N° d'ordre : 3402

THÈSE

Présentée à

L'UNIVERSITÉ BORDEAUX 1

ÉCOLE DOCTORALE DES SCIENCES CHIMIQUES

Par **Cristiano GIACOMELLI**

Pour obtenir le grade de

DOCTEUR

Spécialité : **POLYMÈRES**

****

Nouveaux Développements dans l'Encapsulation de Molécules Hydrophobes via l'Auto-Assemblage de Copolymères à Blocs Amphiphiles

****

Soutenue le : 06 Juillet 2007

Après avis de :

M. R. PECORA	Professeur, Stanford University	**Rapporteur**
M. T. P. RUSSELL	Professeur, University of Massachusetts	**Rapporteur**

Devant la commission d'examen formée par :

M. Y. GNANOU	Directeur de Recherches, Université Bordeaux 1	**Président**
M. R. PECORA	Professeur, Stanford University	**Rapporteur**
M. T. P. RUSSELL	Professeur, University of Massachusetts	**Rapporteur**
M. A. R. BRISSON	Professeur, Université Bordeaux 1	**Examinateur**
M. V. SOLDI	Professeur, Universidade Federal de Santa Catarina	**Examinateur**
M. R. BORSALI	Directeur de Recherches, Université Bordeaux 1	**Examinateur**

- 2007 -

To my wife, Vanessa

To my parents, Domingos and Rosalina

Acknowledgments

This manuscript reports the results obtained during a 3-year period of work at the Laboratoire de Chimie des Polymères Organiques (LCPO-ENSCPB-U. BX 1), in Pessac, France.

I would like to sincerely thank Dr. Y. Gnanou (Director of LCPO) for giving such a precious opportunity to prepare my thesis. I am lucky enough to have spent the last three years in one of the best centers of macromolecular chemistry and physics.

I owe special thanks for all the members of the committee – Dr. A. R. Brisson (Université Bordeaux 1, France), Dr. T. P. Russell (University of Massachusetts, USA), Dr. R. Pecora (Stanford University, USA), Dr. V. Soldi (Universidade Federal de Santa Catarina, Brazil), Dr. Y. Gnanou (Université Bordeaux 1, France) and Dr. R. Borsali (Université Bordeaux 1, France) – for helpful discussions, comments and contributions that have clarified, improved and created new perspectives related to the present work.

The financial support from the Coordenação de Aperfeiçoamento de Pessoal de Nível Superior (CAPES, Ministry of Education, Brazil) is deeply acknowledged. I am particularly grateful to Dr. A. Spinelli (UFSC, Brazil), Dr. V. Soldi (UFSC, Brazil) and Dr. D. Zanette (UFSC, Brazil) for the encouragement they gave me during the early stages of my applications for the fellowships.

I would like to tender my heartfelt thanks to Dr. Redouane Borsali for giving me the opportunity to do my PhD thesis under his supervision, with a forefront, multifaceted and interdisciplinary research topic spanning from polymer synthesis to the preparation and study of nanostructured materials that find application in diverse fields. I express my appreciation to him for giving me in the mean time enough freedom and independence in the quest of novel aspects in soft-matter organization, and his constant readiness for open discussions in all the movements of the day. I greatly appreciated his guidance through the theoretical and practical aspects of my work. I am also delighted with the opportunities I have had to meet many distinguished scientists in the field. Thank you, Dr. Borsali, for all of the guidance, trust, and understanding. Personally, I am also very happy to have come to the end of this 3-year PhD studies with a trustful friendship with Dr. Borsali and his family.

I would like to thank Dr. F. Lecolley for his valued contribution to my work regarding the polymer synthesis. With an ever-present and unparalleled enthusiasm in teaching how to

perform successful controlled radical polymerizations, his outstanding knowledge and friendship were essential in the roadmap of this thesis. Special thanks are also owed to Dr. I. Ydens for her very important advices in the beginning of this work.

I am grateful to Dr. A. R. Brisson for allowing easy access to microscopy facilities available at his research laboratory (Laboratoire d'Imagerie Moléculaire et NanoBioTechnologie (IECB)), as well as for helpful discussions on electron microscopy images along with Dr. J. Lai-Kee-Him and V. Schmidt.

I would like to thank Dr. S. P. Armes (Univeristy of Scheffield, UK) for the very important collaboration within the context of this work.

Ever since my arrival at the LCPO, all the people have been extremely important both professionally and personally. Everyone is acknowledged both professional- and personal-wise.

The understanding, support and collaboration from all my family (Domingos, Rosalina, Fernando and Filipe) have been a building stone in my achievements. They inspire me a lot, and they are heartily thanked.

Last but not least, a very special "thank you very much" goes to my wife Vanessa for her moral support throughout these years, for her sharpness in the decisions we have made so far, for her understanding of the fact that my best paragraphs usually come through in late night writings. This successful 3-year period has been achieved with a very important touch by Vanessa. Thanks!

Thank you all!

Cris

Table of Contents

List of Abbreviations and Symbols

A_2	Second virial coefficient
Abs.	Absorbance
AROP	Anionic ring-opening polymerization
ATRP	Atom transfer radical polymerization
B-IND	Indomethacin covalently bound to the polymer
bpy	2,2'-bipyridyl
χ	Flory-Huggins interaction parameter
CCL	Core crosslinked micelles
CMC	Critical micelle concentration
C_p	Concentration of polymer
CRP	Controlled radical polymerization
D	Diffusion coefficient
DIP	Dipyridamole
DLS	Dynamic light scattering
DMF	*N*-*N*-Dimethylformamide
DOX	Doxorubicin
DP	Degree of polymerization
DPE	Diphenyl ether
DPMK	Diphenyl methyl potassium
DVS	Divinyl sulfone
EPR	Enhanced permeability and retention effect
Et_3N	Triethylamine
f	Overall composition
ϕ	Volume fraction
F	Fluorescence intensity
F-CIN	*trans*-3,5-Bis(trifluoromethyl)cinnamic acid
F-IND	Indomethacin not linked to the polymer
Γ	Relaxation frequency
GPC	Gel permeation chromatography
η	Viscosity
HCST	High critical solubility temperature
HMTETA	1,1,4,7,10,10-Hexamethyltriethylenetetramine
$I(q)$	Scattered intensity at the wavevector q
IBFN	Ibuprofen
IND	Indomethacin
IND-Et	Indomethacin ethyl ester
IND-M	Indomethacin morpholinylamide
K_a	Acid dissociation constant
k_B	Boltzmann constant
K_V	Partition Coefficient
λ	Wavelength

L.C.	Loading Content
L.E.	Loading efficiency
LCST	Low critical solubility temperature
LS	Light scattering
M_n	Number average molecular weight
M_w	Weight average molecular weight
$M_{w,mic}$	Weight average molecular weight of micelles
$M_{w,unimers}$	Weight average molecular weight of unimers
M_w/M_n	Polydispersity
n	Refractive index
N_{agg}	Aggregation number
NMR	Nuclear magnetic resonance
N_x	Degree of polymerization of monomer X
PAA	Poly(acrylic acid)
PCL	Polycaprolactone
PDMA	Poly[2-(dimethylamino)ethyl methacrylate]
PDPA	Poly[2-(diisopropylamino)ethyl methacrylate]
PEO	Poly(ethylene oxide)
PG2MA	Poly(glycerol monomethacrylate)
PGMA	Poly(glycidyl methacrylate)
pH_{mic}	pH of micellization
PLA	Poly(lactic acid)
PMAA	Poly(methacrylic acid)
PMDETA	*N,N,N',N'',N''*-Pentamethyldiethylenetriamine
PMMA	Poly(methyl methacrylate)
PMPC	Poly[2-(methacryloyloxy)ethyl phosphorylcholine]
PPO	Poly(propylene oxide)
PS	Polystyrene
PTX	Paclitaxel
Py	Pyrene
q	Wavevector
R_{core}	Core radius
R_g	Radius of gyration
R_H	Hydrodynamic radius
ROP	Ring-opening polymerization
SCL	Shell cross-linked micelles
SK	Solketal
SLS	Static light scattering
τ	Relaxation time
T	Temperature
TEM	Transmission electron microscopy
T_g	Glass transition temperature
W	Corona width

Introduction

Ever more, the concept and excitement of nanoscience and technology reaches out to the general public through daily newspapers. Over $ 30 million were granted by the National Science Foundation (NSF) in 2005 to set up programs to inform the public about nanotechnology, and address social issues.[1] The scientific articles being published in high-impact journals make widespread use of the prefix "nano".[2]

Such a vast interest in nanoscience and technology derives from the promise of manipulating matter atom-by-atom, molecule-by-molecule to create devices with performances and functionalities that are orders-of-magnitude better and efficient than those provided by current manufacturing technologies.[3]

Two general approaches known as *top-down* and *bottom-up* apply to the preparation of nanosized structures. The *top-down* strategy, which has been used principally by physicists and engineers, consists in "carving" a preexistent macroscopic material through, for example, chemical, mechanical or optical processes to obtain final materials with precisely designed shape, dimensions and properties. Although industry-wise this procedure has the noteworthy advantage of offering straightforward automation possibilities and nearly perfect reproducibility, it is neither atom- nor energy-efficient, as well as irreversible and limited to the production of structures with dimensions approaching 100 nm.

The challenge facing the nanotechnology community is consequently the development of novel structures whose sizes range between 10 – 100 nm. Such a task can be readily accomplished by chemists via the so-called *bottom-up* approach.[4, 5] The latter consists in hierarchically assembling (chemically or physically) a finite amount of elementary building-blocks (atoms, molecules and macromolecules).[6] In addition to the reduced number steps associated with this strategy, it is in most cases reversible, and allows the combination of different materials (minerals, metals, synthetic and natural polymers, etc.). By bottom-up methods, one can elaborate tailored and complex materials via assembling processes driven by chemical and/or physical forces.[7, 8]

It is also possible to combine bottom-up and top-down strategies by inducing the assembly processes (bottom-up) onto already shaped (top-down) nano-scaffolds.[4, 9-11]

Definitely, polymer chemists and physicists share a key contribution to the milestone so far achieved in this domain, as a result of their ability to accurately manipulate small molecules (monomers) that ultimately shall originate 'smart' macromolecules (polymers). Within the large variety of polymer architectures, linear block copolymers certainly play a distinguished, multifaceted role in nanoscience.

The recent advances in controlled/living polymerization processes have encouraged the synthesis of a multitude of macromolecules with controllable architecture, functionality, composition and topology. Through procedures often combining successive polymerization techniques, well-defined amphiphilic copolymers comprising two or more segments of different chemical structures and with hydrophilic and hydrophobic components, have been prepared and injected into the ever-increasing soft mater market.[12]

One of the most interesting and fascinating properties of such precisely engineered macromolecules is their ability to self-assemble into a wide variety of morphologies either in solution (spherical micelles, vesicles, cylinders, etc.) or in bulk (lamellas, bicontineous gyriods and hexagonally or tetragonally packed cylinders, cubic phases, etc.). They constitute, therefore, a collection of elementary building-blocks for the precise construction of novel materials via bottom-up, atom- and energy-efficient approaches.

Figure I-1 summarizes one route for bottom-up construction of nanostructures based on polymeric self-assembly. It is schematically shown how different sizes of construction units can be systematically combined to obtain progressively higher levels of structural hierarchy incorporating different length scales.

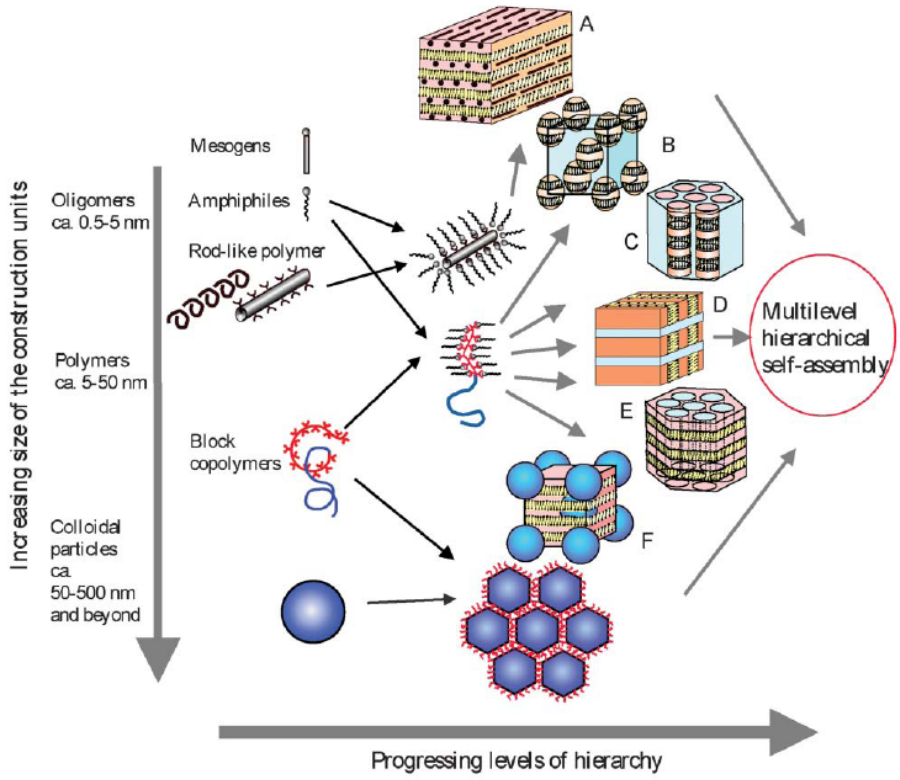

Figure I-1. One of the potential scenarios to construct hierarchically self-assembled polymeric structures.[6]

Particularly, in the biomedical applications the notion of nanorobots roaming within the

blood circulation, detecting and treating diseases, has certainly gained remarkable contributions from block copolymer nanoparticle manipulation. The forefront in the realization of such concepts seems to consist in the development of hybrid, hierarchical nanoparticulate systems that make use of block copolymer scaffolds and mimic the nature in relative simple ways.

Micellar nanoparticles in solution are characterized by a unique core-shell arrangement, where in an aqueous environment the hydrophobic blocks of the copolymer are segregated from the aqueous exterior to form the inner core, and the hydrophilic blocks form the corona or the outer shell. Such nano-objects have been increasingly and successfully tested as nanosized containers in many fields (drug delivery, cosmetics, fragrances, flavor-masking, pesticides, pollution remediation, colloids stabilization, etc.), as a result of their ability to incorporate, retain and release poorly water-soluble, hydrophobic and/or highly toxic compounds, also minimizing degradation and wastage. At the same time, specific targeting can be envisaged through molecular recognition processes imparted by natural bio(macro)molecules attached to micelle periphery such as oligo- and polysaccharides, proteins and antibodies.

On the core (cargo space) side, and independently of the field of application, considerable efforts have focused on the enhancement of micellar loading capacity. Ideally, the solubility parameters of the guest molecules (probe or drug) and the core-forming polymer block should be the same in order to achieve very high loading into micelles. However, there is no universal core-forming segment, because each probe or drug is unique. It is important, therefore, to develop systems in which the latter “matches” in terms of compatibility with the micellar core. As of this moment, however, high micelle payloads have been rarely reported in the literature for physical encapsulation of hydrophobic guest molecules. A few examples do exist, but they appear to be restricted to unique combinations of polymers and guest molecules.

Further development toward general approaches to prepare high payload micellar nanocarriers with widened applications is therefore exceedingly welcome.

Objectives

The central objective of the present work was the conception of original approaches to develop smart block copolymer nanocontainers exhibiting distinguished ability to encapsulate, retain, transport and deliver hydrophobic guest molecules.

Through the roadmap undertaken in such a direction, the goals were positioned on the following aspects, in this order: (*i*) further advance into the understanding of loading and release processes of hydrophobic guest molecules encapsulated inside block copolymer micelles; (*ii*) improve significantly the loading capacity of micellar nanoparticles; (*iii*) establish an copolymer structure – cargo capability relationship; (*iv*) determine the effect of large amounts of hydrophobic guest molecules entrapped inside the nanocontainers on their physical chemical parameters (size, shape, polydispersity, stability, etc.); (*v*) afford access to the control of release mechanisms and kinetics in highly loaded micellar systems through clever manipulation of their structure.

Outline of the thesis

The present manuscript is organized in four principal parts. In *Chapter I*, the fundamentals along with a literature review covering the state-of-the-art of block copolymer self-assembly and micelle-mediated solubilization (encapsulation), transport and delivery of hydrophobic active molecules, will be presented.

In view of the aforementioned objectives, we begin reporting in *Chapter II* on the synthesis and characterization of seven distinct block copolymer systems able to form micellar nanoparticles in selective solvents. The choices of initiators, monomers and the most suitable strategy to carry on the polymerizations in each case are discussed therein. Standard atom transfer radical polymerization (ATRP) and ring opening polymerization (ROP) procedures were used to obtain the macromolecules.

The physical chemical properties of the micellar nanoparticles resulting from the self-assembly of as-synthesized di- and triblocks are subsequently investigated in *Chapter III* mainly by means of scattering and imaging techniques. A brief description of basic concepts underlying the study of micellar systems will precede the results and discussion section. Within the latter, special attention will be given to the effect of the block copolymer composition and architecture on the size, shape and stability of micellar nanoparticles, since all these parameters have important implications on their drug delivery performance.

The loading and release properties of the block copolymer nanocontainers is then presented in *Chapter IV*, which is organized in three principal parts that represent the astonishing differences in terms of probe contents that could be encapsulated by the particles:

A) Low Loading Capacity Nanoparticles: Correlation between Physical Chemical Parameters and Delivery Performance;

B) Moderate Loading Capacity Nanoparticles via Polymer – Probe Conjugates: Multiple Encapsulation and Release Kinetics;

C) High Loading Capacity Nanoparticles via Specific Interactions: Toward a General Approach.

Finally, the *Experimental Part* provides comprehensive details on the synthesis, characterization and manipulation of amphiphilic block copolymers herein investigated, as well as the description of equipments and respective setups used during the present work.

****

Introduction (Français)

****

En solution, les nanoparticules micellaires obtenues à partir de l'auto-assemblage de copolymères à blocs amphiphiles sont caractérisés par une architecture unique du type cœur-couronne. Dans un environnement aqueux, les blocs hydrophobes du copolymère sont isolés de l'extérieur pour former le cœur, tandis que les blocs hydrophiles forment la couronne externe.

Ces particules compartimentées sont investigués de plus en plus en tant que des récipients nanométriques dans divers domaines (vectorisation de médicaments, produits de beauté, parfums, pesticides, récupération de pollutions, stabilisation de colloïdes, etc.), en raison de leur capacité d'incorporer, maintenir, transporter et libérer les composés faiblement hydrosolubles, hydrophobes et/ou fortement toxiques, réduisant également au minimum leur dégradation par différents mécanismes. Parallèlement, des approches pour cibler certains locales spécifiques peut être envisagée via des processus de reconnaissance moléculaire dont certaines (macro)molécules attachées à la périphérie des micelles sont responsables, tels que les saccharides, les protéines et les anticorps.

Indépendamment du champ de l'application, des efforts considérables sont concentrés sur l'amélioration de la capacité d'encapsulation de ces systèmes auto-organisés. Idéalement,

les paramètres de solubilité de la molécule encapsulée et du bloc formant le cœur de la nanoparticule doivent être identiques. Cependant, dans aucun cas il est possible de préparer des systèmes du type universel, car chaque molécule est unique. Par conséquence, le développement de systèmes micellaires avec lesquels les molécules encapsulées seront compatibles est très important. À présent, la préparation de nanoparticules à haute capacité d'encapsulation a été rarement rapportée dans la littérature. Quelques exemples existent, toutefois ils semblent être limités aux combinaisons uniques et très précises des polymères et des molécules hydrophobes.

De ces faits, nouveaux développements dans l'encapsulation de molécules hydrophobes via l'auto-assemblabe de copolymères à blocs amphiphiles sont stratégiquement importants pour l'avancée de ce domaine multidisciplinaire.

Objectifs

L'objectif principal de ce travail était le design d'approches originales pour développer des nanocontainers ayant une excellente capacité d'encapsuler, retenir, transporter et délivrer des molécules hydrophobes. Dans une telle direction, les objectifs ont été focalisés sur les aspects suivants, dans cet ordre : (i) comprendre de manière claire les processus d'encapsulation et de libération de molécules hydrophobes par des systèmes micellaires obtenus à partir de l'auto-assemblage de copolymères à blocs ; (ii) améliorer significativement la capacité d'encapsulation de molécules hydrophobes par des nanoparticles micellaires ; (iii) établir une corrélation entre la structure macromoléculaire et la capacité d'encapsulation ; (iv) déterminer l'effet de grandes quantités de molécules hydrophobes encapsulés à l'intérieur des nanocontainers sur leurs paramètres physico-chimiques (taille, forme, polydispersité, stabilité, etc.) ; (v) contrôler le mécanisme et cinétique de libération des systèmes micellaires via manipulation intelligente de leur structure.

Organisation du manuscrit

Ce manuscrit est organisé en quatre parties principales. Dans le Chapitre I, les principes fondamentaux et les revues bibliographiques seront présentés. En vue des objectifs mentionnés ci-dessus, nous décriront en Chapitre II la synthèse et la caractérisation de sept systèmes distincts de copolymère à blocs capables de former des nanoparticles micellaires dans les solvants sélectifs. Les choix des amorceurs, des monomères et des stratégies plus appropriées pour bien mener les polymérisations dans chaque cas seront discutés.

Les propriétés physico-chimiques des nanoparticles micellaires résultant de l'auto-organisation de copolymères à di- et triblocs sont ensuite étudiées en chapitre III, principalement à travers des techniques de diffusion de lumière et imagerie.

Les performances d'encapsulation et de libération de chaque système de nanocontainers à base de copolymère à blocs sont alors présentées en Chapitre IV, lequel est organisé dans trois parties principales représentant les différences très intéressantes par rapport à la quantité maximale de molécules hydrophobes encapsulées dans le cœur de la micelle. Ces nanoparticules sont classées en trois groupes principaux, correspondant à leur capacités d'encapsulation (LC) *A*) faibles, *B*) modérées et *C*) élevées.

Les résultats ont très clairement montré que la capacité d'encapsulation des systèmes micellaires stimulables que nous avons développés peut être contrôlée avantageusement via les propriétés structurelles des molécules hydrophobes et des blocs formant le cœur de la nanoparticule.

Chapter I

Fundamentals and Literature Review

Introduction

This chapter is devoted to the review of fundamentals aspects on block copolymer systems and the principal breakthroughs achieved through their applications, especially in the biomedical field.

In *Part A*, an overview of synthetic strategies to obtain such segmented macromolecules will initially be given, followed a brief discussion on the thermodynamic driving forces underlying the fascinating self-assembly phenomena occurring in block copolymer systems.

The solution behavior of amphiphilic macromolecules is contemplated in *Part B*, with emphasis to effect of the polymer chain characteristics (architecture, molar mass, composition and polydispersity) on the properties (morphology, size, stability) of self-organized objects (spherical core-shell micelles and vesicles) in aqueous media.

The use of nanostructured materials as carrier/container systems for hydrophobic guest molecules is then highlighted in *Part C*.

A) Block Copolymers: From Molecules to Objects.

A-1. Approaches for Block Copolymer Synthesis

As of today, the knowledge of synthetic tools in macromolecular chemistry allows almost all types of block copolymers to be prepared, provided that certain conditions are fulfilled.[13] The limit seems to be the creativity of polymer chemists face to the emerging challenges in nanoscience. Experimental procedures for "on-demand" synthesis of polymer chains are increasingly undertaken after careful pre-analysis and establishment of properties desired for the resulting materials, and choice of convenient polymerization methods. Certainly, this scenario has been made possible in recent decades through the development of "controlled/living" polymerization (CLP) techniques, which have permitted block copolymers to be prepared and arranged in miscellaneous of architectures, compositions, etc.

The state-of-the-art in block copolymer synthesis has been comprehensively discussed and reviewed in the last couple of years.[13-20] The reader is referred to the cited review articles[14-18] and books[13, 19, 20] for detailed information.

In the present section, we survey the typical strategies for block copolymer synthesis, as recently reviewed by Taton and Gnanou[13] and Hadjichristidis et al.[14] The former authors summarized the possible routes to prepared AB diblock copolymer structures as shown in

Figure I-2. In addition to the sequential monomer addition technique (*route A*), other strategies can be used. These include coupling of two preformed (co)polymer segments with antagonist functional end-groups X and Y (*route B*), combination of different modes of polymerization (switching from one to another) for the preparation of specific block copolymers that are not accessible from one polymerization mechanism only (*route C*), and one-pot initiation from dual bifunctional initiators for AB block copolymer synthesis (*route D*).

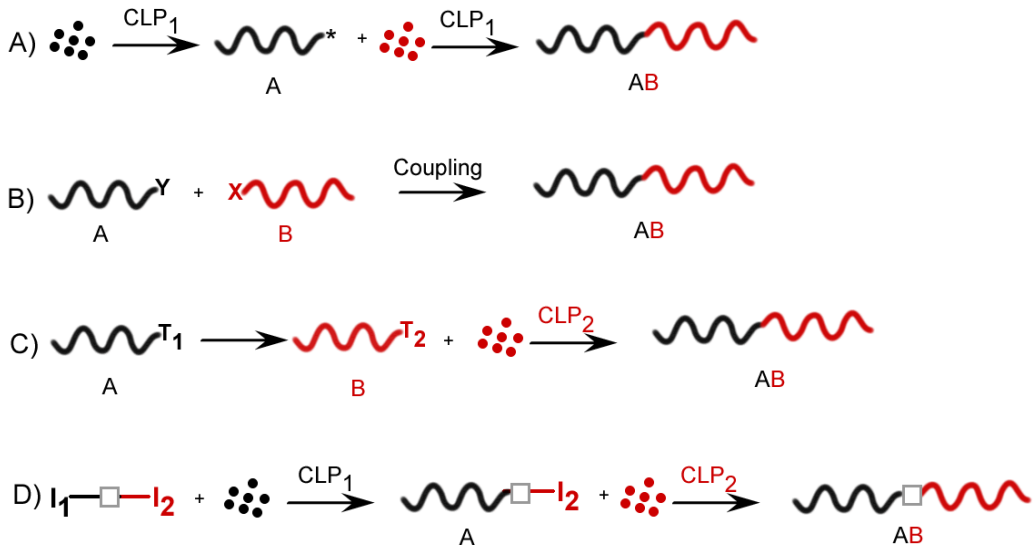

Figure I-2. Illustration of possible routes toward the synthesis of di- or triblock copolymers, as proposed by Taton and Gnanou.[13]

In *route A*, the order of monomer addition is an essential consideration for its successful employment. The growing chains from the polymerization of the first monomer A must be able to efficiently initiate the polymerization of the second monomer B. Another important requirement is that the conversion of the first monomer must be near quantitative in order to prepare well-segmented, structurally homogeneous macromolecules.

The r*oute B* is also a common synthetic approach to multiblock copolymers. A forefront example is the one-pot synthesis of ABC type triblock copolymers via in situ click [3 + 2] and Diels-Alder [4 + 2] reactions.[21] In fact, during the last five years, click chemistry has been extensively developed and applied for the preparation of a multitude of novel amphiphilic macromolecules through coupling of pre-formed chains.[21-26] Perhaps no reaction in the click family has received more attention than Cu(I)-catalyzed Huisgen 1,3-dipolar cycloaddition of terminal alkynes with organoazides to yield 1,4-disubstituted 1,2,3-triazoles. True to a good click reaction, the process is reliable and high yielding, easy to perform, invariant to the

presence of air or moisture, and tolerant of a wide range of functional groups.[22] The 1,2,3-triazole ring is resistant to hydrolysis, oxidation, reduction, and other modes of cleavage. In order to perform a coupling reaction between two A and B homopolymers, both should carry azide ($R–N_3$) and alkyne ($R–C\equiv C$) complementary/antagonist groups.

Switching from one polymerization technique to another as illustrated by *route C* is probably the most largely used synthetic approach in block copolymer nanoscience ever since the emergence of controlled radical polymerization (CRP) in the mid-1990s.[13, 14] It is a useful strategy whenever two or more monomers (A, B, etc.) that are to be paired in a targeted block structure do not polymerize by the same mechanism. The active center T_1 can be transformed into an initiating-capable function T_2 either *in situ* or after isolation of the first block followed by chemical modification of chain ends. The newly formed active center is then able to initiate the subsequent chain growth to generate the n^{th} block. Such an approach has encountered widespread used in the preparation of a multitude block copolymer systems exhibiting adequate properties for biomedical applications, especially in drug delivery.

The *route D* has also gained considerable attention in the last decade because of its particular capability of allowing the combination of mechanistically distinct polymerization reactions without the need of intermediate transformations or protective chemistry steps.[15]

The classical approaches represented by *route A* and *route C* were used during this work to prepare amphiphilic di- and triblock copolymers able to form micellar nanoparticles in water, as is the case of an expressive number of drug delivery systems so far investigated and also those in clinical trial development (see *Part C*).

A-2. General Self-Assembly Behavior

In the simplest block copolymer architecture, an AB diblock, a sequence of N_A monomers are covalently linked to a sequence of N_B monomers, with an overall composition $f = N_A/N$, where $N = N_A + N_B$. Most AB polymer pairs are immiscible, due to a characteristically small entropy of mixing (~1/N) and a positive heat of mixing (~χ_{AB}, the Flory-Huggins interaction parameter), and consequently such mixtures are thermodynamically unstable. Thus, the mixing of two different types of polymer chains often results in macroscopic phase separation.

Block copolymers offer an attractive route to circumvent this problem, in that the covalent linkage between blocks suppresses phase separation. Instead, it can undergo a so-called microphase separation in bulk, or self-assembly process in solution. As a result, each block will reside in its own phase leading to the formation of ordered domains as a result of short range attractive and long-range repulsive forces co-existing at the same time.[18, 27-29]

The resulting materials thus combine properties of both components, with predictable microstructures within 10-200 nm length scale. They may adopt a wide variety of structures and morphologies either in bulk phase or in solution.[30-34] Figure I-3 shows an overview of the most common structures formed by diblock copolymers, as given by Förster and Plantenberg,[30] and Bucknall and Anderson.[31] This is in reality a very simplified representation. Several more complex morphologies such as lamellar in lamellar (LL),[35] hexagonal in lamellar (HL),[32] hexagonal in hexagonal (HH) have been evidenced.[32] The more recent observation is probably the formation of tetragonally (instead of hexagonally) packed cylinders.[33]

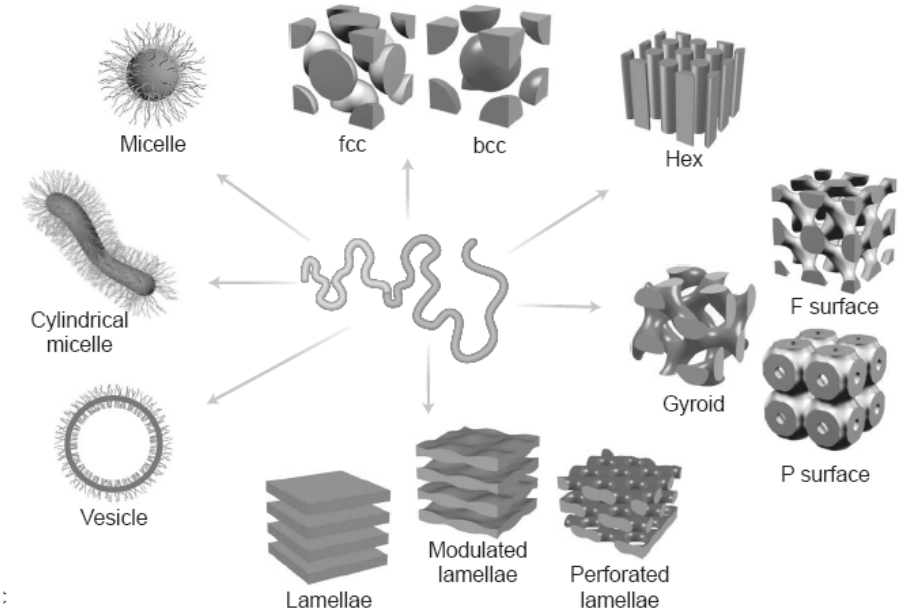

Figure I-3. Schematic representation of the most common self-organized structures in solution (left) and in bulk phase (right). Scheme formerly proposed by Förster and Plantenberg,[30] and Bucknall and Anderson.[31]

In the present work, the interest is evidently centered on block copolymer morphologies in aqueous solution. Objectively, a review of the micellization phenomena and physical chemical properties of the resulting nano-objects is given in the next section.

B) Self-Assembly of Block Copolymers in Aqueous Media

B-1. The Micellization Process

The ability of amphiphilic block copolymers to self-assemble when dissolved in a selective solvent (*i.e.*, a solvent thermodynamically good for one block and poor for the other) is well-documented, and constitutes a hot research topic in modern polymer science.[31, 36-42] The micellization process leads to the formation of ordered structures in which the contact between the insoluble block and the solvent is minimized. The soluble block is then oriented towards the continuous solvent phase and becomes the "corona" of the formed micelle, whereas the insoluble part will be shielded from the solvent in the "core" of the structure, and therefore protected from the external environment (Figure I-4). Important aspects of micelle-mediated drug delivery are also indicated in this figure, and will be discussed in detail in *Section C*, *Chapter I*.

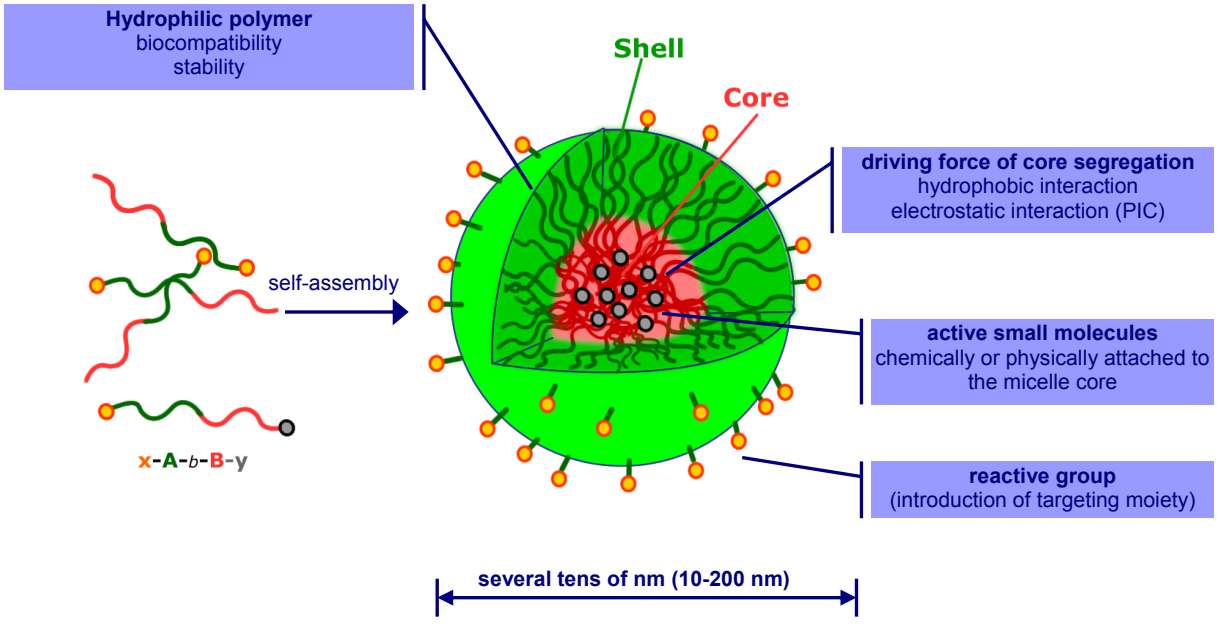

Figure I-4. Micellization of an amphiphilic linear AB diblock copolymer leading to the formation of spherical core-corona micelles.[43]

Two principal opposing forces are responsible for such segregation of the polymer chains. The first force is an attraction between the insoluble blocks, which induces the aggregation. The second force is the repulsion between the soluble blocks, leading to a limitation in the size of the aggregates.[36] The balance between these two forces is generally defined by the stretching of polymer chains in the core, the surface tension at the core-corona interface, the interactions between chains forming the micellar corona, the strength of interaction between the blocks (represented by the Flory–Huggins interaction parameter, χ), and the volume fraction (ϕ) of each constituting segment.

Indeed, these physical chemical parameters can be finely adjusted via macromolecular engineering and clever manipulation strategies.

Depending on the equilibrium between the aforementioned forces during and after the micellization process of block copolymers, micelles with varying size, morphology and structural organization may be obtained, as outlined hereafter.

B-2. Micelle Preparation Methods and Manipulation

The methodology of micellar nanoparticles preparation is a key parameter controlling the mechanism (kinetics and thermodynamics) of self-assembling processes of block copolymers. However it is neither fully described in the literature nor unique. Lately, the large variety of amphiphilic polymers (linear and cyclic blocks, stars, dendritic, hyperbranched, etc.) synthesized through procedures often combining successive polymerization techniques and chemically distinct monomers[20], has demanded increasing efforts in terms of their manipulation, especially in solution. Frequently, the preparation of well-defined (near monodisperse) self-assembled structures requires detailed optimization studies, and creativity of polymer chemists and physicists.

Since the self-organization of polymer chains in solution constitutes a bottom-up approach, several experimental factors (concentration, temperature, presence of additives, etc) can potentially influence the packing of the elementary building-blocks (unimers), and therefore the physicochemical parameters of the resulting objects (aggregation number (N_{agg}), hydrodynamic radius (R_H), density of packing, etc.). Indeed, the number of experimental variables can increase quite rapidly among the preparation methods, and strict control and knowledge of these methods is certainly needed to achieve a good degree of reproducibly.

In this section, we describe five principal micelle preparation methods based on recent

results and some practical information that have been employed so far in macromolecular self-assembling field, highlighting the main adjustable variables in each case. As stated above, there is no universal strategy to prepare nano-structured polymer-based materials in solution. In fact, the considerable body of work currently available has demonstrated that in the research for original aggregates, the precise control over the manipulation of macromolecular chains is as much important as the design of new monomers and polymers.

The following preparation methods have been largely applied: **1**) direct dissolution, **2**) indirect dissolution method (also called dialysis method), **3**) stimuli-induced self-assembling, **4**) solvent casting/film re-hydratation and **5**) emulsion method. The choice of which approach to use depends mostly on the copolymer solubility in the medium wherein the assemblies are to be formed. Whenever the resulting assemblies are to exert a given function in a system, the choice of the method must consider the constraints of the latter.

B-2-1. Direct dissolution

The direct dissolution method simply consists in dissolving a given amount of amphiphilic block copolymer in a solvent in which at least one of the segments is marginally soluble. In general, self-assembly takes place progressively upon stirring until the thermodynamic equilibrium is reached within a period of time varying from minutes to weeks. The self-organization kinetics depends not only on experimental parameters such as solvent, temperature, presence of additives, etc., but also on intrinsic macromolecular properties such as the molecular weight, volume fraction ratio between solvophilic and solvophobic segments, and glass transition temperature (T_g).

The manipulation of amphiphilic block copolymers in aqueous environment appears to be a quite difficult, and direct dissolution has been considered suitable for star-like micelles ($R_{corona} >> R_{core}$) from systems exhibiting corona-forming blocks longer that the core-forming blocks [40]. Still, the preparation of micellar nanoparticles in water frequently requires the solution temperature during the preparation protocol to be higher than the T_g of the constituting blocks [44-46], in order to give mobility to the individual chains. For example, the hydrodynamic diameter ($2R_H$) of the micelles originated from self-assembling of polystyrene$_{21}$-*b*-poly(acrylic acid)$_{77}$ (PS_{21}-*b*-$PAA_{77;}$ $T_g(PS_{21})$ = 55 ^oC using DSC) diblocks, reaches a stable value after 4 hours of stirring at 90^{o}C, [46] whereas at room temperature the size distribution of particles remains very large.

Meanwhile, such a straightforward approach has been extensively used for micelle preparations in organic media, principally because the polymer-solvent interactions (*i.e.*, χ parameter) can be tuned by changing (even slightly) the solvent quality, often giving rise also to different morphologies. This is illustrated in a recent communication by Liu et al.[47] showing that the self-assembling of polystyrene-*b*-poly(4-vinylpyridine) (PS-*b*-P4VP) in low-alcohol solvents originates multiple morphologies, which can in fact be tailored by choosing the adequate experimental protocol. In the mentioned work, those authors dispersed PS-*b*-P4VP diblocks in alcohol solvents at high temperatures in order to improve the solubility of PS block, and then the influence of rate of decreasing temperature on multiple morphologies (including spheres, rods, vesicles, porous vesicles, large compound vesicles, and large compound micelles) was observed. The transformation of spheres to rods, to large compound micelles, and to sphere-shaped large compound micelles was also realized.

The presence of additives (low molecular weight compounds or polymers) during the micellization of block copolymers affects dramatically the thermodynamic equilibrium of the system as well. For example, Ouarti et al. [48] have demonstrated that small amounts of PS_{50} homopolymer (2 – 5 %) in linear and cyclic PS_{290}-*b*-PI_{110} block copolymers govern morphology of the resulting objects in heptane. PS and PI chains constitute the core and the corona of these micelles, respectively, due to the different affinity of the blocks for heptane (good solvent for PI). Consequently, the PS homopolymer added is "solubilized" into the micellar core. Indeed, a morphological transition, from spheres to cylinders for the linear copolymer, and from cylinders to vesicles for the cyclic copolymer was observed.

B-2-2. Indirect dissolution, co-solvent or dialysis method

When the block copolymer solubility in water is too low, indirect methods of dissolution are needed. Broadly also known as co-solvent or dialysis method, the indirect dissolution strategy (Figure I-5) consists in dissolving the block copolymer in a common organic solvent (*i.e.,* thermodynamically good for both blocks) that is miscible with water such as *N,N*-Dimethylformamide (DMF), *N,N*-Dimethylacetamide (DMAc), tetrahydrofuran (THF) and acetone. Subsequently, water is added to the organic phase containing molecularly dissolved chains at controlled rate and amount. Gradually, the solvent quality changes towards opposite directions for each block, becoming increasingly good for one block and poor for the other. At the Critical Water Concentration (CWC), the micellization occurs in order to minimize the

contact between the solvophobic block and the solvent. As a result, self-assembled objects are generated in solution. It was found that the CWC depends, in addition to the nature of the common solvent in which the block copolymers are initially dissolved,[49] on both the polymer concentration and the molecular weight.[50] The higher the polymer concentration, and the higher the molecular weight, the lower the CWC. The morphology of the objects originated at this point (onset of the micellization) might not necessarily be in thermodynamic equilibrium. In fact, the size and shape of the aggregated may evolve not only as a function of the time, but also the water content.[51]

Next, the copolymer/organic solvent/water mixture is dialyzed against water in order to remove the organic solvent. Alternatively, the mixture can be left to evaporate and/or purged gently with N_2 during ca. 24 – 48 h to speed up evaporation in the case of volatile solvents such as THF and acetone. Technically, the removal of the organic fraction can be followed, for example, by GC, HPLC and NMR, analysis, as demonstrated in Figure I-6 for poly(ethylene oxide)$_{45}$-*b*-polycaprolatone$_{24}$ (PEO_{45}-*b*-PCL_{24}) micellar solutions prepared using THF as co-solvent. For a 1.0 mg/mL PEO-*b*-PCL in a mixture of 4:96 v/v THF:water, ^{1}H NMR spectra recorded before (control) and after such a solvent removal procedure (12h under N_2 purge) reveal the complete disappearance of chemical shifts associated with protons in the THF structure, although traces might not be detectable.

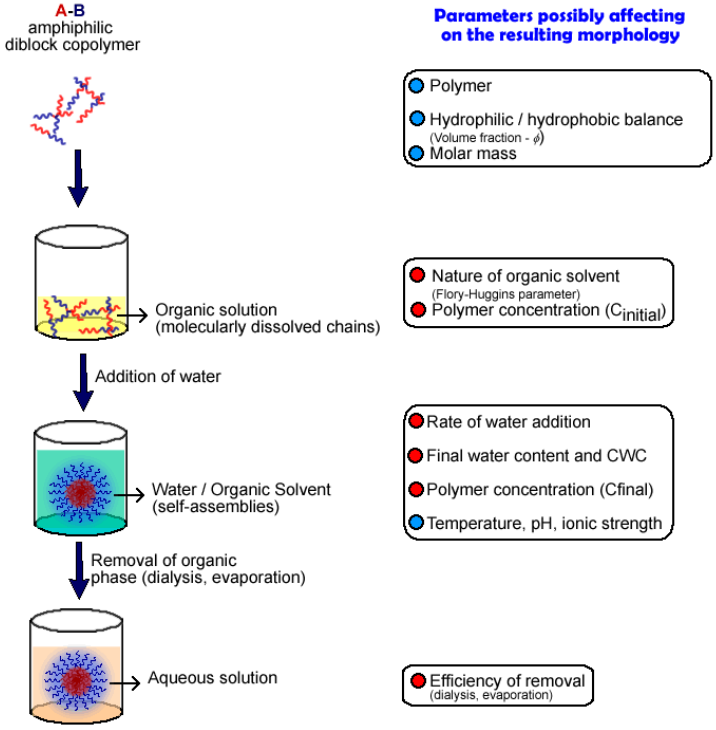

Figure I-5. Schematic representation of preparation of micellar nanoparticles by indirect dissolution method.[40]

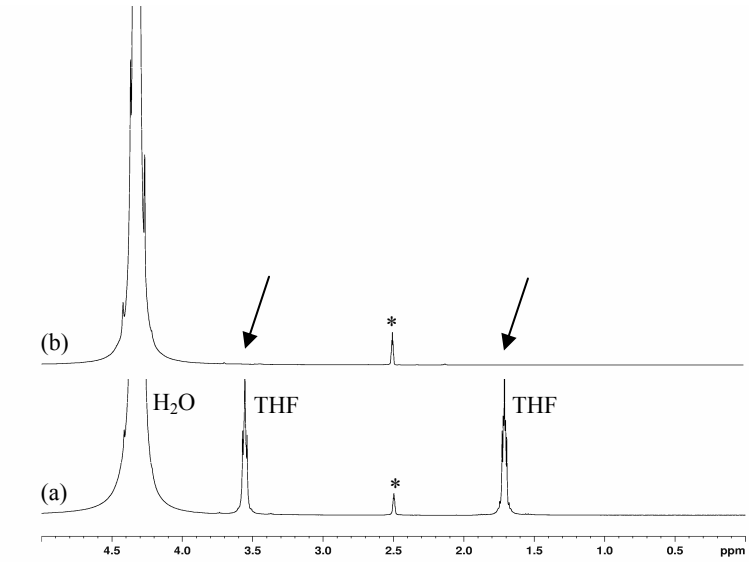

Figure I-6. ^{1}H NMR spectra in 62% DMSO-d_6 of a 1.0 mg/mL PEO-*b*-PCL micelles in a mixture of 4:96 v/v THF:water recorded before (a) and after solvent removal by evaporation under N_2 purge (b) (* = solvent residual peak). Results obtained in this work.

The indirect dissolution method – often combined with quenching techniques – has contributed enormously to the visualization, characterization and application of unprecedented block copolymer morphologies. Although this procedure is experimentally simple, it involves a much higher number of controllable parameters (Figure I-5, right), which in turn affect the properties of self-assemblies.

B-2-3. Stimulus-induced self-organization

Stimuli-responsive macromolecules are characterized by their ability to respond with abrupt changes in the respective properties, to physical (temperature, light, ionic strength solvent, etc.) and/or chemical (pH, reactants, molecular recognition) external stimuli. Among the vast diversity of smart polymeric materials,[52, 53] those exhibiting pH- and temperature-responsiveness have been studied the most, due to their contrasting simplicity in terms of manipulation, and exceptional morphological behavior.

The preparation of micellar aggregates from responsive amphiphilic block copolymers involves, in a first step, the molecular dissolution individual building blocks in the water. Subsequently, an external stimulus is applied to the system in order to provoke changes in the solubility of at least one segment, which then segregates from the aqueous exterior to reduce unfavorable contact with the latter. This behavior is illustrated below for poly[2-(methacryloyloxy)ethyl phosphorylcholine]-*b*-poly[2-(diisopropylamino)ethyl methacrylate]

(PMPC-*b*-PDPA) diblock copolymers. PMPC-*b*-PDPA chains can be molecularly dissolved in dilute acid solution, since the PDPA block is protonated and hence hydrophilic under these conditions. On adjusting the copolymer solution to around pH 5-7, the PDPA blocks become deprotonated and hence hydrophobic, leading to the formation of micelles[54] or vesicles[55] with dehydrated PDPA cores, and PMPC coronas, depending on the volume fraction of PDPA segment (Figure I-7).

The self-assembling of pH-responsive polymer is often sensitive to the ionic strength of the medium because of the polyelectrolyte nature of the species at some point (before or after protonation/deprotonation). The aqueous solution behavior of polyelectrolytes has been extensively investigated, and certain features are now well established.[56-58] For example, it is known that the presence of charge on a polymer chain leads to its expansion with respect to the equivalent neutral polymer chain (or highly screened equivalent polyelectrolyte chain), and that lowering the ionic strength also leads to expansion of the polyelectrolyte coils. As the ionic strength decreases, the repulsion between polyelectrolyte chains increases, leading to a change in the second virial coefficient, A_2, and a reduction in light scattering intensity due to osmotic pressure.[56-58] Furthermore, the ionic strength also affects the critical degree of protonation of weak polyelectrolytes by stabilizing (screening) charged structures.[59] As a result, the equilibrium constant shifts towards the formation of charged structures and the critical micellization pH (pH_{mic}) increases. Thus, the polyelectrolyte nature of weak polybases leads to a rich structural dependence of unimers and micelles on parameters such as ionic strength and pH for these copolymers.

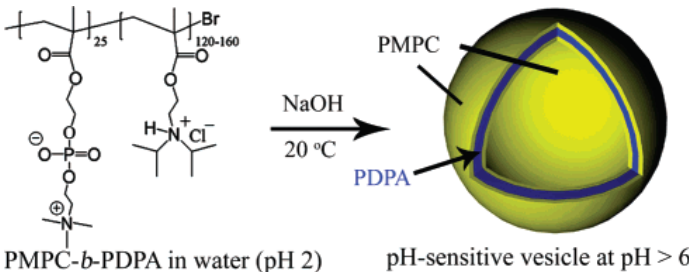

Figure I-7. Formation of PMPC-*b*-PDPA block copolymer vesicles.[55]

B-2-4. Film casting/film re-hydratation

The solvent casting/film re-hydration protocol comprises the copolymer dissolution in an organic solvent which may not necessarily be miscible with water (such as methylene chloride, chloroform, toluene, xylene), followed by slow evaporation of the organic phase. Removing the organic solvent yields to microphase separated systems in bulk, in a process favored by incompatibility between constituting blocks. After obtaining a nano-organized film, an appropriate amount of water can then be added, and the resulting solutions are stirred in sealed vials for quite long periods of time (at least 1 week) prior to analysis. During this time, the bulk films are progressively re-hydrated leading to the formation of self-assembled structures in solutions from pre-organized systems. In fact, this approach has been successfully applied to the preparation of small unilamellar vesicles (SUVs) from phospholipids.[60]

The preparation of block copolymer self-assemblies by solvent casting/film re-hydration method has been reported recently, for example by Bates[61] and Discher,[62] for PEO-*b*-PCL copolymers having $0.30 < \phi_{PCL} < 0.70$. In those experiments, the copolymer was initially dissolved in methylene chloride[61] or chloroform.[62] After evaporation of the solvent, the resulting thin films were re-hydrated to give the desired aqueous micellar solutions.

B-2-5. Emulsion method

The preparation of block copolymer nanoparticles by oil-in-water (o/w) emulsion method (Figure I-8) comprises first the copolymer dissolution in a mixture of water and a water-immiscible organic solvent (or oils such as Lipiodol,[63] for instance) at a precise volume ratio. While the hydrophilic segment dissolves in the aqueous phase, the hydrophobic block solubilizes within nano-sized droplets forming the organic phase. Micellar nanoparticles are then obtained after removal of the organic phase by dialysis or evaporation.

The oil-in-water emulsion method has been preferentially used for the preparation of micellar systems containing relatively high payloads of guest hydrophobic molecules (active drugs, cosmetics, fragrances, toxic or unstable compound, etc.). Its distinguished potential in such a case originates from the fact that both the guest molecule and the core-forming block are dissolved together in an organic micro-environment, thus ensuring that the former is indeed stabilized in a segregated compartment. Upon removal of organic solvent, the drug is

entrapped inside the nanocontainer, allowing appreciably high loadings (> 50 % w/w_p) to be achieved.

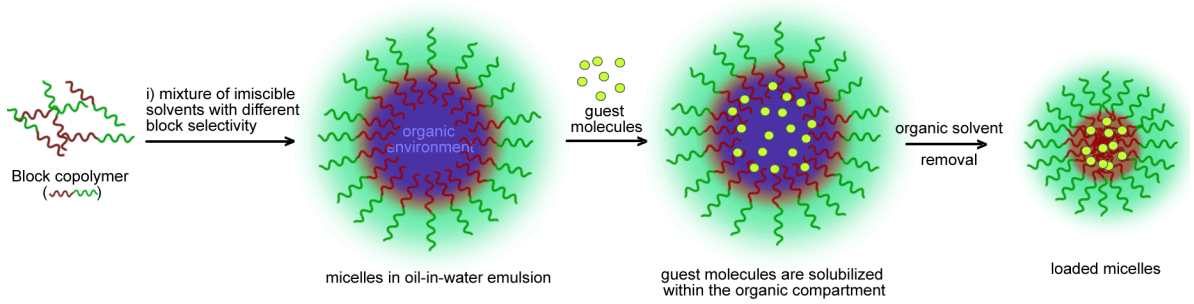

Figure I-8. Schematic representation of preparation of loaded micellar nanoparticles by oil-in-water emulsion method.

B-3. Morphology of Micellar Aggregates

As mentioned above, a variety of morphologies have been accurately characterized mainly by imaging and scattering techniques. Spheres (including hairy, crew-cut, and large compound micelles),[64-67] slight elliptic objects,[68] cylinders[69] and worm-like (i.e., micrometer-long cylinders),[49, 69-71] vesicles,[39, 67, 71, 72] large compound vesicles,[73] disks,[65] bicontinuous rods,[74] hollow tubes,[75] and hexagonally packed hollow hoops,[76] are some of the structures reportedly observed in macromolecular self-assembly. The current understanding so far achieved in this field suggests that in the research for original aggregates, the precise control over the manipulation of polymer chains is as important as the design of new monomers and polymers. For example, Figure I-9 shows how the morphology of self-assemblies made from highly asymmetric PAA_{25}-*b*-PS_{410} diblocks progressively changes as a function of added salt, which acts on the weak polyacid PAA segment.[73] As salts are added to such a system, the morphological spectrum of spheres, rods, vesicles and large compound vesicles can be traversed.

A question of immediate interest is whether all the structures mentioned in the beginning of the preceding paragraph are indeed in simultaneous thermodynamic and kinetic equilibria. The most probable answer is that they are in kinetic equilibrium, but might not necessarily be in thermodynamic equilibrium.[77] Such an affirmation is reinforced by the usual observation of co-existing morphologies even for narrowly distributed block copolymers. This fact is not surprising, however, for rather polydisperse systems inasmuch as they might contain chains with sufficiently different volume fractions of hydrophilic and hydrophobic segments to give rise to more than one type of aggregates within the same solution.

The co-existence of multiple morphologies in solution is frequently observed when micellar nanoparticles are prepared by methods other than direct dissolution of polymer chains in the desired solvent. In part, this is due to the fact that the aggregation process takes place in a solvent mixture, and the newly formed particles might remain in a frozen, kinetically stable state depending on the block copolymer properties. Within the time, the dynamics of polymer chains (see *Section B-5*) can however lead to a re-arrangement of the micellar structure toward the most thermodynamically stable morphology. Although seldom discussed in the literature, the evolution of micellar systems with time after preparation is a phenomenon often observed experimentally.

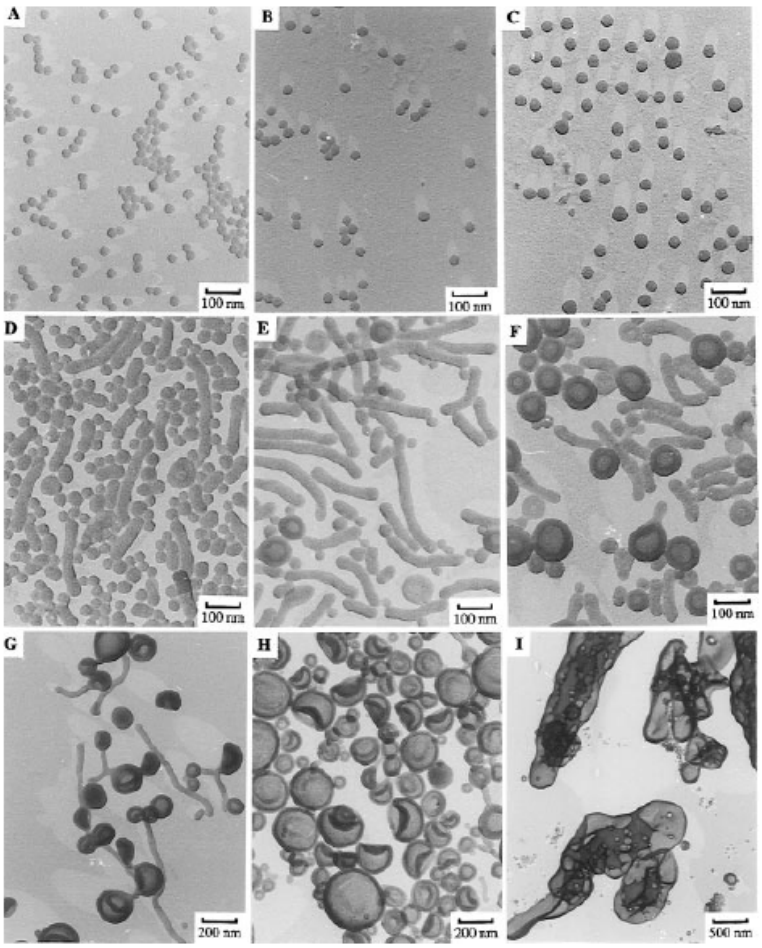

Figure I-9. Micellar aggregates from PS_{410}-*b*-PAA_{25} without any additive (a) and with added NaCl to different final concentrations (in mmol/L): (b) 1.1; (c) 2.1; (d) 3.2; (e) 4.3; (f) 5.3; (g) 10.6; (h) 16.0; (i) 21.0. Adapted from the work by Zhang and Eisenberg.[73]

Whenever diblock copolymer aqueous micellar solutions are prepared by direct dissolution, three principal morphologies (among all those mentioned above) are observed, which consist in spherical core-corona micelles, cylinders and vesicles. Roughly, the formation of spherical micelles are favored for $0.30 < \phi_{hydrophobic} < 0.70$, whereas vesicles are expected for $\phi_{hydrophobic} > 0.70$.[42, 71, 78] This is illustrated in Figure I-10 for poly(1,2-butadiene)-*b*-poly(ethylene oxide) (PB-*b*-PEO) diblocks, as reported by Jain and Bates.[71] These authors observed that at constant degree of polymerization of the PB block (N_{PB}), the increase in volume fraction of PEO (w_{PEO}) segment results in a change in the morphology from vesicles (here called bilayers – B, micrograph A) to cylinders (C, micrograph B) and then to spheres (S, micrograph C).

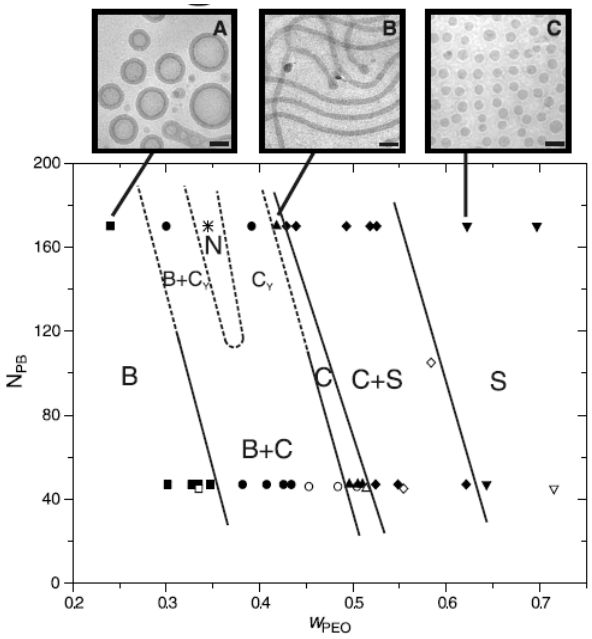

Figure I-10. Morphology diagram for 10 mg/mL PB-*b*-PEO micellar solution in water. N_{PB} and w_{PEO} are the degree of polymerization and weight fraction of the PB and PEO blocks, respectively. Results reported by Jain and Bates.[71]

Among the myriad of block copolymer nano-objects that can be prepared in aqueous solution, spherical core-corona micelles and vesicles are the most interesting morphologies for the encapsulation of hydrophobic and/or hydrophilic compounds (see *Section C*, *Chapter I*). For the sake of simplicity, and unless otherwise specified, from now on the general term "micelle(s)" will refer to spherical micelle(s).

In the sequence we outline concisely the physical chemical micellar properties and experimental parameters affecting their structures.

B-4. Rationalization of the Micelle Structure

An important body of work has been devoted to the systematic study of structural parameters of micelles (e.g.: core radius (R_c), corona width (W), number of aggregation (N_{agg}) and molar mass ($M_{w,mic}$)) as a function of the molecular characteristics of block copolymers (e.g.: M_w, N_A, N_B, ϕ_A, ϕ_B).[41, 64, 79]

In the case of neutral micelles, the principal approaches predicting the variations of physical chemical parameters are based on the scaling concepts formerly described by Alexander and de Gennes,[80] and on the self-consistent mean field theory developed by Noolandi and Hong,[81] Nagarajan and Ganesh,[82] Leibler et al.,[83] and by Hurter et al.[84] These approaches have been used to examine two extreme cases: hairy or star-like micelles and crew-cut micelles. The so-called hairy or star-like micelles ($R_c << W$, Figure I-11a) are formed by block copolymers whose insoluble block is much smaller than the soluble block ($N_B << N_A$). On the contrary, crew-cut micelles ($R_c >> W$, Figure I-11b) are made from samples in which $N_B >> N_A$.

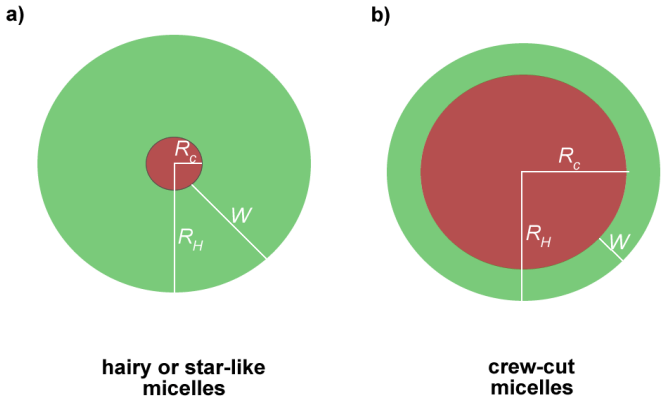

Figure I-11. Schematic representation of hairy or star-like (a) and crew-cut (b) micelles.

The star polymer theory of Daoud and Cotton[85] can be applied in the case of star-like micelles. By defining the segment density profile as a function of the distance of the core center for star-like polymers in good solvents, those authors found that the star polymer radius scales as

$$R \sim N_A^{3/5} f^{1/5} \qquad \text{(I-1)}$$

with f corresponding the number of arms. In a block copolymer micelle, the number of arms corresponds to the aggregation number N_{agg}. The latter being described by the relation

$$N_{agg} \sim N_A^{4/5} \qquad \text{(I-2)}$$

it follows that

$$R \sim N_A^{3/5} N_B^{4/25} \qquad \text{(I-3)}$$

The scaling theory applied to crew-cut micelles assuming a uniform stretching of polymer chains in the core, describes the variation of R_c and N_{agg} as a function of N_B as follows:

$$R_c \sim \gamma^{1/3} N_B^{2/3} a \qquad \text{(I-4)}$$

$$N_{agg} \sim \gamma N_B \qquad \text{(I-5)}$$

where γ is the surface tension between block A (solvophilic) and block B (solvophobic), and a is the segment length. It is interesting to note that the dependence of the micellar properties on N_A disappears, and therefore the ultimate micelle size is dictated mainly by the length of the core-forming block (N_B), as demonstrated by Zhulina and Birshtein.[86] These authors also considered four distinct regimes associated to the relative values of N_A and N_B in their modelization, as listed in Table I-1.

Table I-1. Scaling laws for micelles as a function of N_A and N_B relative values.

Regime	Composition	R_c	W	N_{agg}
I	$N_A < N_B^{\nu/6}$	$N_B^{2/3}$	N_A^{ν}	N_B
II	$N_B^{\nu/6} < N_A < N_B^{\nu(1+2\nu)/6\nu}$		$N_A\, N_B^{(\nu-1)/6\nu}$	
III	$N_B^{\nu(1+2\nu)/6\nu} < N_A < N_B^{\nu(1+2\nu)/5\nu}$	$N_A^{-2\nu/(1+2\nu)} N_B$	$N_A^{3\nu/(1+3\nu)}$	$N_A^{-6\nu/(1+2\nu)} N_B^2$
IV	$N_A > N_B^{\nu(1+2\nu)/5\nu}$	$N_B^{3/5}$	$N_A^{\nu} N_B^{2(1-\nu)/5}$	$N_B^{4/5}$

ν is Flory's exponent which is equal to 1/2 for θ-solvents and 3/5 for good solvents, respectively.[87]

However, such scaling models do not allow the numerical values of structural micellar parameters characteristics to be directly accessed, since they only predict the trends (i.e., how a given micellar parameter scales with a given copolymer parameter). Thus, the scaling models have to be complemented by more detailed mean-field calculations and molecular simulations.

Using the self-consistent mean field theory,[81-83, 88] which takes into account the molecular characteristics of the polymer, the concentration in solution, and the core-corona surface tension, it was shown that the micelle size at equilibrium and the variation of the N_{agg} as a function of the degree of polymerization can be predicted. A representative study dealing with the application of these theories (both scaling and self-consistent mean field) has been given by Förster et al.[87] for polystyrene-*b*-poly(4-vinylpyridine) (PS-*b*-P4VP) system in toluene (selective solvent for the PS block).

B-5. Dynamics of Micellar Systems

The dynamics of block copolymer micelles is a relevant issue in the field of macromolecular self-assembly, especially when such objects are to be used as nanocontainers. It concerns *i*) the unimers exchange processes perpetually taking place between chains molecularly dissolved in the medium and those forming the self-assembly, *ii*) the so-called micelle hybridization process and also *iii*) the dynamics of chains in the micellar core and corona. According to Riess[41] and Gohy[64] in their comparable reviews on these topics, there is still a lack of direct measurements of such physical chemical properties of micellar systems.

B-5-1. Critical micelle concentration

The critical micelle concentration (CMC) is defined as the copolymer concentration below which only molecularly dissolved chains exist but above which both micelles and single chains (unimers) are present simultaneously. However, even if a micelle system is below its CMC (C_p < CMC), it may still be kinetically stable and survive at least for some period or time, if *i*) the core is large, *ii*) the core material is below the T_g (i.e., in a glassy state) or crystalline, and *iii*) the $\chi_{PolymerCore\text{-}Solvent}$ parameter associated with the interaction between the hydrophobic core-forming block and the external selective solvent is high.

In drug delivery, it is very important to know the critical micelle concentration of a particular copolymer micellar system as far as the latter is subjected to 'sink conditions' or severe dilution upon intravenous injection. For example, considering an average individual with total blood volume of approximately 5 L, the concentration of copolymer in the blood would be ca. 0.2 g/L following the intravenous injection of 100 mL (i.e. 0.3 mL/kg.min for 5 min.) of a 10.0 mg/mL micelle solution. Fortunately, most of the block copolymer systems present a CMC well-above this value, with same exceptions.[40]

B-5-2. Unimers exchange and micelle hybridization

For $C_p \geq$ CMC, chains molecularly dissolved in the medium and those forming the micelle interchange at a constant rate (k_{ex}). The k_{ex} is dictated almost exclusively by the molecular characteristics of the polymers, in particular by the $\chi_{PolymerCore\text{-}Solvent}$ Flory-Huggins parameter. In contrast to classical low molecular weight surfactants (e.g., SDS, CTAB), which are known to easily exchange ($k_{ex} \sim 10^6$ and 10^8 s^{-1}),[89] the k_{ex} of block copolymers is substantially lower,

as is the CMC. For example, in aqueous solutions, PEO-*b*-PPO-*b*-PEO micelles have a typical k_{ex} of the order of 10^3 s^{-1}, which is still markedly higher in comparison with micelles having poly[2-(dimethylamino)ethyl methacrylates] (PDMA) ($k_{ex} \sim 10^{-3}$ s^{-1}) as core-forming segment, as reported by Jerome et al.[90] Those authors also found that it is possible to tune the exchange rate in a controlled way; for instance, an extension or branching of the alkyl chain slows down the exchange rate. The same effect is observed when the hydrophobic/hydrophilic balance of these copolymers is increased or when either the hydrophilic or the hydrophobic moiety of diblocks is divided into two external blocks, leading to an ABA triblock copolymer.

In the case of polyisoprene-*b*-poly(methyl methacrylate) (PI-*b*-PMMA) micelles in acetonitrile (PI and PMMA being the core- and corona-forming blocks, respectively) the k_{ex} is immensurable (extremely low), as a result of a very strong segregation of PI ($T_g \sim -12^oC$) chains from the solvent.[91]

Another interesting example is the polystyrene-*b*-poly(sodium methacrylate) (PS-*b*-PMANa) and poly(*t*-butylstyrene)-*b*-poly(sodium methacrylate) (PtBS-*b*-PMANa) micellar systems.[92] In these cases, the kinetics are so slow at room temperature that no exchange could be detected over several hours, while at 60°C the k_{ex}-values could be estimated. In addition to the temperature, the exchange can also be tuned by the addition of either a co-solvent or a co-surfactant. The efficiency of these additives to speed up the exchange process was related to their water solubility and their compatibility with the hydrophobic core of the micelles (plasticizing effect).

The rate limiting step in these processes is the escape of unimers from the micelles. To do so, the hydrophobic block has first to escape from the core, whereupon the unimer has to diffuse out of the outer layer of the micelle to the bulk solution. The reptation of the hydrophobic block is slowed down by increasing the $\chi_{PolymerCore\text{-}Solvent}$ parameter and molecular weight. The probability of recapture of the unimers is proportional to the corona thickness.

The so-called micelle hybridization process corresponds to the same phenomenon as described above, but involving structurally distinct micelles (e.g., mixture of micelles made from different copolymers), thus yielding to the formation of "mixed micelles". This is a rather complex process provided that it is governed by thermodynamic and kinetic parameters, which in turn are very sensitive to the copolymer structures, to their molecular weights and compositions. Evidently, the compatibility between the different copolymers is

one of main parameters along with the mobility of chains, controlling the whole unimers exchange process.

The results reviewed above emphasize that the presence of small amounts of a thermodynamically good solvent in a micellar system can strongly affect the behavior of the aggregates. This is of particular interest especially when block copolymer micelles are prepared by indirect dissolution methods using organic solvents (see *Section B-2-2* above). If they are not completely removed after micellization, they may affect significantly the dynamics of the resulting nano-objects.

To the best of our knowledge, unimer exchange and micelle hybridization processes have not been so far discussed from a drug delivery standpoint. Certainly, this is an important and basic subject in view of the fact that pharmacists usually use "formulations" that often contain more than one type of block copolymer micellar aggregates.

B-5-3. Dynamics of self-assembled copolymer chains

Scattering, fluorescence, and NMR techniques are excellent tools for studying the dynamics and the chain conformation in the micellar core as well as in its corona.[41]

A very interesting study on the mobility of chains inside hairy micelles made from polystyrene-*b*-poly(deuterated styrene)-*b*-polystyrene-*b*-poly(sodium acrylate) (PS_j-*b*-PSd_k-*b*-PS_m-*b*-$PANa_n$) using ^2H NMR measurements in CCl_4 – a solvent in which PANa forms the core, whilst PS_j-*b*-PSd_k-*b*-PS_m forms the corona – was reported by Gao et al.[93] Those authors synthesized a series of 23 samples having a short ^2H-labeled PSd_k block incorporated between PS_j and PS_m segments. The ^2H-labeled segments were strategically placed at different distances from the micelle core by controlling the degree of polymerization of the PS_m block separating the ^2H-labeled PSd_k segments from the $PANa_n$ block. The results clearly indicate that the mobility of the soluble segments near the ionic $PANa_n$ cores is reduced dramatically. At a distance of 25 repeat units (m = 25) from the PS_m-*b*-$PANa_n$ block junctions, the mobility is still significantly lower than that in molecularly dissolved chains, while at a distance of 50 repeat units (m = 50), the mobility is essentially the same as that in the single chains. Another interesting finding in this investigation was that the longer the ionic $PANa_n$ block, the slower the motion in the coronas. Nonetheless, only very short $PANa_n$ blocks were prepared in the mentioned work ($1 \leq n \leq 13$).

C) Block Copolymer Carrier Systems in Aqueous Media

As stated before, micellar nanoparticles have been increasingly and successfully tested as nanosized containers in many fields (drug delivery, cosmetics, fragrances, flavor-masking, pesticides, pollution remediation, colloids stabilization, etc.).[5] Indeed, a strong research activity on this topic has been witnessed in recent years, as represented by the large number of review articles available at the moment.[40, 43, 94-109] Several research teams have developed their own micelle systems made from block copolymers which contain unique combinations of architectures and compositions, thus bringing a great deal of diversity to the field.

The advantages offered by block copolymer micelles in these applications include the facts, among others, that they:

(i) exhibit the ability to incorporate and release active poorly water-soluble, hydrophobic, and/or highly toxic compounds;

(ii) minimize degradation and wastage of compounds, hence increasing availability of the latter.

(iii) can be designed to be either biocompatible and biodegradable;

(iv) are nano-sized (10 – 100 nm in diameter) and have a narrow size distribution;

(v) can be used in specific targeting applications simply by functionalizing their periphery through rather uncomplicated macromolecular engineering.

In the sequence, the foremost structural features of block copolymer micelles will be addressed from an encapsulation point of view.

C-1. The Micelle Corona (Stabilizing Interface)

In an aqueous environment, the micelle corona acts as a stabilizing interface between the hydrophobic core and the external medium. The stabilizing moieties create steric repulsive forces which will compete with the interparticle van der Waals attractive forces. Coagulation does not commonly take place because repulsive forces overwhelm the attractive forces operative between the particles.[43, 94]

Logically, the properties of this outer shell have important implications for various encapsulation related parameters, as summarized in Figure I-12. In this regard, poly(ethylene oxide) (PEO), poly(2-(methacryloyloxy)ethyl phosphorylcholine) (PMPC), and more recently the so-called glycopolymers, have been preferred as corona-forming blocks of assemblies

used in biomedical applications due to their clinically proven exceptional biocompatibility, in spite of the large variety of synthetic polymers easily accessible.[40, 110]

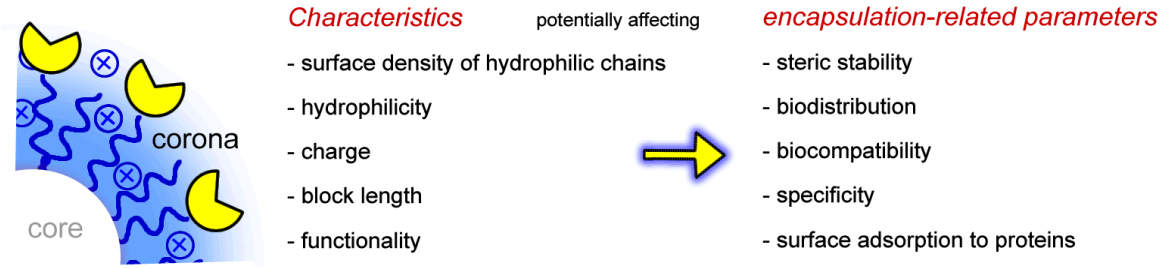

Figure I-12. Micelle corona properties that influence important encapsulation-related parameters.

C-1-1. Poly(ethylene oxide) (PEO)

The vast majority of micellar systems thus far developed and applied as drug delivery nanocarriers have PEO as the corona-forming polymer.[40] Often referred to as PEG (poly(ethylene glycol)), PEO is commercially available in wide range of molecular weights, and is a non-ionic, biocompatible, and water-soluble macromolecule. Studies of the behavior of PEO in aqueous solution have shown that two or three water molecules are typically bound to each EO unit. Its solubility in water is reported to be unlimited at room temperature for all degrees of polymerization.[40, 111]

The PEO coating has been shown to prevent recognition by the macrophages of the reticuloendothelial system (RES).[111] Being "invisible" to the immunological system, micelles (and other particles) with an outer PEO corona can therefore circulate in the human body for a prolonged time ("stealth" effect).[112] The benefits of using such a corona-forming polymer also include the fact that surface adsorption of biological components – proteins can rapidly adsorb to the surface of foreign materials within a few minutes of exposure to the blood – is inhibited.

C-1-2. Poly[2-(methacryloyloxy)ethyl phosphorylcholine] (PMPC)

Over the past few decades, cellular membrane mimicking in relatively simple models has inspired many advances in the biomedical and nanotechnology fields, especially in terms of self-assembly processes involving phospholipid-like molecules.[113] These naturally-occurring

compounds usually comprise double hydrophobic tails and a polar head group, which in many cases contains the phosphorylcholine (PC) motif. On this basis, PC-based macromolecules of clinically-proven biocompatibility have been successfully synthesized either by grafting PC moieties onto a reactive polymer backbone, or by polymerizing PC-containing vinyl monomers such as 2-(methacryloyloxy)ethyl phosphorylcholine (MPC).[110, 114] For example, Winnik and collaborators[115, 116] reported the synthesis of hydrophobically-modified PC-based polybetaines via reductive amination of phosphorylcholine glyceraldehyde by primary amine groups attached to the polymer. On the other hand, Atom Transfer Radical Polymerization (ATRP)[20] has been used by Armes and co-workers[117-120] to copolymerize MPC with various stimuli-responsive (pH, temperature, ionic strength) vinyl monomers to give a range of well-defined amphiphilic diblock and triblock copolymers.

PMPC shows extremely high water solubility and high biocompatibility. Particles and surfaces coated with PMPC also exhibited reduce protein adsorption.[121] On the other hand, this polymer has a major drawback from the encapsulation point of view, because it is insoluble in most of the organic solvents, thus severely restricting the possibilities of manipulating PMPC-containing systems.

C-1-3. Glycopolymers

Within the same context as described above (i.e., mimicking the nature in simple manners), a relatively recent class of polymers containing pendant sugar groups (the so-called glycopolymers or carbohydrate polymers) has attracted considerable attention over the last two decades. Recent developments in polymerization techniques, as reviewed by Haddleton et al.,[122] have prompted the synthesis of glycopolymers featuring a wide range of controlled architectures and functionalities. The high biocompatibility as well as the excellent solubility in water of glycopolymers makes them ideal candidates for the synthesis and preparation of novel nature-inspired sugar-based hybrid materials, such as nonionic polymeric nanoparticles and surfactants, surface modifiers and hydrogels.

Upon the combination to another hydrophobic segment, the resulting amphiphilic carbohydrate-carrying block copolymers can originate micellar aggregates with carbohydrate-based coronas. These original objects show not only distinct properties as such, but also distinguished ability to participate in very specific molecular recognition processes within

human body. At this moment, however, only few works have addressed the preparation of micellar systems having glycopolymers as corona-forming segments.[123-125] The reason for such an observation most probably relies on the fact that convenient, undemanding experimental procedures for the synthesis of sugar-carrying monomers have been only recently developed.[26, 122, 123, 126]

C-2. The Micelle Core (Cargo Space)

The micelle core is formed by hydrophobic polymer chains that segregated from the aqueous external medium to avoid unfavorable interactions with the latter. As a hydrophobic micro-environment, the micelle core serves as the cargo space for various small molecules having comparable solubility properties. This cargo space is, however, limited. For example, if one considers the density of water and copolymers to be equal to 1.0 g/mL, a 1.0 mL of a 10 mg/mL $PMPC_{30}$-*b*-$PDPA_{60}$ (ϕ_{DPA} = 0.59)[54] solution would have a cargo volume of ~ 5.9 µL (0.59 % of the total solution volume). Consequently, one has to develop clever strategies in order to exploit maximally such a minimal loading space available. As stated previously, considerable efforts have focused on the enhancement of micellar payload capacity, which is influenced by a number of parameters as illustrated in Figure I-13.

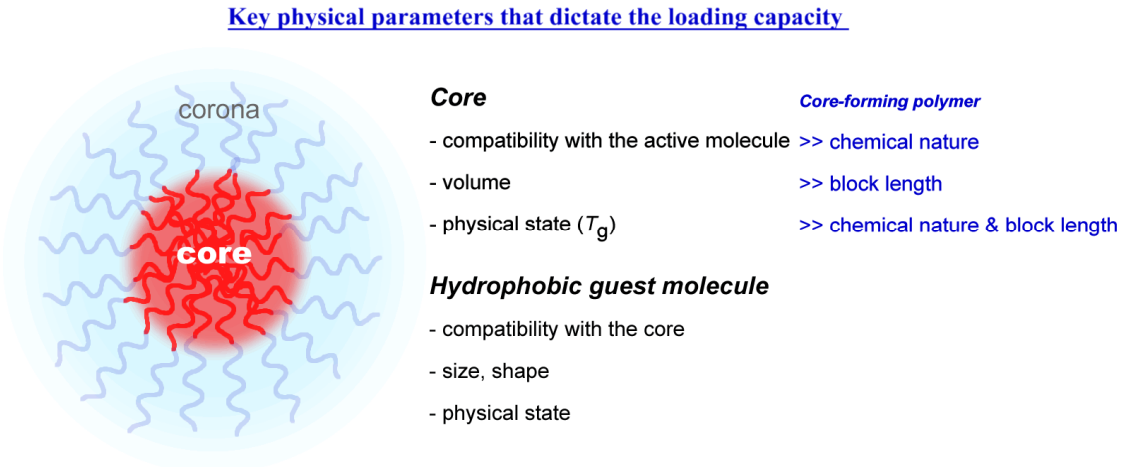

Figure I-13. Micelle core and probe (any hydrophobic guest molecules such as cosmetics, drugs and fragrances) properties dictating the ultimate loading capacity of micellar nanocontainers.

The current understanding of encapsulation of hydrophobic guest molecules by copolymer micelles clearly demonstrates that the compatibility between the probe and the core-forming block is the physical chemical parameter having the most profound influence on these

systems. Fortunately, given that the inner core is presumably surrounded by a biocompatible shell, the selection of core-forming blocks comprises much wider variety of polymers (as compared to the possibilities of corona-forming polymers), thus allowing fine tuning of micelle properties in order to reach acceptable loading contents.

The block copolymer composition and molecular weight as well as architecture (flexibility, rigidity, linear, cyclic, miktoarms, stars, etc), physical state of the core, nature, concentration, size and shape of the probe, and preparation method also affect the loading capacity.

C-2-1. Micelle core – probe compatibility

Ideally, to achieve high loading into micelles, the solubility parameters of the solubilizate (probe) and the core-forming polymer block should be the same. Therefore, they must be perfectly compatible or "invisible" to each other. The degree of compatibility can be estimated from the respective Scatchard-Hildebrand solubility parameters (δ_s and δ_p, accounting for the solubilizate and polymer, respectively) using the Flory-Huggins interaction parameter (χ_{sp}), which is described by eqn. I-6 where V_s is the solubilizate molar volume, R is the universal gas constant and T is the temperature.[127, 128]

$$\chi_{sp} = (\delta_s - \delta_p)^2 \frac{V_s}{RT} \qquad \text{(I-6)}$$

The lower the positive value of χ_{sp}, the greater the compatibility between the probe and the core-forming block. In the case that $\delta_s \approx \delta_p$, the probe can be regarded as a good solvent for the polymer. Therefore, the more closely χ_{sp} approaches zero, the greater will be the extent of encapsulation. If specific interactions are present, the value of χ_{sp} may even be negative.[127, 129]

In practice, however, such an interpretation of loading capacity based on χ_{sp}-values seems to be limited to model compounds (benzene, toluene, chlorobenzene and *p*-xylene) and block copolymer systems (PEO-*b*-PPO-*b*-PEO, PVP-*b*-PS).[127, 128] The most probable reason for this might rely on the uniqueness of each hydrophobic guest molecules – block copolymer combination. Also, these thermodynamic data might not have been determined for novel systems that effectively exhibited good loading capacities (see below).

It is interesting to note that as far as each hydrophobic guest molecule is unique, this suggests that none core-forming block will enable maximum loading levels to be achieved for

all hydrophobic molecules. For this reason, it is unlikely that a given micelle system will serve as a universal delivery vehicle for all probes or drugs.

Recently, the simultaneous encapsulation of two different molecules within the core of a micellar nanoparticle has been made possible through the development of multicompartment micelles.[130] Such objects are characterized by a hydrophilic corona (as for regular micelles) and a hydrophobic core, which exhibits segregated subdomains of incompatible polymers. The so-called "hamburger micelles" (Figure I-14) is typical example of this type of structure.[131] ABC miktoarm star terpolymers with two hydrophobic and incompatible segments are apparently the most suitable candidates for these purposes.

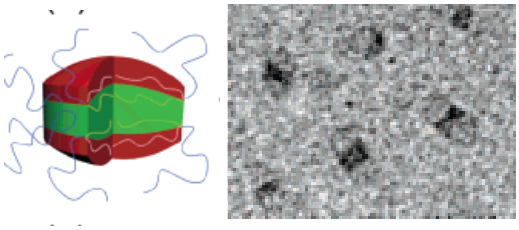

Figure I-14. Illustration showing structural details for the so-called "hamburger micelles", and the corresponding Cryo-TEM image.[131]

In the next section, we describe the state-of-the of the encapsulation of hydrophobic active molecules by copolymer micelles.

C-3. Loading of Guest Molecules

The loading efficiency and the loading content were calculated using the following equations I-7 and I-8, respectively.

$$\text{Loading Efficiency (LE) (\%)} = \frac{\text{mass of probe in micelles (g)}}{\text{mass of probe used (g)}} \text{x } 100 \qquad \text{(I-7)}$$

$$\text{Loading Content (\% w/w}_p\text{)} = \frac{\text{mass of probe in micelles (g)}}{\text{mass of micelles (g)}} \text{x } 100 \qquad \text{(I-8)}$$

As contemplated before, the ability to encapsulate hydrophobic active compounds is an intrinsic feature of block copolymer micelles, finding application in various industrial segments. As an example, Figure I-15 shows digital photographs of 20 % w/w_p chromophore-loaded 2.0 mg/mL copolymer micelles in aqueous media taken before (left) and after (right) exposure to sunlight (UV radiation) – unpublished results obtained in this work –. The red chromophore (hydrophobic and insoluble in water) is physically encapsulated inside the

micellar core. The color of this solution can be accurately tuned (red, green, dark yellow, blue and violet) via rather simple chemistry on the chromophore side-groups. Then, by mixing these compounds, other colors can be obtained. These systems find application in the cosmetic industry. Users could have make-up with changing, personalized, daylight-dependent intensity colors upon exposure to outdoor environment.

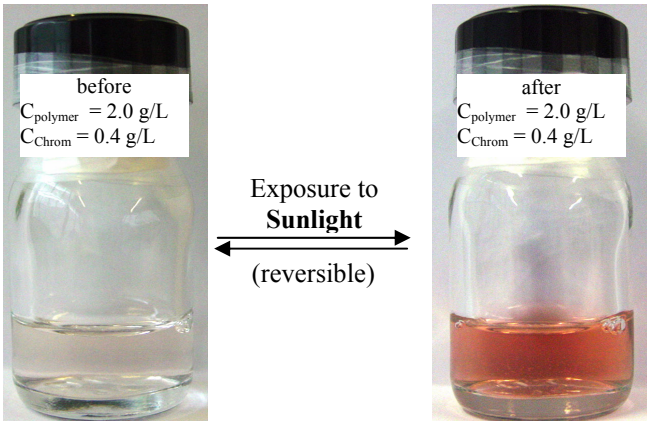

Figure I-15. Digital photographs of chromophore-loaded copolymer micelles in aqueous media taken before (left) and after (right) exposure to sunlight (UV radiation).

Independently of the field of application, the golden rule to achieve acceptable payloads (> 5 % w/w_p) into the cargo space is that the building-blocks of a polymeric nanocarriers should be solubilized along with the probe at some point of the preparation. This also includes systems exhibiting stimulus responsiveness. In fact, the latter presents great potential for controlled release (see *Section C-4*).

In the sequence, we review the representative contributions to this field, with emphasis to biomedical applications (micelle mediated drug delivery).

C-3-1. Representative micellar systems

Table I-2 summarize the literature data regarding some block copolymer micelles loaded with various hydrophobic guest molecules.

Table I-2. Literature data for block copolymer micelles loaded with hydrophobic molecules.[a]

	Hydrophobic Guest Molecule	Block Copolymer[ref]	Payload (% w/w_p)	Remarks concerning the cited study
1	17β-estradiol	PEO-*b*-PCL[132]	190.0	Biocompatible; high partition coefficient.
2	Adryamicin	PEO-*b*-P(AspA-co-AspAADR)	10.2-17.8	Conjugate; linked fraction is not active.
3	Cyclosporin	DEX-*g*-PEO-C_{16}[104]	0.6-17.5	Saccharide-based corona
4		PEO-*b*-PCL[133]	9.9-12.7	Biocompatible
5	Dihydrotestosterone	PEO-*b*-PCL[134]	130.0	Biocompatible; high partition coefficient.
6	Doxorubicin	PEO-*b*-PBLA[135, 136]	5.0-20.0	Biocompatible
7		PEO-*b*-PAGE[137]	3.0	pH-sensitive
8		PEO-*b*-PCL[138]	3.1-4.3	Biocompatible
9		PEO-*b*-PLA[139]	17.0	Biodegradation was accessed
10		PEO-*b*-PLA[140]	2.7	Surface-functionalized micelle
11		PEO-*b*-P(NIPAN-*co*-AlKMA)[141]	< 3.0	pH- and T-sensitive
12		PEO-*b*-P(Asp-*co*-DOXAsp))[142]	8.0	Conjugate; linked fraction is not active; clinical trial
13		PMPC-*b*-PDPA	16.0	Vesicles; pH-sensitive; PC-based shell
14	Ibuprofen	PEO-*b*-PDPA	> 100.0	This work
15		PG2MA-*b*-PDPA	> 100.0	This work
16	Indomethacin	PEO-*b*-PBLA[143]	20.0-22.0	Biocompatible
17		PEO-*b*-PCL[144, 145]	17.0-42.0	Biocompatible
18		PEO-*b*-PGMA	6.0-7.0	This work
19		PEO-*b*-PLA[146, 147]	8.0-9.0	Biocompatible
20		PEO-*b*-PAlkMA[148]	6.0-14.0	pH-sensitive
21		PEO-*b*-P(G2MA-IND)[149]	28.0-58.0	This work; conjugate
22		PEO-*b*-PDPA	> 100.0	This work
23		PG2MA-*b*-PDPA	> 100.0	This work
24	Paclitaxel	PEO-*b*-PCL[150]	0.2-5.1	Core cross-linked micelles
25		P(NIPAN-*co*-DMA)-*b*-P(LA-*co*-GL)[151]	12.0	Temperature-sensitive
26		P(LGG-PTX)-*b*-PEO-*b*-P(LGG-PTX)[152]	16.5	Conjugate
27		PEO-*b*-PVBODENA[153]	18.4-37.4	Hydrotropic acrylate-based micelle core; low citotoxity
28		PEO-*b*-PLA[153]	24.0	-
29		PEtOz-*b*-PCL[154]	0.5-7.6	-
30	Papaverine	PEO-*b*-P(LA-*co*-BMD)[155]	4.0-18.0	-

a) the reader is refereed to the List of Abbreviations for full nomenclature of copolymers.

Through a careful analysis of the data in Table I-2, it is possible to verify that many polymeric micelles have shown only limited loading capacity, regardless of the hydrophobic guest molecule. Remarkable examples of optimal drug delivery performance are the 17*β*-estradiol/PEO-*b*-PCL dihydrotestosterone/PEO-*b*-PCL systems, for which loadings as high as 190 % w/w_p[132] (Table I-2, entry 1) and 130 % w/w_p,[134] (Table I-2, entry 5) respectively, were determined. The respective authors observed that 17*β*-estradiol and dihydrotestosterone molecules exhibit a strong partition coefficient between the micelle core and the aqueous exterior, implying an excellent compatibility with the PCL.

Conversely, if we consider all the other probes used for studying micelle formation, the referenced data demonstrate that micellar loading capacities remain well below 50 % w/w_p.

In the case of paclitaxel (PTX), which is a potent drug whose application in cancer therapy has been limited by its extremely low water solubility, the most satisfactory results (Table I-2, entry 27) were lately reported by Park et al.,[153] who developed the concept of hydrotropic polymeric micelles. Hydrotropic agents are additives that help solubilization of hydrophobic molecules in aqueous media. Based on experimental evidences that *N*,*N*-diethylnicotinamide (DENA) and *N*-picolylnicotinamide (PNA) were excellent hydrotropes for solubilizing PTX, those authors synthesized an original block copolymer system in which the core-forming block contained a given amount of covalently bound hydrotropic agent. As one can see, the micellar loading capacity was effectively improved as compared to other ordinary systems.

The results summarized in Table I-2 clearly demonstrate the importance of developing novel systems in which the active molecule "matches" the micellar core in terms of compatibility, in order to achieve maximal loading into the micelles. Further advances toward general approaches to prepare high loading capacity micellar nanocarriers with widened applications are therefore highly desired.

C-3-2. Micellar systems on (pre-)clinical trial development

In these days, one observes a high activity in the field of micellar encapsulation, and much investigation has been justified by such possibility. In stark contrast, only a few micellar systems have reached (pre-)clinical trial development. One of them is for DOX

delivery (Table I-2, entry 12), and has been coded as NK911. As reported by Nakanishi et al.,[142] DOX was physically entrapped inside spherical micellar aggregates having poly(aspartic acid-*stat*-doxorubicin aspartate) (P(Asp-*stat*-DOXAsp)) cores. The loading capacity (ca. 8% w/w_p) and stability of such micellar systems was attributed to favorable P(Asp-*stat*-DOXAsp)-DOX interactions. Those authors noted, however, that the conjugated DOX fraction does not show biological activity with respect to cancer treatment.[142, 156]

Another recent example is the micelle-encapsulated PTX, which has been coded as NK105. In the latter case, micelles are made from PEO-*b*-P(Asp) modified with 4-phenyl-1-butanolate.[157, 158]

C-4. Release Mechanisms

The probe release from micellar nanocarriers systems can take place via two principal mechanisms, which are diffusional (for nearly all systems under stable conditions; Figure I-16, left) or triggered (for stimulus-responsive systems only; Figure I-16, right) release.

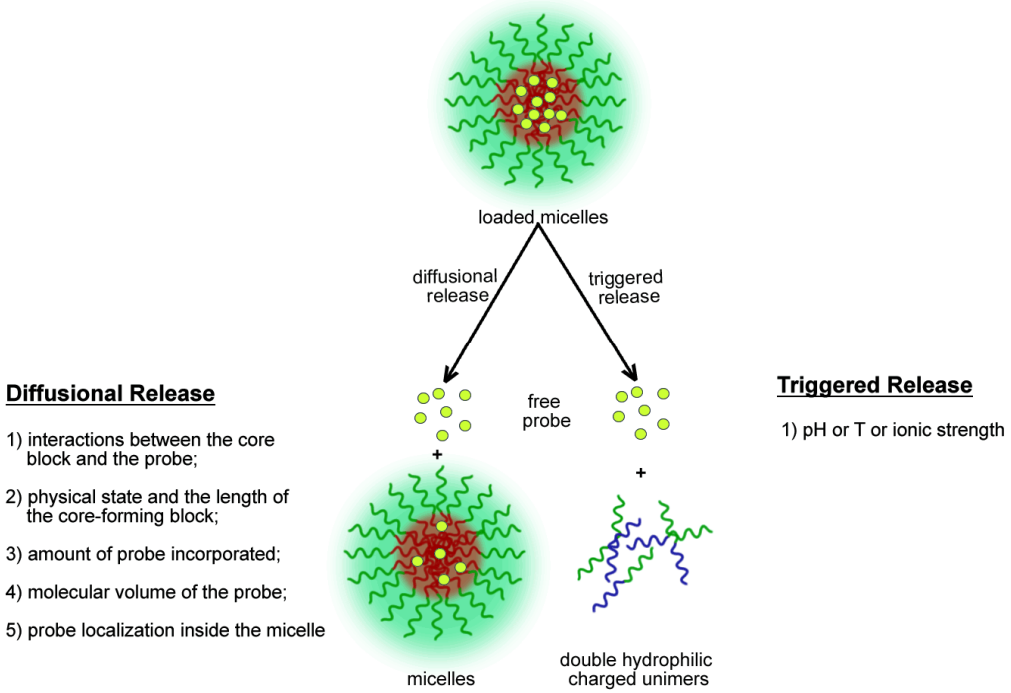

Figure I-16. Triggered *vs.* diffusion-controlled probe release mechanisms.

C-4-1. Diffusion-controlled release

Several factors affect the diffusion-controlled release of a given probe payload encapsulated inside a block copolymer micelle. Assuming that the rate of biodegradation is

slow and that the micelle is stable, then under sink (very dilute) conditions, the probe release is influenced by *i*) the physical state and the length of the core-forming block, *ii*) the amount of probe incorporated, *iii*) the molecular volume of the probe and its localization within the micelle (i.e., in the core, at the interface of the core and the corona, or in the corona itself), and most importantly, *iv*) interactions between the core-forming block and the probe (χ parameter and partition coefficient). If the interaction between the probe and polymer is strong and the rate of biodegradation is fast, then this governs the rate of release.[40] Similarly, for systems in which the probe is covalently bound to the polymer backbone, the release might be governed by the rate of hydrolysis of the linker.

Usually, diffusion-controlled release processes can be identified by applying the Higuchi model[159] to the release data. This model is defined by eqn. I-9 where Q is the amount of drug released per unit area of micelles, C_0 is the initial drug concentration per volume of core-forming block (expressed in mol/cm^3), and t is the release time (expressed in seconds). A detailed description of its use was given recently.[132]

$$Q = 2C_0\left(\frac{Dt}{\pi}\right)^{1/2} \qquad \text{(I-9)}$$

As one can conclude from eqn. I-9, plots of released content as a function of the square root of time give a straight line if the rate-limiting process is diffusion toward the external medium. The slope of the curve is directly proportional to the diffusion coefficient (D) of the probe, which can be determined straightforwardly when some of the micelle (core radius) and polymer (density and weight fraction of the core-forming block) properties are known. Indeed, the Higuchi model has been successfully used to fit the release of hydrophobic probes from various block copolymer micellar systems.[54, 129, 132, 149]

C-4-2. Triggered release

The triggered release (Figure I-16, right) is based on the sharp system response to changes (stimulus) in a certain parameter (pH, temperature, ionic strength, etc.) of the external environment. In most cases, such stimuli render the copolymer chains double hydrophilic, and therefore perfectly soluble in the medium, whereupon demicellization

(disassembly) takes place and any active compound encapsulated inside the nanoparticle is consequently released to the medium.

As mentioned before, the pH-triggered release is an extremely important mechanism for the treatment of pathological areas, which are in general characterized by local acidosis – the pH within those areas can be as low as 5.0 –. In principle, the easiest way to achieve site-specific pH-triggered drug release into cells is by intravenous injection, assuming that the carriers are stable at physiological pH (pH = 7.2 – 7.4, but release their payload once an acid pathological area is encountered (around pH 5.0-5.5), as illustrated in Figure I-17. The disassembly is not represented in the mentioned picture.

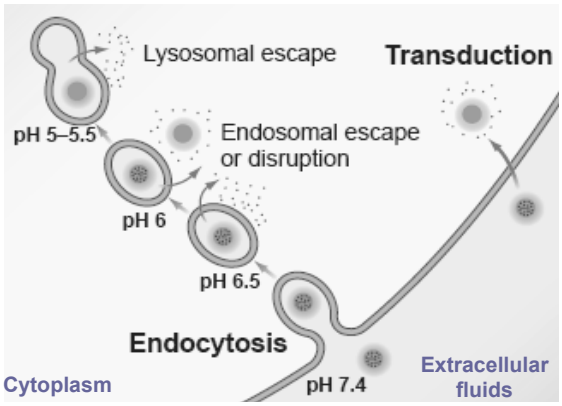

Figure I-17. Micelle-mediated drug delivery into the cell by endocytosis and transduction, as proposed by Hubbell.[160]

One of the major challenges in this regard is the relatively narrow pH range over which the micellar carrier must both retain the drug over prolonged periods and then release it rapidly. This can be tuned, for example, by appropriate selection of the alkyl substituents on the nitrogen atoms in poly[2-(dialkylamino)ethyl methacrylates].[53]

Release processes can also be triggered when changing the solution temperature and exposure to light.[41, 52, 64, 161]

C-5. Guiding Micelles to Specific Sites

The introduction of piloting (targeting) molecules to the surface of micellar nanoparticles is a key step toward further development and precise construction of supramolecular architectures (nano-objects) via bottom-up approaches, given that such functionalization

enables tuning of interactions not only among the particles themselves, but also with the surrounding environment.

Within this context, surface-functionalized micelles have brought a great deal of enthusiasm thanks to the real possibility of selectively targeting specific functional sites.[162] It has been reported that micellar nanoparticles can be conjugated with biotin,[163, 164] folic acid,[165, 166] saccharies,[167, 168] peptides[169] and proteins.[170, 171] These bio-inspired entities show, for instance, specific interactions with antagonist functions (see illustration in Figure I-18) present in the human organism (cell membrane) under given circumstances.

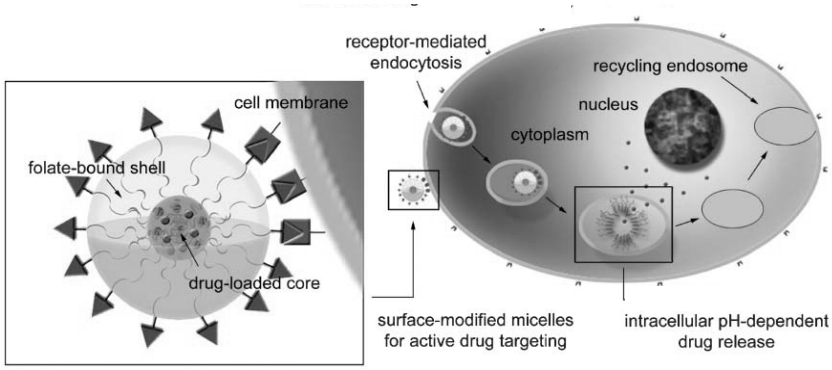

Figure I-18. Principle of targeted micelle-mediated drug delivery. Example using folic acid as piloting molecule, which exhibits high-tumor affinity due to the overexpression of its receptors.[166]

An original methodology to build protein-decorated polymeric micellar nanoparticles that are capable of participating in molecular recognition processes, while having a cargo space for hydrophobic molecules, has been developed at the LCPO (Borsali's group) and at the IECE (Brisson's group) within the frame work of V. Schmidt's thesis.[170, 171]

C-6. Control of Micelle Behavior at Core and Corona Levels

The solution behavior of block copolymer self-organized structures (micelles, vesicles, cylinders, etc) can be controlled using a range of chemistries within the assembly to afford robust functional nanoparticles. The formation of cross-links throughout the core or shell of polymeric micelles confers stability to the nanostructured assemblies, by providing reinforcement to the interactions that facilitate micelle existence. Core cross-linked (CCL) or shell cross-linked (SCL) nanoparticles can, as a result, be manipulated and used in demanding

applications where extreme pHs, high temperatures, concentrations or dilutions, presence of additives, etc., are often required.[52, 172]

Several groups have focused on the development/stabilization of micellar morphologies originated from the self-assembly of amphiphilic macromolecules in selective solvents. The principal breakthroughs achieved so far in this area have been reviewed recently by Lecommandoux,[52] Armes[173] and Wooley.[172] Certainly, the distinguished contributions have come from Wooley's group,[172, 174-180] who was the pioneer to report on the preparation of SCL micelles back in 1996.[180] In that seminal work, polystyrene-*b*-poly(4-vinylpyridine) (PS-*b*-P4VP) diblocks were used as precursors. The P4VP segment was quaternized with *p*-(chloromethyl)styrene, and served as corona-forming block, while the hydrophobic PS chains formed the micellar core. After micellization, the cross-linking reaction of the styrenyl side chain groups in the quaternized P4VP block (micellar corona) was initiated by the photodegradation of 4,4'-azobis(4-cyanovaleric acid), a water-soluble radical initiator (Figure I-19).

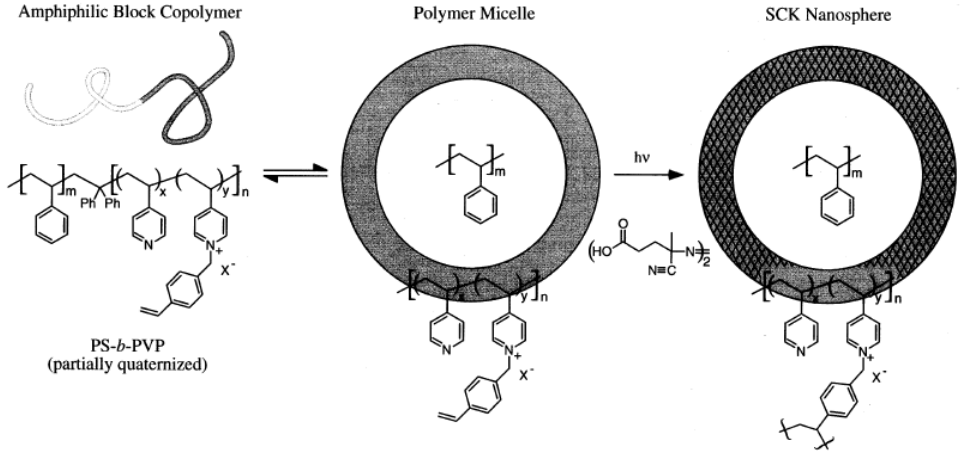

Figure I-19. First shell cross-liking approach reported in the literature by Wooley et al.[180]

Still in the forefront of stabilization and functionalization approaches to make block copolymer micelles in selective solvents a never-ending source of original smart materials, the same research team has succeeded to combine core and shell cross-liking techniques with click chemistry.[174, 181] Click reactions have been extensively developed and applied for the preparation of a multitude of novel functional particulate systems mainly during the last 5 years, thanks to its characteristics such as reliability and high yielding, easy to perform, invariant to the presence of air or moisture, and tolerant of a wide range of functional groups.

An example of their approach is illustrated in Figure I-20, which shows the preparation of permanently stable block copolymer micelles having fluorescent tags attached to their cross-linked shell for application in imaging and detection assays.

The macromolecular architecture is a decisive parameter in the preparation of SCL micelles.[173] Whenever inter-micelle fusion is to be avoided during the cross-liking, the use of ABC triblock copolymers capable of forming three layered (onion-like) core(A)-shell(B)-corona(C) micelles is advantageous when B is the cross-linkable interface. In such a case, the covalent bond formation between different polymeric chains will occur inside each aggregate, and the micro-environment of the reaction will be isolated/protected from the exterior. Thus micelle-micelle collisions will not lead to inter-micelle fusion (formation of large, shapeless aggregates and possibly permanent network gels), therefore enabling the cross-linking experiments to be carried out at high solids.[182]

Indeed, the covalent stabilization of ABC triblock copolymer micelles has open new horizons in biomedical applications, namely in terms of encapsulation, transport, and delivery of hydrophobic active molecules. The hypothetical nanocontainer shown in Figure I-21 presents clear advantages over regular AB diblock copolymer micelles.

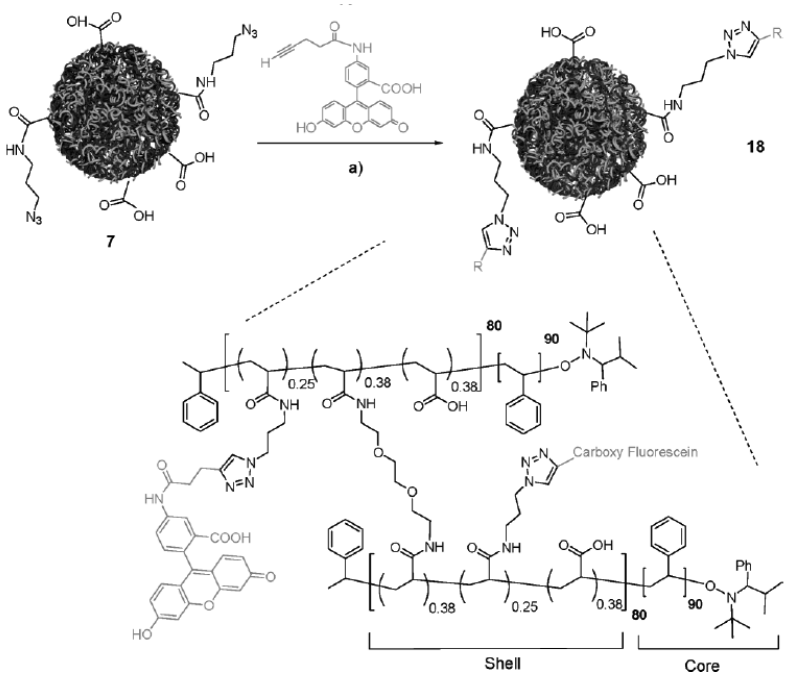

Figure I-20. Functionalization of shell cross-linked micelles using click chemistry.[174, 183]

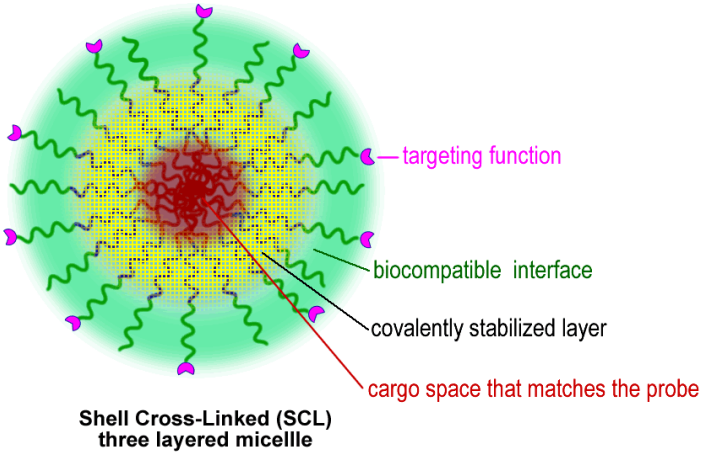

Figure I-21. Important aspects of SCL ABC triblock copolymer micelles when used for encapsulation, transport and delivery of hydrophobic guest molecules.

First, not only the stability of the nanocarriers is guaranteed, but also their biocompatibility if the permanent external layer is a biocompatible polymer such as PEO, PMPC, oligo- and polysaccharides, etc.

Second, the characteristics of the cargo space become easily tunable to match with the probe, via an enlarged range of possibilities regarding the choice of core-forming blocks.

Third, CMC, LCST or HCST and pH_{mic} are typical physical chemical parameters associated with micellar aggregates that no longer have influence or significance in SCL nanoparticles. Accordingly, they are not subjected to *in vivo* disintegration upon dilution (C_p << CMC) that occurs in biological fluids, also favoring the processability in presence of surfactants and oils, for example.[150]

Fourth, the permeability or porosity of the B-C shell-corona interface can be changed by varying the extent covalent bound formation within the latter.[52] The hydrophobicity normally increases with the density of cross-links. Control over the drug/probe release rates becomes then accessible.[184] To date, however, this later feature remains rather unexplored.

Within this idealized framework, an expressive number of ABC triblock copolymer systems able to form core-shell-corona micelles while having a biocompatible segment connected to a cross-linkable one, have been synthesized basically by ATRP using sequential monomer addition techniques.[173, 177] Elegant approaches have been communicated mainly by Armes' group.[182, 184-186]An example of such systems is shown in Figure I-22.[185] In this case, PEO-*b*-PDMA-*b*-PDEA triblock copolymers dissolved molecularly in aqueous solution at low pH; micellization occurred above pH 7.0 to form three-layer micelles with DEA (hydrophobic cargo space) cores, DMA (cross-linkable block) inner shells, and PEO

(biocompatible) coronas. Efficient shell cross-linking was achieved in aqueous solution at room temperature using 1,2-bis(2-iodoethoxy)ethane (BIEE). The SCL micelles exhibit enhanced colloid stabilities at elevated temperatures due to the increased hydrophilicity imparted by the quaternization/cross-linking chemistry. Very importantly, the DEA cores of these SCL micelles had tunable hydrophobicity depending on the solution pH. Reversible swelling was observed on lowering the solution pH from 9 to 2 due to protonation of the DEA chains inside the micellar core.

Curiously, a lack of interest in the stabilization of block copolymer vesicular morphologies is noted,[187, 188] in spite the fact that such hollow nanoparticles are extremely attractive in many fields.[39, 189, 190] The reasons for this are not clear, since the same cross-linking methodologies mentioned above could, in principle, be applied for the covalent stabilization of the vesicle wall.

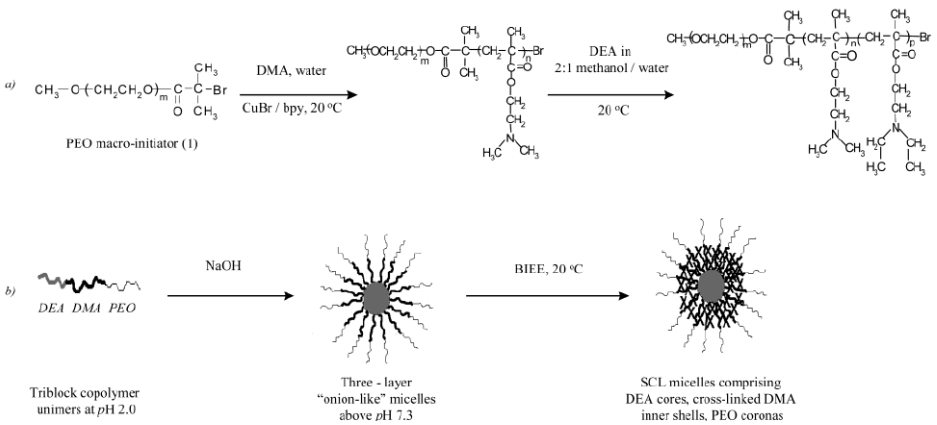

Figure I-22. Formation of three layered shell cross-linked micelles using PEO-*b*-PDMA-*b*-PDEA triblock copolymers prepared by a convenient one-pot ATRP procedure.[185]

A very interesting approach was reported recently by Zhu et al.,[188] who explored at the same time the hydrophobic character and the reactivity of poly(glycidyl methacrylate) (PGMA) chains through the pendant epoxy rings. These three-member heterocyclic functions can be used for nucleophilic attack by various compounds, which will be ultimate grafted to the macromolecule.[191] The authors found that PEO-*b*-PGMA aggregated into vesicles above a given volume fraction of GMA. What was interesting in that approach is the fact that hydrophobic primary amines were added to the organic solution before the micellization, and than they reacted with the epoxy ring to covalently stabilize the vesicles, as depicted in Figure I-23.

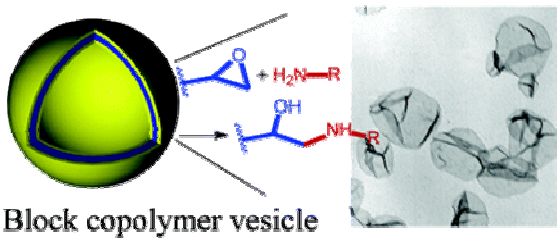

Figure I-23. Vesicle wall cross-linking (WCL) using reactive PEO-*b*-PGMA diblock copolymers.[188]

In summary, control of architecture (macromolecular size, shape and behavior) is achievable through the incorporation of branching sites (cross-links) into polymer within the copolymer assemblies.

As of this moment, it also appears that such permanent, smart and biocompatible nanoparticles are interesting pre-assembled templates (scaffolds) for the subsequent construction of novel hierarchical assemblies either via covalent or non-covalent interactions. One could imagine that such scaffolds already responding to external stimuli can be designed to carry specific functions responding themselves to other complementary stimuli.

The synthesis and molecular characteristics of the amphiphilic block copolymer used in the present study are described in detail in the next chapter.

Chapter II

Synthesis and Molecular Characteristics of Amphiphilic Block Copolymers

Introduction

The synthesis and characterization of the block copolymers used in this work is described in the present chapter. Convenient atom transfer radical polymerization (ATRP) and ring opening polymerization (ROP) procedures were applied to prepare amphiphilic macromolecules showing the ability to form self-assembled structures in water. The molecular weights and compositions were carefully targeted in order to design spherical core-corona micelles. To this, the volume fraction of the hydrophobic block ($\phi_{hydrophobic}$) was purposely chosen to lie in the range $0.30 < \phi_{hydrophobic} < 0.70$. [42, 78]

The choice of monomers was driven, obviously, by the aims established within the framework of this PhD thesis. Most of the efforts were thus focused on the development of the cargo space of nanocontainers. With the (original) discovery of high loading capacity systems among those herein examined, interest was also placed on the strategies to render such objects stable in solution with respect to external environment.

We elected to make use of ATRP technique as the main approach to prepare amphiphilic block copolymers that could fulfill the objectives defined earlier. ATRP not only allows the controlled polymerization of diverse monomers (methacrylates, acrylates, styrenes, etc.) exhibiting rather reactive groups (acids, hydroxyls, amines, epoxy rings, etc.), but also is undemanding with respect, for example, to purity of monomers, solvents and reaction apparatus, when compared to anionic and cationic polymerization. Equally truth for other controlled radical polymerizations (CRP), ATRP is a cost-effective experimental procedure. In view of future work in the area, such a characteristic played a decisive role on its choice as well.

This chapter is divided in two mains parts. Firstly, in *Part A*, the basic aspects and reaction mechanisms underlying a typical ATRP and ROP processes will be presented, before entering *Part B*, in which the synthesis and characterization of initiators and di- and triblock copolymers will be described in details.

A) Polymerization Techniques

A-1 Atom Transfer Radical Polymerization (ATRP)

The concept of using transition metal complexes to mediate radical polymerizations developed out of the so-called metal-catalyzed Kharasch addition or atom transfer radical addition reactions (ATRA), so named because it employs atom transfer from an organic halide to a transition metal complex to generate the reactive radicals. As shown in Scheme II-1, a lower oxidation state metal complexed by suitable ligands ($M_t^{+z}L_n$) abstracts a halogen atom from an alkyl radical ($R^{\bullet}$), which can then add across the double bound of an alkene (R'). The newly formed radical ($RR'^{\bullet}$) reabstracts the halogen atom from the higher oxidation state metal ($M_t^{+(z+1)}L_nX$) to form an alkene-alkyl halide adduct (RR'X) and regenerates the lower oxidation state metal ($M_t^{+z}L_n$).[192, 193 (and references therein)]

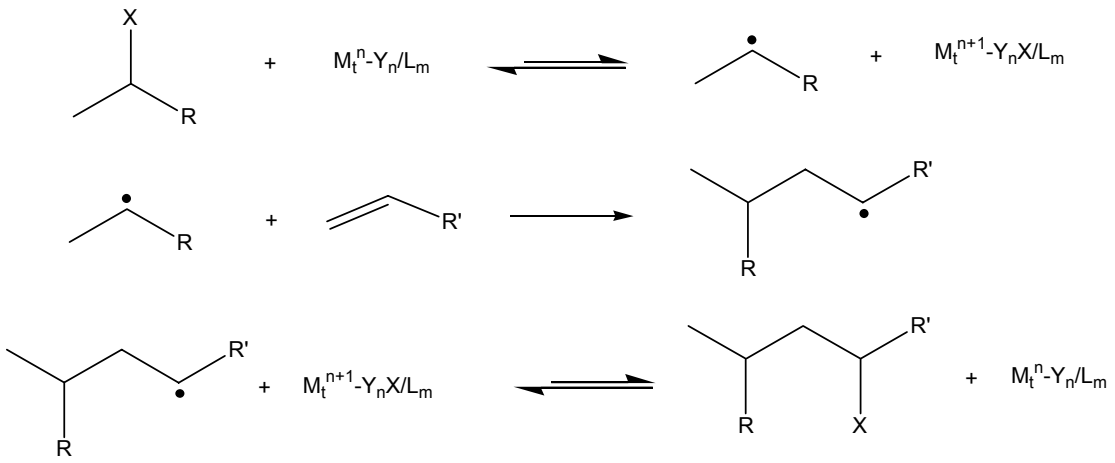

Scheme II-1. General mechanism of ATRA.

In an efficient ATRA, trapping of the product radical should be faster than the subsequent propagation step and reactivation of the adduct should be very slow, maximizing the yield of the targeted product. To promote a polymerization, the newly formed carbon-halogen bond (RR'X) must be capable of being reactivated and the new radical must be able to add another alkene [$R(R')_nX$]. This idea was realized around 1995 almost simultaneously by Matyjaszewski and Sawamoto.[194, 195] The process was called "Atom Transfer Radical Polymerization" (ATRP) to reflect its origins in ATRA[194] and Transition Metal Mediated Living Radical Polymerization (TMMLRP) by Sawamoto.[195] In the first publication, Matyjaszewski et al.[194] reported on the ATRP of styrene at 130 ^{o}C using CuCl/2,2'-bipyridine

as catalytic system. They intentionally use 1-penhylethyl chloride as the initiator to mimic the structure of dormant extremity of the PS chain. The controlled character of this polymerization was supported by the linear dependence of the number average molar mass (M_n) with the monomer conversion. Also, pseudo first-order kinetics indicated that the concentration of the growing radical chains remained constant during the propagation and that termination was not significant, accordingly to a controlled radical polymerization (CRP). The polydispersity was relatively narrow (M_w/M_n = 1.5). The number average molar mass (M_n) of the resulting polymers could be easily controlled by the monomer/initiator ratio. Finally, a good agreement between theoretical M_n ($M_{n,theo}$) and experimental M_n ($M_{n,exp}$) values measured by GPC supported a high initiation efficiency (e.g., $f = M_{n,theo}/M_{n,exp}$ = 0.93. The synthesis of block copolymers was also reported by heating chloride end-capped PS in presence of methyl acrylate (MA) and the copper catalyst, thus yielding PS-*b*-PMA copolymer.

Independently and at the same time, Sawamoto[195] demonstrated that methyl methacrylate (MMA) could be polymerized using a ruthenium catalyst ($RuCl_2(PPh_3)_3$) and CCl_4 as the initiator. In that approach, the addition of an aluminum alkoxide was needed. Although its role is not clear, the authors proposed that it activated the C-Cl bound at the polymer chain end through coordination of the methyl ester group. In absence of this Lewis acid, only the mono-adduct was formed. Linear pseudo first order kinetic plots were obtained, in contrast to the dependence of $M_{n,exp}$ on the monomer conversion, while $M_{n,exp}$ was smaller than $M_{n,theo}$, suggesting that transfer reactions occurred.

Since these early and pioneering works, ATRP became among the most rapid developing areas in chemistry, especially in polymer chemistry.[192] To date, very important developments have been achieved in ATRP processes, which are currently available for "everyone".[196, 197]

Mechanism of ATRP

The principles and mechanism of ATRP have been recently reviewed in detail by Matyjaszewski[192] and Sawamoto.[198] The reader is refereed to the mentioned literature for a deeper discussion on the aspects underlying an ATRP process.

As a multicomponent system, ATRP is composed of a monomer, an initiator with a transferable (pseudo)halogen, and a catalyst (composed of a transition metal species (Mt) with counter ions (Y) a suitable ligand (L)). Sometimes an additive is used. The general ATRP mechanism is illustrated in Scheme II-2. The reaction is usually initiated by the activation

(hemolytic cleavage) of the carbon-halogen bond in an appropriate organic halide (RX) via one-electron oxidation of the metal center ($M_t^nY_n/L_m$) to form an initiating radical species ($R^\bullet$) and an oxidized metal compound ($X\text{-}M_t^{n+1}Y_n/L_m$). The $R^\bullet$ reacts with the halogen atom on the oxidized metal to regenerate RX or adds to the monomer to generate a radical species ($RM^\bullet$). It is sooner or later transformed into the adduct of RX and monomer(s) (RM_pX with $p \geq 1$) via abstraction of a halogen atom from $X\text{-}M_t^{n+1}Y_n/L_m$. The carbon-halogen bond of the adduct is subsequently activated by the metal complex, similarly to RX, to result in a similar carbon-halogen bound at the polymer chain end via a repetitive set of reactions.

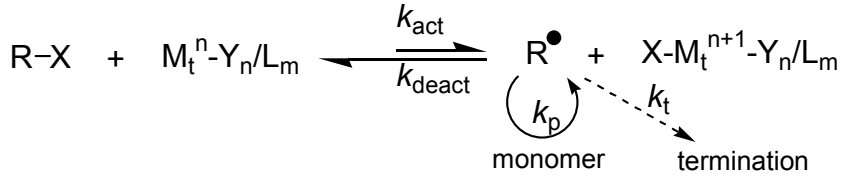

Scheme II-2. General transition-metal-catalyzed ATRP mechanism, as proposed by Matyjaszewski.[192, 193, 199]

The key factors for these reactions[192, 198] are the low concentration of the radical intermediates (~10^{-9} – 10^{-8} mol/L) at a given time and their fast but reversible transformation into the dormant species. Polymer chains grow by the addition of the free radicals to monomers in a manner similar to a conventional radical polymerization. Termination reactions (k_t) also take place in ATRP, principally through radical coupling and disproportionation; however, in a well-controlled ATRP, no more than a few percent of the polymer chains undergo termination. Other side reactions may additionally limit the achievable molar masses. Typically no more than 5% of the total growing chains terminate during the initial, short, non-stationary stage of polymerization. This process generates oxidized metal complexes (deactivators), which behave as persistent radicals to reduce the stationary concentration of growing radicals and thereby minimize the contribution of termination at later stages.

The equilibrium constant ($K_{eq} = k_{act}/k_{deact}$) determines the polymerization rate. ATRP will not occur or occur very slowly if the equilibrium constant is too small. In contrast, large equilibrium constants will lead to a large amount of termination because of a high radical concentration. This will be accompanied by a large amount of deactivating higher oxidation state metal complex, which will shift the equilibrium toward dormant species and may result

in an apparently slower polymerization. Each monomer possesses its own intrinsic radical propagation rate. Thus, for a specific monomer, the concentration of propagating radicals and the rate of radical deactivation need to be adjusted to maintain polymerization control.

So far, a variety of transition metal complexes have been successfully used for ATRP. They include compounds from group VI (Mo), VII (Re), VIII (Ru, Fe), IX (Co, Rh), X (Ni, Pd) and XI (Cu), and are used almost invariably with halides and suitable ligands such as bipyridyls, aryl phosphines, aliphatic amines, able not only to facilitate solubility of the halide salts but also to modify the electronic (redox potential) and steric nature of the complexes. Typical initiators are halogenated alkanes, haloesteres, (haloalkyl)benzenes, sulfonyl halides, etc.

Using ATRP protocols, control of polymerization has been achieved for various monomers including methacrylates, acrylates, styrenes, etc., most of which are radically polymerizable conjugated monomers. This technique has been also proven to be a valuable tool for the synthesis of a variety of polymers with reactive groups (acids, hydroxyls, amines, etc.).[192, 198]

Definitely, ATRP has contributed enormously to the macromolecular domain,[20, 122, 126, 200] allowing the preparation of a multitude of macromolecules with controllable architecture, functionality, composition and topology, as illustrate in Figure II-1.

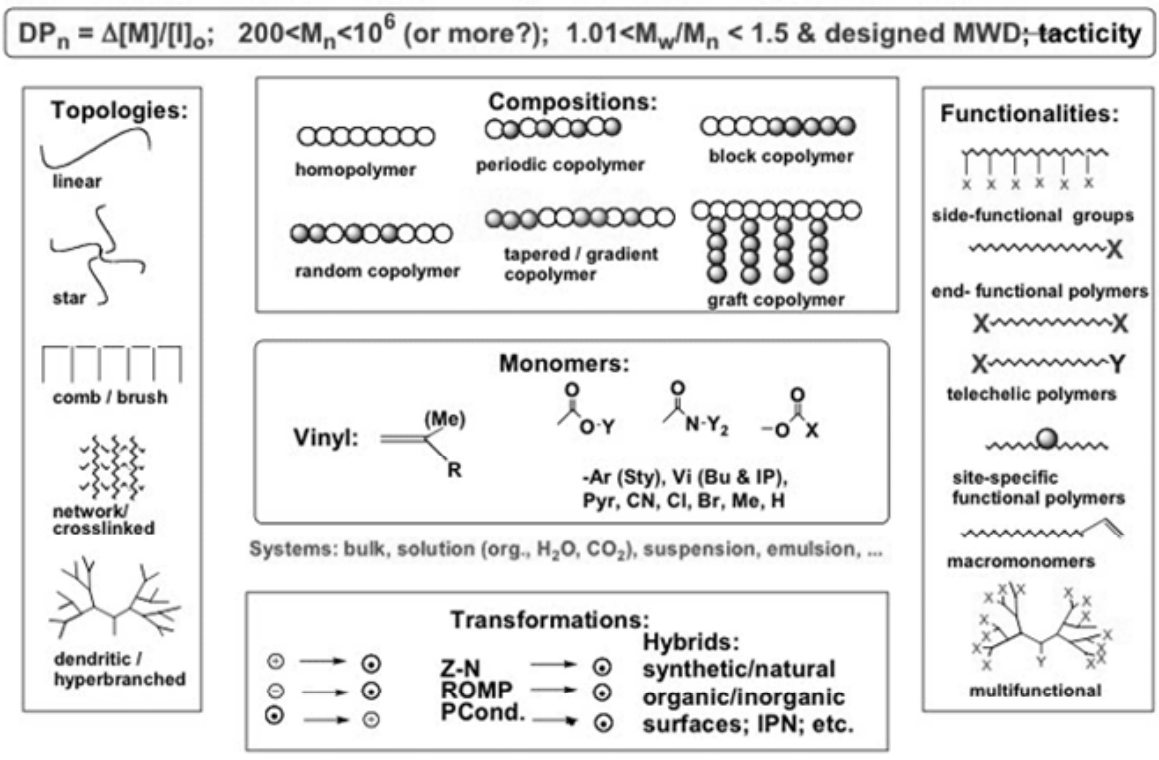

Figure II-1. Illustration of the versatile ATRP toolbox.[201]

A-2 Ring Opening Polymerization (ROP)

The existence of electrophilic carbon atoms in a vast number of heterocyclic rings is a ubiquitous characteristic that has been increasingly explored to prepare and develop novel day-life products. Several technical polymers made by ring opening polymerization (ROP) of such heterocyclic compounds could hardly be replaced by any other synthetic or natural materials in a short term,[202] thus permanently representing a strategic segment of the polymeric materials market.

Depending on the monomers, initiators, catalysts, solvents, etc., several different reaction pathways may take place in ROP polymerizations, which constitute a broad, forefront topic in polymer science.

In the present section, we focus on the ROP of lactones to prepare aliphatic polyesters, which find particular relevance in biomedical applications (controlled drug delivery, artificial skin, prosthetics, vascular grafts, bone screws, dental implants, pins, stents, plates for temporary internal fracture fixation, etc.) owning to their mechanical properties, hydrolyzability and, foremost, biocompatibility.[203-207] One reason for the growing interest in these systems is that their physical and chemical properties can be tuned over a wide range by copolymerization of distinct lactones and precise macromolecular engineering leading to a diversity of homo and block copolymers, stars, brushes, hyperbranched and cross-linked materials.[207]

The ROP of lactones – first explored by Carothers et al.[208] – is generally performed in bulk or in solution (toluene, dioxane, etc.), emulsion or dispersion. Depending on the initiator/catalyst, the polymerization proceeds according to three major reaction mechanisms: carbocationic, anionic and coordination-insertion.[204] A convenient experimental approach to prepare biocompatible amphiphilic block copolymers having a polyester segment (in particular, poly(lactic acid) (PLA) and polycaprolactone (PCL)) is through the use of metal carboxylates along with rather active hydrogen compounds as co-initiators, via coordination-insertion pathway.[207]

The most widely used initiators are organometallic derivatives of Zn, Ti, Ge and, mainly, Al and Sn.[205] The covalent metal alkoxides or carboxylates with vacant "d" orbitals react as coordination initiators in these polymerizations. Among others, tin (II) 2-ethylhexanoate – also kwon as stannous octanoate ($Sn(Oct)_2$) –, which was applied to the synthesis of PEO-*b*-PCL diblocks in this work, is probably the most commonly used catalyst/initiator for ROP of lactones. Special attention is also given to this organometallic compound due to its biological

tolerable effects. Indeed, $Sn(Oct)_2$ has been approved by the Food and Drug Administration (FDA) for its application as food additive.[206] As mentioned earlier, ROP reaction with $Sn(Oct)_2$ is carried out in the presence of active hydrogen compounds (e.g., alcohols – ROH), which are in fact the initiating species. In case that no active hydrogen compound is added, impurities in the medium are believed to initiate the polymerization.[204-207] As reviewed by Albertsson and Varma,[204] the polymerization mechanism in presence of $Sn(Oct)_2$/ROH catalyst/initiator system is rather complex and at least two mechanisms have been proposed. In the activated monomer mechanism (Scheme II-3), it is proposed that the monomer is coordinated with the catalyst and is activated. The ROP then proceeds via a nucleophilic attack of alcohol leading to the insertion of monomer into metal-oxygen bond by rearrangement of the electrons. The alcohol functionality and the monomer are both coordinated to the $Sn(Oct)_2$ complex during propagation. The reaction is terminated by hydrolysis forming a hydroxyl end group.

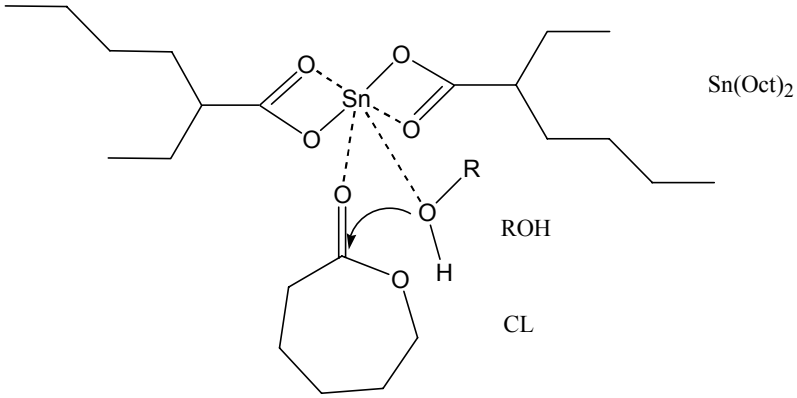

Scheme II-3. Activated monomer mechanism for ROP of lactones.[204]

An alternative mechanism, for which a series of experimental evidences have been also collected, suggests that when $Sn(Oct)_2$ is mixed with an alcohol, an initiating complex is formed prior to polymerization. The establishment of equilibrium between $Sn(Oct)_2$ and alcohol results in the liberation of acid from the catalyst. The tin alkoxide complex (OctSnRO) thus formed initiates the polymerization (Scheme II-4).

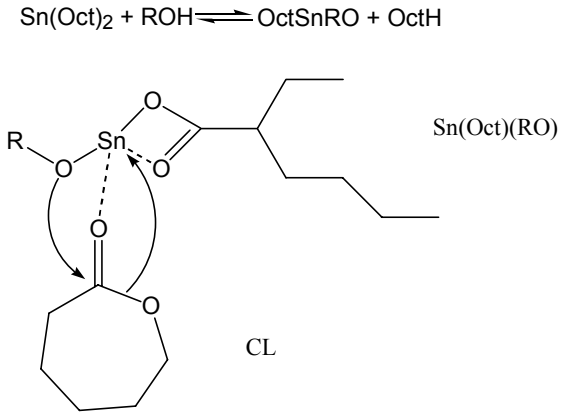

Scheme II-4. Tin alkoxide complex initiating the polymerization of lactones.[204]

Depending mainly on the temperature and the reaction time, inter- and intramolecular (back-biting) transesterification reactions may occur in the polymerization medium during the ROP of lactones in presence of $Sn(Oct)_2$/ROH, leading not only an increase in the polydispersity of the resulting macromolecules, but also changes in the end-chain groups. Fortunately, under optimized conditions, polyesters can be prepared with low molecular weight distributions ($M_w/M_n < 1.40$) and near quantitative hydroxyl end-chain functionality. Thus, the latter can be subsequently transformed to continue the chain growth by other polymerization techniques, such as ATRP.[209, 210]

B) Copolymer Synthesis and Characterization

B-1. Preparation of Initiators

In this study, four types of ATRP macroinitiators based on poly(ethylene oxide) (PEO), and two low molecular weight hydrophilic initiators based on solketal (SK), were employed (Scheme II-5).

Here is described the preparation of α,ω-heterodifunctional PEO ATRP macroinitiators (Scheme II-6). Essentially the same comments also apply, however, for the other cases, and the reader is referred to the *Experimental Part, Section B* for details on syntheses and characterization data of such (macro)molecules.

The interest in α,ω-heterodifunctional macromolecules originates from the possibility of preparing micelles or vesicles with controlled functionality at their periphery. These precisely functionalized structures have attracted increasing attention at the LCPO, and constitute important material for ongoing studies.[170, 171] As shown in Scheme II-6, SK-PEO-OH was

firstly synthesized by AROP of EO in THF using SK-OH as initiator (targeted hydroxyl deprotonation extent by DPMK of 70%).[211] As expected, the reaction proceeded in a controlled way, yielding SK-PEO-OH of targeted molar masses and low polydispersities (M_w/M_n = 1.10). M_n(NMR) determined using the solketal moiety as reference (δ = 1.45 – 1.38 ppm, Figure II-2) showed very good agreement with M_n(GPC) in water with PEO standards. Subsequently, the procedure consisted in the nucleophilic attack by hydroxyl groups on the positively polarized unsaturated carbon atom of α-bromoisobutyryl bromide, in presence of triethylamine. In general, these reactions were performed with a slight excess (1.1 eq.) of α-bromoisobutyryl bromide to ensure complete reaction of hydroxyl moieties, and the excess was removed during the purification procedure. The quantitative coupling efficiency could be determined straightforwardly by ^{1}H NMR spectroscopy on basis, for example, of the ratio between integrals from solketal (δ = 1.35 – 1.28 ppm) and isobutyryl (δ = 1.97 ppm) protons (Figure II-2). Finally, the selective solketal hydrolysis under acid conditions yielded the α-ω-heterodifunctional PEO-based ATRP macroinitiator, thus enabling the preparation of block copolymer micelles with controllable shell functionally.

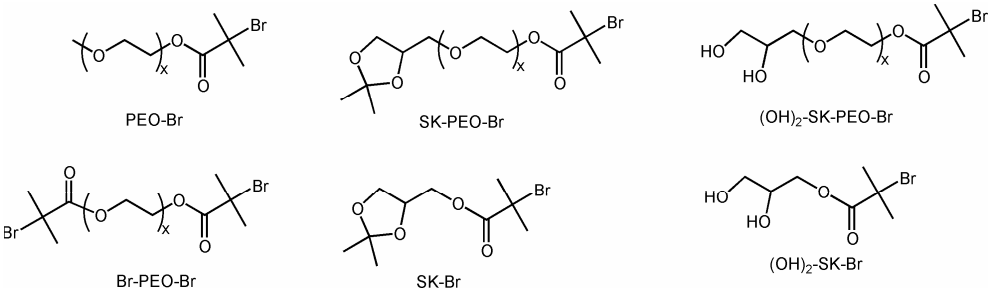

Scheme II-5. Chemical structures of the ATRP initiators used in this work.

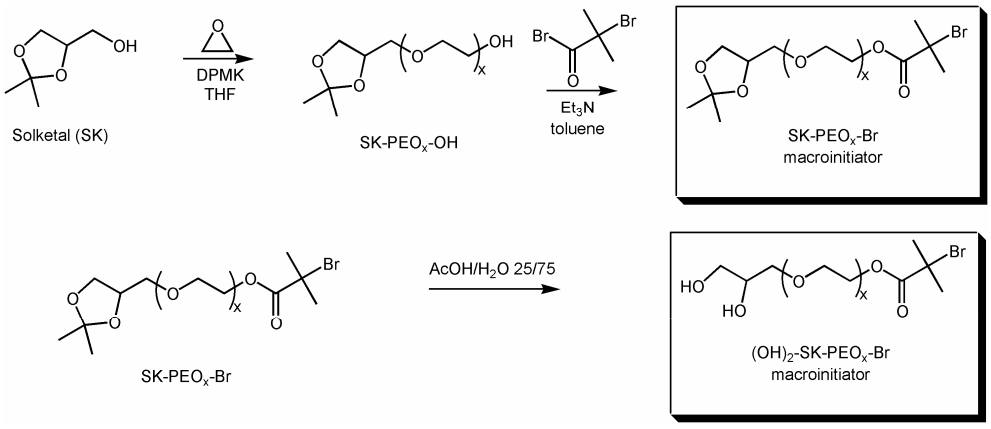

Scheme II-6. Synthesis of α,ω-heterodifunctional PEO-based ATRP macroinitiator.

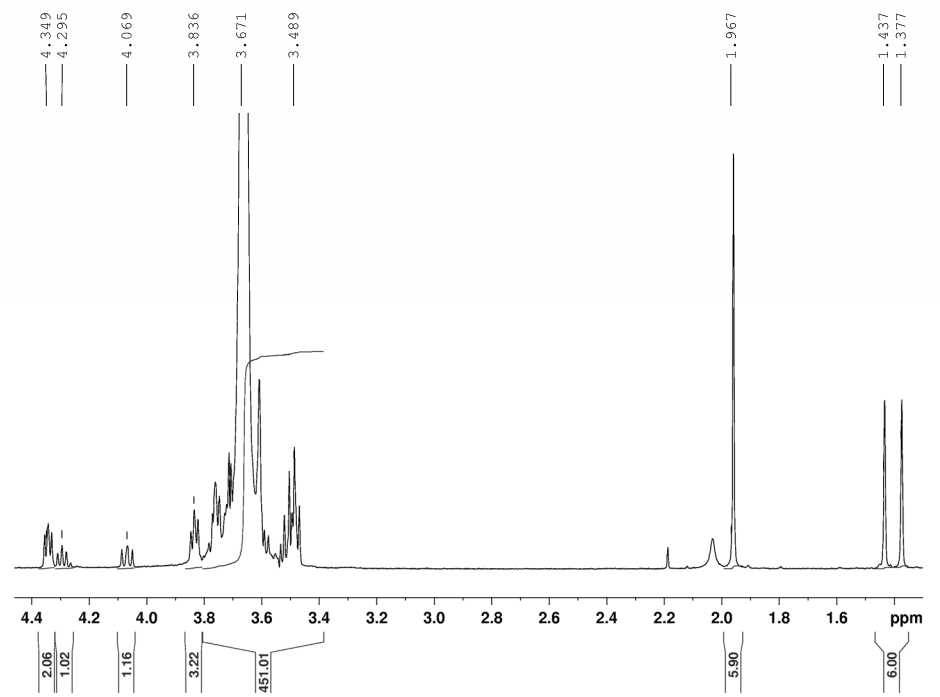

Figure II-2: ^{1}H NMR spectrum of SK-PEO_{95}-Br ATRP macroinitiator in $CDCl_3$.

B-2. Stimulus-Responsive Systems

B-2-1. PMPC-b-PDPA

In the framework of a collaboration with Steven P. Armes (University of Scheffield, UK), the PMPC-*b*-PDPA diblocks herein investigated were prepared by his group, using sequential monomer addition and ATRP techniques (Scheme II-7).[212] The controlled polymerization of MPC monomer was initiated by an oligo(ethylene glycol)-based water-soluble initiator (OEGBr), and carried out in MeOH at 20 ^{o}C in presence of Cu(I)Br/bpy as catalyst. Generally high conversions were achieved under mild conditions in protic media, with reasonably low polydispersities (M_w/M_n < 1.30) and good blocking efficiencies (no traces of PMPC homopolymer). Following, DPA monomer was added to the reaction. The characteristics of the PMPC-*b*-PDPA block copolymers used in this work are summarized in Table II-1.

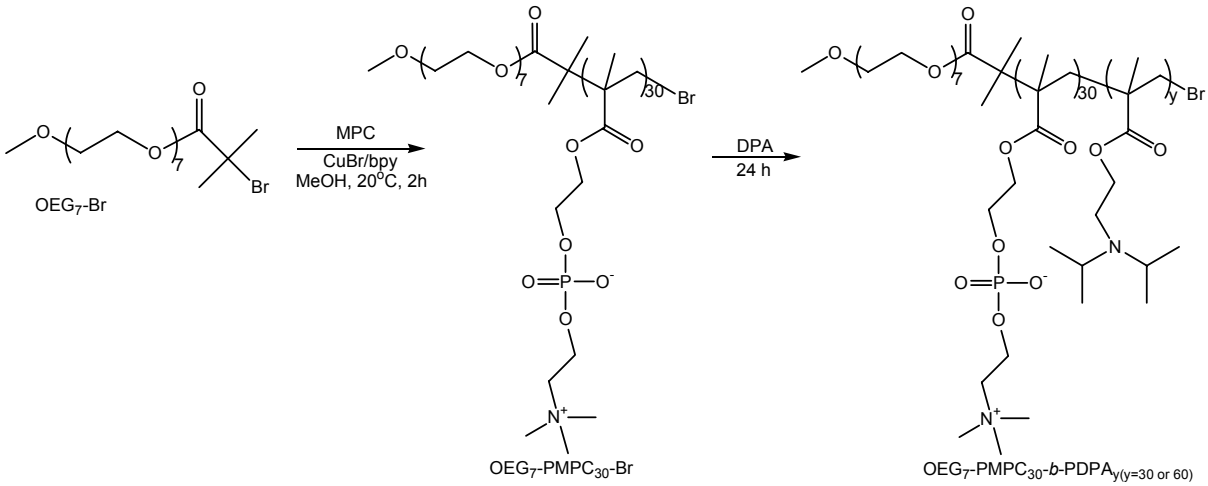

Scheme II-7. Synthesis of amphiphilic PMPC-*b*-PDPA diblock copolymers by ATRP.

Table II-1. Characteristics of PMPC-*b*-PDPA copolymers.

Copolymer $PMPC_x$-*b*-$PDPA_y$	M_n (g/mol)[a]	M_w/M_n[a]	ϕ_{DPA}[b]
30-30	14 000	1.20	0.42
30-60	21 000	1.27	0.59

[a] Extracted from literature data.[212] [b] Volume fraction of DPA segment assuming that the polymer density is equal to 1.0 g/mL.

B-2-2. PEO-b-PDPA

The PEO-*b*-PDPA diblock copolymers studied hereinafter, were synthesized by ATRP of DPA initiated by bromo-terminated poly(ethylene oxide) using CuBr/HMTETA as catalyst in THF (50 % v/v) at 60 °C, and [Initiator]:[Metal]:[Ligand] = 1:1:2 (Scheme II-8). Since data for these exact polymerization conditions were not found in the literature, a kinetic study was undertaken to verify the controlled character of the chain growth. The evolution of conversion *vs.* time and the corresponding semilogarithmic plot are shown together in Figure II-3a. The linearity observed in the semilogarithmic plot indicates that the polymerization is first order with respect to the DPA, and implies that the polymer radical concentration remains constant on the timescale of the reaction. M_n(GPC)-values depended linearly on the conversion (data not shown). Illustrative GPC curves for the PEO_{113}-Br macroinitiator and PEO_{113}-*b*-$PDPA_{74}$ diblock copolymers are shown in Figure II-3b. There is a clear shift to higher molecular weight for diblock compared to the homopolymer, with no apparent contribution from the latter, thus indicating high macroinitiator efficiency. An assigned ^{1}H NMR spectrum for this

system is depicted in Figure II-4, which shows clearly the presence of chemical shifts from both segments, and the absence of unreacted monomer.

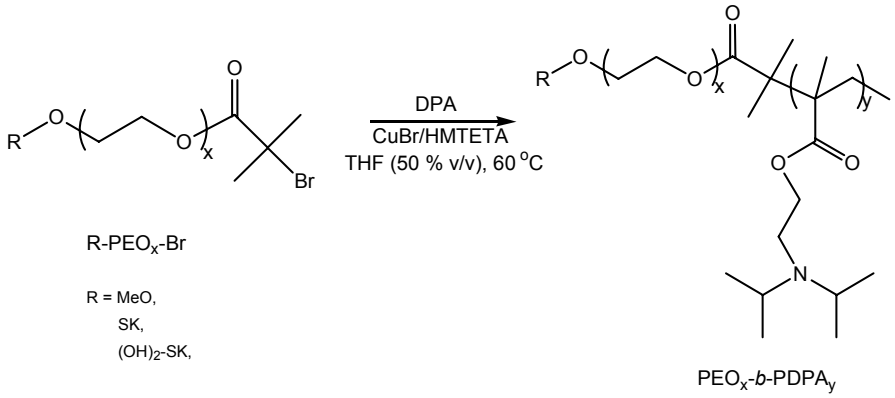

Scheme II-8. Synthesis of amphiphilic PEO-*b*-PDPA block copolymers by ATRP.

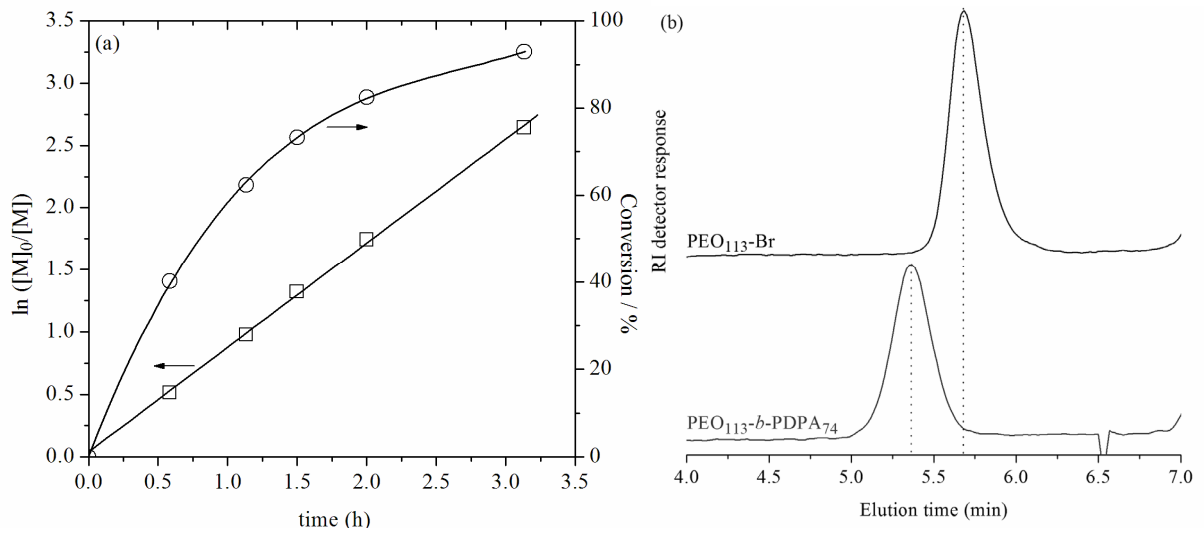

Figure II-3. (a) First order kinetic plot for ATRP of DPA in THF (50% v/v) at 60 °C. Conditions: [DPA]/[PEO_{113}-Br]/[CuBr]/[HMTETA] = 112/1.0/1.0/2.0. (b) GPC traces in THF of PEO_{113}-Br and PEO_{113}-*b*-$PDPA_{74}$ diblock copolymer.

On adjusting the stoichiometry of these polymerizations ([monomer]/[initiator] ratio), a set of well-defined PEO-*b*-PDPA diblocks ($M_w/M_n \leq 1.28$) having different compositions (volume fractions of the hydrophobic segment; $0.34 \leq \phi_{PDPA} \leq 0.93$), and molar masses, were thus obtained. These results are listed in Table II-2.

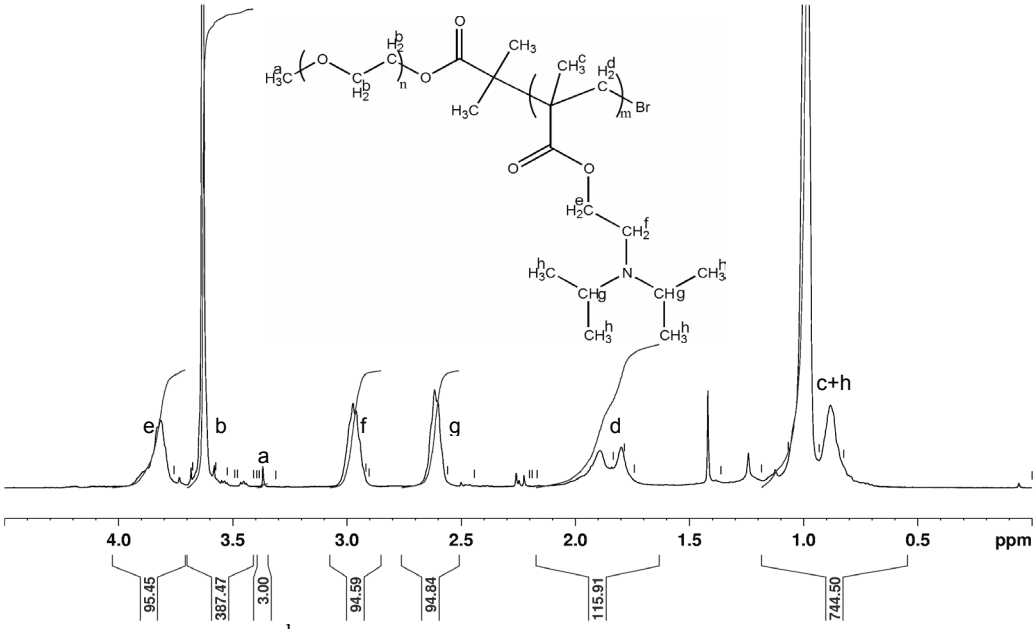

Figure II-4. Assigned ^{1}H NMR spectrum for PEO-*b*-PDPA copolymer in $CDCl_3$.

Table II-2. Molecular characteristics of PEO-*b*-PDPA diblock copolymers.

Copolymer PEO_x-*b*-$PDPA_y$	time (h)	Convn.[a] (%)	M_n(target)[b] g/mol	M_n(NMR)[c] g/mol	M_n(GPC)[d] g/mol	M_w/M_n[d]	ϕ_{PDPA}[f]
45-25	1.5	97	9 000	7 500	9 600	1.28	0.72
45-47	2.0	98	13 100	12 000	14 300	1.20	0.83
45-85	4.0	ND[e]	21 000	20 100	19 600	1.16	0.90
45-120	5.3	98	28 000	27 600	25 100	1.17	0.93
113-12	1.0	93	8 000	7 600	9 800	1.18	0.34
113-28	1.3	ND[e]	10 300	11 000	12 000	1.16	0.54
113-50	3.0	95	15 000	15 700	15 300	1.15	0.68
113-74	4.3	93	23 100	20 800	19 500	1.13	0.76
16-106-16	1.5	95	10 600	11 800	18 100	1.21	0.58
25-106-25	1.5	91	15 600	15 300	20 400	1.20	0.68

[a] Calculated based on the conversion estimated by ^{1}H NMR; [b] At quantitative monomer conversion; [c] Determined by ^{1}H NMR measurements in $CDCl_3$ using the initiator methoxy moiety as reference; [d] Determined by GPC measurements in THF with PS standards; [e] Not determined; [f] Volume fraction of DPA segment assuming that the polymer density is equal 1.0 g/mL.

B-2-3. PEO-b-PG2MA-b-PDPA and PG2MA-b-PDPA

As outlined earlier in this chapter, the interest in the synthesis of PEO-*b*-PG2MA-*b*-PDPA triblock and PG2MA-*b*-PDPA diblock copolymers was prompted by the possibility of,

respectively, i) stabilizing highly loaded micellar structures through cross-linking, and ii) verifying possible effects of the corona-forming block structure on the micellar payload capacity.

The PEO-*b*-PG2MA-*b*-PDPA triblock and PG2MA-*b*-PDPA diblock copolymers were synthesized via sequential monomer addition and ATRP techniques (one-pot reaction) (Scheme II-9). The experimental parameters (such as solvent, temperature, concentration of reactants, catalyst, etc.) for the controlled polymerization of G2MA and DPA monomers have been reported before,[182] being essentially the same as for PMPC-*b*-PDPA diblocks (see *Section B-2-1*).

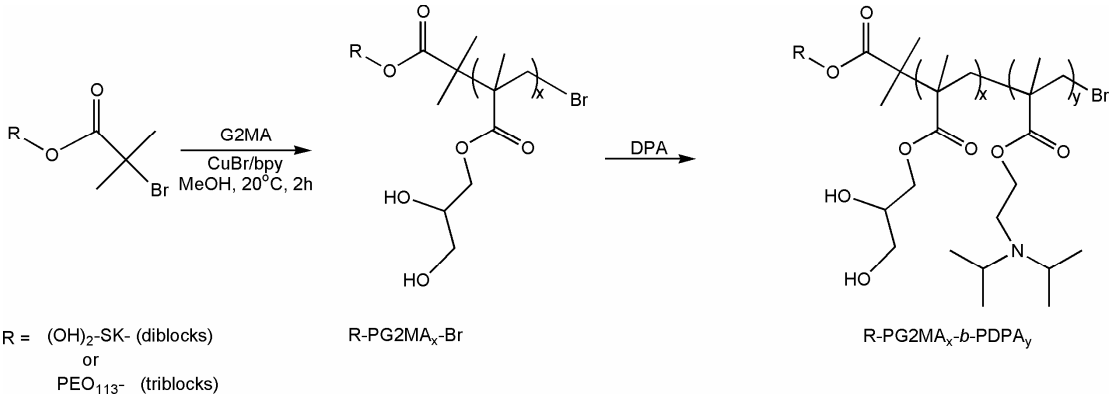

Scheme II-9. Synthesis of amphiphilic PEO-*b*-PG2MA-*b*-PDPA and PG2MA-*b*-PDPA copolymers by ATRP.

G2MA was polymerized first by ATRP in MeOH at 20°C using either PEO_{113}-Br (for triblocks) or $(OH)_2$-SK-Br (for diblocks) initiators and Cu/bpy as catalyst. In all cases, the first stage of the polymerization was allowed to continue for approximately 2 h, point at which the monomer conversion was virtually complete as indicted by ^{1}H NMR analysis. The spectrum **a** in Figure II-5 recorded after 2h and just before addition of the second monomer corroborates the near quantitative disappearance of signals associated to vinyl groups. Thus, the possibility of statistical copolymerization of G2MA with DPA in the next stage was minimized. Subsequently, the second monomer (30-min N_2-purged 50 % v/v DPA in MeOH) was cannulated into the reaction, which was allowed to proceed until the desired conversion or until complete monomer consumption (typically after 20 – 24h). For the synthesis of $PG2MA_{40}$-*b*-$PDPA_{15}$ (target DP_n = 50) for example, the polymerization was stopped after 6h (conversion = 56 %, Figure II-5, spectrum **b**). The assigned ^{1}H NMR spectrum for this copolymer is depicted in Figure II-6, which shows clearly the presence of chemical shifts from both segments and the absence of unreacted monomer after purification.

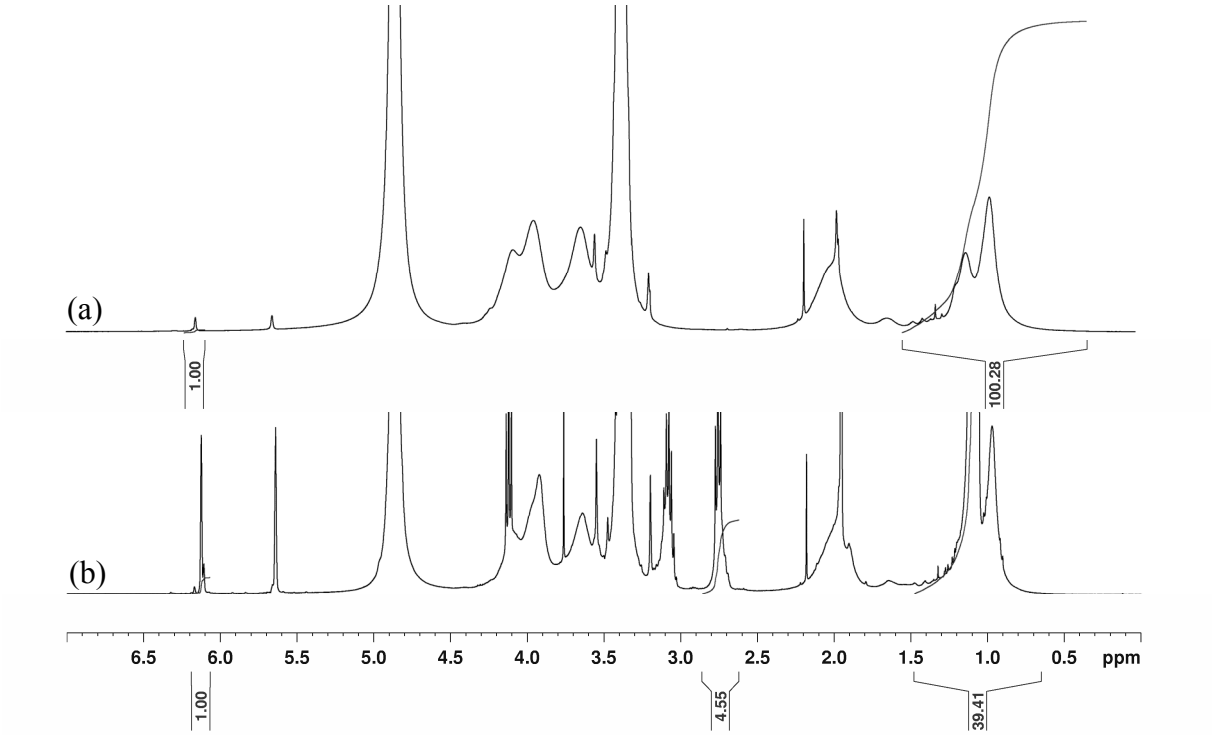

Figure II-5. 1H NMR spectra recorded in MeOD during a typical one-pot polymerization procedure used to synthesize R-PG2MA-b-PDPA di- and triblock copolymers: (a) first stage: after 2h of G2MA polymerization and just before addition of the second monomer and (b) second stage: after 6h of DPA polymerization.

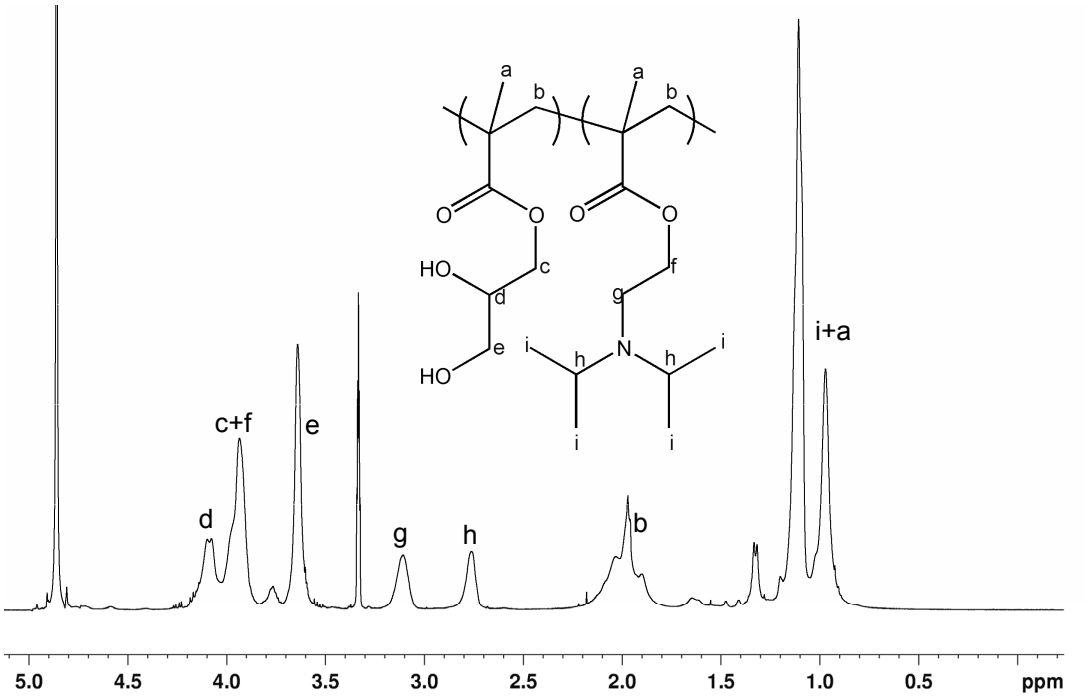

Figure II-6. Assigned [1]H NMR spectrum for PG2MA-*b*-PDPA copolymer in MeOD.

The GPC traces recorded for the polymers obtained by this one-pot approach indicated that premature termination of R-PG2MA-Br chains likely occurred, but was a minor phenomenon given that just a weakly pronounced peak broadening (low molecular weight region) was observed, as exemplified by the arrow in Figure II-7.

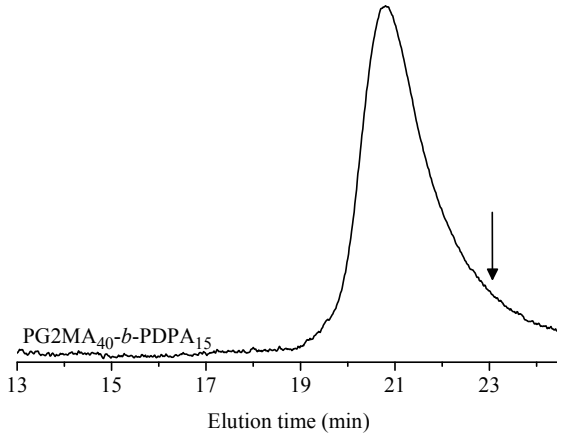

Figure II-7. GPC trace in DMF of $PG2MA_{40}$-*b*-$PDPA_{15}$ diblock copolymer.

Table II-3. Characteristics of PG2MA-*b*-PDPA diblock copolymer.

Copolymer	M_n (target)[a] g/mol	M_n (theo)[b] g/mol	M_n (GPC)[c] g/mol	M_w/M_n[c]
$PG2MA_{40}$-*b*-$PDPA_{15}$	13 600	10 600	14 300	1.17
PEO_{113}-*b*-$PG2MA_{40}$-*b*-$PDPA_{50}$	20 500	20 500	38 000	1.30

[a] At quantitative monomer conversion; [b] Determined based on the conversion estimated by ^{1}H NMR measurements in MeOD considering quantitative initiation. [c] Determined by GPC measurements in 1.0 g/L LiBr DMF at 60°C DMF with PS standards.

B-3. Non-Responsive Systems

B-3-1. PEO-b-PGMA

The ATRP of GMA is very sensitive to the different components present in the polymerization mixture, such as the initiator, catalyst, ligand and solvent.[191, 213-216] A distinctive report was given recently by Canãmero,[214] who observed that the high polymerization rate in bulk did not permit the polymerization control. However, the homopolymerization in solution exhibited a behavior typical of controlled processes, and enabled the evaluation of different experimental parameters, such as temperature, solvent and initiator concentration. In the mentioned work, an impressive solvent effect was established,

and the lowest polydispersity indices and the highest initiation efficiencies were observed using diphenyl ether (DPE) in combination with a mixed halide technique.

Base on those already reported observations, the ATRP of GMA was performed in DPE at 30 °C in presence of CuBr/PMDETA as catalyst (Scheme II-10). The controllability of GMA chain growth under these conditions was corroborated by first order kinetic plot (Figure II-8a) and linear dependence of M_n(GPC)-values on the conversion (see inset). It is verified that the plots do not pass through the origin, which is ascribed to changes in the catalyst in the early stages of the reaction leading to an observed change in rate. There can also be a higher concentration of free radicals formed, which in tandem with the higher rate of diffusion of the low mass chains can lead to increases in radical-radical termination reactions.[20, 192] GPC curves for this system (Figure II-8b) clearly indicated the increase in the molar mass, however we do see also a broadening at low molar masses (arrow). The presence of chemical shifts from both segments, and the absence of unreacted monomer were corroborated by ^{1}H NMR experiments (Figure II-9).

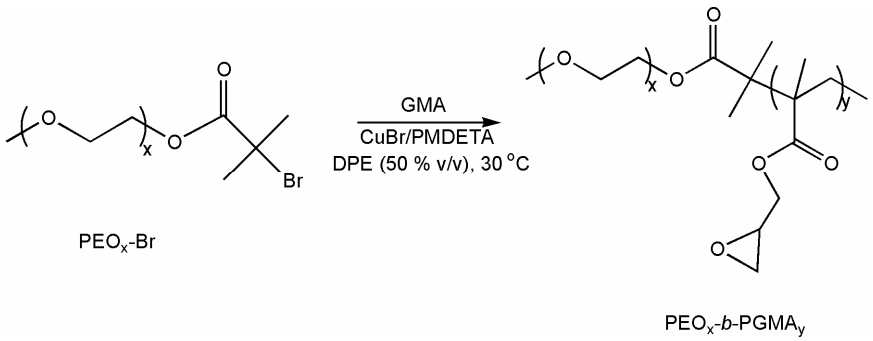

Scheme II-10. Synthesis of amphiphilic PEO-*b*-PGMA copolymers by ATRP.

The results of PEO-*b*-PGMA diblock copolymers characterization are summarized in Table II-4. Narrow polydispersity indexes were determined for the three different molar masses and compositions, which remained in the range $0.50 \leq \phi_{PGMA} \leq 0.60$, thus favoring the formation of spherical core-shell micelles and fitting into the objectives of this work.

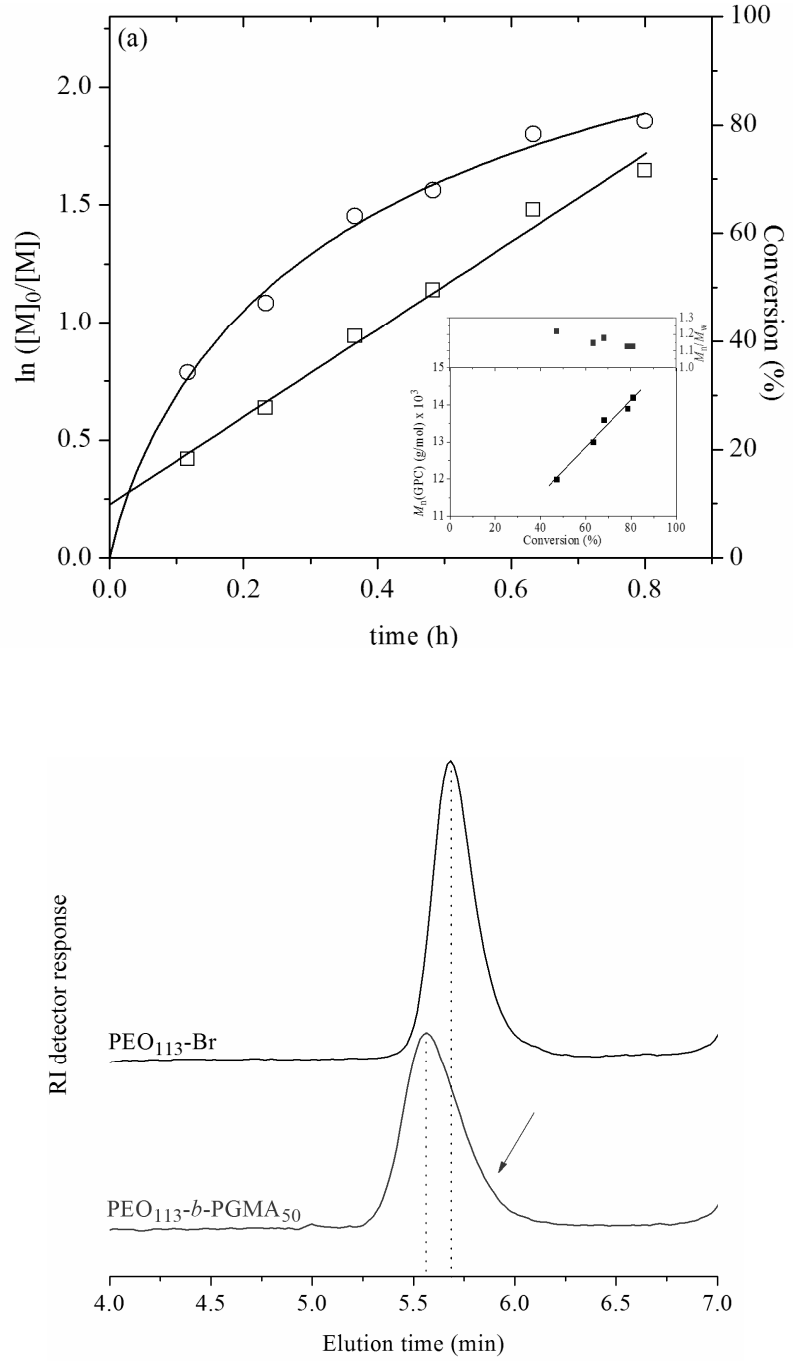

Figure II-8. (a) First order kinetic plot for ATRP of GMA in DPE (50% v/v) at 30 °C. Conditions: [GMA]/[PEO_{113}-Br]/[CuBr]/[PMDETA] = 65/1.0/1.0/2.0. The inset shows the evolution of *M*n-values as a function of the conversion. (b) GPC traces in THF of PEO_{113}-Br and PEO_{113}-*b*-$PGMA_{50}$ diblock copolymer.

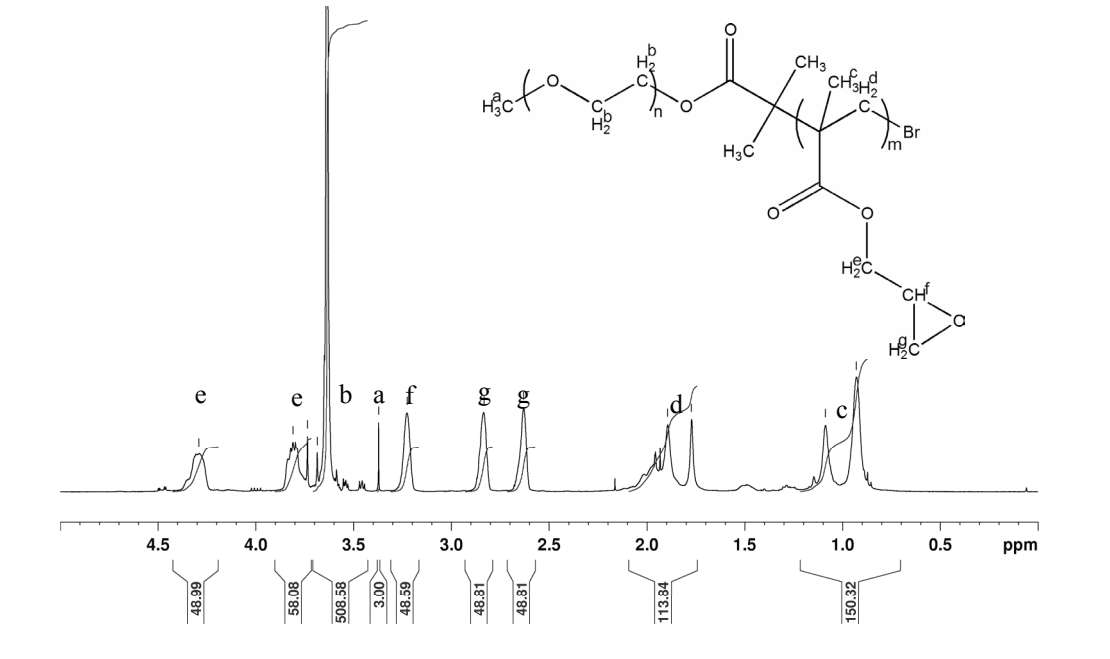

Figure II-9. Assigned ^{1}H NMR spectrum for PEO-*b*-PDPA copolymer in $CDCl_3$.

Table II-4. Molecular characteristics of PEO-*b*-PGMA diblock copolymers.

Copolymer PEO_x-*b*-$PGMA_y$	time (h)	Convn.[a] (%)	M_n(target)[b] g/mol	M_n(NMR)[c] g/mol	M_n(GPC)[d] g/mol	M_w/M_n[d]	ϕ_{PGMA}[e]
113-35	0.3	50	14 100	10 000	8 900	1.20	0.50
113-50	0.5	70	14 100	12 100	9 500	1.25	0.60

[a] Calculated based on the conversion estimated by ^{1}H NMR; [b] At quantitative monomer conversion; [c] Determined by ^{1}H NMR measurements in $CDCl_3$ using the initiator methoxy moiety as reference; [d] Determined by GPC measurements in THF with PS standards; [e] Volume fraction of GMA segment assuming that the polymer density is equal 1.0 g/mL.

B-3-2. PEO-b-PCL

PEO-*b*-PCL diblocks were either synthesized via ROP of ε-CL in toluene from the hydroxyl end-group of α-methoxy-ω-hydroxy PEO chains in presence of $Sn(Oct)_2$ as illustrated in Scheme II-11, or commercially available. In the former case, the reaction proceeded for ca. 12 h at 115 ^{o}C. The resulting diblock copolymers obtained after precipitation into diethyl ether, and exhibited narrow molecular weight distributions (M_w/M_n < 1.25) in all cases (Table II-5). Notably, however, the samples prepared in this work via $Sn(Oct)_2$ were characterized by a higher polydispersity indexes as compared to those prepared

using $Al(iPrO)_3$. The lower temperature and shorter polymerization time in the latter case minimize the occurrence of undesirable reactions already discussed in this chapter, thus yielding final products not only with narrower size distributions but also excellent degree of end-chain functionality.

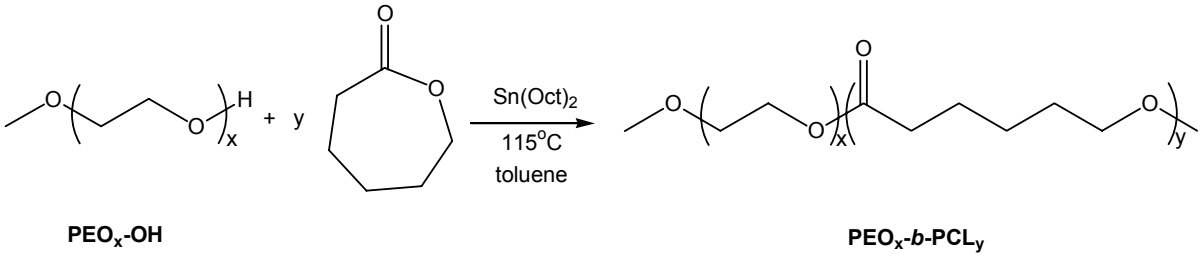

Scheme II-11. Synthesis of amphiphilic PEO-*b*-PCL copolymers by ROP of CL from PEO-OH.

Table II-5. Molecular characteristics of PEO-*b*-PCL diblock copolymers.

PEO_x-*b*-PCL_y	M_n(target) g/mol	M_n(NMR)[c] g/mol	M_n(GPC)[d] g/mol	M_w/M_n	ϕ_{PCL}[e]
45-9[a]	-	-	3 000[a]	1.10[a]	0.34
45-24[a]	-	-	4 700[a]	1.19[a]	0.58
114-24[a]	-	-	7 900[a]	1.11[a]	0.35
114-44[a]	-	-	10 000[a]	1.06[a]	0.50
113-95[b]	16 400	15 800	47 900	1.23[c]	0.68
114-44[b]	27800	27 200	67 600	1.24[c]	0.82

[a] Data provided by the manufacturer (Polymer Source Inc.); [b] Synthesized in this work; [c] Determined by ^1H NMR measurements in $CDCl_3$ using the ratio between integrals relative to $-C\mathbf{H_2}C\mathbf{H_2}O-$ protons at $\delta = 3.4 - 3.8$ ppm (PEO chain) and $-C(O)C\mathbf{H_2}(CH_2)_4O-$ protons 3.8 – 4.2 ppm (PCL chain) [d] Determined by GPC measurements in DMF with PS standards; [e] Volume fraction of PCL segment assuming that the polymer density is equal 1.0 g/mL.

The M_n(NMR)-values of as-synthesized PEO-b-PCL diblocks (calculated from the ratio of integrals shown in the ^1H NMR assigned spectrum in Figure II-10) were in excellent agreement with M_n(target)-values (see Table II-5) suggesting near quantitative consumption of CL monomer. The GPC analysis of PEO macroinitiator and a selected PEO-*b*-PCL diblock are depicted in Figure II-11. The results revealed the shift in M_n toward higher molar masses after polymerization of CL initiated from PEO. Importantly, no traces of PEO homopolymer were detected suggesting good initiation efficiency. A slightly pronounced shoulder indicative of side reactions is however apparent in the chromatogram of the diblock.

The M_n(GPC)-values were obviously overestimated. Such an observation can be attributed to differences in hydrodynamic volumes between PEO-*b*-PCL and PS standards.

The series of PEO-*b*-PCL diblocks finally available for this work covered a wide range of hydrophobic volume fractions ($0.34 \leq \phi_{PCL} \leq 0.82$), and consequently allowed a systematic study of the PCL block length effect on the size, morphology, and loading capacity of the nanocontainers.

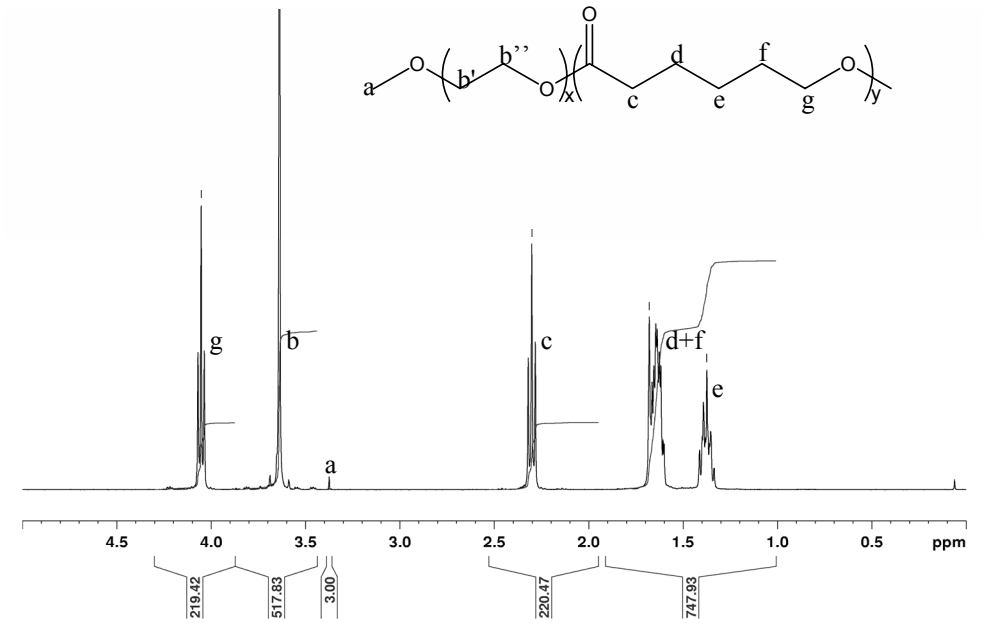

Figure II-10. Assigned ^{1}H NMR spectrum for PEO-*b*-PCL copolymer in $CDCl_3$.

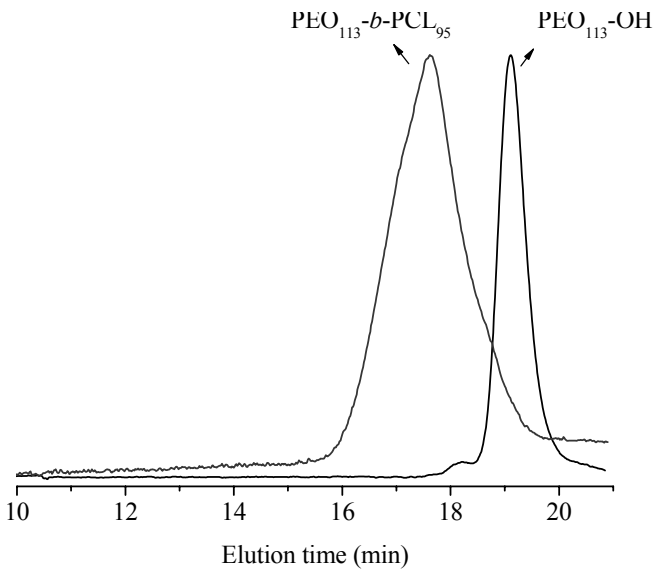

Figure II-11. Representative GPC traces in DMF of PEO_{113}-OH and PEO_{113}-*b*-PCL_{95} diblock copolymer.

B-3-3. PEO-b-PG2MA and PEO-b-(PG2MA-IND)

Double hydrophilic diblock copolymer–drug conjugates presenting self-assembly properties have been prepared as illustrated in Scheme II-12. Firstly, poly(ethylene oxide)-*b*-poly(glycerol monomethacrylate) (PEO-*b*-PG2MA) block copolymers were synthesized by ATRP of G2MA in methanol using PEO macro-initiators and Cu/bpy catalyst, as previously described elsewhere by Armes *et al*.[182] Block copolymers systems with narrow molecular weight distributions ($M_w/M_n < 1.20$) were obtained, as shown in Table II-6 and in Figure II-12. The large discrepancy between M_n-values calculated from ^{1}H NMR (Figure II-13) and DMF GPC analysis of these polymers is attributed to the differences in hydrodynamic volumes between PEO-*b*-PG2MA and PS standards.

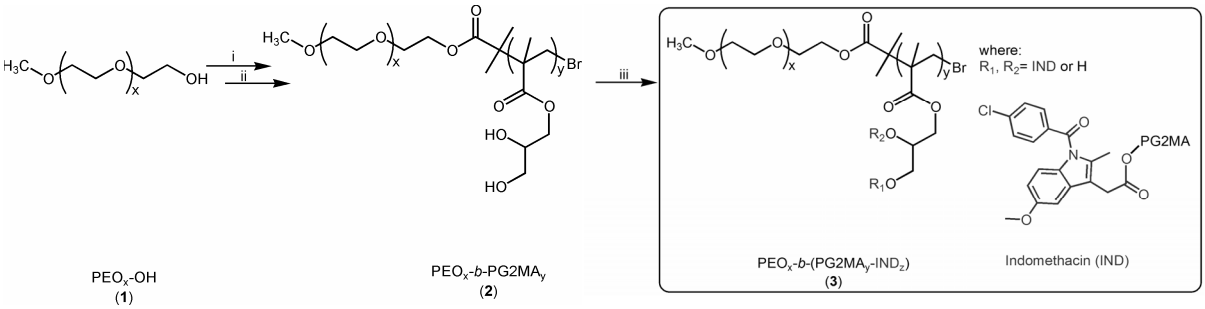

Scheme II-12. Synthesis of amphiphilic PEO-*b*-(PG2MA-IND) polymer-drug conjugates and their precursors; i) α-bromoisobutyryl bromide, Et3N, toluene, overnight, RT; ii) G2MA, CuBr/bpy, MeOH, 20°C; iii) Indomethacin, DCC/DMAP, DMF, 72h, RT.

Table II-6. ATRP of G2MA in MeOH at 20°C using CuBr/bpy as catalyst, and characteristics of resulting PEO-*b*-PG2MA diblock copolymers.

Diblock PEO_x-*b*-$PG2MA_y$	time (h)	Convn. (%)	M_n (target)[a] g/mol	M_n (theo)[b] g/mol	M_n (NMR)[c] g/mol	M_w/M_n[d]
113-40	4.0	96	11,400	11,200	11,400	1.10
113-65	2.0	62	19,400	14,000	15,500	1.12
113-85	5.0	91	19,400	18,200	18,600	1.16

[a] At quantitative monomer conversion.
[b] Calculated based on the conversion estimated by ^{1}H NMR in MeOD.
[c] Determined by ^{1}H NMR measurements in D_2O using the initiator methoxy moiety as reference.
[d] Determined by GPC measurements in 1.0 g/L LiBr DMF at 60 °C with PS standards.

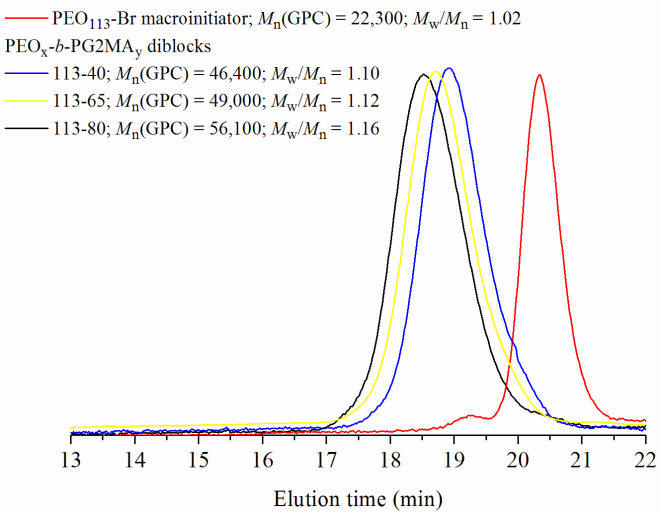

Figure II-12. GPC traces of PEO_{113}-Br macroinitiator and PEO-*b*-PG2MA diblock copolymers in 1.0 g/L LiBr DMF at 60°C DMF (Table II-1).

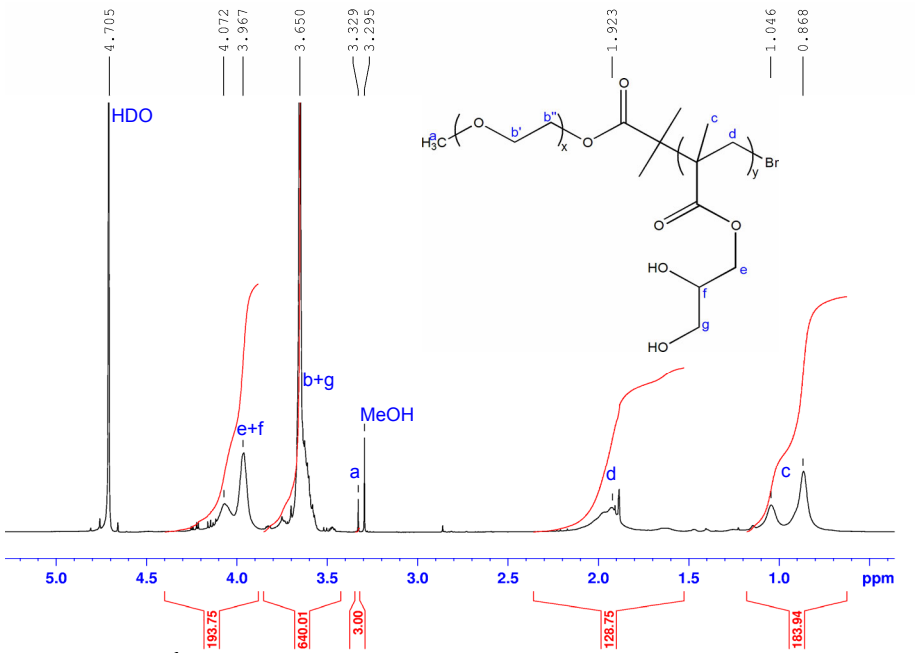

Figure II-13. Assigned ^{1}H NMR spectrum for MeO-PEO_{113}-*b*-$PG2MA_{65}$ diblock copolymer in D_2O. Integrals illustrate the determination of M_n using methoxy groups as internal reference.

In the following step, the pendant hydroxyl groups of PG2MA blocks were used for post-polymerization conjugation to the hydrophobic drug IND by Steglich esterification (Scheme II-12), which is a mild reaction allowing the conversion of sterically demanding systems. In contrast to the quite simple organic chemistry implied in esterification reactions between hydroxylated and carboxylated small molecules, analogous polymers frequently require forcing conditions to achieve the desired degree of modification.[217] Table II-7 shows the

molecular characteristics of amphiphilic block copolymer – drug conjugates synthesized and hereinafter investigated, as assessed by ^{1}H NMR and UV-vis.

In the case of ^{1}H NMR analysis, the efficiency of esterification reactions was calculated on basis of the integral ratio between aromatic IND proton at δ = 6.9 ppm and methacrylate signal of PG2MA block at δ = 1.6 – 0.5 ppm (normalized to 3H), also taking in account the polymerization degree of PG2MA (DP_{G2MA}). Figure II-14 depicts a typical ^{1}H NMR spectrum for IND in DMSO-d_6 (a) and PEO_{113}-*b*-($PG2MA_{40}$-IND_{21}) conjugate in DMF-d_7 (b), showing regions of interest integrated. The unreacted IND molecules were almost completely removed during polymer precipitation in cold diethyl ether, solvent in which free IND is soluble.

Table II-7. Molecular characteristics of PEO-*b*-(PG2MA–IND) conjugates.

	Conjugate PEO_x-*b*-($PG2MA_y$–IND_z)	Targeted esterif. degree (%)	Achieved esterif. degree (%)[a]	Convn.[a] (%)	# of IND per chain[a/b]	wt. % B-IND[b]	$\phi_{PG2MA\text{-}IND}$[c]
1	113-(40-10)	25	18	72	14 / 10	21	0.33
2	113-(40-17)	50	25	50	20 / 17	33	0.49
3	113-(40-21)	50	28	56	22 / 21	40	0.56
4	113-(40-29)	100	52	52	42 / 29	49	0.68
5	113-(65-08)	25	08	32	11 / 08	15	0.22
6	113-(65-28)	50	25	50	33 / 28	39	0.56
7	113-(85-10)	25	06	24	11 / 10	16	0.22
8	113-(85-29)	50	24	48	40 / 29	32	0.50

[a] Calculated by ^{1}H NMR in DMF-d_7 on basis of the integral ratio between aromatic IND proton at 6.9 ppm and methacrylate signal of PG2MA block between 1.6 – 0.5 ppm, after purification; [b] Determined by UV-vis spectroscopy using typical absorption maximum of IND (λ_{max}) at 320 nm; [c] Volume fraction of PG2MA-IND in the resulting polymer – drug conjugate, assuming that the polymer density is equal to 1.0 g/mL.

As can be observed in Table II-7, satisfactory agreement between results collected using NMR or UV was observed, and UV analysis was chosen to discuss the data due to its good analytical reliability. The coupling was also confirmed in all cases by GPC–UV analysis (data not shown). The conversions typically remained in the range of 24 – 72 %, whereas a slight decrease apparently occurred upon the increase in the molecular weight of PG2MA block. The incomplete reaction is most probably explained by the sterical hindrance imposed by firstly grafted IND bulky molecules and the difference in the reactivity of primary and secondary hydroxyl groups in the PG2MA structure.[217, 218] These results are in good agreement with other reports on the esterification of hydroxyl substituted macromolecules.[218, 219]

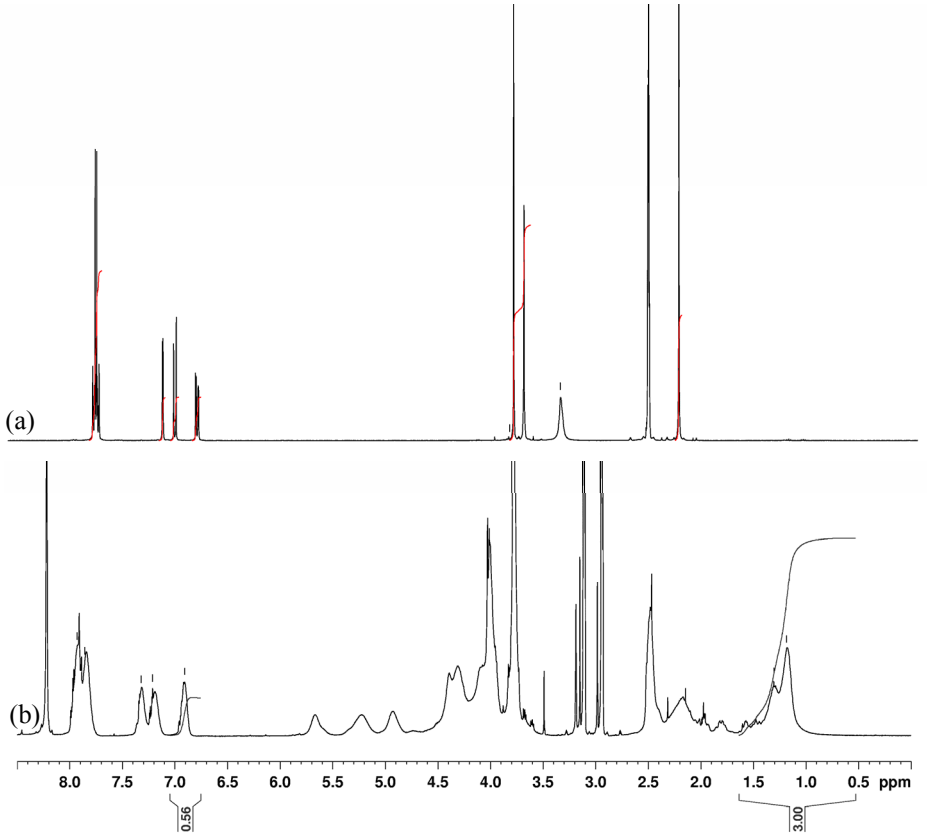

Figure II-14. ^{1}H NMR spectrum for IND in DMSO-d_6 (a) and PEO_{113}-*b*-($PG2MA_{40}$-IND_{21}) conjugate in DMF-d_7 (b).

The final drug content clearly depended, however, on the targeted IND/OH molar ratio. As a result, distinct drug amounts were covalently attached to the same polymer precursor, yielding block copolymer – drug conjugates in which the volume fraction of G2MA-IND ($\phi_{G2MA\text{-}IND}$) varied from 0.22 to 0.68. Besides, samples exhibiting fairly similar $\phi_{G2MA\text{-}IND}$ values but different PG2MA block lengths were synthesized. It is also meaningful to note the weight percentage (wt. %) of IND in the polymer – indomethacin conjugates, which varied between 15 and 49 %. These values are fairly comparable to those reported by Bertin et al.[220] and Quémener et al.,[221] who polymerized norbornenyl-modified indomethacin monomers.

The self-assembly of block copolymers has been the subject of comprehensive theoretical and experimental studies,[42] and it is nowadays well-established that the volume fraction (ϕ) of each constituting segments is a major driving force – along with the overall degree of polymerization (DP) and Flory-Huggins interaction parameter(χ) – that defines the thermodynamic-stable morphology (see *Chapter III*). Roughly, spherical core-shell micelles are favored for $0.30 < \phi_{hydrophobic} < 0.70$, whereas vesicles are expected for $\phi_{hydrophobic} > 0.70$.[42,

[78] Therefore, self-assembly into spherical micelles is anticipated for most of the samples listed in Table II-7, fulfilling the objective of preparing micelles with IND-based cores.

In the next chapter the self-assembly properties in water of the as-synthesized block copolymers is presented.

Chapter III

Self-Assembly of As-Synthesized Amphiphilic Block Copolymers

Introduction

In this chapter, the self-assembly of the aforementioned copolymers in water is described. True to any macromolecular self-organization study, the strategy to obtain compartmented core-corona nanoparticles such as micelles, vesicles, cylinders, etc., depends mostly on the solubility properties of the building-blocks (the polymer chains). Whenever the resulting objects are to perform certain functions (*e.g.:* act as nanocontainers in this study), additional constraints may eventually be imposed to the preparation methods, and demand clever manipulation approaches. Two of the principal micellar preparation methods already described in *Chapter I* (indirect dissolution (*Section B-2-2*) and stimulus-induced self-assembly (*Section B-2-3*)) have been used in this work, as explained below.

This chapter begins, therefore, with a brief description of the fundamentals of techniques used to access the physical chemical properties of block copolymer nano-structured materials in solution (*Part A*). Such an introduction to the theory underlying the experiments is superficial in the sense that it only highlights the main ideas and assumptions. The reader is refereed to the cited literature for complete and very understandable information.

After describing basic concepts in the study of macromolecular aggregates, the self-assembly processes of the amphiphilic copolymers synthesized in this work and the physical chemical properties of the resulting nano-objects, are presented (*Part B*). This latter and most important section is sub-divided according to the strategy used to induce the formation of micellar morphologies: *B-1*) stimulus-responsive systems: pH-induced micellization and *B-2*) non-responsive systems: micellization from organic solvents. In some cases, nevertheless, the micellization of samples exhibiting pH-responsiveness was also performed from organic media. Such an interest relies on the fact that the solvent-free pH-induced protocol is often not suitable for encapsulation of hydrophobic guest molecules (probes), due to the reasons described before (*Chapter I*, *Sections C-3 and C-4*). Instead, it presents great potential in the controlled/triggered payload release.

Encapsulation-wise, there is consequently an advantage of using PEO as corona-forming block instead of PMPC, provided that excellent solubility in most of the organic solvents is achievable in the former case. Such a difference represents a much large range of possibilities in the manipulation, as discussed later in this document.

A) Assessment of Nanoparticle Properties: Fundamentals

A-1. Light Scattering (LS)

Electromagnetic radiation is one of the most important probes of structure and dynamics of matter.[222] Certainly, the most important advances in the knowledge of phenomena occurring in our day-life have been achieved by observing interactions between electro-magnetic waves and materials. Depending on the characteristics of both the incident radiation and the objects exposed to it, distinct physical chemical processes may take place, which truthfully constitute a toolbox for scientists.

In the polymer field, probably no other technique has contributed more to the elucidation of local macromolecular structures and dynamics at submicron scale than light, x-rays and neutron scattering. To a large extent, these techniques are complementary. They do share several similarities, and perhaps the most important of these is the fact that, with minor adjustments to account for the different types of radiation, the same basic equations and laws can be used to analyze the data.

In LS experiments, a monochromatic beam impinges on a sample and is scattered into a detector placed at an angle θ with respect to the transmitted beam, as illustrated in Figure III-1. The intersection between the incident and the scattered beams defines a volume V, called scattering volume or illuminated volume.[222] All the elements (solvent and particles such as micelles, cylinders, vesicles, etc) within such a space will scatter the light in all directions at a given intensity, which depends on their polarizability. The latter can be thought as a difference in the refractive index between the particles and the solvent. In other words, light scattering only occurs in media having an inhomogeneous refractive index.

Depending on the data treatment applied to the scattered intensity arriving at the detector, different information can be obtained. Whilst in static light scattering (SLS) measurements one makes use of the time-average intensity of scattered light arriving at the detector, in dynamic light scattering (DLS) the information comes from the fluctuations of the scattered light intensity as a function of time.

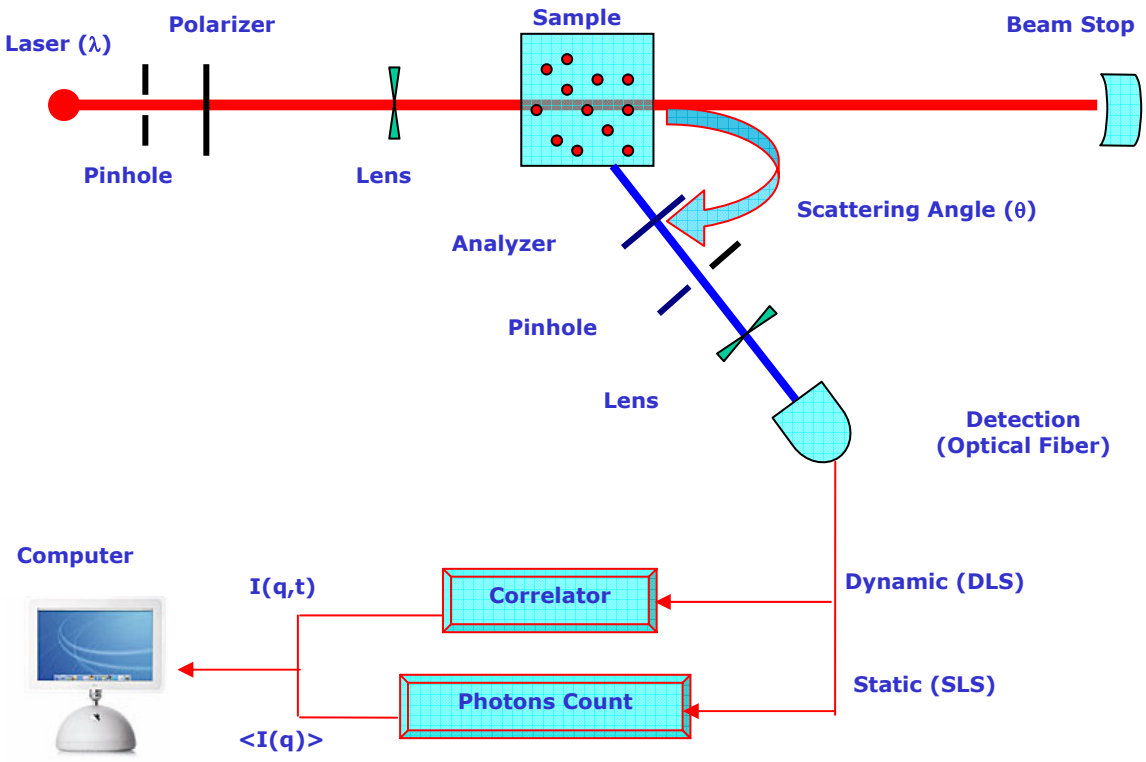

Figure III-1. Schematic representation of a light scattering setup.

A-1-1. Static Light Scattering (SLS)

The classical LS theory was derived by Rayleigh, who studied the phenomenon for gaseous molecules. However, his considerations are valid only for small, non-interacting particles. By small particles, it is meant those whose size is much less than λ, where λ is the wavelength of the light that is being scattered. More precisely, $R_g < \lambda/20$. It is easy to conclude that such a rule is often violated in polymer solutions (especially in those cases where chains are self-assembled or aggregated), because for a monochromatic laser with for example λ = 632.8 nm (as used in this work), the R_g should be less than approximately 30 nm. The original Rayleigh theory also does not take into account possible interactions between the scattering particles (non-ideal solutions). Thus, the analysis of light scattering date requires two extrapolations/corrections: i) for large particles effect and ii) for non-ideal effect.

Ideal polymer solution with small particles

Beginning with the case of an ideal polymer solution with small particles, we should first establish a quantitative relation between the scattered light intensity and the properties of the particles.

The Rayleigh ratio (R_θ) is defined by eqn. III-1,

$$R_\theta = \frac{I_\theta}{I_0} r^2 \qquad \text{(III-1)}$$

where I_θ is the scattered intensity at an angle θ, I_0 is the intensity of the incident radiation, and r is distance between the particle and the observer. The origin of I_θ is associated with the interaction of the incident light I_0 with the particles located along its propagating direction. The result is the formation of a dipole, which produces an oscillating secondary electromagnetic field, with the same frequency (same λ, elastic scattering) as that of the incident one. The intensity of such an induced dipole is correlated with the incident intensity through a proportionally constant, which is the polarizability (α) of the particle or molecule. The latter is defined by eqn III-2,

$$\alpha = \frac{nC}{2\pi N}\left(\frac{dn}{dC}\right) \qquad \text{(III-2)}$$

where C is concentration, N is the number of particles and dn/dC is the increment in n as a function of C. This quantity can be easily measured using a differential refractometer.

The I_θ/I_0 ratio for one single and small particle is defined by eqn III-3, which can be deduced using an electromagnetism approach to describe the light scattering phenomenon.[19]

$$\frac{I_\theta}{I_0} = \frac{16\pi^4\alpha^2 \sin^2\theta}{\lambda^4 r^2} \qquad \text{(III-3)}$$

By replacing α in eqn III-3, one gets

$$\frac{I_\theta}{I_0} = \frac{\frac{16\pi^4 C^2}{4\pi N}\left(\frac{dn}{dC}\right)\sin^2\theta}{\lambda^4 r^2} \qquad \text{(III-4)}$$

The number of scattering particles can be expressed as follows:

$$N = \frac{cN_A}{M_w} \qquad \text{(III-5)}$$

After substitution of eqn III-5 into eqn III-4, and rearrangement, the result reads:

$$\frac{I_\theta}{I_0} r^2 = \frac{4\pi^2 C M_w}{\lambda^4 N_A}\left(\frac{dn}{dC}\right)\sin^2\theta \qquad \text{(III-6)}$$

The lhs of eqn III-6 is the Rayleigh ratio, which is now related the molecular weight of the scattering particle. For the sake of clarity and simplicity, all constant values are grouped into a constant *K* (eqn. III-7), giving the eqn III-8 after rearrangement and considering $\theta = 90^o$.

$$K = \frac{4\pi^2 n^2}{\lambda^4 N_A}\left(\frac{dn}{dC}\right)^2 \qquad \text{(III-7)}$$

$$\frac{KC}{\Delta R_\theta} = \frac{1}{M_w} \qquad \text{(III-8)}$$

Experimentally, the value of ΔR_θ at different scattering angles θ can be determined indirectly by measuring the light scattered by a standard, the solvent and the sample as given in eqn III-9.

$$\Delta R_\theta = \frac{I - I_{solvent}}{I_{standard}}\left(\frac{n_{solvent}}{n_{standard}}\right)^2 R_{standard} \qquad \text{(III-9)}$$

Non-ideal polymer solutions

The eqn. III-8 is valid for non-interacting small particles, that is, for near infinite dilution ($C \to 0$). The possibility of non-ideal behavior should however be taken into consideration at finite concentration. Following the fact that fluctuations in the polarizability due to intermolecular interactions depend on the chemical potential, and can be related to the osmotic pressure, the non-ideal case was handled by adding virial coefficients and concentration terms to the ideal result. Hence, expanding eqn III-8 gives

$$\frac{KC}{\Delta R_\theta} = \frac{1}{M_w} + 2A_2 C + 3A_3 C^2 + \ldots \qquad \text{(III-10)}$$

Normally, the terms beyond the second virial coefficient are negligible, so that $KC/\Delta R_\theta$ is linearly dependent on *C*, originating a straight line were the slope is $2A_2$, and the linear coefficient is $1/M_w$. The A_2 parameter depends on the inter-particle interactions in solution. Whereas A_2 is zero for θ-conditions, it is positive in the case of inter-particle repulsions, and negative in the case of attractive interactions.

In summary, for small particles (*i.e.*, $R_g < \lambda/20$) the respective M_w can be technically determined at a fixed angle.

Scattering from large particles

When the particle is not small compared to the wavelength of light, the latter can scatter from different parts of the object, thus traveling different path lengths before reaching the detector. Such a difference can lead to destructive interference, which reduces the intensity of the scattered light. The net effect is that the scattering diagram for large particles is reduced in intensity from the scattering diagram for small particles. As depicted in Figure III-2, the amount of intensity reduction or the amount of destructive interference depends on the scattering angle. By looking at this diagram, we would merely have to carry on the LS experiment at $\theta = 0$. However, under a such condition the transmitted light masks the scattered part of it. Instead, the LS analysis can be performed at $\theta > 0$ and than extrapolate to $\theta = 0$.

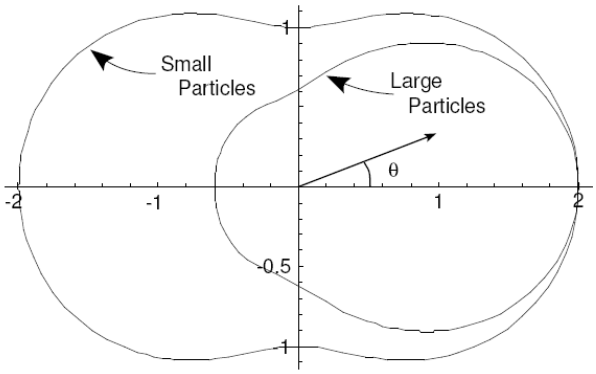

Figure III-2. Scattering diagrams for both small and large particles.

This question was handled by introducing a form factor ($P(\theta)$) to eqn III-10 that contains the description of the large particle effect, yielding the relation represented by eqn III-11, which was written as a function of the wavevector q. At a scattering angle θ, q is defined by eqn III-12, and its inverse value (q^{-1}) is assimilated to the scale of observation.

$$\frac{KC}{\Delta R_\theta} = \frac{1}{M_w P(\theta)} + 2A_2 C \qquad \text{(III-11)}$$

$$q = \frac{4\pi n}{\lambda} \sin\left(\frac{\theta}{2}\right) \qquad \text{(III-12)}$$

In the Guinier region where $qR_g << 1$, the form factor $P(q)$ for is defined as

$$P(q)_{q\to 0} \approx 1 - \frac{q^2}{3}\left\langle R_g^2 \right\rangle \qquad \text{(III-13)}$$

Finally, one gets the Debye relation:

$$\frac{KC}{I(q)} = \frac{1}{M_w}\left(1 + \frac{R_g^2}{3}q^2\right) + 2A_2C \qquad \text{(III-14)}$$

By measuring *I(q)* for a set of θ and C_p, values of M_w, R_g, and A_2 can be estimated from typical Zimm plots after extrapolation to $C \to 0$ and $q \to 0$, as illustrate in Figure III-3.

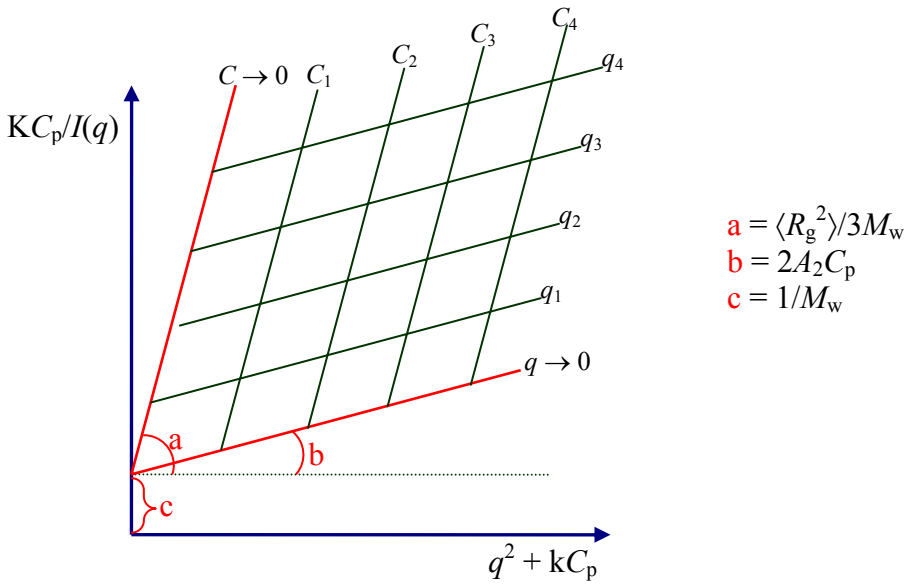

Figure III-3. Typical Zimm plot showing the determination of M_w, R_g and A_2 values, as indicated.

A-1-2. Dynamic Light Scattering (DLS)

Dynamic light scattering (DLS) is the most versatile and useful technique for measuring *in situ* the sizes, size distributions, and (in some cases) the shapes of nanoparticles in solution.[222-224] The rapid development and widespread use of DLS in multidisciplinary fields (physics, chemistry, biology, pharmacy, etc) is certainly related to the advances in fabrication of electronic devices (correlators).

The principle of DLS is shown in Figure III-4. On the left, the signal detected at a given observation scale (*q*-value) is shown. The perpetual particle motion (Brownian motion or "random walk") causes statistic fluctuations in *I*(*q*) as a function of time. Definitely, such fluctuations carry very important information about the dynamics of the scattering particles, which is ultimately defined by the properties of the latter such as size, shape, molecular interactions, repulsions, etc.[19, 222, 224] The detailed analysis of these fluctuation with the aid of electrodynamics and theory of time dependent statistical mechanics, is at the origin of DLS techniques.[222] The fluctuation pattern is firstly transferred into an intensity correlation

function, using the following scheme: the time-dependent scattered intensity is multiplied with itself shifted by a distance τ in time, and these products are averaged over the total measurement time.

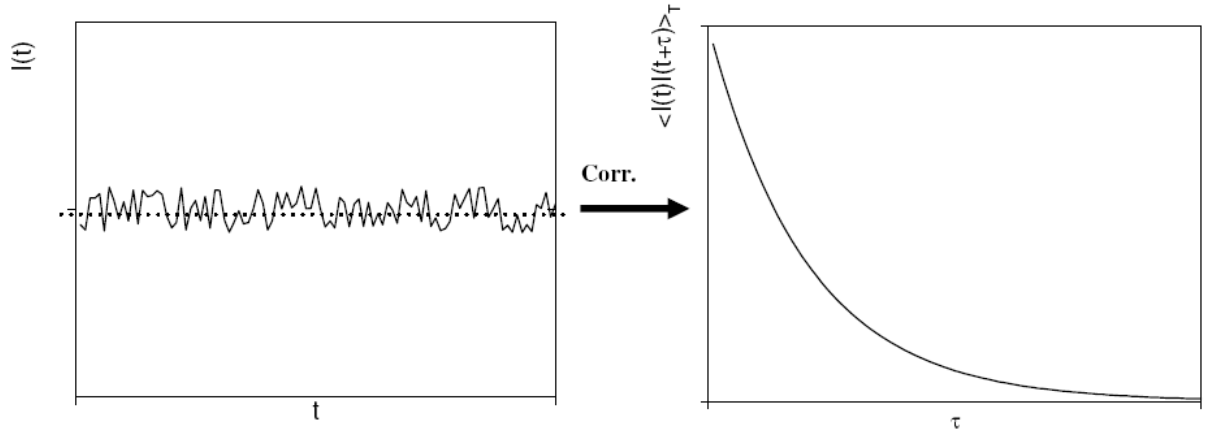

Figure III-4. Principle of a DLS measurement.

The auto-correlation function can be defines as

$$g^2(q,t) = \frac{\langle I(q,0)I(q,t)\rangle}{\langle I(q,t)\rangle^2} \qquad \text{(III-15)}$$

where t is the time. Through this relation, it is possible to determine the variations in the scattered light intensity at a given observation scale (q-value) at two different moments ($I(q,0)$ and $I(q,t)$). It is easy to conclude from eqn III-15 that when the signal at an instant t is compared to itself, the correlation is perfect and $g^2(q,t) = 1$. Inversely, $g^2(q,t) = 0$ when no correlation exist; i.e., the particle "lost" the information regarding its initial position due to the random walk. Assuming a Gaussian distribution of the electrical field, one can use the Siegert approach to obtain a relation between the auto-correlation functions of the scattered intensity $g^2(q,t)$ and the scattered electric field $g^1(q,t)$, which corresponds to the inverse Laplace transformation of the relaxation times. As a consequence, the relaxation times for a given q-value can be obtained from information contained in $g^2(q,t)$ function.

$$g^2(q,t) = 1 + \left|g^1(q,t)\right|^2 \qquad \text{(III-16)}$$

However, different methods apply to the analysis of the auto-correlation functions. In the present work, the CONTIN analysis[225] was used in most of the cases, while cumulants analysis was applied to estimate the polydispersity of the particles.

In the cumulants method,[226] the first order electric field correlation function of laser light scattered by polydisperse solutions of macromolecules is written as a sum or distribution of

exponentials (eqn III-17), with decay rates proportional to the diffusion coefficients of the solute molecules. The coefficients Γ_n are the so-called cumulants. For an ideal solution containing monodisperse scattering particles, the development of eqn III-17 stops at Γ_1 (or simply Γ). In the case of a polydisperse systems, though, the first cumulant Γ corresponds to an average relaxation time, while the second cumulant μ_2 is related to the distribution of the relaxation times, and thus to the extent of polydispersity index (PDI = μ_2/Γ^2).

$$\ln(g^1(q,t)) = \ln(A) - \Gamma t + \mu_2 \frac{t^2}{2} + \ldots \qquad \text{(III-17)}$$

A more powerful method, which has become the standard in analyzing DLS data, uses mathematical algorithms to perform an inverse Laplace transform on the data (described by eqn III-18) to obtain the distribution function of relaxation times $A(\Gamma)$.[223] In eqn. III-18, $A(\Gamma)\mathrm{d}\Gamma$ is the fraction of the correlation function decaying with reciprocal relaxation time between Γ and $\Gamma + d\Gamma$. To find $A(\Gamma)$ from $g^1(q,t)$, which is the Laplace transformation of the former, is a non-simple problem.[223] In fact, mathematical techniques for performing such transformations known as regularization techniques were developed, and applied to the analysis of DLS by Provencher,[225] who wrote the CONTIN program.

$$g^1(q,t) = \int_0^\infty A(\Gamma) e^{-\Gamma t} dt \qquad \text{(III-18)}$$

The CONTIN routine is probably the most interesting approach to fit auto-correlation functions recorded from solutions of macromolecules and their self-assemblies.[222-224] It allows the analysis of multi-modal distribution of scattering particles, within limitations in terms of the separation of $A(\Gamma)$ peaks, which should be about a factor of five or more as, experienced during this work.

The relaxation frequency, Γ ($\Gamma = \tau^{-1}$) depends generally on the scattering angle, and in the case of a diffusive particle, this frequency is q^2-dependent.[224] The apparent diffusion coefficient (D_{app}) at a given copolymer concentration (C_p) is calculated from

$$\left.\frac{\Gamma}{q^2}\right|_{q\to 0} = D_{app} \qquad \text{(III-19)}$$

The hydrodynamic radius (R_H) (or diameter, $2R_H$) is then calculated from the Stokes-Einstein relation when assuming a spherical shape

$$R_H = \frac{k_B T}{6\pi\eta\Gamma} q^2 = \frac{k_B T}{6\pi\eta D_{app}} \qquad \text{(III-20)}$$

where k_B is Boltzmann constant, T is the temperature of the sample, and η is the viscosity of the medium.

A-1-3. The micellar structure accessed by combining SLS and DLS experiments.

Depending on the "scale of observation", different information on a given block copolymer nanoparticle system can be obtained, as pictured in Figure III-5. Taking q^{-1} (the inverse of the wavevector q - eqn III-12) as the "inverse magnification glass", one can straightforwardly conclude that by varying the wavelength λ of the incident beam (4000 Å < λ < 7000 Å for LS, 1 Å < λ < 20 Å for NS and 0.2 Å < λ < 2 Å for XS) and the angle of detection θ, a broad range of q-values is probed. Light, x-rays and neutron scattering techniques are therefore complementary to each other.

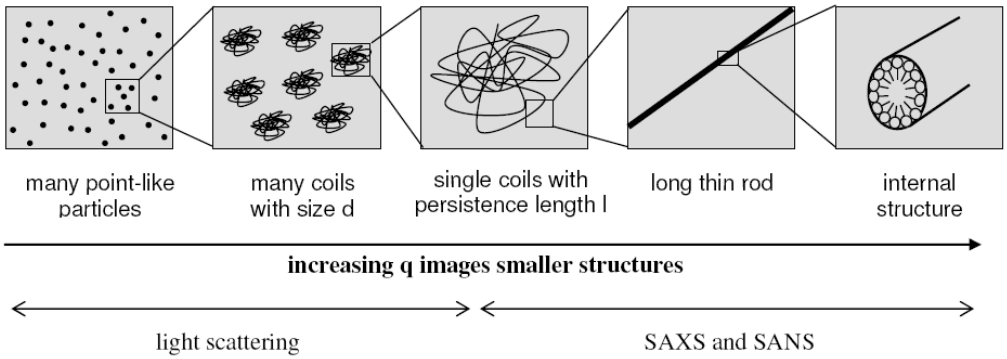

Figure III-5. Representation of q as the observation scale, and its correlation with the scattering technique.

In the case of block copolymer micelles, however, one can have access to the inner structure not only via measurements using large instruments (SANS and SAXS), but also via a rather simple combination of results from SLS and DLS experiments. The following physical chemical parameters can be determined using the approach described below:

- Micelle molar mass ($M_{w,mic}$) - SLS
- Micelle aggregation number (N_{agg}) - SLS
- Radius of gyration (R_g) - SLS
- Interparticle interactions (A_2) - SLS
- Hydrodynamic radius (R_H) - DLS
- Corona thickness (W) - SLS + DLS
- Core radius (R_c) - SLS + DLS
- Compactness of the core ($V_{monomer}$) - SLS + DLS

The N_{agg} is calculated using eqn. III-21, where $M_{w,mic}$ is the micelle molar mass determined by SLS, and $M_{w,unimers}$ is the molar mass of the respective individual block copolymer chains.[227]

$$N_{agg} = \frac{M_{w,mic}}{M_{w,unimers}} \qquad \text{(III-21)}$$

The R_c can be derived from eqn. III-22, where N_A is the Avogadro number, $wt_{hydrophobic}$ is the weight fraction of hydrophobic block in the copolymer chain, $d_{hydrophobic}$ is its solid-state density, and $\Phi_{hydrophobic}$ is its volume fraction in the micelle core, which was assumed to be equal to unity (*i.e.* all the hydrophobic segments chains are located within the micelle core).[227] Thus the volume occupied by a single monomer unit inside the micelle core ($V_{monomer}$) can be estimated from eqn. III-23 on the basis of R_c-values, where $DP_{hydrophobic}$ is the mean degree of polymerization of the hydrophobic block.

$$R_c = \left(\frac{3M_{w,mic} wt_{hydrophobic}}{4\pi N_A d_{hydrophobic} \Phi_{hydrophobic}} \right)^{1/3} \qquad \text{(III-22)}$$

$$V_{monomer} = \frac{4\pi R_c^3}{3N_{agg} DP_{hydrophobic}} \qquad \text{(III-23)}$$

The corona width (W) is then calculated from the following relation

$$W = R_H - R_c \qquad \text{(III-24)}$$

The R_g/R_H ratio is often useful to characterize and block copolymer self-assembly with respect to its morphology.[228, 229] The theoretical value of R_g/R_H for a homogenous hard sphere is 0.779, and it increases substantially for less dense structures. For vesicular structure, R_g/R_H is close to 1, whereas for coils R_g/R_H = 1.5 (θ-solvent) or R_g/R_H = 1.8 (good solvent).

A-2. Transmission Electron Microscopy (TEM)

Imaging techniques are crucial to explore the morphologies of block copolymer aggregates, especially in cases of co-existing morphologies or wide size distributions. Indeed, comprehensive information on nanoparticle systems can be achieved by combining scattering and imaging methods.

In very simple words, transmission electron microscopy (TEM) is a technique where a beam of electrons is focused onto a specimen supported on a thin film, and an enlarged electron scattering map is created using CCD cameras or photographic films. The analysis of copolymer nanoparticles often requires staining to improve the electron contrast. Among

other methods, the negative staining provides high contrast by surrounding or embedding the objects in an electron rich material (Figure III-6). Besides, it has advantage in terms of simplicity and speed of preparation. The staining agent (in most cases an inorganic acid such as sodium phosphotungstate at pH ~ 7.4, or and an organic acid combined with a heavy metal such as uranyl acetate at pH ~ 3.0) should obviously preserve the sample characteristics. As of this work, it must not provoke the demicellization of pH-sensitive chains, and therefore sodium phosphotungstate was chosen.

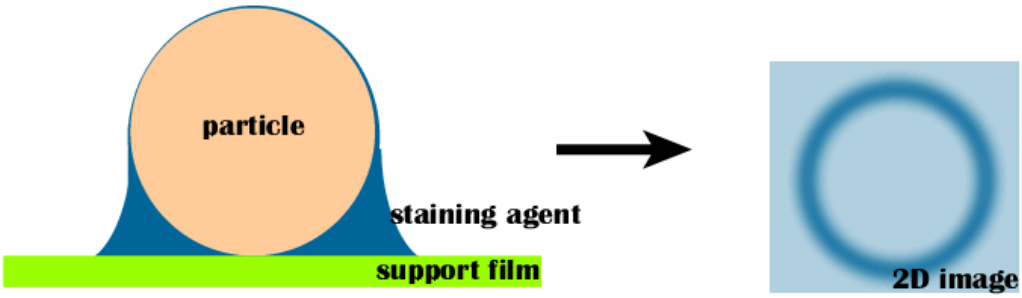

Figure III-6. Schematic representation of a micelle with hydrophilic coronas embedded in a negative staining agent on a hydrophilic support.

Once the processing manipulations have been carefully establish, the most important step of any study is to objectively assess and interpret the observed structural features. In case of copolymer nano-assemblies, not only the characteristics of the particles themselves but also those of the building-blocks (glassy *vs.* rubber-like polymeric chains) can play a decisive role on the imaging results and possibly on the data interpretation. For example, Figure III-7 is a schematic explanation of the difference between soft and hard vesicles when viewed under TEM. Due to the rubber-like wall, the deformed vesicles have an almost constant thickness from the edge to the center and do not show any electron contrast, but hard (or plastic) vesicles do.[230]

Therefore, these experimental observations give emphasis to the correlation between scattering and imaging techniques in the field of block copolymer self-assembly.

It is worth mentioning, however, that for a particle system with a given size distribution and finite polydispersity, TEM analysis will usually undersize the size of particles relative to DLS, because while the former reports a number-average diameter, the latter indicate an intensity-average diameter; the scattered light intensity is higher for larger particles, so that the resulting intensity-average size will tend to be slightly larger that the number-average size.

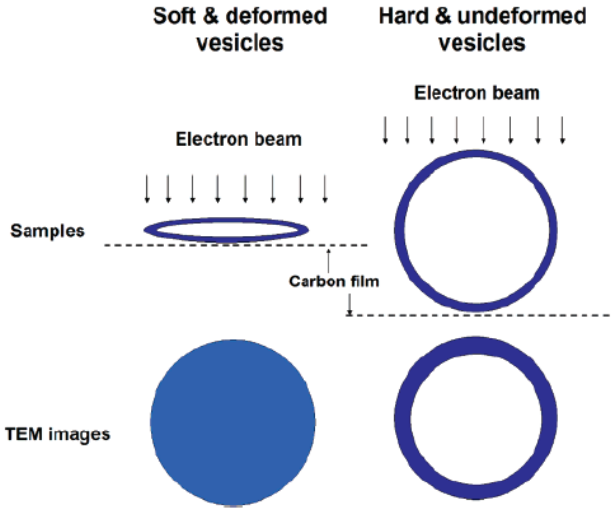

Figure III-7. Illustration of the difference between soft and hard vesicles when viewed under TEM (cartoon proposed by Yang et al).[230]

A-3. Fluorescence Spectroscopy

Fluorescent probes have been widely used in the field of self-assembly to assess the polarity of various microenvironments. Pyrene (and derivatives) is indeed an interesting molecule for these purposes. Its emission spectrum displays several absorption bands, and two among them (F_1 at 372 nm and F_2 at 383 nm for λ_{ex} = 335 nm) are affected the most by the polarity of the probe surroundings, as shown in Figure III-8a. The changes in their relative intensity have been proven to be useful tools to investigate not only self-assembly processes in general, but also the local structure of the resulting objects.[231] In fact, it is possible to follow the transfer of pyrene molecules from the solvent (polar) to inside micellar core (apolar) during the micellization of amphiphilic copolymers in aqueous media. As a consequence, the critical micelle concentration (CMC), which is the copolymer concentration below which only molecularly dissolved chains exist but above which both micelles and single chains are present simultaneously, can be determined as illustrated in Figure III-8b.

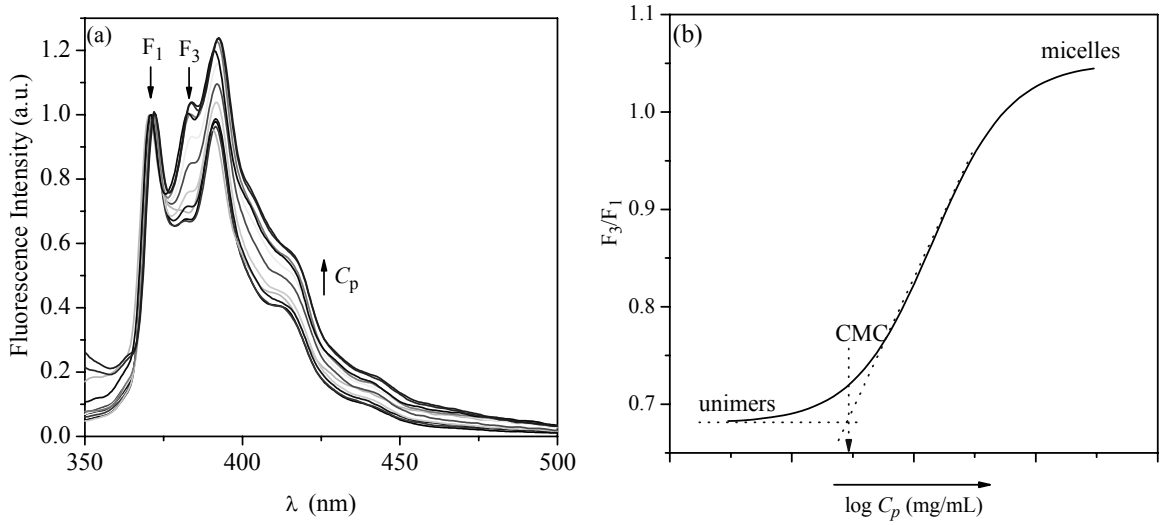

Figure III-8. Pyrene fluorescence emission spectra (a) and the corresponding variation in the F_3/F_1 ratio (b) as a function of the copolymer concentration ($[pyrene]_{ct}$ = 6.0x10^{-7} mol/L, λ_{ex} = 335 nm).

The CMC is relevant in self-assembly processes and therefore in drug delivery applications since it is related to micelle stability, and in turn to the partition coefficient, drug loading efficiency and ultimately to the drug release profile.[107] A micelle is thermodynamically stable with respect to dissociation provided that the copolymer concentration C_p is above the CMC. If C_p < CMC, micelles may still be kinetically stable and survive for a given period of time, which will depend on the characteristics of the core-forming block (size, glass transition temperature, crystallinity, etc).[40, 129]

A-4. Potentiometric Titration

Potentiometric measurements are of particular importance in the study of pH-responsive systems, allowing direct determination of the i) polymerization degree of the weak polybases or weak polyacids, ii) critical micellization pH (pH_{mic}), iii) protonation/deprotonation equilibrium during micellization process, and iv) effects of ionic strength and other additives on charged chains. In the case of PDPA-containing systems (this work), the titration can be modeled as the neutralization of a weak acid with a strong base, where the copolymer comprises DPA repeat units having an average pK_a.[232] Thus, the acid-base equilibrium can be represented as described below, where HP^+ denotes the copolymer with positively charged (protonated) PDPA blocks, H^+ is the proton (note: H^+ is a simplified notation for H_3O^+ ion), and P is the neutralized (deprotonated) copolymer. It is easy to understand that the progressive addition of salt to such systems will cause screening of the charges along the PDPA block,

thus stabilizing the HP^+ species. Consequently, the equilibrium constant, K_a, which is defined by eqn. III-25 and dictates the micellization thermodynamics, decreases due to the change in $[HP^+]$ (square brackets stand for molar concentration), and therefore the micellization process changes.

The average pK_a associated with the DPA groups in PDPA-containing copolymers can be readily estimated from titration curves, being equal to the solution pH at 50% neutralization (i.e., where $[HP^+] = [P]$), whereupon eqn. III-25 simplifies to eqn. III-26.

$$HP^+ \rightleftharpoons P + H^+$$

$$K_a = \frac{[P].[H^+]}{[HP^+]} \qquad \text{(III-25)}$$

$$K_a = [H^+] \therefore pH = pKa = -\log(K_a) \qquad \text{(III-26)}$$

The degree of protonation (or the extent of micellization process) can be approximated by the eqn. III-27, whereas the mean degree of polymerization of the polybase segment can be estimated from eqn. III-28.

$$\alpha = \frac{1}{(1+10^{pH-pKa})} \qquad \text{(III-27)}$$

$$DP(polybase) = \frac{mmolsOH}{mmolsPolymer} \qquad \text{(III-28)}$$

B) Physical Chemical Parameters of the Nano-Assemblies

B-1. Stimulus-Responsive Systems: pH-induced Micellization

B-1-1. PMPC-b-PDPA

Figure III-9 shows typical autocorrelation functions $C(q,t)$ and distributions of the relaxation times $A(t)$ at scattering angle of 90° as revealed by CONTIN analysis for 0.5 mg/mL solutions of (a) $PMPC_{30}$-*b*-$PDPA_{30}$ and (b) $PMPC_{30}$-*b*-$PDPA_{60}$ at pH = 9.0 and I ~ zero (*i.e.*, no added salt; a small amount of NaCl is nevertheless present due to the pH adjustment during the micelle preparation procedure). In both cases (Figures III-9a and III-9b), narrow distributions of relaxation times were obtained, with a single dominant mode corresponding to the diffusive motion of the micelles in solution, whose characteristic hydrodynamic diameter ($2R_H$) was 30 nm for $PMPC_{30}$-*b*-$PDPA_{30}$ and 58 nm for $PMPC_{30}$-*b*-

$PDPA_{60}$. The insets in Figure III-9 depict the typical q^2-dependence of the relaxation frequency (Γ) for diffusive scattering particles.[224]

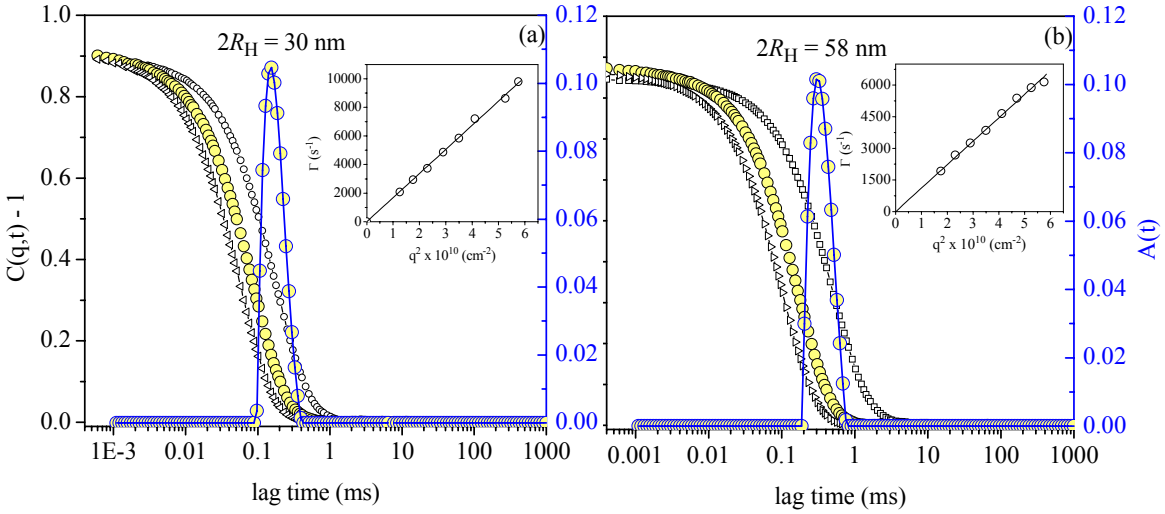

Figure III-9. Autocorrelation functions C(q,t) measured at scattering angles between 50° and 130°, and distributions of the relaxation times A(t) at 90° as revealed by CONTIN analysis for 0.50 mg/mL solutions of (a) $PMPC_{30}$-*b*-$PDPA_{30}$ and (b) $PMPC_{30}$-*b*-$PDPA_{60}$ at pH = 9.0 and zero added salt.

The molecular features of PMPC-*b*-PDPA unimers at pH = 3.0 are characteristic of a diblock linear polyelectrolyte (the PMPC chains have permanent zwitterionic character and the PDPA chains are cationic at this pH due to protonation). The variation in hydrodynamic diameter ($2R_H$) as a function of the solution pH at different ionic strengths (I) is shown in Figure III-10. Micellar aggregates formed by the pH-induced self-assembly of the copolymer with the shorter hydrophobic block ($PMPC_{30}$-*b*-$PDPA_{30}$; Figure III-10a) presented virtually the same $2R_H$ values (ca. 30 nm) regardless of the ionic strength. In contrast, the $2R_H$ of the $PMPC_{30}$-*b*-$PDPA_{60}$ micelles (Figure III-10b) decreased from 58 nm at I ~ zero down to 38 nm at I = 0.10 mol/L. However, in both cases a shift in the critical micellization pH (pH_{mic}) occurred, which corresponds to the inflection point of the sigmoidal curves shown in Figure III-10. The pH_{mic} was accurately determined from acid-base titration experiments (see below).

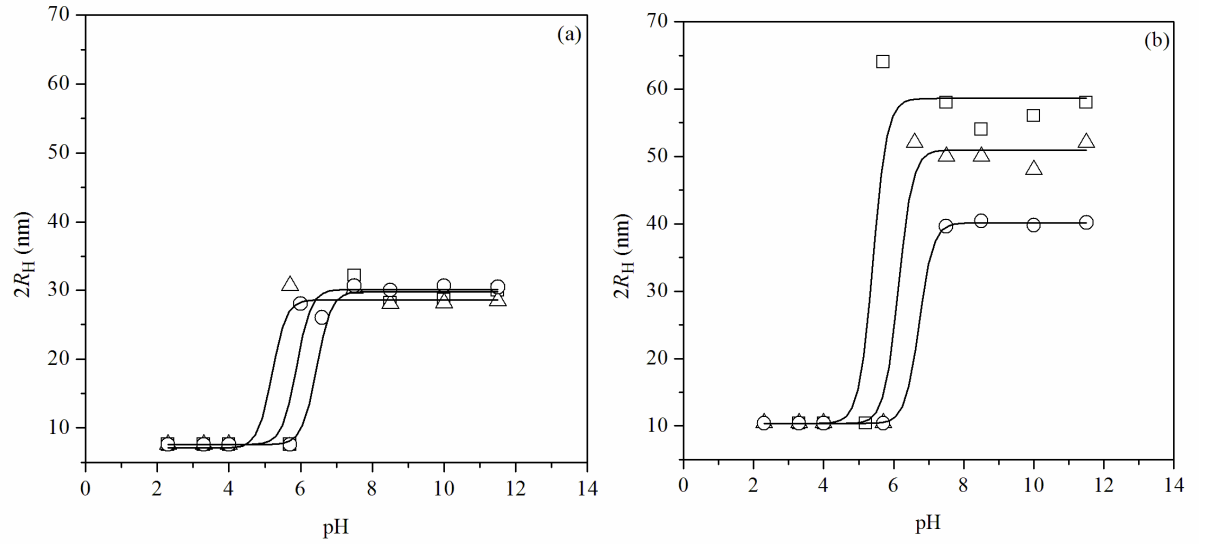

Figure III-10. Variation of hydrodynamic diameter ($2R_H$) with solution pH at different ionic strengths (I ~ zero, □; I = 0.05 mol/L,△; I = 0.1 mol/L,○) (I) for (a) $PMPC_{30}$-*b*-$PDPA_{30}$ and (b) $PMPC_{30}$-*b*-$PDPA_{60}$ solutions.

The effect of adding salt on the properties of micelles consisting polyelectrolyte-type coronas (*e.g.* polystyrene-b-poly(acrylic acid) (PS-*b*-PAA) micelles has been extensively studied by Eisenberg.[73] In general, charge screening leads to a reduction in the coil dimensions and, in turn, in the corona width. Conversely, the addition of salt after micellization does not affect the properties of $PMPC_{30}$-*b*-$PDPA_{60}$ micelles initially prepared at I ~ zero, while $PMPC_{30}$-*b*-$PDPA_{30}$ micelles are unaffected by ionic strength neither before nor after micellization. This unique behavior is most likely due to the polyzwitterionic nature of the PMPC block, which minimizes the effect of ionic strength on local charges at the coronal chains.

Hence, the differences in terms of size observed in Figure III-10b ($PMPC_{30}$-*b*-$PDPA_{60}$ micelles) are attributable to changes in the micelle aggregation number (N_{agg}) and micelle molar mass ($M_{w,mic}$).

The existence of a narrow, unimodal particle size distribution for the micelles formed by the $PMPC_{30}$-*b*-$PDPA_{30}$ (Figure III-9a) and $PMPC_{30}$-*b*-$PDPA_{60}$ (Figure III-9b) copolymers in aqueous solution allowed SLS measurements to be carried out with very high accuracy. Figure III-11 shows typical Zimm plots obtained for $PMPC_{30}$-*b*-$PDPA_{30}$ (Figure III-4a) and $PMPC_{30}$-*b*-$PDPA_{60}$ (Figure III-4b) micelles investigated in this work, and the values of R_g (or $2R_g$), A_2 and $M_{w,mic}$ were calculated after extrapolation to $C_p \rightarrow 0$ and $q \rightarrow 0$.

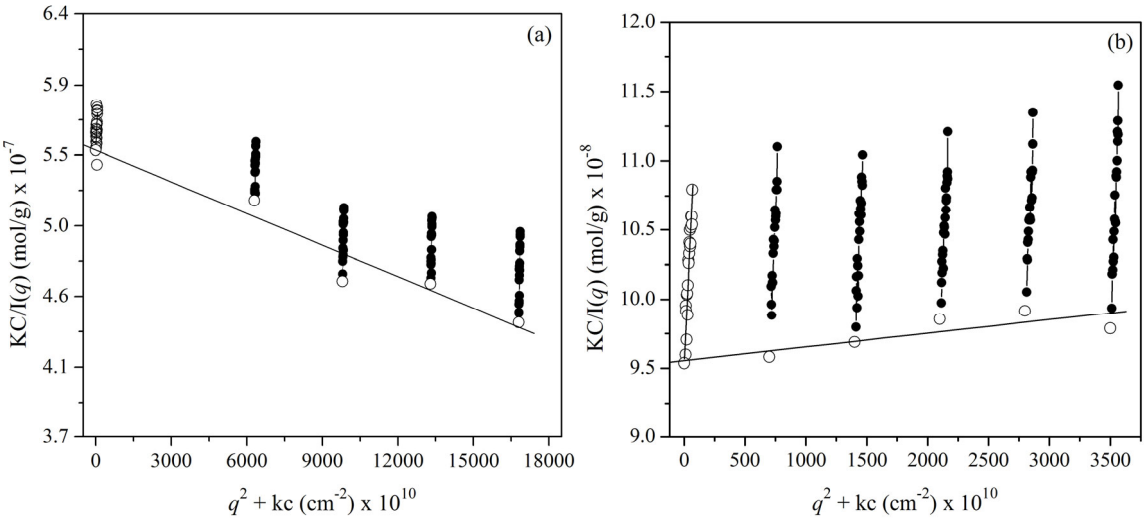

Figure III-11. Typical Zimm plots (a,b) and C_p-dependence of the averaged light scattering intensity (c,d) obtained for aqueous micellar solutions of (a,c) $PMPC_{30}$-*b*-$PDPA_{30}$ (C_p = 1.8 – 4.8 mg/mL) and (b,d) $PMPC_{30}$-*b*-$PDPA_{60}$ (C_p = 0.2 – 1.0 mg/mL).

According to results summarized in Table III-1, the micellar self-assembly of PMPC-*b*-PDPA block copolymers exhibiting different volume fractions of DPA (ϕ_{DPA}) clearly results in well-defined but structurally distinct nano-objects. At low ionic strength (*i.e.* no added salt), the increase in the PDPA block length induces a significant increase in the micelle molar mass ($M_{w,mic}$) from 1.82 x 10^6 g/mol for $PMPC_{30}$-*b*-$PDPA_{30}$ to 1.05 x 10^7 g/mol for $PMPC_{30}$-*b*-$PDPA_{60}$. Such behavior reflects a substantial change in the respective N_{agg} from 130 to 500, respectively. Likewise, the $2R_g$ and $2R_H$ values increase significantly on increasing the mean degree of polymerization (DP) of the PDPA block (Table 2). The R_g/R_H values for $PMPC_{30}$-*b*-$PDPA_{30}$ and $PMPC_{30}$-*b*-$PDPA_{60}$ micelles are 0.86 and 0.92, respectively, suggesting the formation of approximately spherical micellar aggregates.[233]

Although the micelles studied in this work are spherical, their structures can vary significantly. Assuming that the terminal oligo(ethylene glycol)-based fragment (from the ATRP initiator) has typical C—C and C—O bond lengths of 1.53 and 1.43 Å, respectively, the corona width (W) value should be around 10 nm (the 2-bromoisobutyryl spacer at the block junction not included). Inspecting Table III-1, the highly hydrophilic PMPC chains are clearly stretched into the solvent (W = 11 nm) in the case of $PMPC_{30}$-*b*-$PDPA_{60}$ micelles. In contrast, a coil-like conformation is most likely present for the $PMPC_{30}$-b-$PDPA_{30}$ micelles, since W is only 5 nm. Such variation in W-values is accompanied by changes in the micelle core diameter ($2R_c$), which are obviously due to the increase in the length of the core-forming block. Considering that all the PDPA chains are located inside the micelle core, it is also observed that the volume occupied by a single DPA repeat unit is smaller for more

hydrophobic $PMPC_{30}$-*b*-$PDPA_{60}$ micelles (0.57 nm^3/monomer) than for $PMPC_{30}$-*b*-$PDPA_{30}$ micelles (0.84 nm^3/monomer) (Table III-1). This suggests that the core is more compact in the former case. From a drug delivery point of view, these aspects clearly have implications for drug loading efficiency, drug release kinetics and micelle stability.

Table III-1. Physical chemical parameters of PMPC-*b*-PDPA micelles obtained by combining SLS and DLS results.

$PMPC_x$-*b*-$PDPA_y$	$M_{w,mic}$ (g/mol)	N_{agg}	$2R_H$ (nm)	$2R_g$ (nm)	R_g/R_H	$2R_c$ (nm)	W (nm)	$V_{monomer}$ nm^3/monomer
30-30	$1.82x10^6$	130	28.0	24.2	0.86	18.4	4.8	0.84
30-60	$1.05x10^7$	500	54.2	50.0	0.92	32.2	11.0	0.57

The results in Figure III-11a and III-11b also indicate gradients of opposite sign for the two straight lines generated by extrapolating the $\frac{KC_p}{I(q)}\Big|_{q\to 0}$ values to zero C_p, from which the second virial coefficients (A_2) were estimated as being -1.33 x 10^{-8} mol L/g^2 and 1.38 x 10^{-9} mol L/g^2 for $PMPC_{30}$-*b*-$PDPA_{30}$ and $PMPC_{30}$-*b*-$PDPA_{60}$ copolymers, respectively. The A_2 parameter depends on the inter-particle interactions in solution. Whereas A_2 is zero for θ-conditions, it is positive in the case of inter-particle repulsions, and negative in the case of attractive interactions. Unfortunately, it is not possible to draw reliable conclusions for these small A_2 values obtained for our systems. Besides, it is well-known that A_2 obtained by SLS for micelles may depend not only on the solvent nature but also on the surface tension at the core-corona interface.

Figure III-12 shows a representative plot for the q^2-dependence of the averaged light scattering intensity for 0.1 mg/mL $PMPC_{30}$-*b*-$PDPA_{60}$ micellar solutions prepared at different ionic strengths (I). As $q \to 0$, eqn. III-14 can be rewritten in the form of eqn. III-29, which can be further simplified to eqn. III-30 if the $2A_2C_p$ term is negligible. Assuming that A_2 is of the order of 10^{-8} mol L/g^2 (see above) regardless of the ionic strength, $2A_2C_p$ term is approximately two orders of magnitude lower than $1/M_w$ (~ 10^{-7} mol/g) for C_p = 0.1 mg/mL.

$$\frac{KC_p}{I(q)}\Big|_{q\to 0} = \frac{1}{M_w} + 2A_2C_p \qquad \text{(III-29)}$$

$$\frac{KC_p}{I(q)}\Big|_{q\to 0;\,2A_2C_p\to 0} = \frac{1}{M_w} \qquad \text{(III-30)}$$

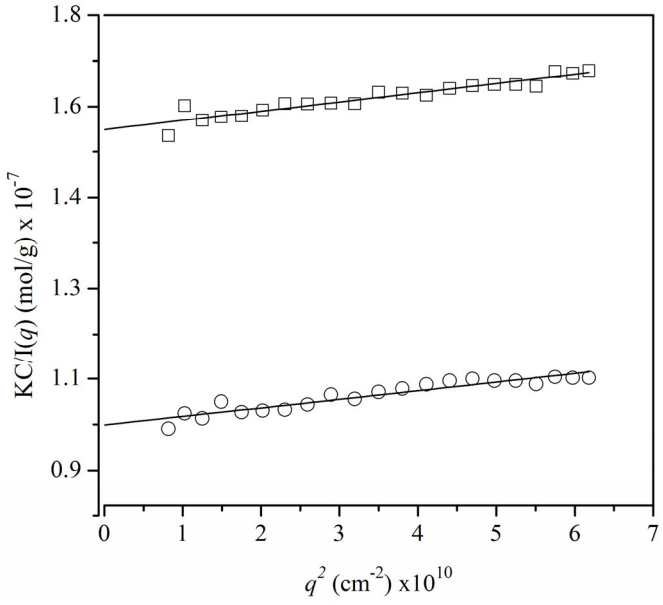

Figure III-12. q^2-dependence of the averaged light scattering intensity for 0.10 mg/mL $PMPC_{30}$-*b*-$PDPA_{60}$ micellar solutions prepared at $I \sim$ zero (○) and $I = 0.10$ mol/L (□) .

$M_{w,mic}$ calculated from eq. 11 is 1.0 x 10^7 g/mol at $I \sim$ zero and 6.3 x 10^6 g/mol at $I = 0.1$ mol/L. Under these conditions N_{agg} decreases from ca. 476 to ca. 300 with increasing I. Thus it is obvious that varying the ionic strength primarily affects the polymer chain conformation prior to micellization, rather than electrostatic shielding effects between adjacent chains within the micellar corona. This interpretation seems reasonable since, below the critical micellization pH, the molecularly dissolved diblock copolymer comprises a polyzwitterionic-type PMPC block and a cationic PDPA block, which is certainly sensitive to the presence of added counter-ions.

Figure III-13 shows TEM images of negatively stained $PMPC_{30}$-*b*-$PDPA_{60}$ micelles prepared at (a) $I \sim$ zero and (b) $I = 0.1$ mol/L. In general, narrowly distributed nano-sized spherical micelles are observed in Figures III-13a and III-13b. The mean micelle diameter in these micrographs ($2R$ = 40 - 50 nm at $I \sim$ zero and $2R$ = 20 - 30 nm at $I = 0.1$ mol/L) are evidently smaller than those determined by DLS measurements. The reasons for these observations were discussed above. The images shown in Figure III-13 corroborate the observed differences in terms of $M_{w,mic}$, $2R_H$ and N_{agg} revealed by DLS (Figure III-10b) and SLS (Figure III-12) experiments, as deduced by comparing the mean micellar diameters in Figures III-13a and III-13b.

The comments above also apply to micrographs taken for $PMPC_{30}$-*b*-$PDPA_{30}$ micelles (not shown) prepared using the same protocol, except that no noticeable size differences were observed on varying the ionic strength.

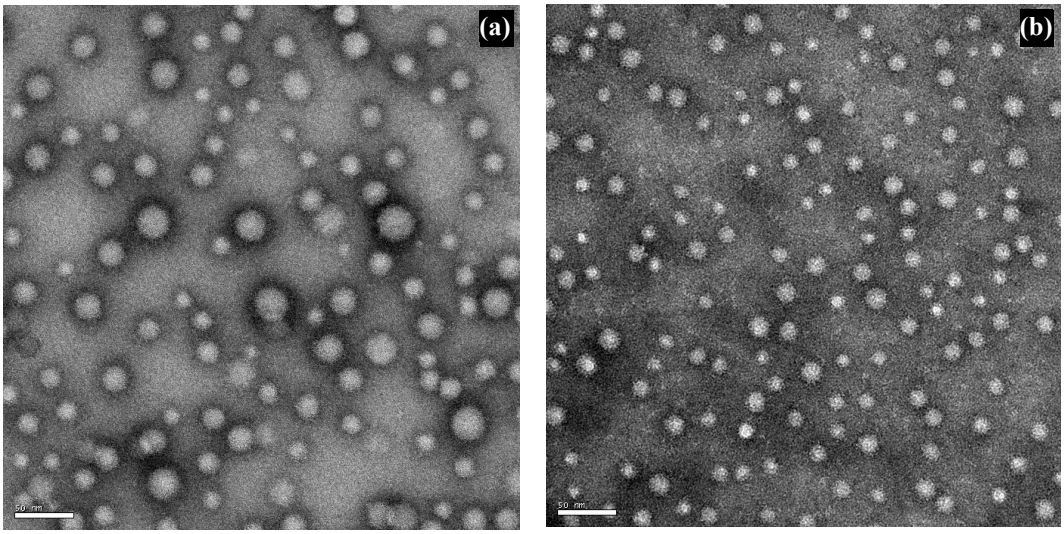

Figure III-13. TEM images of negatively stained $PMPC_{30}$-*b*-$PDPA_{60}$ micelles prepared at (a) I ~ zero and (b) I = 0.10 mol/L. Scale bar is 50 nm.

Potentiometric measurements were performed in order to gain insight into the effect of ionic strength on the copolymer chains prior, and during the micellization process. Figure III-14 shows the potentiometric titration curves for 0.5 mg/mL $PMPC_{30}$-*b*-$PDPA_{60}$ copolymer solutions at different ionic strengths (no added salt; 0.05 mol/L and 0.10 mol/L). The small amounts of additional salt inevitably formed during titration were not taken into account. Starting from pH ~ 3, the addition of small amounts of NaOH increases the solution pH until a plateau is reached. In this buffering region, the added NaOH is consumed by the titration of the tertiary amine groups on the DPA repeat units, leading to micellization. After this process is complete, further addition of base merely elevates the solution pH. The average pK_a clearly depended on the salt concentration (ionic strength), varying from 5.7 (no added salt) up to 6.6 (I = 0.1 mol/L) (Figure III-14), as discussed above. These findings indicate that the critical micellization pH (pH_{mic}) of PMPC-*b*-PDPA copolymers vary, and can be controlled by adjusting the ionic strength. The same observations also apply to the $PMPC_{30}$-*b*-$PDPA_{30}$ copolymer (data not shown).

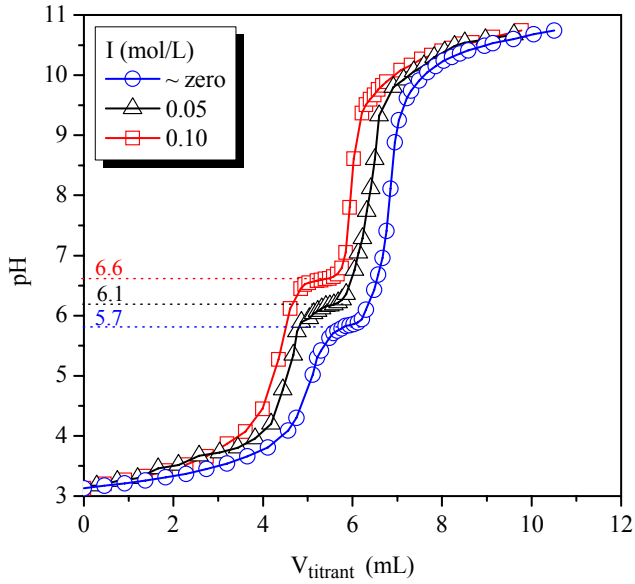

Figure III-14. Potentiometric acid-base titration curves for 0.50 mg/mL $PMPC_{30}$-*b*-$PDPA_{60}$ solutions at different ionic strengths, as indicated ($V_{aliquot}$ = 10.0 mL; 8 mmol/L NaOH as titrant).

The CMC values for the PMPC-*b*-PDPA diblocks were determined by fluorescence spectroscopy using pyrene as probe. In the case of $PMPC_{30}$-*b*-$PDPA_{30}$ and $PMPC_{30}$-*b*-$PDPA_{60}$ these values were found to be 0.025 and 0.014 mg/mL, respectively. As expected, the longer the core-forming block, the lower the CMC because the chains segregate earlier from the aqueous environment in order to minimize the unfavorable interactions with the selective solvent.

The CMC values obtained for the PMPC-*b*-PDPA system are slightly lower than, for example, those reported for PEO_{25}-*b*-PPO_{38}-*b*-PEO_{25} and PEO_{148}-*b*-PPO_{56}-*b*-PEO_{148} copolymers (0.03 – 0.3 mg/mL),[234] but somewhat higher than those determined for PEO_{45}-*b*-PCL_{21} (0.0028 mg/mL).[235]

B-1-2. PEO-b-PDPA

Micellar nanoparticles can originate from self-assembly of PEO-*b*-PDPA system via different approaches, as we discussed previously. Hereinafter, pH-induced and indirect dissolution methods were investigated, with emphasis to the former.

Using the pH-based method, it was observed that PEO-*b*-PDPA behaves similarly to PMPC-*b*-PDPA, and therefore representative results that illustrate globally the characteristics of the nanoparticles are shown in the sequence. Figure III-15 displays the autocorrelation

functions C(q,t) and distributions of the relaxation times A(t) at scattering angle of 90° as revealed by CONTIN analysis for 0.5 mg/mL solutions of (a) PEO_{45}-*b*-$PDPA_{47}$ and (b) PEO_{113}-*b*-$PDPA_{50}$ at pH = 9.0 and I ~ zero. In both cases, one relaxation mode associated with the diffusive behavior of vesicles (a) and spherical core-shell micelles (b) was evidenced. The polymer concentration (within the range of interest in the present case) had a minor influence on this system. Second cumulant analyses applied to C(q,t) functions generally yielded $\mu_2/\Gamma^2 < 0.25$. The narrow polydispersity and the morphology of PEO-*b*-PDPA assemblies were also corroborated by TEM experiments (Figure III-16).

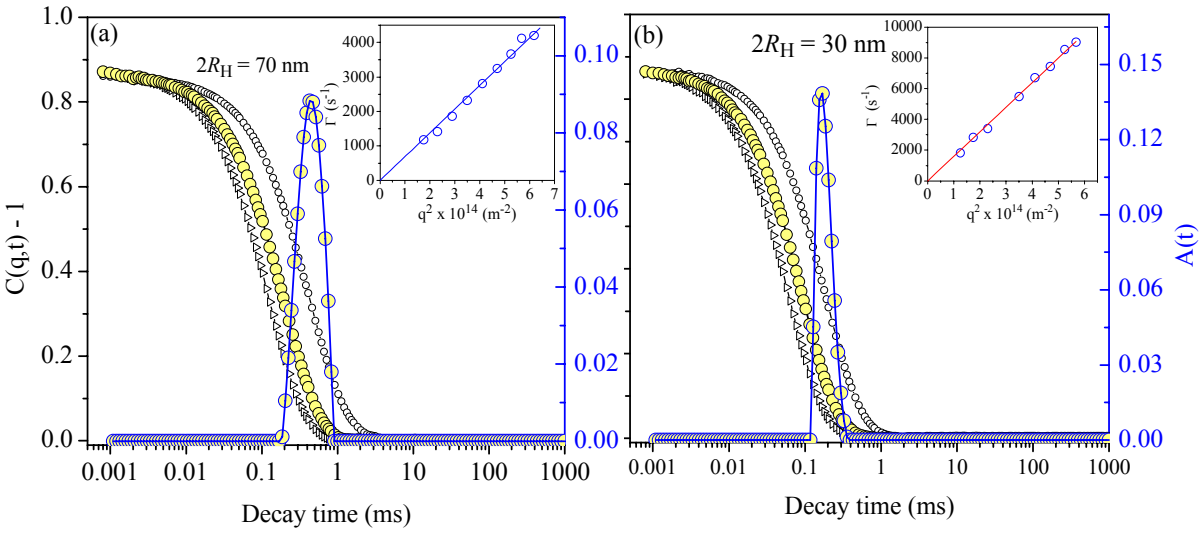

Figure III-15. Autocorrelation functions C(q,t) measured at scattering angles between 50° and 130°, and distributions of the relaxation times A(t) at 90° by CONTIN analysis for 0.50 mg/mL solutions of (a) PEO_{45}-*b*-$PDPA_{47}$ and (b) PEO_{113}-*b*-$PDPA_{50}$ at pH = 9.0 and I ~ zero.

The variations in the morphology and hydrodynamic diameter of the resulting nanoparticles as a function of the composition, molar mass and block copolymer architecture (di- or triblock) are summarized in Table III-2. It was observed that copolymers with $\phi_{PDPA} \geq 0.76$ favored the formation of vesicles (entries 2, 3 and 8, Table III-2), while spherical micelles were obtained for samples presenting $\phi_{PDPA} < 0.76$, in very good agreement with theoretical and experimental studies on morphology transitions in block copolymer assemblies.[42, 78, 236] However, highly hydrophobic chains (entry 4, $\phi_{PDPA} = 0.93$, Table III-2) collapsed during the early stages of the preparation procedure, yielding very opaque solutions with sedimentation.

Among the samples exhibiting spherical core-shell micellar morphology (entries 5 – 7, and 9 – 10 in Table III-2, for instance), the hydrodynamic size increased with degree of

polymerization of the PDPA segment, but did not follow the scaling laws observed earlier for star and crew-cut micelles in organic media prepared by direct dissolution.[237]

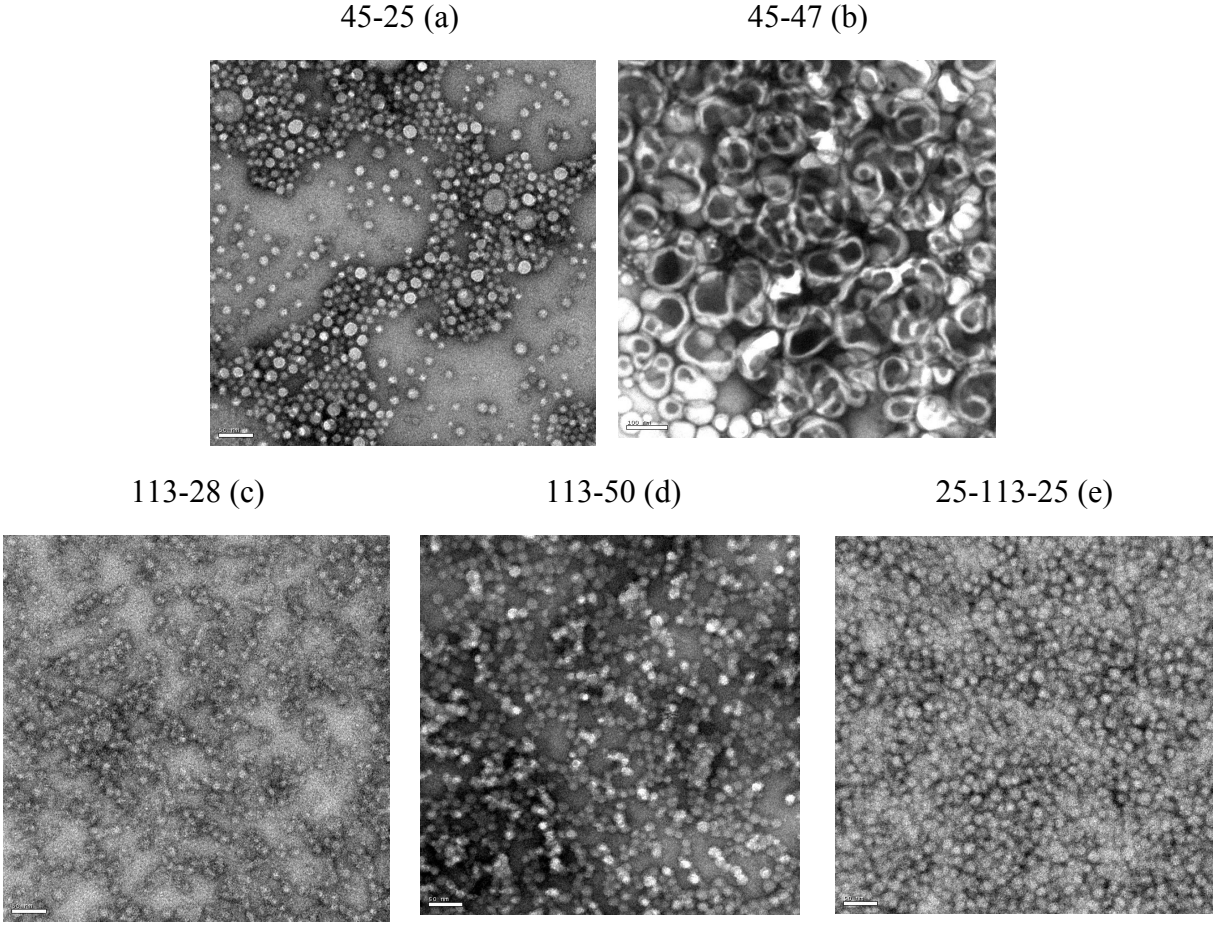

Figure III-16. TEM images of negatively stained PEO_x-*b*-$PDPA_y$ micelles. Scale bar = 50 nm (a,c,d,e) or 100 nm (b)

Table III-2: Hydrodynamic diameter ($2R_H$) and morphology of PEO-*b*-PDPA nano-objects.

Entry	PEO_x-*b*-$PDPA_y$	ϕ_{PDPA}	$2R_H$ (nm)	Morphology[a]
1	45-25	0.72	30	M
2	45-47	0.83	70	V
3	45-85	0.90	190	V
4	45-120	0.93	Precipitate	
5	113-12	0.34	20	M
6	113-28	0.54	22	M
7	113-50	0.68	30	M
8	113-74	0.76	132	V
9	16-106-16	0.58	20	M
10	25-106-25	0.68	34	M

[a] Dominant morphology of self-assemblies by TEM observations (M = Micelles; V = Vesicles).

To better understand such variations in the micellar structure, SLS measurements were carried out on three selected samples (Figure III-17). The properties of the block copolymer nanoparticles were estimated using dilute solutions (C_p = 0.1 mg/mL) and assuming that the second virial coefficient A_2 for the PEO-*b*-PDPA micelles is in the order of 10^{-8} mol L/g^2 (A_2 ~ 10^{-9} – 10^{-8} mol L/g^2 for PMPC-*b*-PDPA[54] and PEO-*b*-PDEA[164] systems). The contribution from $2A_2C_p$ term at the rhs of eqn. III-14 can thus be neglected, so that $\left.\frac{KC}{I(q)}\right|_{q\to 0} \cong \frac{1}{M_{w,mic}}$, since $1/M_{w,mic} > 10^{-7} – 10^{-6}$ mol/g and $A_2 \sim 10^{-9}$ mol L/g^2.

The apparent $M_{w,mic}$-values extracted from the linear coefficients of straight lines in Figure III-17, and physical chemical parameters then calculated, are listed in Table III-3. The results indicate that changes in the length of the core-forming segment and copolymer architecture were at the origin of self-assemblies with different inner structures in terms of N_{agg}, R_H, R_c and W. Definitely, a very interesting architecture effect was evidenced for PEO_{113}-*b*-$PDPA_{50}$ and $PDPA_{25}$-*b*-PEO_{106}-*b*-$PDPA_{25}$ copolymers, which have nearly the same M_n and ϕ_{DPA}. The triblock revealed a clear tendency to give nanoparticles with larger core radius and slightly thicker corona width. The increase in the W-values for the triblock (even if weakly pronounced) was a surprising result, inasmuch as the PEO chains should form loops at the corona in this case, and the opposite behavior would be more obvious. Apparently, the PEO chains in triblock copolymer micelles are much more stretched out (almost twice) into solvent than for its diblock analogous (see Figure III-18).

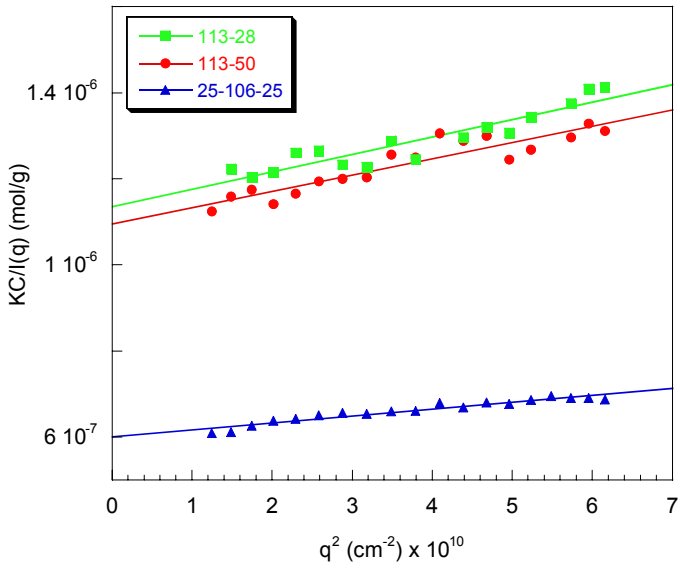

Figure III-17. q^2-dependence of the averaged light scattering intensity for 0.10 mg/mL PEO_x-*b*-$PDPA_y$ micellar solutions prepared at I ~ zero.

Table III-3. Physical chemical parameters of PEO-*b*-PDPA micelles obtained by combining SLS and DLS results.

PEO_x-*b*-$PDPA_y$	$M_{w,mic}^{app}$ (g/mol)	N_{agg}	$2R_H$ (nm)	$2R_c$ (nm)	W (nm)	$V_{monomer}$ nm^3/monomer
113-28	$8.81x10^5$	80	22	11.4	5.3	0.36
113-50	$9.13x10^5$	58	30	12.6	8.7	0.36
25-106-25	$1.66x10^6$	110	34	15.2	9.4	0.33

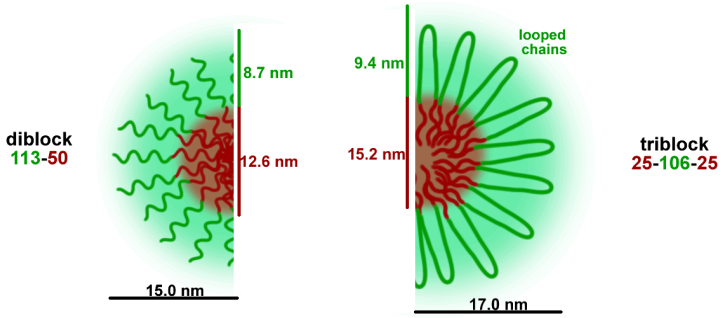

Figure III-18. Structure of PEO_{113}-*b*-$PDPA_{50}$ and $PDPA_{25}$-*b*-PEO_{106}-*b*-$PDPA_{25}$ micelles.

PEO-*b*-PDPA *vs.* PMPC-*b*-PDPA systems: the corona-forming block effect

The careful analysis of the data in Tables III-1 and III-3 suggests a significant effect of the corona-forming block structure on the properties of micelles containing PDPA-based cores. First, as characterized by the larger volume occupied by a monomer unity ($V_{monomer}$) in the former case, the core is apparently less compact in PMPC-*b*-PDPA than in PEO-*b*-PDPA micelles; $V_{monomer}$ decreased from ~ 0.70 down to ~ 0.35 nm^3/DPA (in average) upon substitution of PMPC by PEO in the micellar corona. Second, PMPC chains are more stretched into the solvent than PEO chains; roughly, the same W-values were observed for both systems while the end-to-end distance (fully extended linear chains) of hydrophilic block are 9.2 nm and 49.6 nm for PMPC and PEO, respectively, assuming C—C = 1.53 Å and C—O = 1.43 Å. Finally, at approximately constant hydrophobic block length, larger nanoparticles (higher N_{agg}) can be obtained using PMPC as hydrophilic block.

It should be noted, nevertheless, that such remarks may not necessarily be valid when different experimental conditions are used to prepare the nanoparticles.

B-1-3. PEO-b-PG2MA-b-PDPA

During the developing stages of the roadmap initially envisioned for this thesis, we found out that micellar nanocarriers having weak polybase-based cores were able to encapsulate enormous amounts of hydrophobic guest molecules when those exhibited antagonist weak carboxylic acid groups (see hereinafter in *Chapter IV*). This was indeed the case of PEO-*b*-PDPA micelles, for example. They do exhibit an excellent cargo potential, but also show a major drawback in relation to the lack of stability in different pH conditions. Even though the pH-triggered release is of course very attractive from a drug delivery perspective, it might not be desirable in other fields such as in the cosmetic and flavor-masking.

Therefore, in order to broaden the range of applications of these excellent-performance well-defined micellar carriers, it is necessary to develop strategies to stabilize them while keeping their cargo functionality. Any approach to be undertaken to achieve this goal should 1) use block copolymers soluble in organic solvents that are miscible with water – high loading is only observed by micellization from organic media –, 2) be performed after loading/micellization and in aqueous media and 3) not affect the micellar core.

We elected to use a triblock copolymer able to form three layered core-shell-corona micelles, whose inner shell is cross-linkable. To this end, the methodology formerly proposed by Armes et al.[182] was adapted to fit into our purpose.

The triblock PEO_{113}-*b*-$PG2MA_{30}$-*b*-$PDPA_{50}$ was then prepared in a convenient one-pot ATRP-based procedure (*Chapter II*). The length of the middle $PG2MA_{30}$ segment was deliberately chosen to be short in order to ensure the solubility of the resulting macromolecule in organic medium (namely in THF). In spite the fact that PEO_{113}-*b*-$PG2MA_{30}$ diblocks are insoluble in THF (see results in *Section C-2-3* for PEO-*b*-(PG2MA-IND)), when the third $PDPA_{50}$ block was present, the triblock polymer could be easily solubilized in the mentioned solvent. Very interestingly, however, was the fact that ^{1}H NMR analysis of 10 mg/mL PEO_{113}-*b*-$PG2MA_{30}$-*b*-$PDPA_{50}$ in THF-d_8 (Figure III-19) revealed the near complete absence of PG2MA chemical shifts (see spectrum in Figure II-13 for comparison). In Figure III-19, the signal at δ = 2.9 ppm corresponds to the -C(O)OCH$_2$C$\underline{\boldsymbol{H}}_2$N(*i*Pr)$_2$ protons of the PDPA block. As one can deduce from the integrals between 3.9 – 3.6 ppm (-C(O)OC$\underline{\boldsymbol{H}}_2CH_2$N(*i*Pr)$_2$, 2H), 1.9 – 1.6 ppm (-C$\underline{\boldsymbol{H}}_2$- from the backbone, 2H) and 1.3 – 0.6 ppm (-C$\underline{\boldsymbol{H}}_3$- methacrylic protons and –C-(C$\underline{\boldsymbol{H}}_3$)$_2$ isopropyl protons, 15H), only PDPA protons appear in the spectrum. Such a result is indicative of aggregation involving the solvophobic PG2MA block. Hence, the PEO_{113}-*b*-$PG2MA_{30}$-*b*-$PDPA_{50}$ triblock straightforwardly self-assembles in THF. The

hydrodynamic size ($2R_H$) of the resulting nano-objects was about 28 nm, as judged from DLS measurements shown Figure III-20. Their morphology most likely correspond to (reverse) spherical micelles, since the volume fraction of PG2MA block is low ($\phi_{PG2MA} = 0.24$).[42, 78]

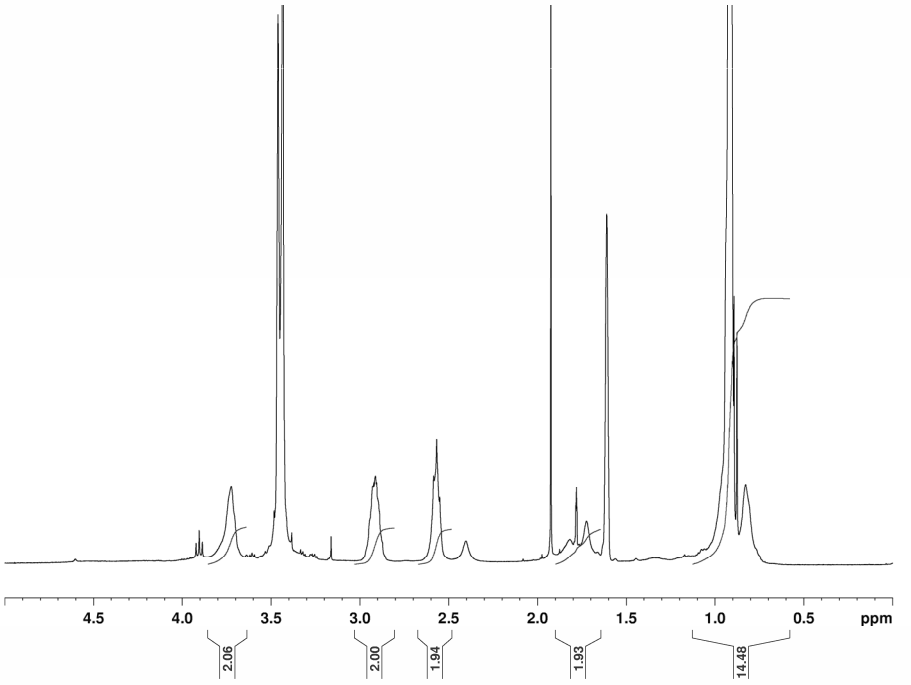

Figure III-19. ^{1}H NMR spectra of 10.0 mg/mL PEO_{113}-*b*-$PG2MA_{30}$-*b*-$PDPA_{50}$ in THF-d_8 (selective solvent for PEO and PDPA blocks).

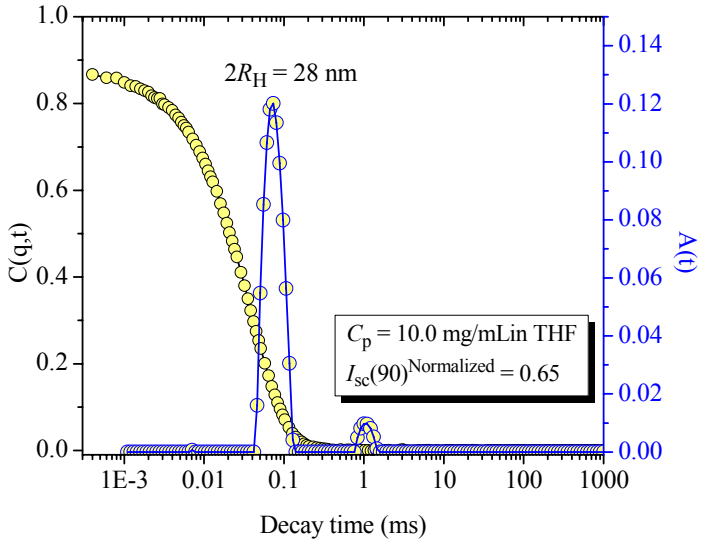

Figure III-20. Autocorrelation function *C*(q,t) measured at scattering angle of 90°, and the corresponding distribution of the relaxation times *A*(t) by CONTIN analysis for 10.0 mg/mL PEO_{113}-*b*-$PG2MA_{30}$-*b*-$PDPA_{50}$ in THF.

Upon the addition of water to such a solution in THF, the pre-assembled aggregates self-reversed to form the so-called three layered (onion-like) core-shell-corona micelles, as illustrated in Figure III-21. DLS measurements shown in Figure III-22 revealed the presence

of 31-nm sized particles in the resulting aqueous solutions after evaporation of the organic phase. A contribution from large aggregates (see the shoulder in the intensity-averaged A(t) profile) was also observed for this system.

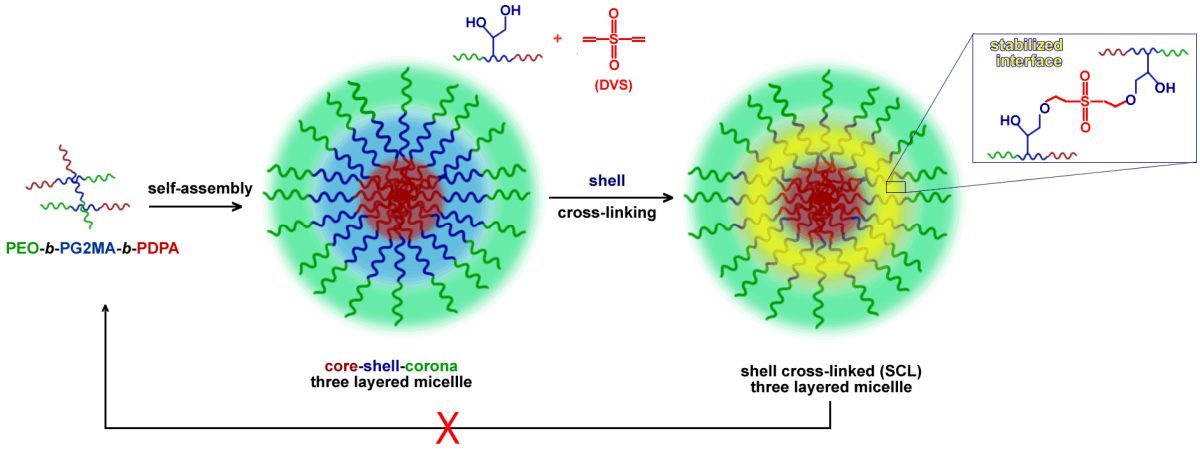

Figure III-21. Self-assembly of PEO-*b*-PG2MA-*b*-PDPA triblocks into three layered core-shell-corona micelles and the selective cross-linking of their inner shell using DVS.

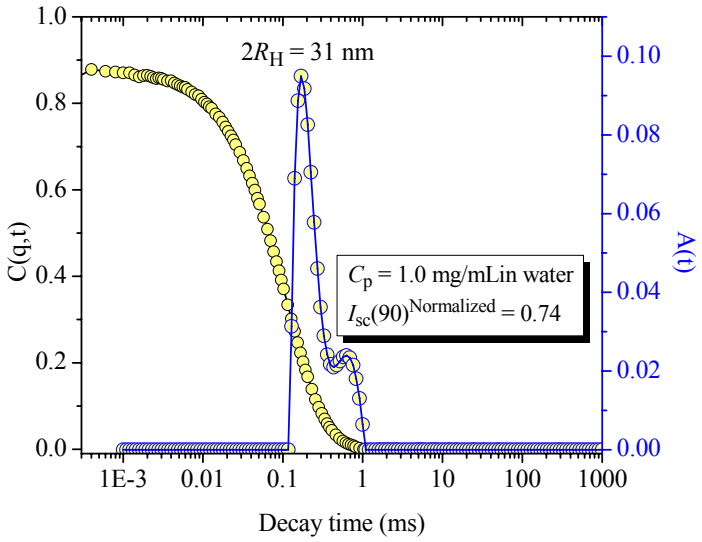

Figure III-22. Autocorrelation function C(q,t) measured at scattering angle of 90°, and the corresponding distribution of the relaxation times A(t) by CONTIN analysis for 1.0 mg/mL PEO_{113}-*b*-$PG2MA_{30}$-*b*-$PDPA_{50}$ in water.

The covalent stabilization of these micelles was then performed via Michael addition chemistry, through the reaction of the pendant hydroxyl groups of PG2MA block with the di-functional cross-linking agent divinyl sulfone (DVS) (Figure III-21, right).[238-241]

DVS, which is prone to hydrolysis in aqueous media but reacts quicker with G2MA, was added directly to the aqueous micellar solution, and the latter was stirred during 24 h at room temperature prior the analysis. The unreacted DVS and other possible by-products were not removed from the medium in this work. We note, nevertheless that dialysis methods would be

suitable to eliminate any undesirable low molecular weight water-soluble compounds, as reported by Wooley et al.[175] for the cross-linking of PAA by 2,2'-(ethylenedioxy)diethylamine. Furthermore, dilute copolymer solutions (C_p = 1.0 mg/mL) were used in order to minimized eventual inter-micelle cross-linking, even though the outer PEO-shell should in principle prevent such phenomena by protecting each individual particle from its neighbors.

The efficiency of such an approach was evaluated by SLS experiments under acid conditions. To this, the solution pH originally at 7.4 was adjusted to 3.0 after the reaction. If no shell cross-linking had occurred, micellar dissociation into individual triblock copolymer chains would be expected, since the DPA core block becomes soluble under these conditions.

Figure III-23 shows the variation of the ratio between the scattered light intensity at pH = 3.0 (successive to cross-linking and pH lowering) and at pH = 7.4 (before cross-linking and pH adjustment) as a function of the [DVS]/[PG2MA] molar ratio. Clearly, non-SCL (regular) micelles dissociated straightforwardly upon decreasing the solution pH, and the scattered light intensity dropped to nearly zero (first filled symbol). However, when small amounts of DVS were used (first open symbol; [DVS]/[PG2MA] = 0.10), the nanoparticles remained in solution provided that the scattered light intensity was still about 50 – 60 % of the initial value. The DLS intensity-average size distributions of regular and SCL PEO_{113}-*b*-$PG2MA_{30}$-*b*-$PDPA_{50}$ micelles indicated a significant increase in the size of the objects upon cross-linking and pH lowering, as demonstrated in Figure III-24.

Such a behavior is in part attributable to the swelling of the micellar core under acid conditions, leading to much less compact objects. Indeed, the PDPA-core forming block is positively charged in acid media, being therefore hydrophilic and well-solvated. The disassembly is however prevented by the covalently stabilized PG2MA shell.

It is also worth to observe that no inter-micelle cross-linking occurred, since large aggregates were not detected by DLS.

The stability of these cross-linked high-payload pH-responsive PEO-*b*-PG2MA-*b*-PDPA micelles was also corroborated by visual inspection of loaded systems, which under acid environment were able to keep their payload stabilized with no apparent precipitation (see digital photographs in *Chapter IV*), which straightforwardly occurs for regular micelles.

Through this approach, not only the stability of the nano-carriers is guaranteed, but also their biocompatibility thanks to the permanent PEO external layer, which will avoid exposition of inner segments.

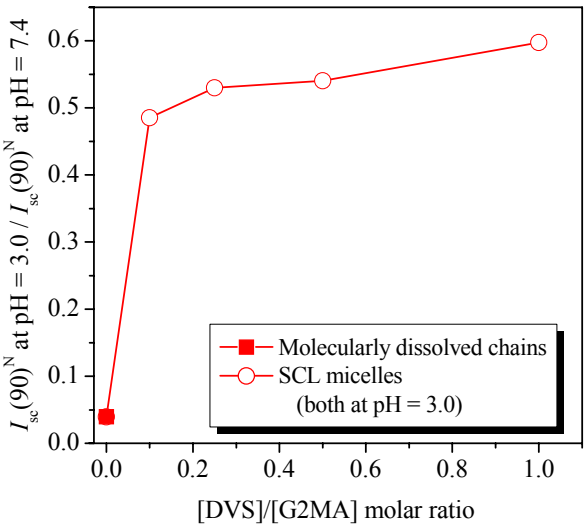

Figure III-23. Variation in the ratio between the scattered light intensities at pH = 3.0 and at pH = 7.4 as a function of the [DVS]/[PG2MA] molar ratio.

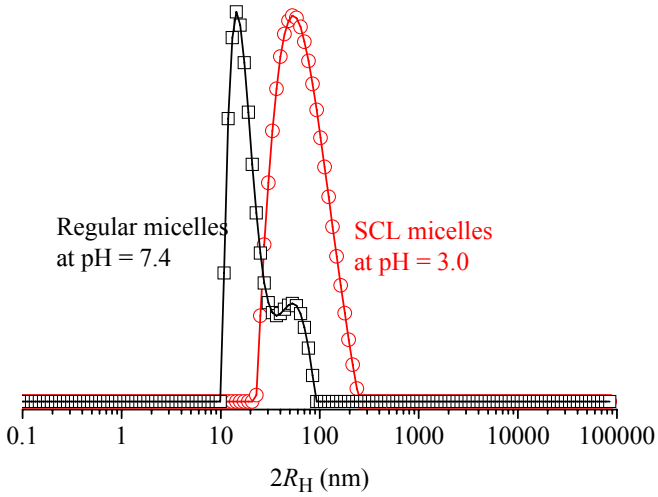

Figure III-24. Distributions of the hydrodynamic diameter ($2R_H$) obtained by DLS using CONTIN analysis for PEO_{113}-*b*-$PG2MA_{30}$-*b*-$PDPA_{50}$ micelles before and after core cross-liking (SCL) followed by pH lowering to 3.0.

B-2. Non-Responsive Systems: Micellization from Organic Medium

B-2-1. PEO-b-PCL

The micellization behavior of PEO-*b*-PCL diblock copolymers with distinct molar masses and volume fractions (Table II-5) is described in this section. The physicochemical parameters of the micellar nano-objects originated from their self-assembly using three different water-miscible organic solvents (DMF, THF and acetone) are summarized in Table

III-4. Several attempts to gain insight into micellar structure by SLS were unfortunately not successful due to non-negligible aggregation phenomena (slow relaxation mode) as the polymer concentration was varied. In fact, such an observation is quite usual for objects presenting PEO-bases coronas.

As observed in Table III-4, all PEO-*b*-PCL samples self-assembled into spherical micelles when either DMF or THF is used as organic solvent to dissolve them before the micellization. Striking different, regular wormlike morphologies were however obtained using acetone as solvent for copolymers with $\phi_{PCL} = 0.50 – 0.58$, as detailed in the sequence.

Table III-4. Physical chemical parameters of PEO-*b*-PCL self-assemblies in water.

Copolymer	DMF		THF		Acetone	
	$2R_H$ (nm)	Morphology[c]	$2R_H$ (nm)	Morphology[c]	$2R_H$ (nm)[c]	Morphology[c]
45-9[a]	16	S	16	S	16	S
45-24[a]	20	S	20	S	60/200/600	W
114-24[b]	40	S	80	S	120	S
114-44[b]	60	S	100	S	80/210/700	W

[a] C_p = 1.0 mg/mL;
[b] C_p = 0.5 mg/mL;
[c] Dominant morphology observed by TEM and/or cryo-TEM experiments; S: spherical; W: wormlike.

Spherical micelles prepared from DMF or THF solutions

Typical autocorrelation functions $C(q,t)$ and distributions of the relaxation times $A(t)$ at scattering angle of 90° as revealed by CONTIN analysis for selected samples (1.0 mg/mL PEO_{45}-*b*-PCL_{24} (A) and 0.5 mg/mL PEO_{114}-*b*-PCL_{44} (B)) prepared from THF are shown in Figure III-15. In general, narrow distributions of relaxation times were observed for the dominant mode, which corresponds to the diffusive motion of the spherical micelles in solution, whose morphology was confirmed by TEM (see below). Their characteristic hydrodynamic diameter ($2R_H$) depended on the overall polymerization degree (DP) of both PEO and PCL segments (Table III-4), irrespective of the organic solvent employed to prepare them. In general, $2R_H$-values increased with the length of the constituting blocks. These results are in very good agreement with other reports suggesting that the size of micelles is controlled by several factors, among which are the length of the corona- and core-forming blocks.[54, 132, 227] However, while the size of PEO_{45}-*b*-$PCL_{y\ (y = 9\ or\ 24)}$ micelles prepared from

DMF or THF was basically the same, PEO_{114}-*b*-$PCL_{y\ (y\ =\ 24\ or\ 44)}$ originated slightly bigger micelles in THF (see data in Table III-4).

The existence of a slow relaxation mode was regularly observed for all PEO-*b*-PCL micellar solutions, as illustrated in Figure III-15 for two selected samples. The respective distribution amplitude decreased upon dilution, thus suggesting their dynamical behavior. Such large macromolecular aggregates (200–700 nm) are probably formed of small individual micelles, as indeed proposed earlier by Allen *et al.*[134, 242] for PEO_{44}-*b*-PCL_{20} micellar solutions.

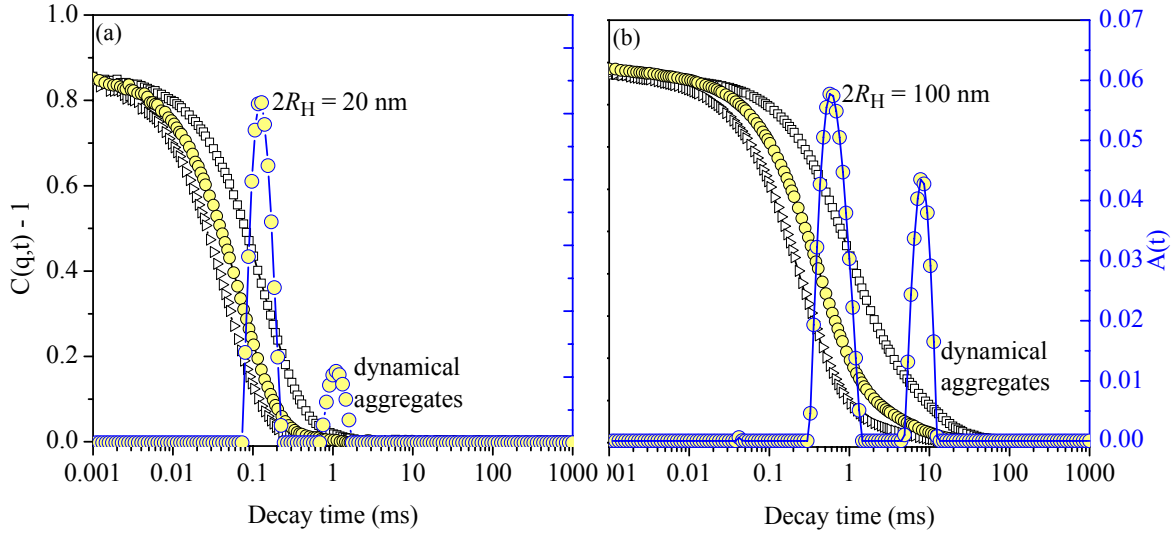

Figure III-25. Autocorrelation functions *C*(q,t) measured at 60°, 90° and 120° scattering angles and distributions of the relaxation times *A*(t) at 90° as revealed by CONTIN analysis for (a) 1.0 mg/mL PEO_{45}-*b*-PCL_{24} and (b) 0.5 mg/mL PEO_{114}-*b*-PCL_{44} micellar solutions prepared using THF as organic solvent.

The spherical morphology of PEO-*b*-PCL micelles prepared using either DMF or THF during initial stages of their preparation was clearly confirmed by TEM experiments, which are shown in Figure III-26 for (a) PEO_{45}-*b*-PCL_9 and (b) PEO_{45}-*b*-PCL_{24} solutions. These micrographs revealed rather monodisperse nano-sized spherical micelles. It is worth to note that no large objects were observed by TEM, hence further suggesting the dynamical behavior of the large aggregates observed in DLS measurements (slow relaxation mode). The above comments also apply to micrographs (not shown) taken for the other samples listed in Table III-4 and prepared using either DMF or THF.

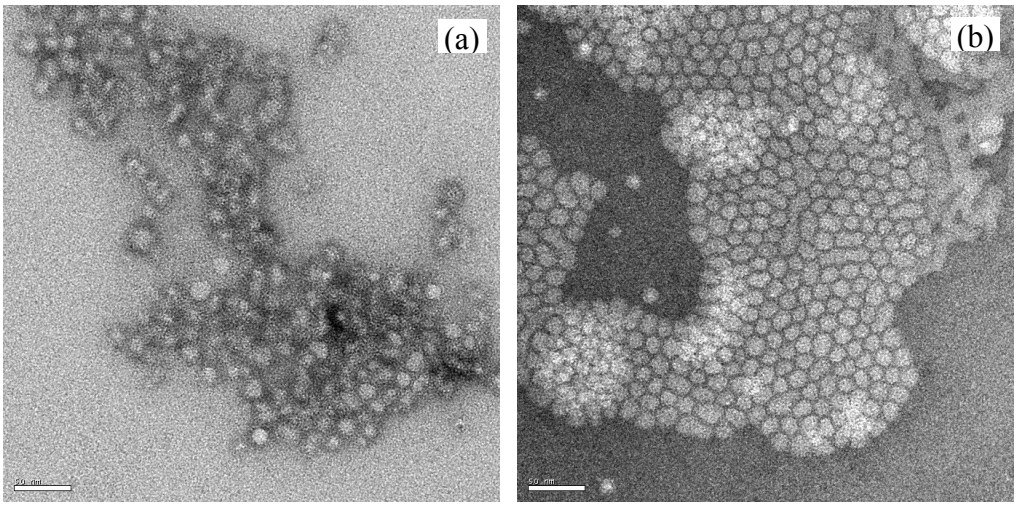

Figure III-26. TEM images of (a) PEO_{45}-*b*-PCL_9 and (b) PEO_{45}-*b*-PCL_{24} micelles prepared using THF as organic solvent. Scale bar = 50 nm.

Wormlike micelles prepared from acetone solutions

When PEO-*b*-PCL diblock copolymers with ϕ_{PCL} = 0.50 – 0.58 were firstly dissolved in acetone, extended cylindrical (wormlike) micelles were formed upon self-assembling in aqueous solutions. For these solutions, DLS measurements revealed multiple (at least three) decay times. Such a behavior is illustrated in Figure III-27, which shows the autocorrelation functions $C(q,t)$ and the distributions of the relaxation times $A(t)$ at three scattering angles ($\theta = 50°$, 90° and 120°) as revealed by CONTIN analysis for 1.0 mg/mL PEO_{45}-*b*-PCL_{24} solutions prepared from acetone. In this figure, it is possible to observe that the amplitude associated to the largest particles is much higher at low θ ($\theta = 50^o$, small q). Besides, the total scattered intensity recorded at $\theta = 50^o$, for instance, was higher than that measured at $\theta = 130^o$, thus suggesting heterogeneous distribution of sizes within the different observation scales reached by varying the scattering angle (or q-values). Also, the relaxation frequencies (Γ) associated to each process eventually deviated from its linear q^2-dependence.

Indeed, direct imaging experiments carried on these micellar solutions have corroborated that self-assembling PEO-*b*-PCL block copolymers from acetone originates wormlike or extended cylindrical morphology instead of spherical. Figure III-28 shows TEM and cryo-TEM micrographs taken exactly for the same solution as that one in Figure III-27. Wormlike objects with nearly constant cross-sectional diameter and lengths of at least several microns are manifestly evident. Examination of large area micrographs shows long cylinders to be the dominant species in solutions, with only occasionally small individual spherical particles

(Figure III-28a). Such well-defined structures probably do exist in solution, since cryo-TEM allows for direct visualization of the aggregate structures in water. In addition, both electron microscopy techniques (cryo-TEM and TEM) gave similar results.

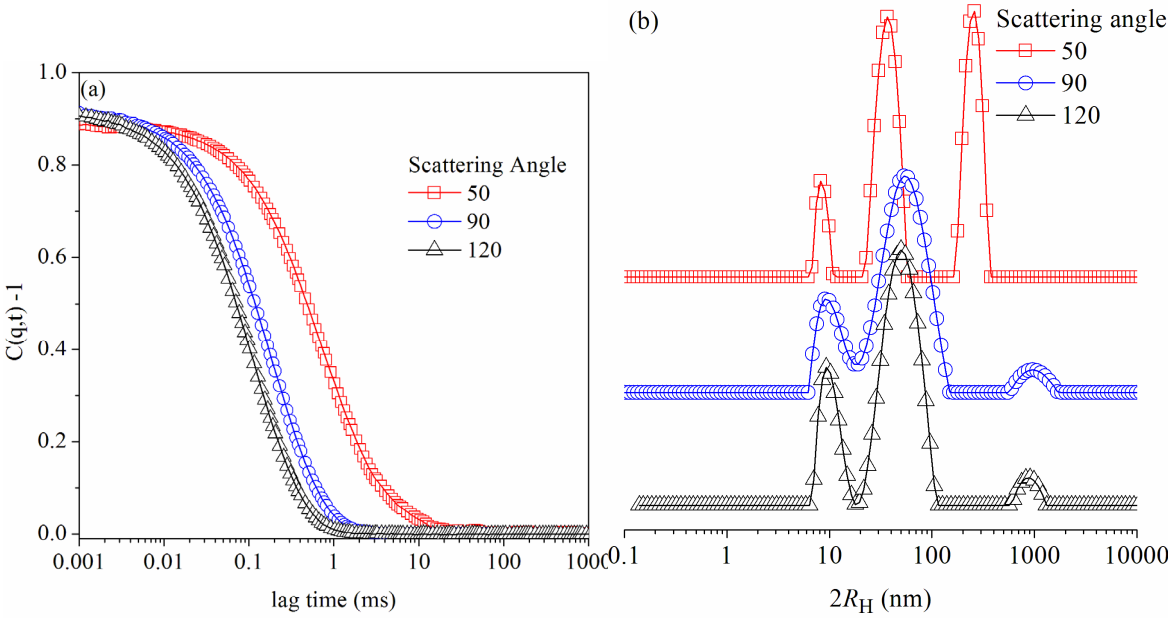

Figure III-27. (a) Autocorrelation functions $C(q,t)$ measured at 50°, 90° and 120° scattering angles and (b) respective distributions of the relaxation times $A(t)$ as revealed by CONTIN analysis for 1.0 mg/mL PEO_{45}-*b*-PCL_{24} micellar solutions prepared using acetone as organic solvent.

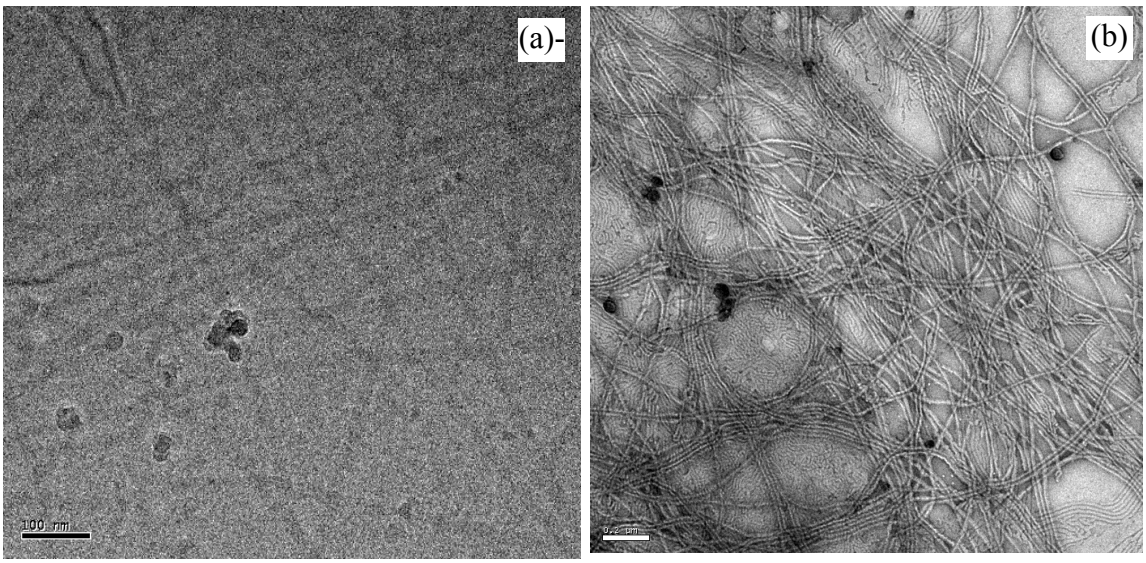

Figure III-28. Cryo-TEM (a) and TEM (b) images of PEO_{45}-*b*-PCL_{24} wormlike micelles prepared using acetone as organic solvent. Scale bar = (a) 100 nm and (b) 200 nm.

B-2-2. PEO-b-PGMA

Spherical core-shell micelles with epoxy-based cross-linkable cores were prepared by indirect dissolution method using THF as organic solvent. Figure III-29a shows the autocorrelation functions $C(q,t)$ and distributions of the relaxation times $A(t)$ at scattering angle of 90° for 0.7 mg/mL PEO_{113}-*b*-$PGMA_{50}$ micellar solutions. In general, narrowly distributed nanoparticles were formed, whose spherical morphology was confirmed by TEM (Figure III-29b). Their characteristic hydrodynamic diameter ($2R_H$) depended on the overall polymerization degree (DP) of PGMA segment ($2R_H$ = 34 nm for PEO_{113}-*b*-$PGMA_{35}$ $2R_H$ = 42 nm for PEO_{113}-*b*-$PGMA_{50}$). Importantly, no substantial difference could be identified using DMF as organic solvent.

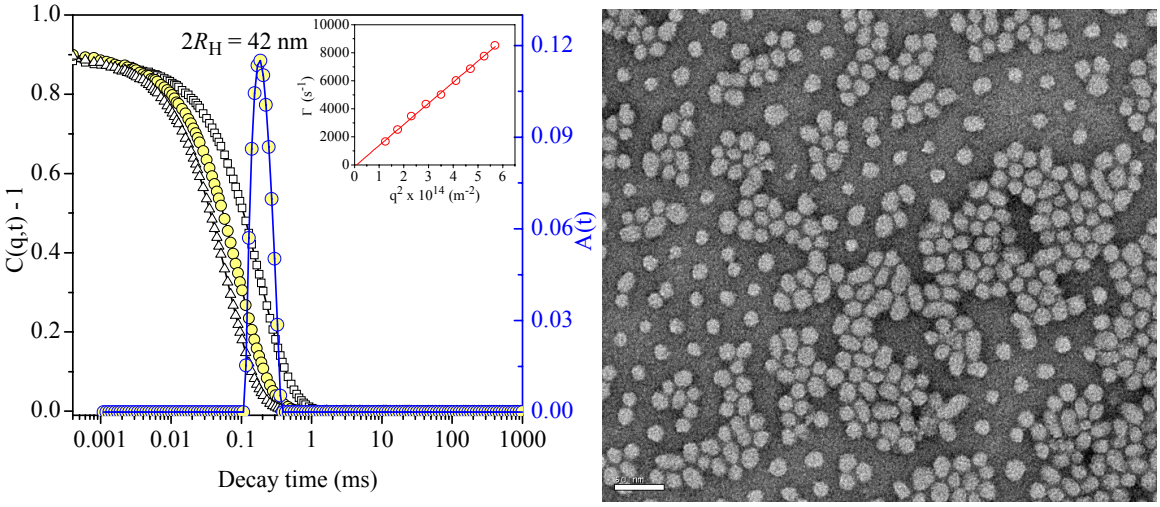

Figure III-29. (a) Autocorrelation functions $C(q,t)$ measured at scattering angles between 60° and 120°, and distributions of the relaxation times $A(t)$ at 90° by CONTIN analysis for 0.7 mg/mL solutions of PEO_{113}-*b*-$PGMA_{50}$ and (b) the respective TEM micrograph. Scale bar = 50 nm.

Core cross-linked micelles

The interest in the use of GMA-compartmented structures relies on the possibility of obtaining permanently stable objects via cross-linking using primary alkyl diamines, as illustrated in Figure III-30. Indeed, this was demonstrated in a parallel independent work published by Zhu et al.[188] dealing exactly with the same copolymer. In the cited study, however, the authors were interested in PEO-*b*-PGMA vesicles (with reactive epoxy walls) formed by copolymer chains having higher ϕ_{GMA} than ours (see also *Chapter I, Section B-6*).

Here, it was anticipated that after diffusion through the PEO corona, the diamine would encounter the hydrophobic reactive epoxy barrier (the PGMA core), then undergoing a cross-linking reaction at the core-corona interface. Afterward, the diamine excess can be easily removed by dialysis.

A primary water-soluble diamine was therefore added to the system following the micellization, and the stability of the resulting objects (in a good solvent) was verified by DLS experiments. Figure III-31 demonstrates that after cross-linking (ethylenediamine (final content = 5 % v/v) was added to a PEO_{113}-*b*-$PGMA_{50}$ micellar solution, which was stirred at room temperature overnight) followed by dilution with DMF (final content = 87 % v/v; good solvent for both blocks) the nanoparticles still remained in solution. The increase in the hydrodynamic size observed in Figure III-31 is ascribed mainly to the swelling of the core by DMF. When the same experiment was carried out on regular micelles, the scattered intensity after dilution was very low and close to that of the solvent ($I_{sc}(90)N \sim 0.04$).

Essentially the same results were reported by Zhu et al.,[188] who employed a rather different approach to perform the stabilization of PEO-*b*-PGMA vesicular walls, through the addition of an hydrophobic primary diamine prior the micellization process (*i.e.* to the organic solvent).

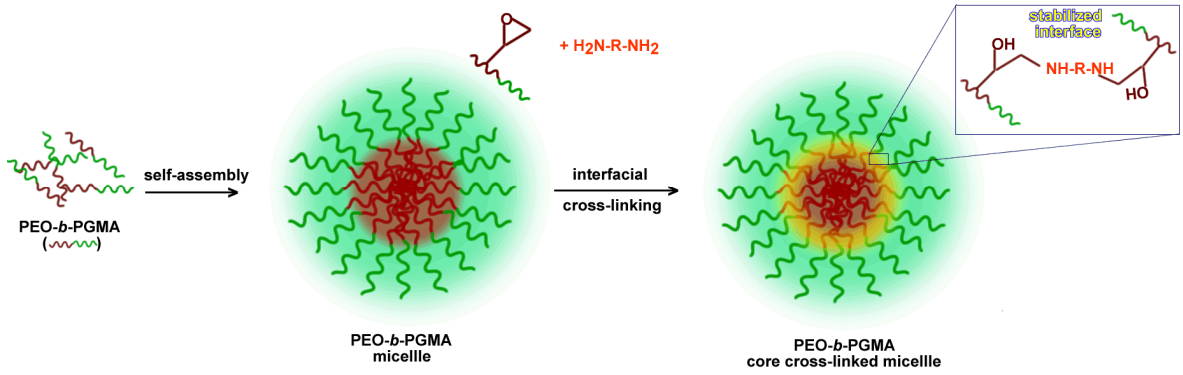

Figure III-30. Formation of core cross-linked micelles via reaction of epoxy-based core and primary alkyl diamines.

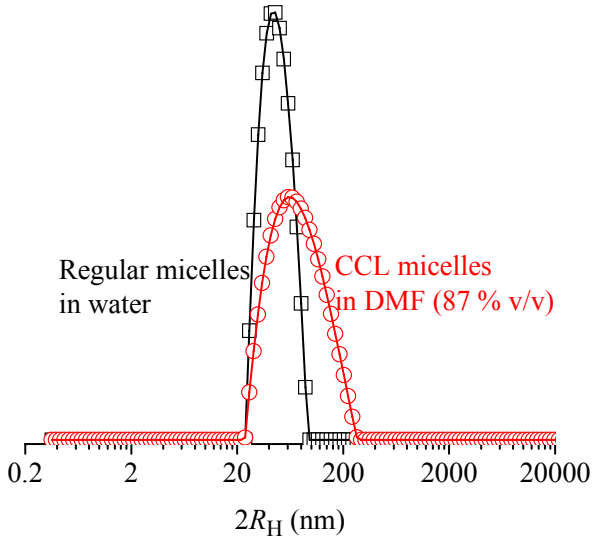

Figure III-31. Distributions of the hydrodynamic diameter ($2R_H$) obtained by DLS using CONTIN analysis for PEO-*b*-PGMA micelles before and after core cross-liking (CCL) followed by dilution with DMF. Solvent viscosity was corrected as follows: $\eta_{water} = 0.89$ cP; $\eta_{DMF\ 87\%} = 0.83$ cP; $\eta_{mixture} = 0.83x0.87 + 0.89x(1-0.87)$.

B-2-3. PEO-b-(PG2MA-IND)

The solution behavior of PEO-*b*-PG2MA and PEO-*b*-(PG2MA-IND) copolymers is schematized in Figure III-32, which is based on DLS measurements carried out for solutions corresponding to steps **I** – **IV**, as depicted in Figure III-33. For instance, PEO_{113}-*b*-$PG2MA_{85}$ is a double hydrophilic diblock copolymer and dissolves molecularly in water (unimers with hydrodynamic size $2R_H$ = 6 – 8 nm, Figure III-33a). However, it becomes amphiphilic upon conjugation to indomethacin, and the PEO_{113}-*b*-($PG2MA_{85}$-IND_{29}) polymer-drug conjugate can then be molecularly dissolved, for example, in THF (unimers with $2R_H$ = 7 – 10 nm in THF, Figure III-33b). In these two later cases, very low scattered light intensities were recorded. The addition of a selective solvent (water at pH = 7.4) to situation **II** (Figure III-32) induces self-assembly, leading to well-defined spherical micelles (Figure III-33c), which contain a hydrophobic drug linked covalently to the core through acid-sensitive ester bounds. The relaxation frequency is q^2-dependent (see insets) for all the systems, thus characterizing the diffusive behavior of scattering particles.

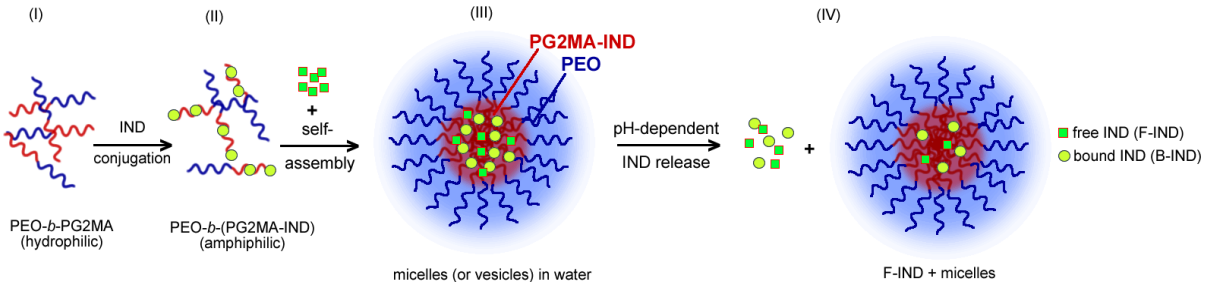

Figure III-32. Solution behavior of amphiphilic PEO-*b*-(PG2MA-IND) polymer-drug conjugates and their precursors.

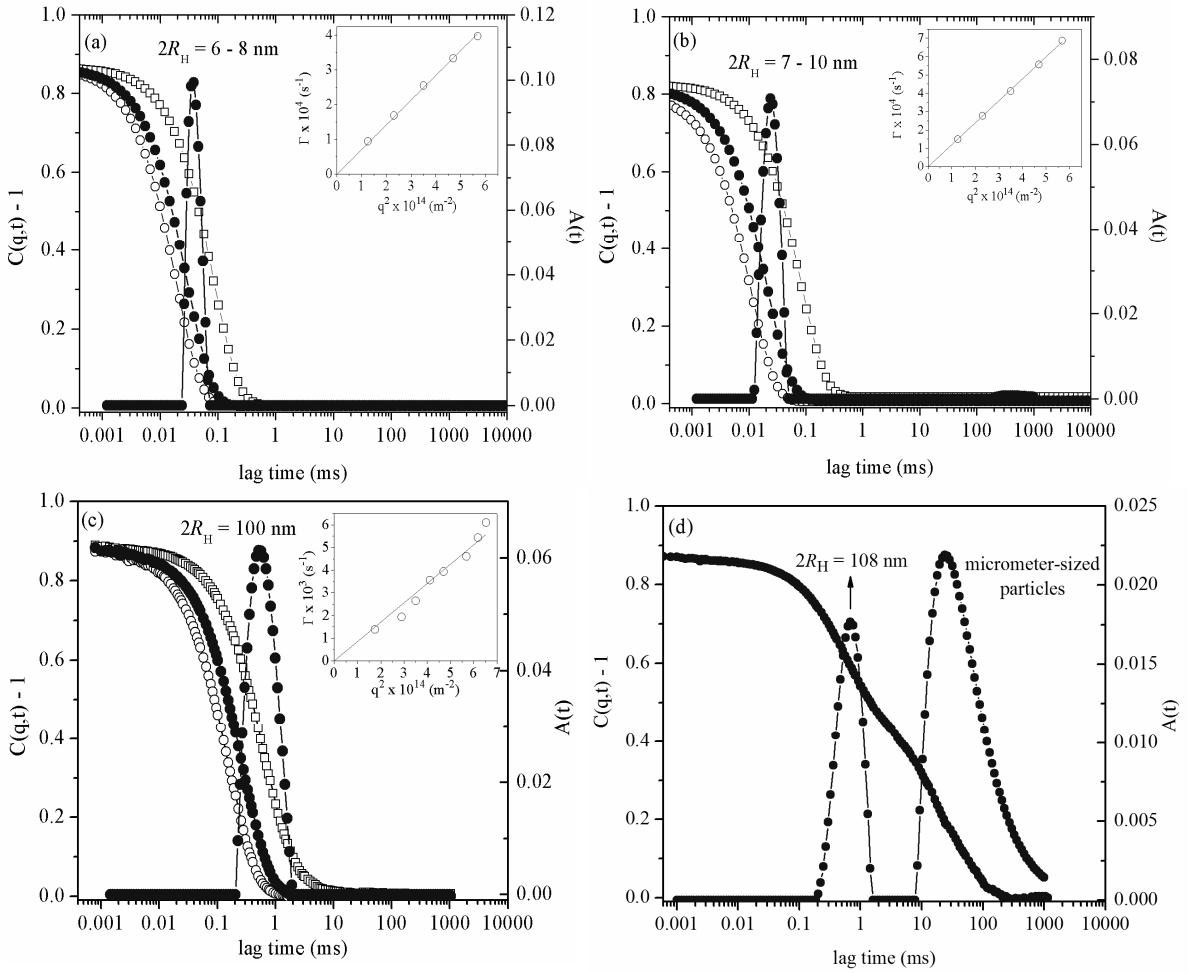

Figure III-33. Autocorrelation functions $C(q,t)$ measured at scattering angles of 50° (□), 90° (●) and 130° (○), and distributions of the relaxation times $A(t)$ at 90° as revealed by CONTIN analysis for solutions corresponding to steps **I** – **IV** in Figure 1b, as follows: 10.0 mg/mL PEO_{113}-*b*-$PG2MA_{85}$ in water (a), 10.0 mg/mL PEO_{113}-*b*-($PG2MA_{85}$–IND_{29}) in THF (b), 0.5 mg/mL PEO_{113}-*b*-($PG2MA_{85}$–IND_{29}) in water (c), and 0.5 mg/mL PEO_{113}-*b*-($PG2MA_{85}$–IND_{29}) after 5h in water at pH = 2.0 – 3.5 (d).

The nanoparticles structure and size was found to be dictated by both the length of PG2MA block and the amount of indomethacin (see below). The ability of these micelles to

release active molecules in response to pH changes is illustrated in Figure III-33d, which shows the auto-correlation function and distribution of relaxation times for the same solution as in Figure III-33c, but after 5h in an acidic environment (pH adjusted to 2.0 – 3.5). Under these circumstances, a very slow relaxation time appeared ($2R_H > 2$ μm), which was related to very large particles in solution formed by precipitation of free indomethacin within the sample holding cell, thus corroborating its pH-dependent release.

Figure III-34 shows autocorrelation functions $C(q,t)$ measured at different scattering angles and distributions of the relaxation times $A(t)$ at 90° as revealed by CONTIN analysis for 1.0 mg/mL PEO-*b*-(PG2MA–IND) block copolymer – drug solutions in water. The insets in Figure III-34 depict the typical q^2-dependence of the relaxation frequency (Γ) for diffusive scattering particles.[224] Thus, the $2R_H$ values discussed hereafter were calculated from the Stokes-Einstein relation (eqn. III-20).

In general, reasonably narrow distributions of relaxation times were obtained (μ_2/Γ^2 = 0.08 – 0.17, Table III-5), with a fast dominant mode corresponding to the diffusive motion of individual particles (micelles or vesicles). For PEO_{113}-*b*-($PG2MA_{65}$–IND_{08}) solutions (Figure III-34c) a slow mode associated with the existence of large aggregates (or other morphologies) was observed. However, the 6-fold difference in the relaxation frequency (and ultimately in the particles size) between the fast and slow modes should be considered to interpret these results. Even though the amplitude is higher for the slow mode than for the fast one, the number of particles with small size prevails because the light scattered intensity strongly depends on particle mass and size, implying that DLS reports an intensity-average size. Moreover, it is important to note that the amplitude of the two relaxation modes (slow and fast) strongly depends on the scattering angle in DLS measurements.[224]

The size and morphology of nano-objects originated from the self assembly of PEO-*b*-(PG2MA–IND) block copolymer – drug solutions depended on both the amount of IND and the PG2MA block length. For the shortest polymer precursor (PEO_{113}-*b*-$PG2MA_{40}$), spherical micelles with diameter ($2R_H$) varying from 24 to 64 nm were obtained with increasing IND contents (21 – 40 wt. %) (Table III-5, entries 1 – 3). According to Static Light Scattering (SLS) measurements (Table III-6), such a behavior is, besides the volume occupied by the drug, in part due to an increase in the respective aggregation number (N_{agg}) of the micelles in a process favored by hydrophobic interactions.

Let us assume that density of hydrophobic block equal to 1.0 mg/mL and that the core is formed, roughly, only by G2MA-IND. The average diameter of the hydrophobic compartment

(the core, $2R_c$) of these spherical micelles can thus be estimated according to eqn. III-22. The results are summarized in Table III-6, and show that $2R_c$ increases from 12 to 25 nm as the amount of B-IND increases from 21 – 40 wt. %, globally representing a ~ 9-fold (entries 1 and 3) augmentation in the cargo space (V_{core}).

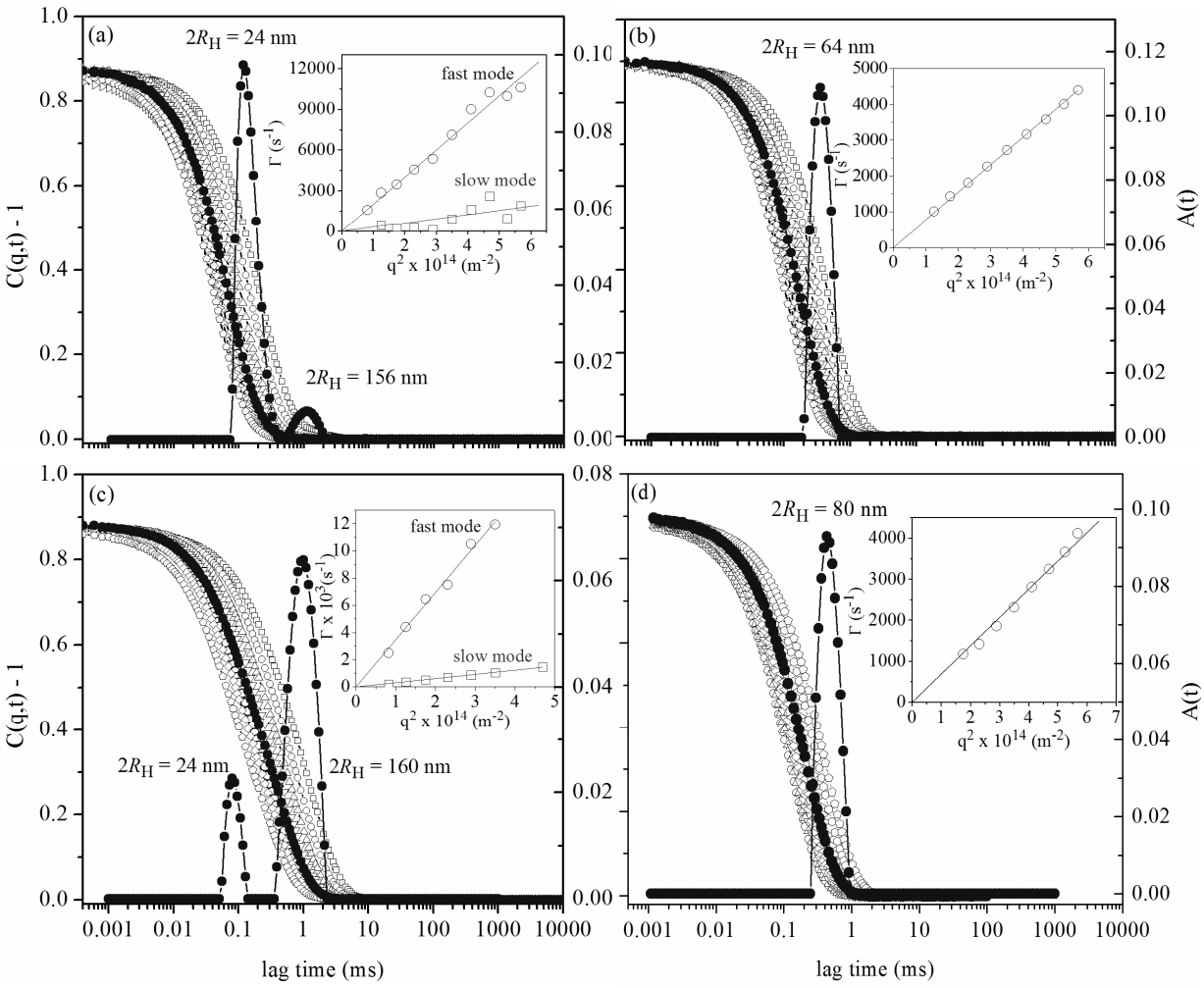

Figure III-34. Autocorrelation functions $C(q,t)$ at scattering angles of 50° (□), 90° (●) and 130° (○), and distributions of the relaxation times $A(t)$ at 90° as revealed by CONTIN analysis for 1.0 mg/mL PEO_x-*b*-($PG2MA_y$–IND_z) block copolymer – drug solutions in water: 113-(40-10) (a), 113-(40-21) (b), 113-(65-08) (c), and 113-(65-28) (d).

The corona width (W) determined using eqn. III-24 ranged from 6 to 19 nm. For PEO_{113}-*b*-($PG2MA_{40}$-IND_{10}) and PEO_{113}-*b*-($PG2MA_{40}$-IND_{17}), W was barely higher than R_g(calc) of unperturbed PEO_{113} homopolymer coil in a good solvent (R_g(calc) ~ 2.0 nm; assuming typical C—C and C—O bond lengths of 1.53 and 1.43 Å), and suggest, therefore, that hydrophilic chains are only slightly stretched into the solvent. In contrast, for PEO_{113}-*b*-($PG2MA_{40}$-IND_{21})

indicating that PEO chains are comparably more stretched into solvent (W = 19 nm; hypothetically, fully stretched PEO_{113} chain can reach ~ 50-nm length).

Table III-5. Physical chemical characteristics of PEO-*b*-(PG2MA–IND) self-assemblies.

Entry	Conjugate PEO_x-*b*-($PG2MA_y$–IND_z)	$\phi_{PG2MA-IND}$ [c]	$2R_H$ [a] (nm)	μ_2/Γ^2 [b]	Morphology [c]
1	113-(40-10)	0.33	24	0.10	M
2	113-(40-17)	0.49	36	0.12	M
3	113-(40-21)	0.56	64	0.08	M
4	113-(40-29)	0.68	ND [d]	ND [d]	ND [d]
5	113-(65-08)	0.22	24	-	M
6	113-(65-28)	0.56	80	0.15	V
7	113-(85-10)	0.22	ND [d]	ND [d]	ND [d]
8	113-(85-29)	0.50	100	0.17	V

[a] Hydrodynamic size of self-assembled PEO-*b*-(PG2MA-IND) particles, as assessed by DLS; [b] Polydispersity estimated by cumulants analysis of $C(q,t)$ auto-correlation functions recorded at 90° scattering angle; [c] Dominant morphology of self-assemblies in solution (M = Micelles; V = Vesicles); [d] Not Determined. Either the polymer was not fully soluble in THF (entry 7) or partially precipitated during micellization (entry 4).

Table III-6. Physical chemical properties of PEO_{113}-*b*-($PG2MA_{40}$-IND_z) spherical micelles determined by combining SLS and DLS results.*

Copolymer	$M_{w,unimers}$ (g/mol)	$M_{w,mic}$ (g/mol)	N_{agg}	$2R_g$ (nm)	$2R_H$ (nm)	$2R_c$ (nm)	W (nm)	R_g/R_H
113-(40-10)	$1.50x10^4$	$1.64x10^6$	109	20	24	12	6	0.83
113-(40-17)	$1.75x10^4$	$3.76x10^6$	215	34	36	18	9	0.89
113-(40-21)	$1.89x10^4$	$8.98\ x10^6$	475	58	64	25	19	0.91

* dn/dC = 0.12 mL/g

These results are in very good agreement with other reports, which suggest that the length and the hydrophobic character of the core-forming block determine the micelle dimensions,[132, 227] and consequently the loading efficiency, drug release profile, partition coefficient, bioavailability and biodistribution of the carrier system.[132] The morphology of

these nano-particles was confirmed by TEM experiments, which are shown in Figure III-35 for selected samples. In general, narrowly distributed nanosized spherical micelles were clearly identified as depicted in Figure III-35, panel **a** for PEO_{113}-*b*-($PG2MA_{40}$–IND_z) samples.

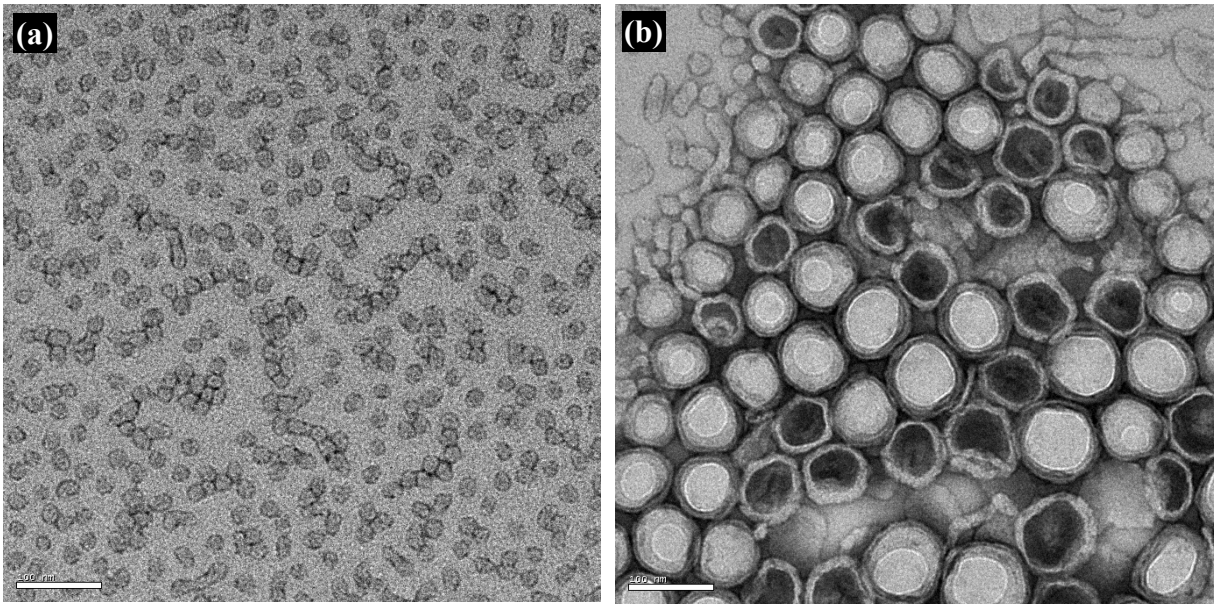

Figure III-35. TEM images of unloaded PEO_x-*b*-($PG2MA_x$–IND_z) assemblies: 113-(40-10) (a) and 113-(65-28) (b). Scale bar is 100 nm.

Very surprisingly, however, was the occurrence of kinetically stable vesicular structures with an average wall thickness of 12 nm by TEM for sample PEO_{113}-*b*-($PG2MA_{65}$–IND_{28}) (Figure III-35, panel **b**), which presents $\phi_{G2MA\text{-}IND} = 0.56$. Normally, the formation of micelles is expected at this volume fraction of the hydrophobic segment.[42, 78] The origin of such an observation may rely on the polymer-drug conjugate structure. It can be noted that in spite of the hydrophobic character of this sample due to the presence of linked IND, it contains a number unsubstituted OH groups in the PG2MA block, thus generating an additional, and important constraint during the micellization that might favor a transition from spheres to vesicles. During such a transition, an intermediate elongated or cylindrical morphology is usually observed for block copolymers systems either in organic or aqueous media.[71, 78] In the present case, a few cylinders can indeed be identified in Figure III-35, panel **b**, as indicated.
The mean nanoparticles (micelles and vesicles) diameter observed in TEM micrographs (for instance, 2R ~ 15 - 20 nm for PEO_{113}-*b*-($PG2MA_{40}$–IND_{10}) (Figure III-35a) and 2R ~ 60 – 70 nm for PEO_{113}-*b*-($PG2MA_{65}$–IND_{28}) (Figure III-35b)) are slightly smaller than those

determined by DLS measurements ($2R_H$ = 24 nm for PEO_{113}-*b*-($PG2MA_{40}$–IND_{10}) (Figure III-34a) and $2R_H$ = 80 nm for PEO_{113}-*b*-($PG2MA_{65}$–IND_{28}) (Figure III-34d)). This is in part due to micelle dehydration caused by solvent evaporation under the high vacuum conditions employed during TEM imaging. However, discrepancies are also expected because DLS reports an intensity-average diameter, whereas TEM reports a number-average diameter. Thus for a given size distribution of finite polydispersity, TEM images will usually undersize relative to DLS data. Overall, the size of PEO-*b*-(PG2MA–IND) nano-delivery system ($2R_H$ < 100 – 200 nm) is considered ideal for avoiding the body's defense mechanisms (the reticuloendothelial system (RES)).[40]

The loading and release properties of the above described micellar systems are presented in the next chapter.

Chapter IV

Loading and Release Properties of Block Copolymer Nanocontainers

Introduction

The loading and release properties of block copolymer nanocontainers is presented in this chapter, which is organized in three principal parts representing the astonishing differences in terms of probe contents that could be encapsulated inside the nanoparticles:

A) Low Payload Capacity Nanoparticles: Correlation between Physical Chemical Parameters and Delivery Performance;

B) Moderated Payload Capacity Nanoparticles via Polymer – Probe Conjugates: Multiple Encapsulation and Release Kinetics;

C) High Payload Capacity Nanoparticles via Specific Interactions: Toward a General Approach.

In *Part A*, the influence of the micellar structure on delivery related parameters is described for systems able to encapsulate up to ~ 30 % w/w_p of a hydrophobic guest molecule (probe). The loading content, loading efficiency, partition coefficient and release kinetics data were correlated with the carrier structure, namely, $M_{w,mic}$, N_{agg}, R_H, R_c and W.

In *Part B*, the suitability of the use of amphiphilic polymer – probe conjugates as building-blocks for nanocontainers is discussed. Through a combination of covalently bound and physically encapsulated fractions of the same probe, the payload capacity could be noticeably improved up to 58 % w/w_p. Such a system also allows different hydrophobic molecules to be loaded simultaneously in a multiple encapsulation strategy (one type of molecule chemically linked to the core-forming polymer and another entrapped inside the cargo space).

In *Part C*, finally, a general and unprecedented approach toward high payload capacity block copolymer micelles is presented. It consists in the use of active molecules (or probes) exhibiting weak carboxylic acid groups in their structure in combination with micellar nanoparticles having weak polybase-based cores (or *vice-versa*). The specific (acid-base) interactions between these species enhance hugely the payload capacity of polymeric nanoparticles (~ 100 % w/w_p). Besides, a possible cross-linking approach to permanently stabilize such highly loaded core-shell-corona micelles is shown.

A general overview of the payload capacities of different probe/nanoparticle systems will be given initially, in order to facilitate the data interpretation, and justify the choices made in this part of the study with respect to the probe and block copolymers systems.

Overview of Probe/Block Copolymer Systems

Aiming to establish a potential macromolecule structure-payload capacity relationship, the encapsulation studies were undertaken using a set of structurally different active molecules and micellar nanocarriers (Scheme IV-1).

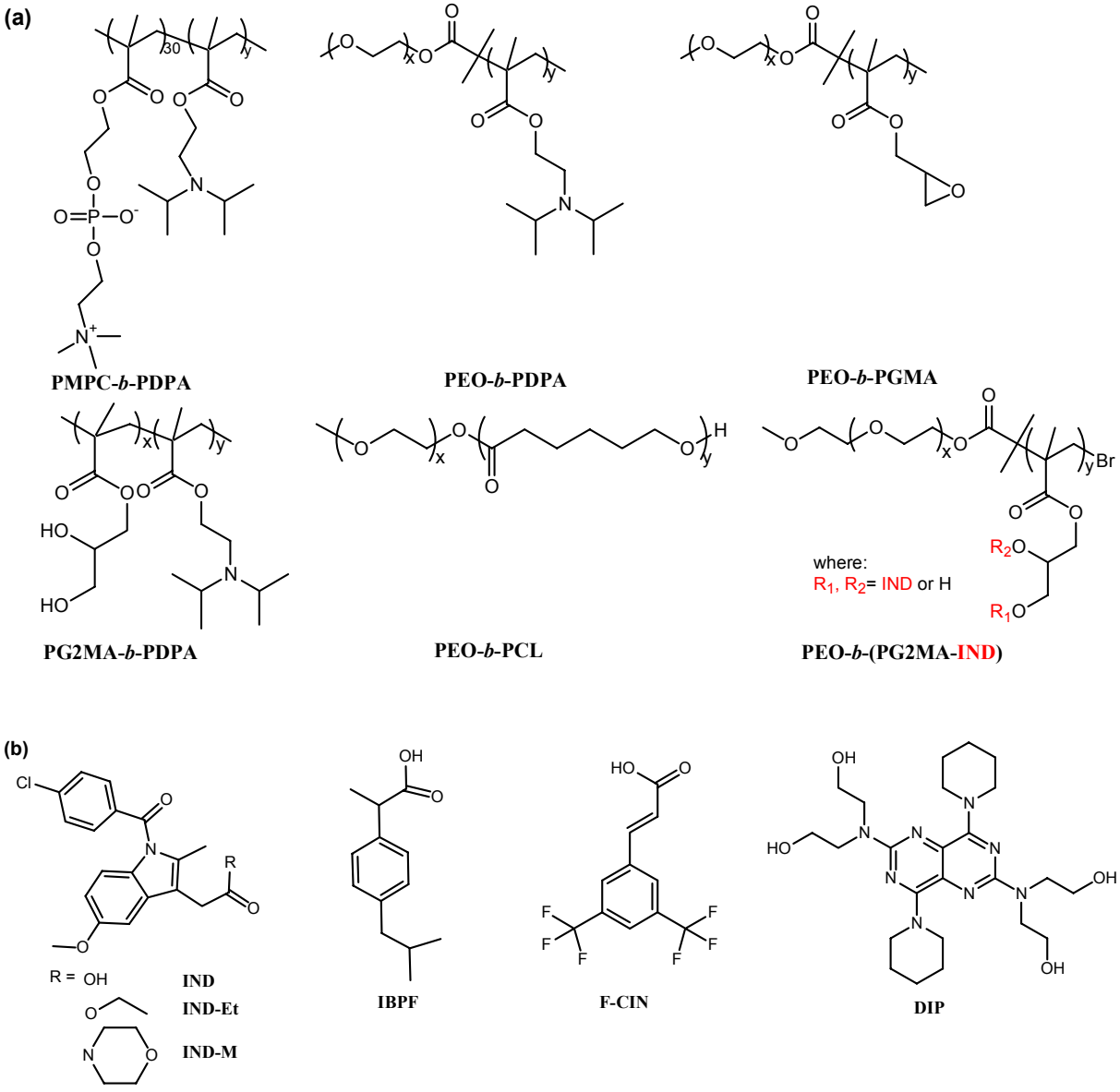

Scheme IV-1. Chemical structure of the diblock copolymers (a) and hydrophobic probes (b) used in this work.

A realistic picture of the principal experimental results collected during this work is given in Table IV-1. The careful analysis of these selected data evidently suggests that the micellar delivery systems can in fact be categorized in three main groups (A, B and C), which were defined earlier in this chapter.

Indeed, according to a recent literature survey (see *Chapter I*), the payload capacity of most of the block copolymer nanocarriers falls below 30 % w/w_p (category A), and in this case the physical chemical properties of the cargo and the guest molecule dictate the maximum loading content. Motivated by the originality of the DIP/PMPC-*b*-PDPA pH-responsive system among the others, we elected to study the latter into more detail so as to determine the effect of the micelle structure on the delivery-related parameters.

Table IV-1. Representative loading results for the encapsulation of distinct hydrophobic guest molecules by copolymers micellar nanocarriers having different core-corona structures.

Nanocarrier [a]	Probe	Acid-Base	Added Probe (% w/w_p)	Encapsulated Probe (% w/w_p)	Category[c]
$PMPC_{30}$-*b*-$PDPA_{60}$	DIP	no	20	12	A
	IND	yes	100	98	C
PEO_{113}-*b*-$PDPA_{50}$	DIP	no	20	04	A
	IND-Et	no	100	15	A
	IND-M	no	100	-	A
	IND	yes	100	99	C
	IBPF	yes	100	100[b]	C
	F-CIN	yes	100	100[b]	C
$PG2MA_{40}$-*b*-$PDPA_{50}$	IND	yes	100	100[b]	C
	IBPF	yes	100	100[b]	C
PEO_{45}-*b*-PCL_{24}	IND	no	100	13	A
	IND-Et	no	100	12	A
PEO_{113}-*b*-$PGMA_{50}$	IND	no	100	07	A
	IND-Et	no	100	06	A
PEO_{113}-*b*-($PG2MA_{40}$–IND_{21})	IND	no	50	40 + 18 = 58 (B-IND + F-IND)	B
	DIP	no	50	40 + 05 = 45 (B-IND + F-DIP)	B

[a] C_p = 1.0 mg/mL; [b]Visual inspection; stable solutions with no apparent precipitation. [c] Classification of the probe/nanocarrier system according the payload capacity: A= Low (LC ≤ 30 % w/w_p), B = Moderated (30 % w/w_p < LC < 70 % w/w_p) and C = High (LC ≥ 70 % w/w_p) Payload Capacity Nanoparticles.

A noticeable improvement in the hydrophobic payloads up to ~ 58 % w/w_p (category B) could be attained through a combination of covalently bound + physically encapsulated fractions of a given probe.

A breakthrough achievement reported herein is, however, related to the fact that specific interactions inside the hydrophobic environment of the nanoparticle enhance dramatically the payload capacity up to ~ 100 % w/w_p (category C). Apparently, such a conclusion can be generalized for other active molecules and polymers, thus suggesting that chemical modification of already-in-use or novel drugs to meet this requirement is a potential strategy to obtain highly loaded nanocontainers. Needless to say though, that this may have implications on biological activity of drugs, and such a point must of course be investigated in the near future.

A) Low Loading Capacity Nanoparticles: Correlation between Physical Chemical Parameters and Delivery Performance

A-1. Loading

A-1-1. Loading of DIP into PMPC-b-PDPA via pH-based method

The so-called solvent-free protocol for the preparation of drug-loaded block copolymer micelles in aqueous solution is a very attractive strategy, particularly if both the copolymer and the drug respond to the same external stimulus.

The chemical structure of DIP (Scheme IV-1) contains both aromatic and aliphatic nitrogen atoms whose pK_a values are 5.7 and 12.5, respectively. The aqueous solubility constant (K_s) of DIP is strictly determined by its degree of protonation. Although completely water-soluble at pH < pK_{a1} (pK_{a1}(DIP)= 5.7), it precipitates out from solution between pH = 5.7 and pH = 12.5 with a K_s of about 1.0 x 10^{-5} mol/L. Above pH = 12.5, the K_s is further reduced by a factor of five.

The pK_{a1} of DIP is in fact very close to the average pK_a for the PDPA block (pK_a(PDPA) = 5.7 – 6.6, see *Chapter III*). Hence, we elected to take advantage of the structure-solubility relationship of DIP and PMPC-*b*-PDPA by using the solvent-free method of drug entrapment. Both the copolymer and the active molecule were first molecularly dissolved in acidic solution (pH < pH_{mic}). Adjusting the solution pH to above the pH_{mic} led to simultaneous micellization and drug encapsulation.

Figure IV-1 shows potentiometric titration curves of 0.5 mg/mL $PMPC_x$-*b*-$PDPA_y$ micellar solutions in presence of 0.1 mg/mL DIP. It is interesting to note that the presence of DIP did not change the profile of titration curves, indicating the concomitant neutralization of

both the copolymer and the drug. Evidently, the plateau region corresponding to the neutralization process was extended in DIP-containing solutions as compared to DIP-free solutions, suggesting that the drug is precipitated and entrapped inside the hydrophobic micellar cores during the onset of micellization. Furthermore, the addition of DIP to copolymer solutions lowered the mean pK_a value of the PDPA block (dotted lines in Figure IV-1), thus favoring (anticipating) the drug/copolymer self-assembly process. We speculate that the hydrophobic probe exerts the opposite effect of the ionic strength, promoting favorable hydrophobic interactions with the deprotonated PDPA. This causes the equilibrium in eqn. III-25 to shift to the right (micellization), with consequent increase in the K_a values (*i.e.*, decrease in the pK_a-values).

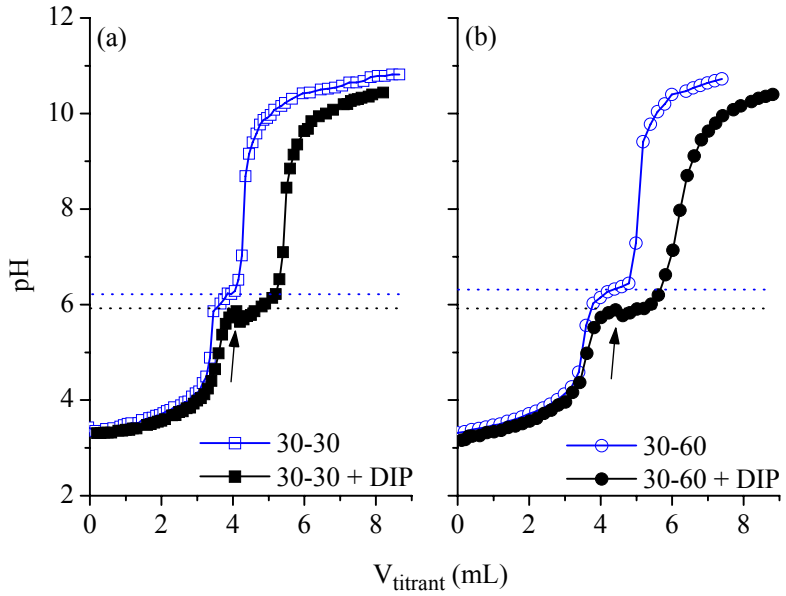

Figure IV-1. Potentiometric acid-base titration curves for 0.50 mg/mL solutions of (a) $PMPC_{30}$-*b*-$PDPA_{30}$ and (b) $PMPC_{30}$-*b*-$PDPA_{60}$ in the absence and presence of 0.1 mg/mL DIP ($V_{aliquot}$ = 10.0 mL; 10 mmol/L NaOH as titrant).

The partition coefficient, K_V, of DIP between the aqueous exterior and the micellar core is defined as

$$K_V = \frac{[PROBE]_{mic}}{[PROBE]_{aq}} \qquad \text{(IV-1)}$$

where $[PROBE]_{mic}$ is the probe concentration in the micellar phase and $[PROBE]_{aq}$ is the probe concentration in the aqueous phase. [234] K_V-values were determined as previously described.[243] For partitioning of a probe molecule between copolymer micelles and solution, with a partition coefficient K_V, it is possible to define the dependence of the maximum

fluorescence emission with respect to the copolymer concentration, C_p, for a constant probe concentration as given in eqn. IV-2,

$$\frac{1}{F - F_{\min}} = \frac{1}{(F_{\max} - F_{\min})} + \frac{\rho}{K_V \phi_{DPA} C_p (F_{\max} - F_{\min})} \qquad \text{(IV-2)}$$

where F_{min} is the fluorescence intensity in absence of micelles, F_{max} is the intensity when essentially all the probe is located within the micelle cores (high C_p), F is the intensity measured at a copolymer concentration C_p, and ρ is the density of the micelle core (taken as 1.0 g/mL).

Thus, K_V can be determined from the slope and intercept of $1/(F\text{-}F_{min})$ against $1/C_p$ plot. Figure IV-2a shows the variation of DIP fluorescence spectra as a function of C_p. As expected, the intensity at the wavelength of maximum emission (λ_{max} = 490 nm) increases with C_p, generating good straight lines when plotted as $1/(F\text{-}F_{min})$ against $1/C_p$ (Figure IV-2b).

The respective partition coefficients for $PMPC_{30}$-*b*-$PDPA_{30}$ and $PMPC_{30}$-*b*-$PDPA_{60}$ were 1.1 x 10^4 and 5.7 x 10^4, respectively. These values reveal strong partitioning of the hydrophobic small molecules into the micellar core, being comparable with those observed for pyrene/crew-cut PAA-*b*-PS (K_V = 1.3 x 10^5) [244] and pyrene/PEO-*b*-PS (K_V = 2.0 – 4.0 x 10^5),[245] Cell Tracker CM-DiI/PEO-*b*-PCL (K_V = 5.8 x 10^3)[129] systems, and relatively higher than for pyrene/PEO-*b*-PCL (K_V = 1.0 x 10^2)[242] system.

The dependence of K_V on the volume fraction of DPA is expected, since the longer the core-forming block the greater the drug entrapment capacity.[107, 235]

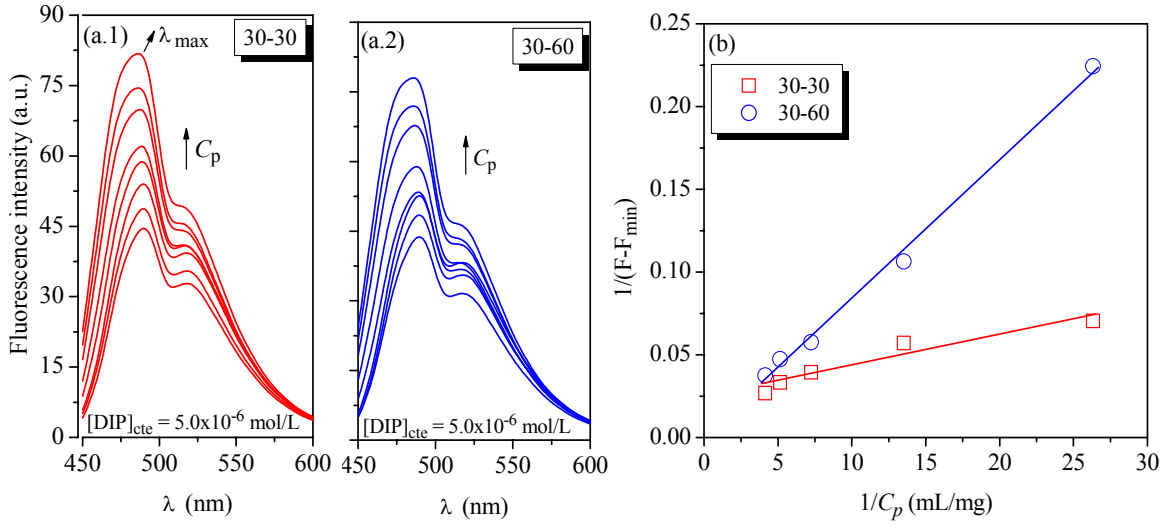

Figure IV-2. DIP fluorescence spectra measured at C_p varying from 0.0 to 1.12 mg/mL as indicated by the arrows, for $PMPC_x$-*b*-$PDPA_y$, as indicated (a), and determination of the partition coefficient of DIP between the aqueous phase and the micelle cores (b).

The amount of DIP incorporated into the PMPC-*b*-PDPA micelles was determined by fluorescence spectroscopy using the standard addition analytical method (see *Experimental Part*). Figure IV-3 shows the variation of the encapsulated probe content and the respective probe loading efficiencies as a function of the total mass of probe used. The dotted line denotes quantitative loading. In general, there is an increase in the encapsulated drug content as its amount in the initial solution increases, but eventually a maximum value is attained. The maximum DIP content loaded into the $PMPC_{30}$-*b*-$PDPA_{30}$ micelles is about 7 % w/w_p (corresponding to a loading efficiency of 36 %) at an initial weight ratio of 20 % w/w_p. However, this value increases up to 12 % w/w_p (68% loading efficiency) for micelles formed by the $PMPC_{30}$-*b*-$PDPA_{60}$ copolymer.

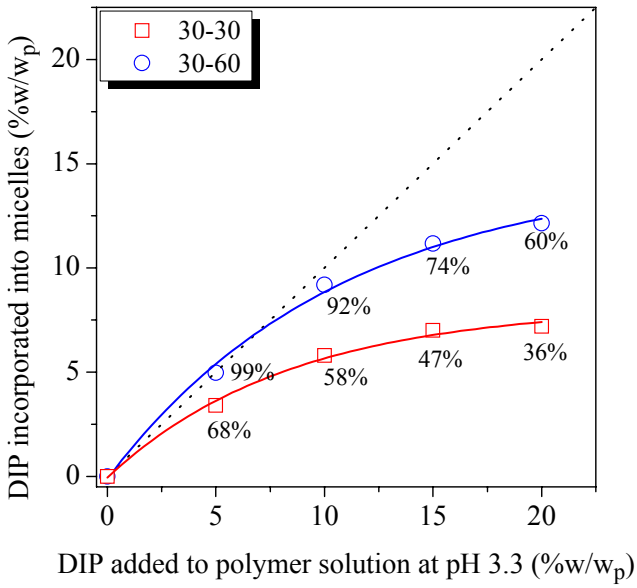

Figure IV-3. Variation of DIP content encapsulated within 0.5 mg/mL $PMPC_x$-*b*-$PDPA_y$ micelles and the respective DIP loading efficiencies as a function of added DIP.

These results suggest that the capacity of PMPC-*b*-PDPA micellar aggregates to carry (deliver) DIP molecules is strongly correlated to their structural properties. According to DLS and SLS experiments (*Chapter III*), the increase in the volume fraction of DPA (ϕ_{DPA}) from 0.42 to 0.59 leads to an increase in the core volume from 3 x 10^3 nm^3 to 2 x 10^4 nm^3. The higher cargo space in the latter case is the main reason for the higher loading efficiency of $PMPC_{30}$-*b*-$PDPA_{60}$, along with non-negligible contributions possibly arising from the higher hydrophobicity of micelle cores formed by longer PDPA blocks, consequently enhancing interactions with the hydrophobic probe.

A-2. Release

The *in vitro* drug release studies were accessed at pH = 7.4, conditions under which the nanoparticles are stable. The amount of DIP released from PMPC-*b*-PDPA micelles as a function of the time is shown in Figure IV-4a. Regardless of the copolymer used, both profiles exhibit an induction period during which the released amount increases slowly and remains below to 10%. This time interval precedes the main release process and is attributed to drug diffusion inside the micelle, predominantly from the inner core towards the outer shell. Once the drug reaches the interface between the aqueous phase and the micelles, it is released at a constant rate (proportional to the slope of straight lines in Figure IV-4b), accounting for a diffusion-controlled mechanism as proposed by Higuchi's model.[159] According to these results, the amount of drug released within a 5-h period from 0.5 mg/mL $PMPC_{30}$-*b*-$PDPA_{30}$ + 7 % w/w_p DIP and 0.5 mg/mL $PMPC_{30}$-*b*-$PDPA_{60}$ + 12 % w/w_p DIP loaded micelles was approximately 80 and 60%, respectively, with almost complete release being achieved after 20 h in the former case. On the other hand, the $PMPC_{30}$-*b*-$PDPA_{60}$ copolymer micelles retained around 20% of their original DIP content after 20 h, which is in agreement with their higher loading capacity and drug retention as the volume fraction of the core-forming block increases. Longer release periods have not been assessed.

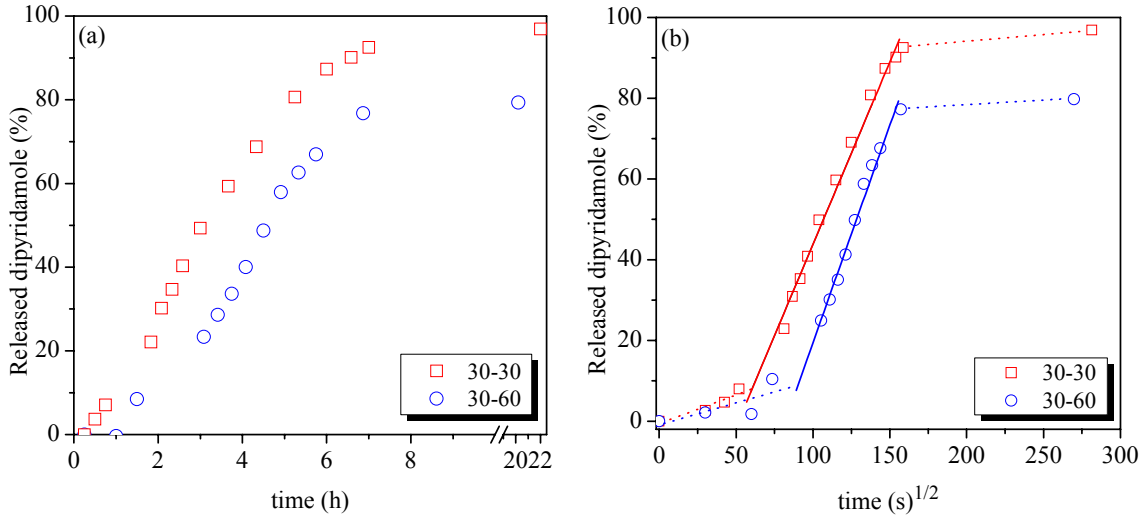

Figure IV-4. Percentage of DIP released as a function of the time for 0.50 mg/mL $PMPC_x$-*b*-$PDPA_y$ micelles (a), and the respective Higuchi plots (b).

B) Moderated Loading Capacity Nanoparticles Using Polymer – Active Molecule Conjugates: Multiple Encapsulation and Release Kinetics

B-1 Loading

B-1-1. Loading of free indomethacin (F-IND) into PEO-b-(PG2MA-IND) nanoparticles

The ability of PEO-*b*-(PG2MA-IND) micelles to physically encapsulate free IND (F-IND) was assessed in order to further improve their loading capacity (*i.e.*, total drug payload), in which the compatibility between solubilizate and micelle core is in principle high. A relationship between B-IND and F-IND can thus be anticipated for these systems, being indeed confirmed by entries 1 and 3 in Table IV-2, which shows loading results for selected samples at constant polymer and added IND concentrations. In these cases, the increase in B-IND from 15 to 21 % w/w_p is accompanied by a parallel increase in F-IND from 13 to 20 % w/w_p. As for other micellar drug carriers, the loading capacity is obviously finite, and a limitation of encapsulation F-IND there appears to exist as B-IND further increases (entries 2 and 4). The amounts of unbound or free IND (F-IND) effectively encapsulated by PEO-*b*-(PG2MA-IND) micelles as prepared in this work are comparable with those reported for other IND micellar delivery systems tested so far: 8 – 9 % w/w_p for PEO-*b*-PLA;[146] 6 - 14 % w/w_p for PEO-*b*-poly(alkyl (meth)acrylates);[148] 20 % w/w_p for PEO-*b*-PBLA;[143] 17 – 42 % w/w_p for PEO-*b*-PCL.[144, 145]

Table IV-2. Loading results for IND encapsulation by nanoparticles made from PEO-*b*-(PG2MA–IND) conjugates (C_p = 1.0 mg/mL; Targeted F-IND loading = 50 % w/w_p).

Entry	PEO_x-*b*-($PG2MA_y$–IND_z)	L.E.[a] (%)	F-IND[b] (% w/w_p)	B-IND (% w/w_p)	Total IND payload[c] (% w/w_p)
1	113-(40-10)	40	20	21	41
2	113-(40-21)	36	18	40	58
3	113-(65-08)	27	13	15	28
4	113-(65-28)	44	15	39	54

[a] Loading efficiency.
[b] Free IND content encapsulated inside the nanoparticles, as determined by UV-vis spectroscopy.
[c] F-IND + B-IND.

Most importantly, however, is the remarkable total IND payload (*i.e.,* covalently bound IND + physically entrapped IND) achieved using micellar nano-containers formed by self-assembly of PEO-*b*-(PG2MA-IND) block copolymer – drug conjugates. IND contents ranging from 28 up to 58 % w/w_p (Table IV-2) were systematically obtained by this facile approach, being entirely comparable with reports by Bertin *et al.*,[220] (30 – 60 % w/w_p) and Quémener *et al.*[221] (5 – 70 % w/w_p).

Interestingly, it has been observed that self-organization for F-IND loaded samples with more than 50 % w/w_p IND payload (Table IV-2, entries 2 and 4) either originated vesicular morphologies instead of micelles or provoked a huge increase in the size of vesicles. The distributions of the hydrodynamic diameter ($2R_H$) determined by DLS for unloaded and F-IND loaded PEO_x-*b*-($PG2MA_x$–IND_z) nanoparticles revealed a remarkable (~ 3-fold) increase in their size (for example, from $2R_H$ = 64 nm to $2R_H$ = 160 nm for PEO_{113}-*b*-($PG2MA_{40}$-IND_{21}) and from $2R_H$ = 80 nm to $2R_H$ = 220 nm for PEO_{113}-*b*-($PG2MA_{65}$-IND_{28})) with a parallel augmentation in the normalized scattered light intensity at 90 scattering angle ($I_{sc}^{90}N$) (see insets) upon F-IND loading, as illustrated in Figure IV-5. These observations are in good agreement with results by TEM, which are shown in Figure IV-6 for the same systems as in Figure 5. Indeed, micrographs taken for F-IND loaded (Figure IV-6, panels **a** and **b**) and unloaded (Figure IV-6, insets in panels **a** and **b**) PEO-*b*-(PG2MA-IND) nanoparticles confirmed the existence of a morphology transition from spheres to vesicles (panel **a**) and/or an important size augmentation upon F-IND loading (panels **a** and **b**). Besides, slightly bluish aspects (visual inspection by digital photographs, not shown) were observed for such solutions, suggesting the presence of relatively large objects in solution.

The above results suggest that the thermodynamics and kinetics of PEO-*b*-(PG2MA-IND) self-organization change dramatically in presence of F-IND, possibly leading to morphology transitions. This is an important observation as far as the structure and dynamics of block copolymer micellar drug delivery vehicles affect parameters such as hydrodynamic diameter, molar mass, etc., therefore exerting huge implications on nanoparticle biodistribution, drug loading capacity and release kinetics.[107]

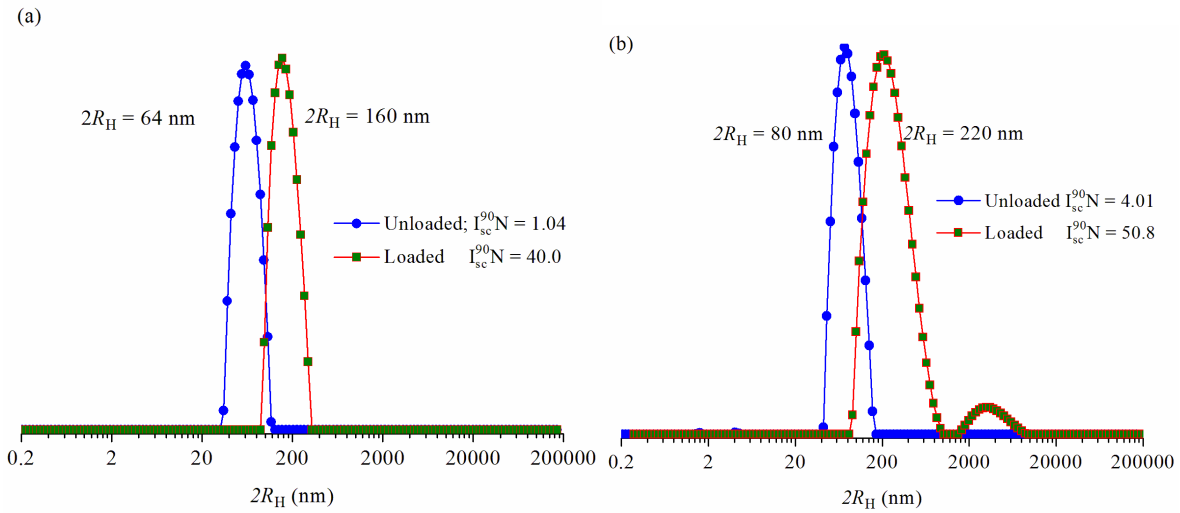

Figure IV-5. Distributions of the hydrodynamic diameter ($2R_H$) obtained by DLS using CONTIN analysis for F-IND loaded 1.0 mg/mL PEO_x-*b*-($PG2MA_x$–IND_z) block copolymer – drug nanoparticles in water: 113-(40-21) + 18 % w/w_p F-IND (a), and 113-(65-28) + 15 % w/w_p F-IND (b).

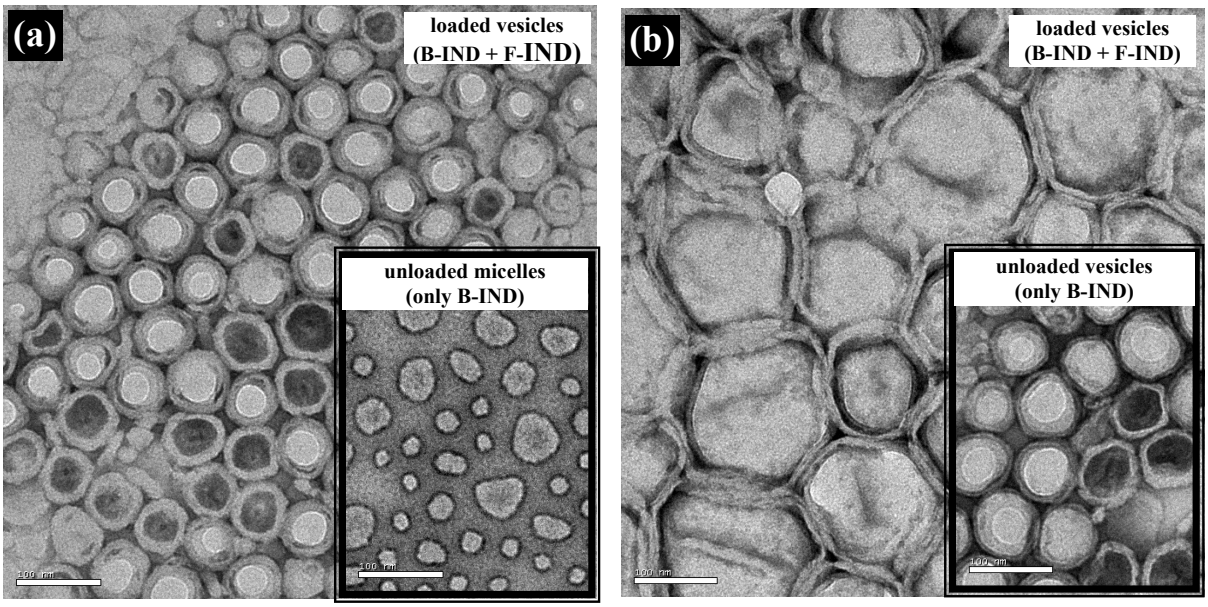

Figure IV-6. TEM images of F-IND loaded PEO_x-*b*-($PG2MA_x$–IND_z) assemblies: 113-(40-21) + 18 % w/w_p F-IND (a) and 113-(65-28) + 15 % w/w_p F-IND (b). Scale bar is 100 nm in all images, including the insets.

B-1-2. Loading of dipyridamole (DIP) into PEO-b-(PG2MA-IND) nanoparticles

In many cases one might envision wishing to deliver two or more active agents to the same place at the same time. Although it is possible that one could prepare micellar aggregates of two distinct types, and thereby encapsulate two agents separately, this does not solve the problem of guaranteeing that both agents arrive at the same place, at the same time, and in a prescribed stoichiometric ratio.[130] The design of multicompartment nanoparticles has then attracted considerable attention during the last decade, but only very recent significant achievements have been made.[246] Such complex systems comprise a hydrophilic shell and a hydrophobic core with segregated incompatible subdomains, which may therefore transport simultaneously different agents.

Within this context, the entrapment of a second probe into PEO-*b*-(PG2MA-IND) micelles was assessed. Differing from multicompartment objects, in our case, one drug is bound to the particle core, while the other is not.

Dipyridamole (DIP) was chosen for these studies owing to its UV-vis absorption characteristics. They diverge sufficiently from those of IND to validate the use of a facile UV-based analytical method for the quantification of loaded DIP amounts. As observed in Figure IV-7, which displays the UV-vis absorption spectra recorded in THF for DIP, IND, and their mixtures, IND practically does not absorb in the $400 < \lambda < 500$ nm range. Therefore, DIP can be easily quantified through variations in the absorbance at $\lambda_{max} = 411$ nm.

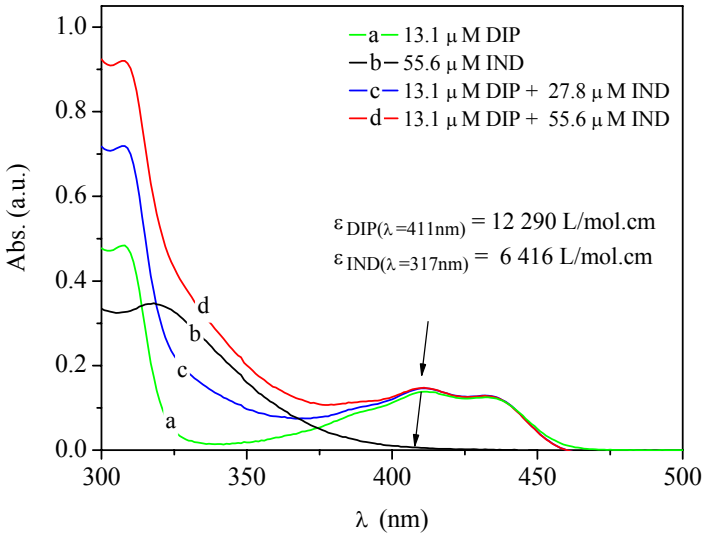

Figure IV-7. UV-vis absorption spectra recorded in THF for DIP, IND and their mixtures.

By applying exactly the same preparation procedure as for IND, the amount of DIP that could be encapsulated inside the PEO-*b*-(PG2MA–IND) nanoparticles was markedly lower, as can be concluded from the data listed in Table IV-3. Regardless of the carrier's size, the DIP loading content was about 5 % w/w_p. Although these results are far from an ideal delivery system, they do support the hypothesis that the compatibility between IND and IND-base core-forming block is at the origin of the moderate payload capacity.

Table IV-3. Loading results for DIP encapsulation by nanoparticles made from PEO-*b*-(PG2MA–IND) conjugates (C_p = 1.0 mg/mL; Targeted DIP loading = 50 % w/w_p).

Entry	PEO_x-*b*-($PG2MA_y$–IND_z)	L.E.[a] (%)	DIP[b] (% w/w_p)	B-IND (% w/w_p)	Total probe payload[c] (% w/w_p)
1	113-(40-21)	9	5	40	45
2	113-(65-28)	9	5	39	44

[a] Loading efficiency.
[b] Free DIP content encapsulated inside the nanoparticles, as determined by UV-vis spectroscopy.
[c] DIP + B-IND.

B-2 Release

The release of drugs from block copolymer nanocarriers depends upon several physical-chemical parameters such as drug diffusion rate, partition coefficient between drug and hydrophobic segment, micelle/vesicle stability and the copolymer biodegradation rate, among others. In the case of stimuli-responsive systems, these parameters can change dramatically as a function of the environmental surroundings, leading to triggered release processes.

Indomethacin release from PEO-*b*-(PG2MA-IND) micelles has been anticipated as being a pH-dependent phenomenon firstly due to intrinsic molecular characteristics of F-IND, and secondly due to pH-sensitivity of ester linkages in the conjugate. Physically encapsulated F-IND has a carboxylic acid group whose pK_a is 4.5.[143, 247] As a result of its aqueous dissociation behavior, neutral (F-IND) and negatively charged ($F\text{-}IND^-$) species coexist in solution, and the respective molar fraction depends on the solution pH (Figure IV-8). The overall aqueous solubility constant (K_s) of F-IND is, for this reason, strictly determined by its degree of protonation. The solubility of F-IND in pH 1.2 and pH 7.2 buffered aqueous media was found to be 0.011 and 2.1 mmol/L, respectively.[247] Therefore, F-IND can be considered as a practically insoluble drug at pH 1.2 and slightly soluble at pH 7.2 buffer solutions. The obvious difference in terms of K_s between F-IND and $F\text{-}IND^-$ species has been highlighted by

Kataoka *et al.*[143] to explain the higher release rate (> 15-fold) of F-IND from micellar nano-carriers at neutral pH as compared to acidic media.

From a drug delivery standpoint, esters, carbonates, amides and urethanes are linkers susceptible towards hydrolysis in acidic media, yielding to the so-called passive hydrolysis, and the rate of hydrolysis decreases in the order ester > carbonate > amides > uretanes.[248, 249] Nevertheless cleavage may also occur between the spacer and the polymeric backbone leading to the release of the spacer – drug moiety. The pH-dependent release of IND molecules linked to polymer chains via amide and anhydride bounds has been formerly reported elsewhere.[220, 221]

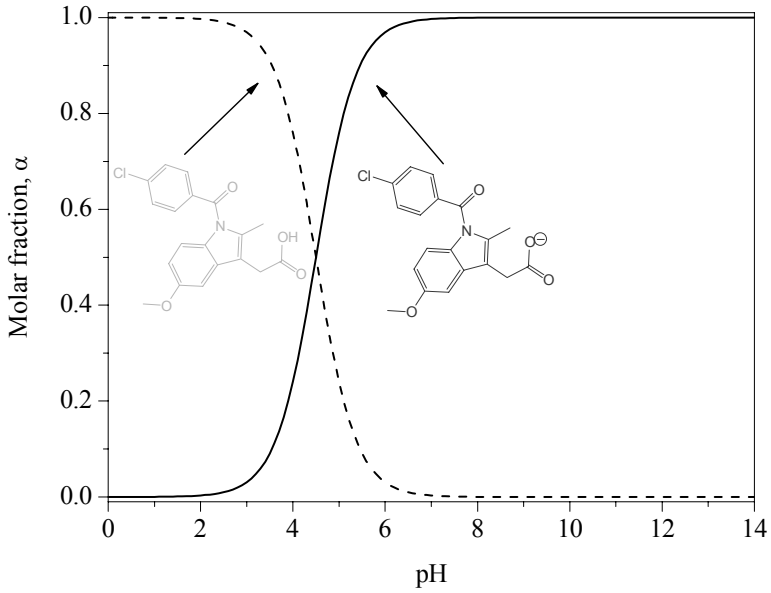

Figure IV-8. Diagram of species distribution as a function of the solution pH for indomethacin in aqueous medium.

In the present work, the release of IND from nano-carries originated from self assembly of PEO-*b*-(PG2MA–IND) block copolymer – drug conjugates was investigated as a function of the solution pH in absence and in presence of F-IND. Figure IV-9 shows the percentage of IND released over time as determined by variations in the UV absorbance at 320 nm. At pH = 7.4 and in absence of F-IND (Figure IV-9a, open symbols) the amount of IND released from the nanoparticles increased slightly as a function of time. After a rapid release of ca. 10% of the initial IND payload (0.40 mg/mL) during the initial 2- 3 h period, a quite stable plateau was systematically observed suggesting that ester bound cleavage hardly occurred. This profile was interpreted as corresponding to the passive diffusion of a given amount (typically 10 – 20%) of unbound IND that could not be completely separated during purification by

selective precipitation of block copolymer drug conjugates. Essentially the same comments also apply for other samples listed in Table 3. On the other hand, nanoparticles carrying both B-IND and F-IND (Figure IV-9a, filled symbols) produced 5-fold faster and sustained release rate of their encapsulated content, following an initial 2-h burst release. After 21 h, nearly 50 % of the total IND payload (0.58 mg/mL) had been released. The undesirable burst effect normally takes place when a significant amount of the drug resides at the core-corona interface or in the corona, because molecules do not have to traverse large core segments to exit the carrier.[129]

The mechanism of IND release from the nanoparticles was diffusional-controlled, as indicated by the linear variation of the released content as a function of the square root of time (Higuchi plot shown in Figure IV-10).[159]

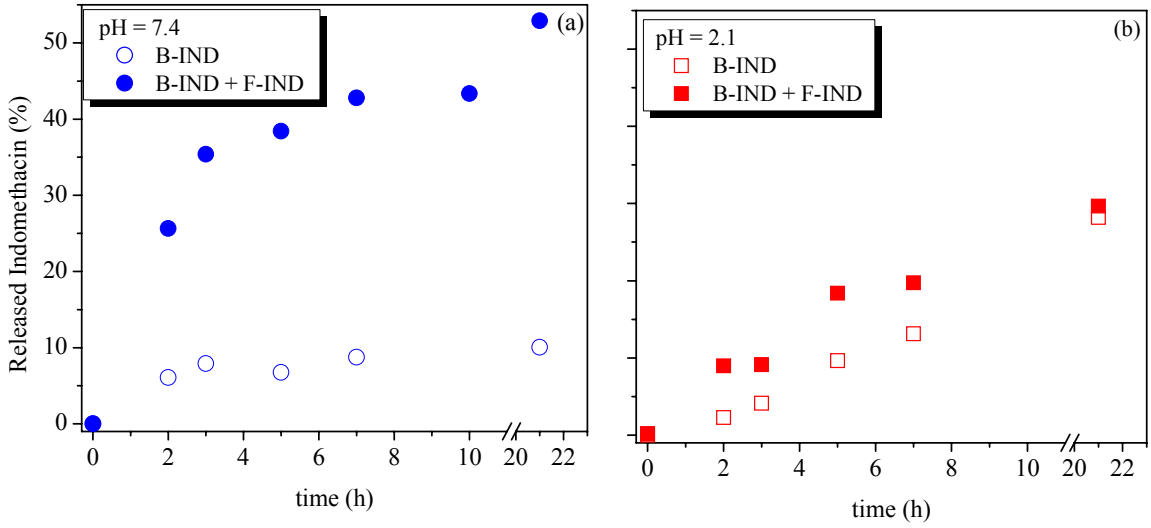

Figure IV-9. Percentage of IND released as a function of time as determined by variations in the UV absorbance at λ_{max} = 320 nm for 1.0 mg/mL PEO_{113}-*b*-($PG2MA_{40}$–IND_{21}) conjugates at pH = 7.4 (a) and pH = 2.1 (b) in absence and in presence of 0.18 mg/mL F-IND, as indicated.

Upon exposure to pH = 2.1 solutions, PEO-*b*-(PG2MA–IND) micellar solutions without added F-IND (Figures IV-9b, open symbols) exhibited sustained release with slow kinetics. Albeit it seems clear that acid medium favored acid hydrolysis of ester bounds, only 25% of total IND payload (0.40 mg/mL) diffused out of the nanoparticles during 21 h. Indeed, from this amount 15% consisted in hydrolyzed B-IND while ~ 10% is F-IND (Figure IV-9a). Likewise, much slower release rate was observed in presence of F-IND (Figure IV-9b, filled symbols) (30% of 0.58 mg/mL released after 21h). Interestingly, minor burst effect occurred at low pH in both cases. The pH-dependent release rate of F-IND herein characterized is in

good agreement with previous reports by other research groups,[143, 250] and can be attributed to the very different solubility of IND as a function of the solution pH, as mentioned above.

The passive hydrolysis of ester linkage in PEO-*b*-(PG2MA–IND) conjugates was found to be a rather slow process (15 % release after 21 h exposure to pH = 2.1 solutions at room temperature), being fairly comparable with findings obtained by Bertin *et al*.[220] These authors determined that 20 % of the amide-bound IND was released from the block copolymer-based nanoparticles after 48-h incubation at pH = 3.0 and at 37°C. Nevertheless, our release studies indicated slower kinetics as compared to the hydrolysis of anhydride-bound IND in polynorbornene colloidal particles (80% release after 48-h incubation at pH = 3.0), as reported by Quémener *et al*.[221]

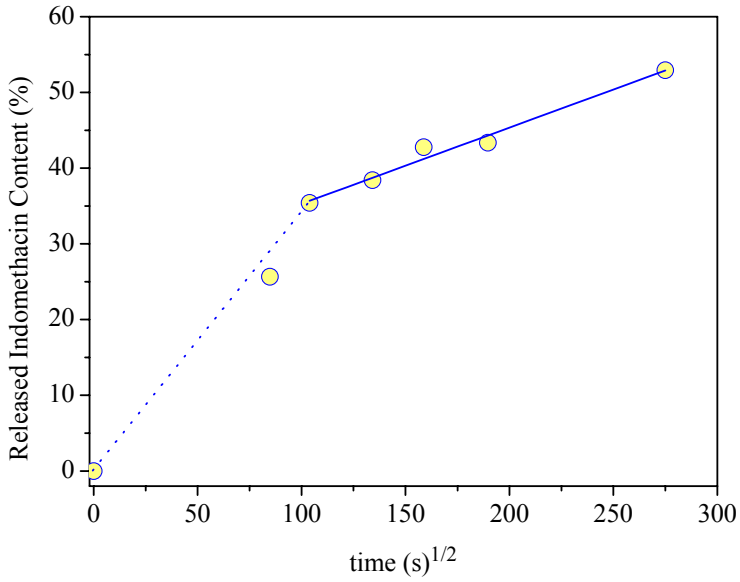

Figure IV-10. Diffusional release of IND from PEO_{113}-*b*-($PG2MA_{40}$-IND_{21}) nanoparticles. Line of best fit suggests diffusional release, not including the initial burst release.

The release profiles observed for IND release from PEO-*b*-(PG2MA–IND) micellar nanoparticles emphasizes their excellent potential as drug delivery vehicles, as judged from their distinguished capacity to transport, retain and deliver indomethacin.

C) High Loading Capacity Nanoparticles via Specific Interactions: Toward a General Approach

C-1 Loading

C-1-1. Loading of guest hydrophobic molecules containing carboxylic acid groups into micelles with weak polybase cores

In general, when a hydrophobic active molecule (probe, drug, fragrance, nanoparticulate metal-base systems, etc.) and an amphiphilic block copolymer are dissolved together into an organic medium, the subsequent addition of water (a selective solvent for the hydrophilic block) induces the self-organization of the copolymer chains, possibly originating a wide range of morphologies (micelles, cylinders, vesicles, etc), which can serve as containers for encapsulation of a given fraction of probe. The unloaded part often precipitates out of the solution, and is removed by uncomplicated separation methods (centrifugation, filtration, etc).

Remarkable high loading capacities have been observed for indomethacin (IND) incorporation into micelles having weak polybase cores (namely, PEO-*b*-PDPA and PG2MA-*b*-PDPA). The variation of the IND content encapsulated by PEO_{113}-*b*-$PDPA_{50}$ micelles as a function of the total mass of IND used for the preparation, is illustrated in Figure IV-11 for different polymer concentrations (C_p = 0.25 – 2.0 mg/mL). The dotted line represents the quantitative loading, while the horizontal lines refer to 100 % w/w_p probe contents inside the micelles (i.e., the concentrations (in mg/mL) of entrapped probe and polymer are equivalent). For the IND/PEO_{113}-*b*-$PDPA_{50}$ system, the drug loading was proportional to the amount of micelles in solution. For 1.0 mg/mL PEO_{113}-*b*-$PDPA_{50}$ micellar solutions (Figure IV-11, squares), nearly quantitative encapsulation was observed as amount of IND in the initial solution increased until target loadings of ~ 150 % w/w_p (1.5 mg/mL IND). Above this point, the curve deviates from the dotted line, indicating partial encapsulation (up to ~ 100 % w/w_p; 1.0 mg/mL IND) regardless of the total amount of IND used. This behavior is also characteristic of diluted copolymer solutions (0.25 and 0.50 mg/mL). For 2.0 mg/mL PEO_{113}-*b*-$PDPA_{50}$ solutions (Figure IV-11, circles), on the other hand, IND was completely entrapped inside the micelles for target loadings lower than 50 % w/w_p (1.0 mg/mL IND). However, the encapsulated content was further improved up to 83 % w/w_p (1.66 mg/mL IND) by increasing the IND amount in the initial solutions. Importantly, only in this latter case the sedimentation of solids was observed typically after one week under steady (shelf) conditions. Otherwise,

the solutions remained stable over periods of weeks (up to 10 weeks), with no apparent material deposition.

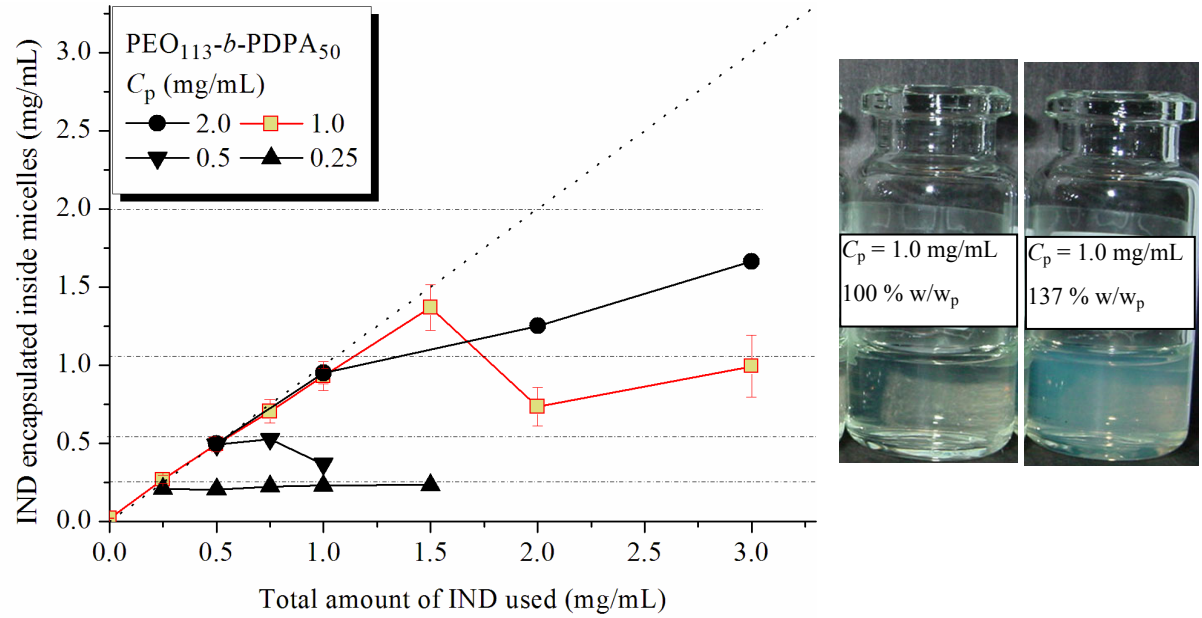

Figure IV-11. Amount of IND loaded into PEO_{113}-*b*-$PDPA_{50}$ micelles as a function of the amount used for different polymer concentrations.

The presence of a hydrophobic probe in such high amounts during the micellization of amphiphilic block copolymers may, of course, affect the thermodynamics and kinetics of the process, leading to aggregates of distinct characteristics. Indeed, IND/PEO_x-*b*-$PDPA_y$ micellar solutions underwent a noticeable visual change towards bluish aspects as the IND content entrapped inside the nano-carriers increased, as illustrated by pictures taken for 1.0 mg/mL PEO_{113}-*b*-$PDPA_{50}$ micelles carrying 100 % w/w_p and 137 % w/w_p IND in their cores (Figure IV-11, insets). This behavior reflects either an important increase in the size of the particles or a transition in the morphology. The onset of this process depended on both the copolymer concentration and the PDPA block length, in agreement with earlier works suggesting that the loading efficiency normally increases with the core-forming block.[54, 94, 129, 132] For PEO_{113}-*b*-$PDPA_{12}$ and $PG2MA_{40}$-*b*-$PDPA_{15}$ (diblocks with short PDPA segments) for instance, such behavior occurred when the targeted loadings were increased from 25 to 50 % w/w_p IND (Figure IV-12).

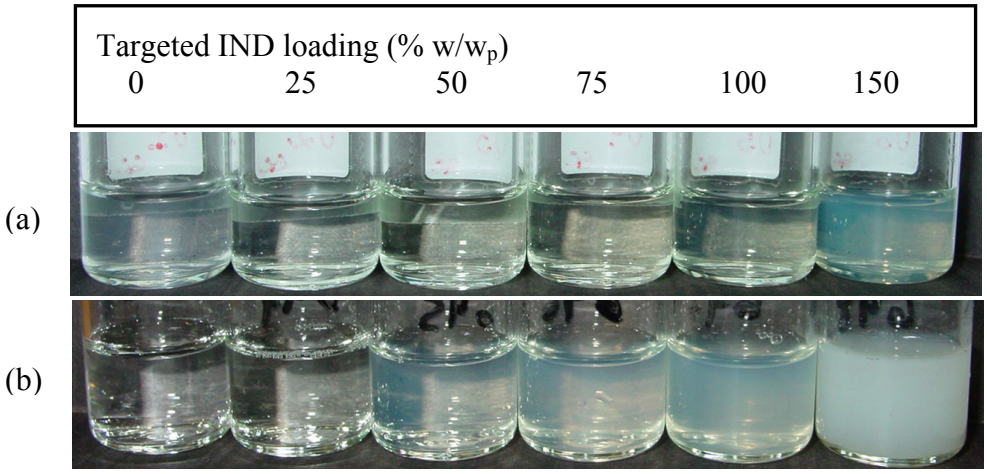

Figure IV-12. Digital photographs taken following a typical IND encapsulation experiment (before separation of unloaded IND) at different targeted loadings (indicated on top) using 1.0 mg/mL PEO_{113}-*b*-$PDPA_{50}$ (a) and PEO_{113}-*b*-$PDPA_{12}$ (b) diblock copolymer solutions.

For a better understanding of the effects of high hydrophobic loadings on the physical chemical properties of the objects, IND-loaded PEO_{113}-*b*-$PDPA_{50}$ micelles were investigated in more details using light scattering (DLS) and microscopy (TEM) techniques. Figure IV-13 shows the variations of the micellar hydrodynamic micelle diameter ($2R_H$) as a function of the IND loading content for 1.0 mg/mL PEO_{113}-*b*-$PDPA_{50}$ solutions. The results revealed a slight decrease in the $2R_H$ values for low IND loadings ($\leq$ 25 % w/w_p) as compared to unloaded particles, suggesting that micelles become slightly more compact. Increasing the IND content above 25 % w/w_p, the size gradually increased until a sharp rise from 33 to 52 nm when probe content finally varied from 99 to 137 % w/w_p. Such a remarkable increase in the size of the nano-objects was also confirmed by TEM. Micrographs recorded for 1.0 mg/mL PEO_{113}-*b*-$PDPA_{50}$ + 137 % w/w_p IND solutions (Figure IV-14a) revealed the presence of much larger objects ($2R$(TEM) = 45 nm) as compared to unloaded counterparts (Figure III-16d; $2R$(TEM) = 16 nm). The effect of high IND loadings on the micelle properties is more pronounced at higher copolymer concentrations. Both DLS and TEM analyses carried out on 2.0 mg/mL PEO_{113}-*b*-$PDPA_{50}$ + 133 % w/w_p IND solutions after adequate dilutions (Figure IV-14b) clearly demonstrated the co-existence of spherical and cylindrical morphologies. Indeed, the formation of cylinders is favored under such circumstances, with a number of Y-junctions sometimes terminated by nearly spherical caps, as observed in this representative TEM picture. Morphology transitions from micelles to cylinders and than to vesicles are usual

responses of block copolymers systems to increases in their solvophobic character, either in organic or aqueous media.[71, 78]

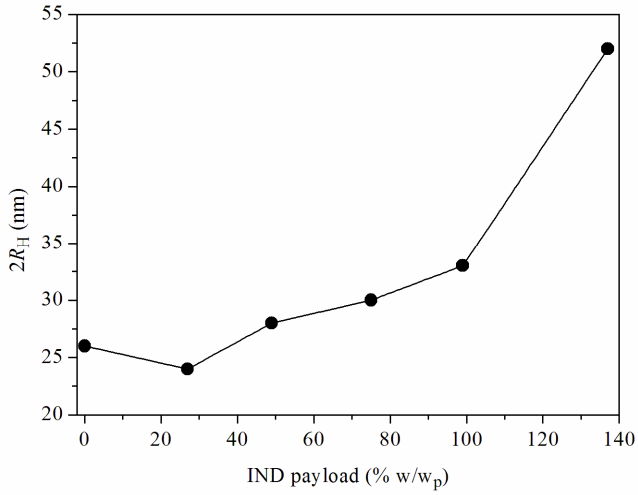

Figure IV-13. Variations in the hydrodynamic micelle diameter ($2R_H$) as a function of the IND payload for 1.0 mg/mL PEO_{113}-*b*-$PDPA_{50}$ solutions.

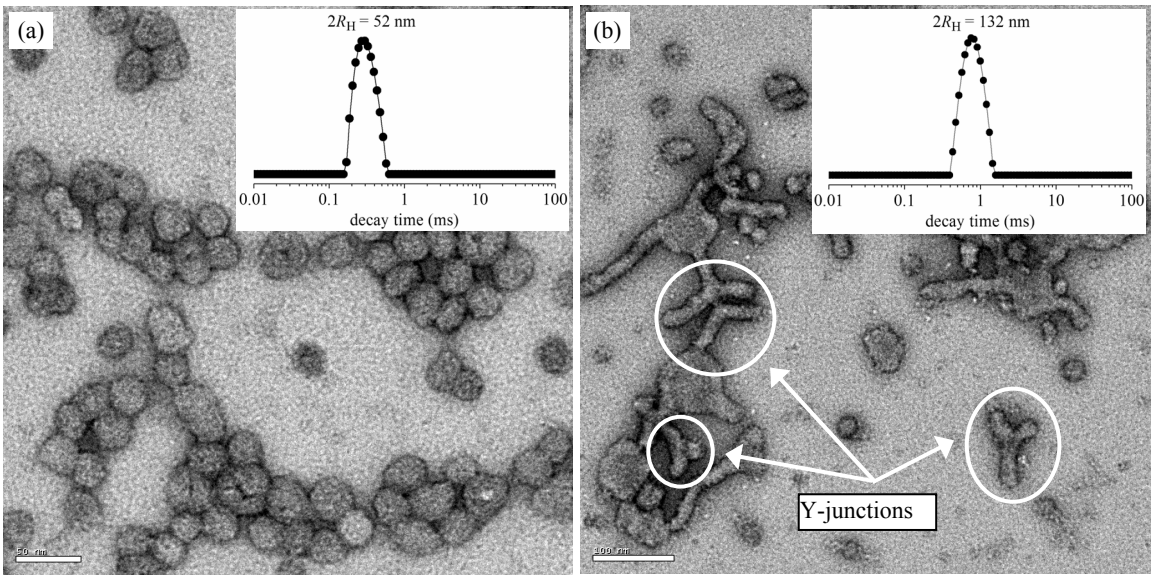

Figure IV-14. TEM images of highly IND-loaded PEO_{113}-*b*-$PDPA_{50}$ micelles: 1.0 mg/mL micelles + 137 % w/w$_p$ drug ((a); scale bar = 50 nm) and 2.0 mg/mL micelles + 133 % w/w$_p$ drug ((b); scale bar = 200 nm). The insets show the respective distributions of the relaxation times $A(t)$ at 90° obtained using CONTIN of DLS results.

Therefore, the results above suggest that the morphology of block copolymer aggregates may change due to the presence of hydrophobic guest molecules, hence characterizing a different strategy to induce morphological changes in block copolymer systems. Nevertheless, this phenomenon represents a significant drawback in drug delivery applications, as far as the

size of nano-delivery systems should ideally remain below 200 nm in order to avoid body's defense mechanisms.[40]

Among the micellar systems with $2R < 200$ nm already described in the literature, the ability to encapsulate IND molecules was markedly lower than for the PEO-*b*-PDPA system (~ 100 % w/w_p IND; stable clear solutions), as concluded by straightforward comparison with data gathered in Table IV-1.

When other hydrophobic molecules such as the ibuprofen (IBPF) drug and the *trans*-3,5-bis(trifluoromethyl)cinnamic acid (F-CIN) probe (Scheme IV-1) were tested with PEO-*b*-PDPA, PEO-*b*-PG2MA-*b*-PDPA, PG2MA-*b*-PDPA and PMPC-*b*-PDPA diblock copolymer micelles, the results revealed essentially the same behavior as described above for IND/PEO-*b*-PDPA system (Table IV-1).

Therefore, micelles having weak polybase-based cores such as poly[2-(dialkylamino)ethyl methacrylate], present an optimized loading capacity for hydrophobic guest molecules containing antagonist carboxylic acid groups. At the best of our knowledge, micelle loading capacities as high as 100 % w/w_p have been rarely reported in the literature for the physical encapsulation (not chemically linked) of hydrophobic molecules by well-defined block copolymer spherical micelles with $2R < 200$ nm. A distinctive result was communicated by Soo *et al.*[132] for the 17β-estradiol/PEO-*b*-PCL system, for which loadings of 190 % w/w_p were reported.

C-1-2. Origins of high micellar payload capacities

Ideally, the solubilizate should match the core-forming polymer in order to achieve high loading into micelles.[40, 77, 129] The reasons for the outstanding loading capacities observed during encapsulation of hydrophobic guest molecules containing carboxylic acid groups into micelles having weak polybase-based cores, were therefore investigated through a combination of structurally different probes and block copolymers (Scheme IV-1) in order to establish a potential macromolecule structure-loading content relationship. The results are listed in Table IV-1 and clearly show that specific (acid-base) interactions between the guest molecules and the core-forming blocks are responsible for the enhanced micellar loading capacities. Indeed, among the probe/micelle systems tested in this work, those exhibiting the capability to form R_1–COOH/NH_2–R_2 pairs (indicated in Table IV-1) were able to stabilize high amounts of hydrophobic probes (~ 100 % w/w_p), as exemplified by IND/PEO-*b*-PDPA,

IBPF/PEO-*b*-PDPA and F-CIN/PEO-*b*-PDPA systems. The esterification of IND yielding to a non-ionizable IND ethyl ester derivative (IND-Et) caused the maximum encapsulated contents to decrease abruptly to 15 % w/w_p, being almost negligible for indomethacin morpholinylamide (IND-M). Similar results were also obtained when IND was combined with non-ionizable block copolymers. For example, the substitution of PEO-*b*-PDPA by PEO-*b*-PCL or PEO-*b*-PGMA provoked a decrease in the loading capacity to ~ 13 % w/w_p or 6 % w/w_p, respectively. Besides, no significant difference between IND and IND-Et loading was evidenced in those cases. (*see also Chapter IV, Section A*).

The existence of specific acid-base interactions between the hydrophobic probes and the block copolymers was corroborated by ^{1}H NMR experiments. Figure IV-15 shows ^{1}H NMR spectra for 15 mg/mL IND in absence (a) and in presence of 16.0 mg/mL PEO_{113}-*b*-$PDPA_{50}$ (20 % excess of DPA units) in THF-d_8, simulating the first step of micelle preparation procedure (i.e., after probe and copolymer dissolution in THF, and before addition of water). In this experiment, the chemical shift at δ ~ 11 ppm associated with the labile acid proton of IND (spectrum **a**) basically disappeared in presence of PEO_{113}-*b*-$PDPA_{50}$ (spectrum **b**).

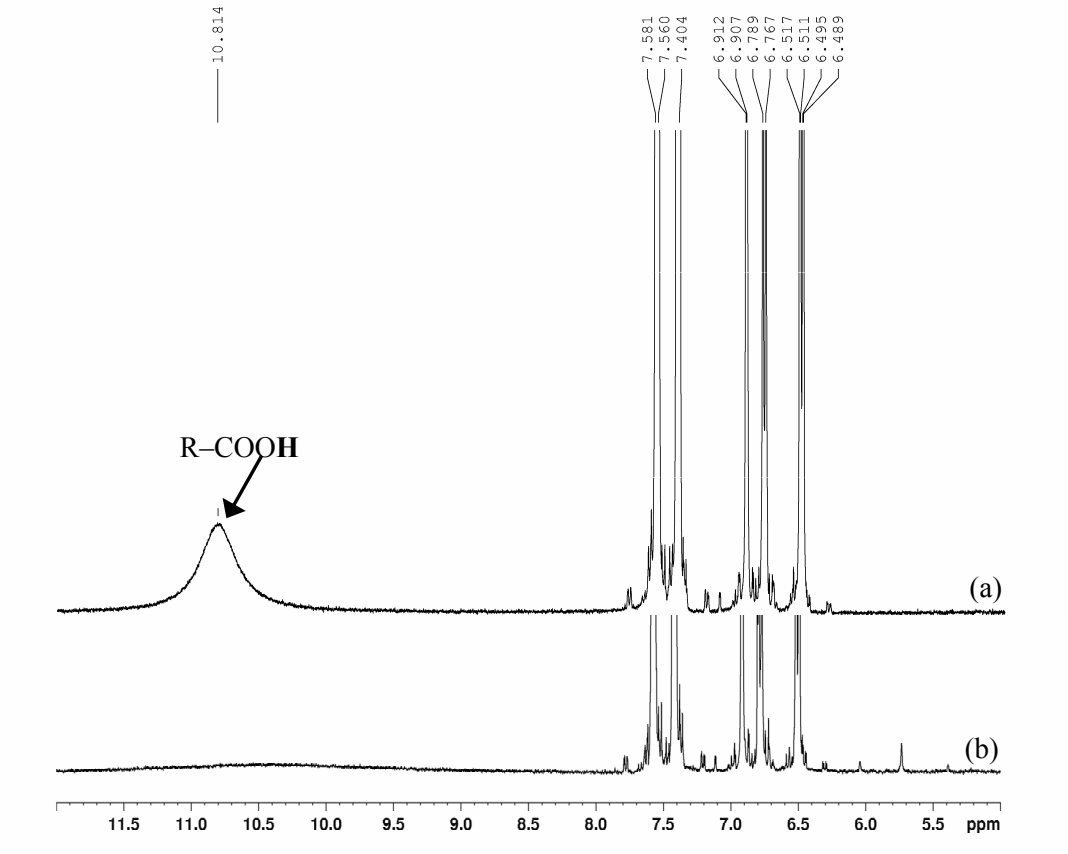

Figure IV-15. ^{1}H NMR spectra for 15 mg/mL IND in absence (a) and in presence (b) of 16.0 mg/mL PEO_{113}-*b*-$PDPA_{50}$ (20 % excess of DPA units) in THF-d_8.

Therefore, the high loading contents of hydrophobic molecules having carboxylic acid groups inside micelles whose core is formed by polybases, is ascribed to acid-base interactions within the latter (Scheme IV-2). The system can be modeled as the neutralization of a weak acid (drug) with a weak base (micelle core), yielding to an inner structure similar to polyion complex (PIC) micelles (Scheme 3).[94] Indeed, this can be easily anticipated on basis of characteristic pK_a-values of the drug to be encapsulated (pK_a(IND) =4.5[143, 247] and pK_a(IBPF) = 4.5[251]) and 2-(dialkylamino) ethyl methacrylate units (pK_a(PDPA-core) = 5.7).[54]

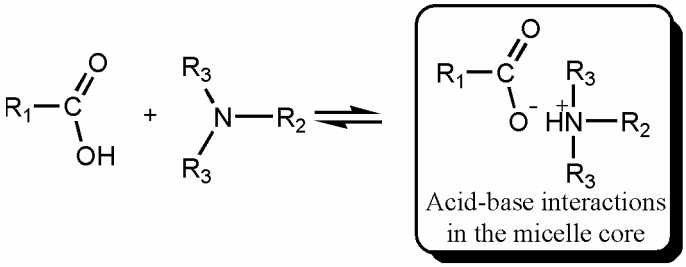

Scheme IV-2. Acid-base interactions inside the micelle core.

C-2 Release

C-2-1. Release kinetics from highly loaded micelles

The release of IND from highly loaded PEO-*b*-PDPA, PEO-*b*-PG2MA-*b*-PDPA and PG2MA-*b*-PDPA micelles may be triggered by lowering the solution pH below pK_a of PDPA, since micellar dissociation occurs rapidly under these conditions. The pH-triggered release of IND is shown in Figure IV-16 for a 1.0 mg/mL PEO_{113}-*b*-$PDPA_{50}$ + 100 % w/w_p IND solution, and corroborates the existence of high drug amounts entrapped inside the micelle cores, simply by visual inspection. In this experiment, the solution pH originally around 7.4 (right) was lowered down to 3.0 (left) by adding 1.0 mol/L HCl. Upon dissociation of PEO-*b*-PDPA micelles due to protonation of the PDPA block at low pH (see the inset), the hydrophobic IND molecules precipitated out of the solution.

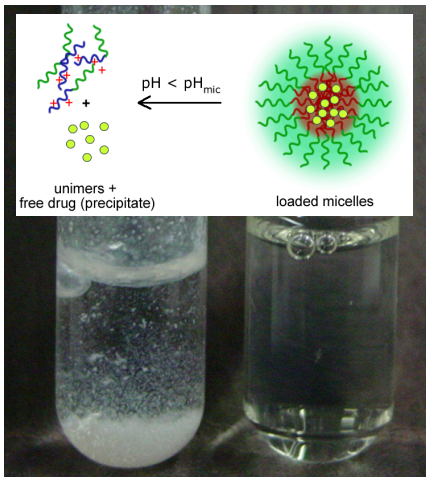

Figure IV-16. Digital picture showing the pH-triggered drug release for a 1.0 mg/mL PEO_{113}-*b*-$PDPA_{50}$ + 100 % w/w_p IND solution.

However, sustained drug release kinetics is normally sought in order to decrease both administration frequency and high plasma levels. The release data are shown in Figure IV-18, which displays (a) the percentage of IND released over time from 1.0 mg/mL PEO_{113}-*b*-$PDPA_{50}$ + 100 w/w_p IND loaded micelles, and (b) the corresponding Higuchi plot. According to these results, the amount of drug released within 8-h period in both cases (di- and triblock micelles) was approximately 85%, with almost complete release being achieved after ~ 24 h. Such an observation suggests, therefore, that the release of hydrophobic drugs with carboxylic acid groups interacting with polybase-based micellar cores basically does not change in comparison to other non-ionizable systems. In fact, the release of molecules such as IND is favored when experiments are carried under nearly sink conditions using buffer solutions at pH > pK_a(drug), because of their dissociation in aqueous media (ionized species are more soluble than non-ionic counterparts, see *Chapter IV, Section B-2*).[143, 149]

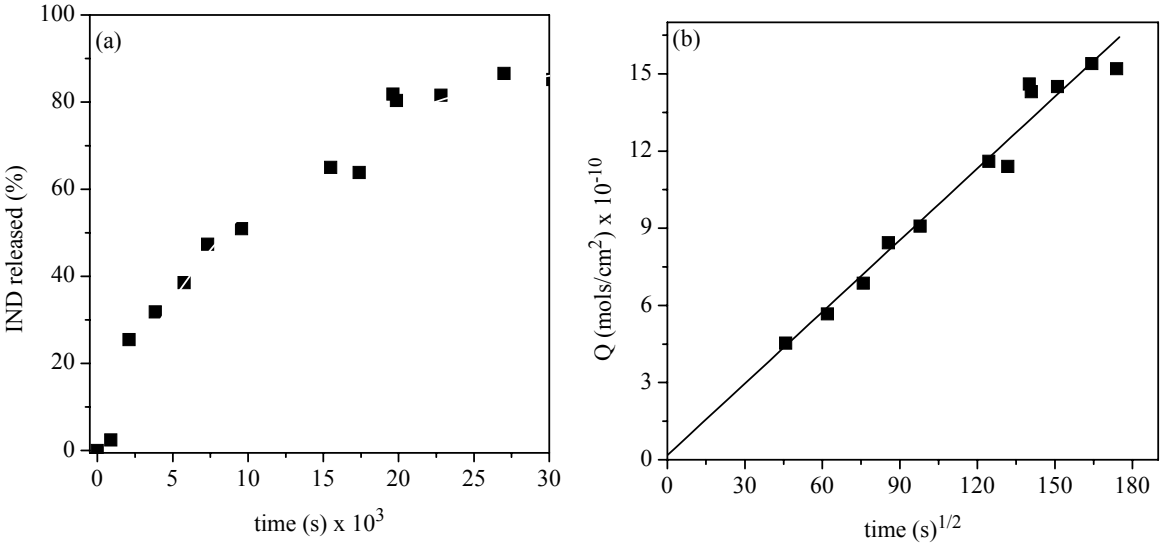

Figure IV-18. Percentage of IND released over time from 1.0 mg/mL PEO_{113}-*b*-$PDPA_{50}$ + 100 %w/w_p IND (a), and the corresponding Higuchi plot (b).

The linearity observed in the Higuchi plot (Figure IV-18b) is indicative of a diffusion-controlled release mechanism,[159] which has been previously used to fit the release of hydrophobic probes from block copolymer micelles.[54, 129, 132, 149] The diffusion coefficient (*D*) extracted from Figure 7 was 6.4×10^{-18} cm^2/s, assuming that the micelle diameter is 33 nm (see Figure 3) and that the density of PDPA is 1.0 g/mL. Comparable *D*-values were also obtained by Soo *et al.*[132] for highly 17*β*-estradiol-loaded PEO_{45}-*b*-PCL_{23} micelles ($D = 8.9 \times 10^{-18}$ cm^2/s).

C-2-2. Effect of probe release on micellar properties

It was shown above (Figures IV-13 and IV-14a) that high payloads of carboxylic acid containing molecules into micelles with weak polybase-based cores provoke a significant increase in the size of the nanocarriers, eventually also leading to changes in the morphology. We elected to use the highest loaded system still exhibiting well-defined spherical aggregates to verify the reversibility of such a "swelling" phenomenon upon release of the probe from the nanoparticles. Figure IV-19a shows the distribution of relaxation times for 1.0 mg/mL PEO_{113}-*b*-$PDPA_{50}$ + 137 % w/w_p IND before and after release experiments, as indicated. Clearly, after a major fraction (86%) of the drug had been released, $2R_H$ decreased from 52 nm down to 33 nm. The latter value is still higher than the typical dimensions of unloaded PEO_{113}-*b*-$PDPA_{50}$ ($2R_H$ = 26 nm). One can thus speculate that N_{agg} may be higher when micellization is carried out in presence of a hydrophobic guest molecule. SLS measurements

have not been performed on these systems. The $2R_H$ decrease upon probe release has been also confirmed by TEM imaging experiments (see Figure IV-14a – loaded micelles – and Figure IV-19b – after release–).

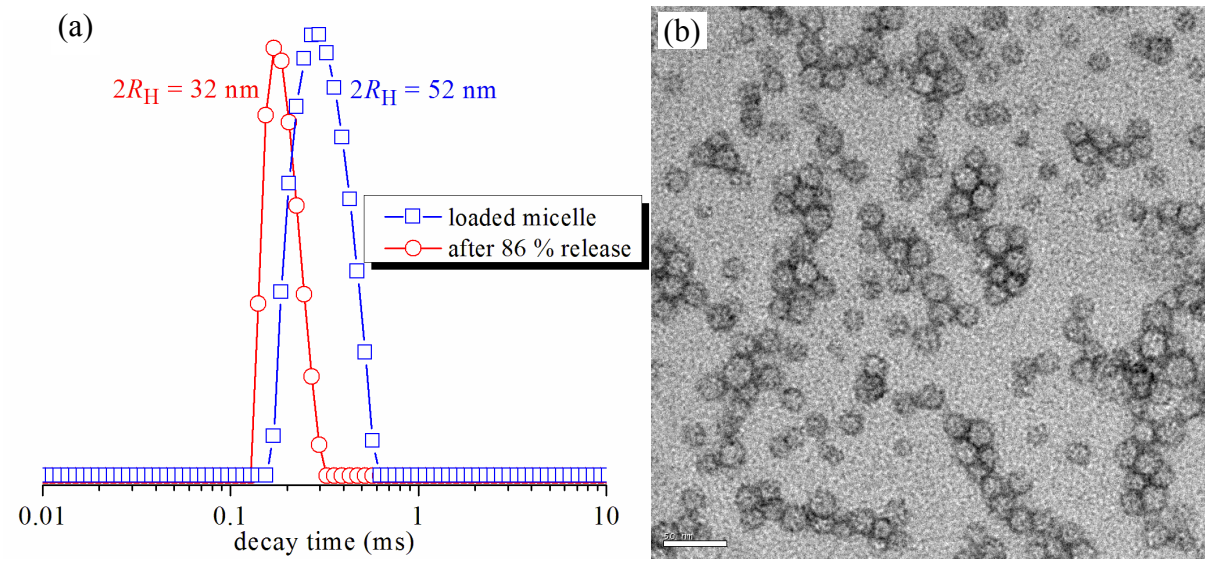

Figure IV-19. Distribution of relaxation times using CONTIN analysis for PEO_{113}-*b*-$PDPA_{50}$ micelles before and after release of their payload (C_p = 1.0 mg/mL, [IND] = 137 % w/w_p) (a), and TEM micrograph taken after release (b). Image showing loaded micellar aggregates is given in Figure IV-14a.

C-3. Nanoparticle Engineering: Control of the Micellar Stability and Release Mechanism

Incontestably, the pH-responsiveness of micellar systems is an extremely useful property for the development of smart materials. Whether or not their complete disassembly upon changes in the external environment is desirable, on the other hand, depends on the purposes of the application.

In the biomedical field, for instance, there is a clear interest in stabilizing these highly loaded objects in order to insure *i*) biocompatibility (provided by the PEO-based corona and *ii*) stability also in acid environments. Indeed, using the cross-linking approach illustrated in Figure III-21 (*Chapter III*), it was found that highly IND-loaded PEO-*b*-PG2MA-*b*-PDPA assemblies can be exposed to acid environment (pH < pH_{mic}), without causing the precipitation of the payload content, as judged simply by visual inspection (Figure IV-20). Nevertheless, the solutions usually became bluish upon decreasing the pH, but regained the original aspect upon re-adjusting the pH to above pH_{mic} (reversible process).

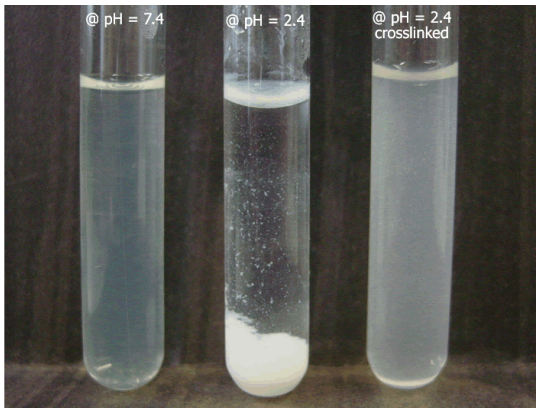

Figure IV-20. Digital picture showing the pH-triggered drug release for a 1.0 mg/mL PEO_{113}-*b*-$PG2MA_{30}$-*b*-$PDPA_{50}$ + 100 % w/w_p IND solution. Left: SCL micelles at pH 7.4; Center: non-SCL micellar solutions with pH lowered down to 2.4; Right: SCL micellar solutions with pH lowered down to 2.4.

Very interestingly, the release kinetics data shown in Figure IV-21 indicated that the insertion of a highly hydrophilic block (PG2MA) as an inner layer between the PDPA core and the PEO corona (Scheme III-21) practically does not affect the release kinetics, even though it represents an additional barrier (hydrophilic) to the diffusion of drug (hydrophobic) toward outside the micellar environment. However, within the timescale of this experiment, such an effect (if it does exist) could not be detected because the drug diffuses quickly through the PG2MA layer,[77] especially at pH > pK_a(IND).

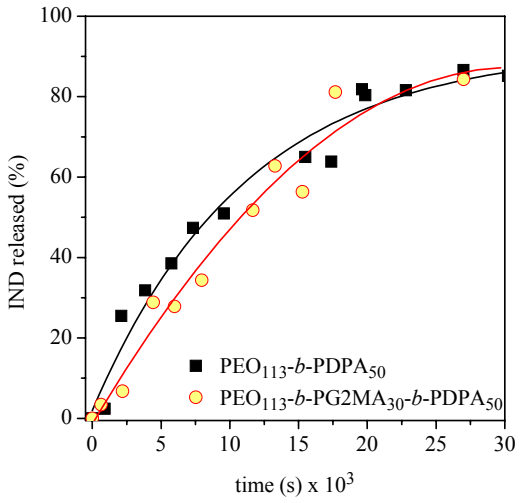

Figure IV-21. Percentage of IND released over time from PEO_{113}-*b*-$PDPA_{50}$ and PEO_{113}-*b*-$PG2MA_{30}$-*b*-$PDPA_{50}$ micelles (C_p = 1.0 mg/mL, [IND] = 100 %w/w_p).

Conclusions and Outlook

The objective of the present work was the conception of original approaches to develop smart block copolymer nanocontainers exhibiting excellent ability to encapsulate, retain, transport and deliver hydrophobic guest molecules. As reviewed in the first chapter, the vast majority of polymeric micelles have shown limited loading capacity, regardless of the hydrophobic guest molecule. The referenced data demonstrate that micellar loading capacities have remained well below 50 % w/wp, thus highlighting the importance of developing novel systems in which the active molecule "matches" the micellar core in terms of compatibility so as to achieve maximal loading into the micelles. Further advances toward general approaches to prepare high loading micellar nanocarriers with widened applications are therefore highly desired.

In an attempt to fulfill such a pressing demand of the nanotechnology field, in the present work efforts were focused on: (*i*) the synthesis and characterization of seven distinct block copolymer systems able to form micellar nanoparticles in selective solvents, (*ii*) the advance in the understanding of encapsulation and release processes of hydrophobic guest molecules by block copolymer micelles, (*iii*) the improvement in the loading capacity of micellar nanoparticles, (*iv*) the influence of the block copolymer structure on the cargo capacity, (*v*) the determination of the effect of large amounts of hydrophobic guest molecules entrapped inside the nanocarriers on their physical chemical parameters (size, shape, polydispersity, stability, etc.), (*vi*) the control of release mechanisms and kinetics in highly loaded micellar systems through clever manipulation of their structure.

Besides the design and characterization of the self-assembled nanoparticles, the results of this work revealed astonishing differences in terms of probe contents that could be encapsulated inside the particles (in most cases core-corona micelles), which could be organized in three principal groups: *A*) Low (LC $\leq$ 30 % w/w_p), *B*) Moderate (30 % < LC < 70 % w/w_p) and *C*) High loading capacity micelles (LC $\geq$ 70 % w/w_p).

For nanoparticles in category *A*, a clear correlation between physical chemical parameters of the micelle structure (namely $M_{w,mic}$, N_{agg}, R_H, W, R_c, and V_c) and encapsulation performance (loading content, loading efficiency, partition coefficient and release kinetics) is observed. Usually, the loading capacity increases with the length of the core-forming blocks, reflecting the increase in the cargo space of the systems. In parallel, there also occurs an increase in the probe partition coefficients (K_V) between the aqueous phase and the micelles.

Using a rather elaborated approach that consisted in the combination of covalently bound (B-probe) and physically encapsulated (F-probe) fractions of the same hydrophobic probe, the loading capacity of block copolymer micelles can be noticeably improved, as observed for nanocarriers corresponding to category *B*. This was demonstrated by investigations carried out on amphiphilic copolymer – probe conjugates prepared via chemical modification of pendant hydroxyl groups in the structure of pre-formed double hydrophilic block copolymers. The resulting amphiphilic conjugates self-assemble into nanometer-sized spherical micelles or vesicles in water, whose hydrodynamic size ($2R_H$) is dictated by both the amount of probe and the length of the core-forming blocks. For all the samples investigated, the micellar size ($2R_H \leq 150$ nm) was adequate for avoiding the body's defense mechanisms. The ability of such micelles to solubilize, transport and deliver a hydrophobic molecule can be further improved by physically encapsulating the same probe, thus reaching moderate payloads (*i.e.,* covalently bound + physically entrapped hydrophobic guest molecules). However, self-organization of samples with more than 50 % w/w_p payload favor the formation of stable vesicular morphologies instead of micelles, and induce a significant increase in the size of the objects, as was highlighted by light scattering and imaging experiments.

A general and unprecedented approach toward high loading capacity block copolymer micelles was then highlighted (micellar systems grouped in category *C*). Clearly, specific interactions between hydrophobic guest molecules and polymer segments forming the micelle core can significantly improve the loading capacity of self-assembled block copolymer particles in aqueous media, whilst still keeping their hydrodynamic size ($2R_H$) below 150 nm. Micelles whose hydrophobic core was formed by poly[2-(dialkylamino)ethyl methacrylate] (i.e., weak polybases), were successfully loaded with high amounts (~ 150 % w/w_p) of lipophilic probes containing antagonist carboxylic acid groups in their structure. The existence of acid-base interactions between the solubilizate and the PDPA block forming the micelle core, was confirmed by ^{1}H NMR measurements and through encapsulation experiments carried out on systems that combined structurally different hydrophobic probes (IND, IND-Et, IND-M, IBPF, F-CIN) and block copolymers (PEO-*b*-PCL, PEO-*b*-PGMA, PEO-*b*-PDPA, PG2MA-*b*-PDPA).

The conception of such systems with high cargo ability also led to original observations in terms of changes in the morphology (from spheres to cylinders, to vesicles) of block copolymer micellar nanoparticles.

In principle, such an approach can be generalized for other active molecules and polymers, suggesting that chemical modification of already-in-use or novel active molecules (cosmetics, drugs, fragrances, etc) to meet this requirement is a prospective strategy toward highly loaded nanoparticles. Needless to say though, that this may have implications on biological activity of drugs, and such a point must of course be investigated in the near future.

In conclusion, the results reported herein strongly suggest that the loading capacity of block copolymer micelles can be tailored through the rational design of core-forming blocks and hydrophobic guest molecules.

As of this moment, the perspectives for future studies are associated mainly with the original observation of high loadings into micelles whenever specific interactions can take place. Polymer-wise, there seems to exist plenty of possibilities to further fine-tuning micellar properties. A very promising approach would be the use of **A**-*block*-(**B**-*stat*-**C**) or **A**-*block*-(**B**-*grad*-**C**) copolymers, where **A** is the hydrophilic block (e.g.: PEO, PG2MA, PMPC), and **B** and **C** form the hydrophobic segment with **B** being a weak polybase (e.g.: PDPA, PDEA) or a weak polyacid (e.g.: PAA) and **C** being a high-T_g polymer (*e.g.*, PS, PMMA). It is anticipated that the use of these architectures will favor the formation of stable but still pH-responsive nanostructures in solution (i.e.: not susceptible to disassembly upon changes in the external pH due to the presence of hydrophobic units of styrene and/or and methyl methacrylate).

We are also looking forward to evaluating the response of biological systems (model cells) upon contact with the micellar systems described above. Certainly, the substitution of poly[2-(dialkylamino)ethyl methacrylate] core-forming segments by biocompatible macromolecules derivatives is recommend, even though shell-crosslinked micelles having a PEO external layer (such as PEO-*b*-PG2MA-*b*-PDPA micelles) should in principle not present major biocompatibility issues.

The triblock PEO-*b*-PG2MA-*b*-PDPA has also been found to be a very interesting material for studying the properties of nanoparticles dispersed in organic media using light scattering under external electrical field (ongoing work in collaboration with Dr. N. P. Silveira).

The microphase separation in bulk of the aforementioned systems still remains unexplored. Preliminary experiments carried out using small angle x-rays scattering (SAXS, ESRF) have confirmed the formation of nano-organized structures.

****

Conclusion (Français)

****

L'objectif central de cette thèse a été le design d'approches originales pour développer des nanocontainers ayant une excellente capacité d'encapsuler, retenir, transporter et délivrer des molécules hydrophobes. Selon la revue bibliographique présentée dans le Chapitre I, la grande majorité de micelles à base de polymères démontrent une capacité d'encapsulation très limitée, indépendamment de la molécule hydrophobe. Les données révèlent que les capacités d'encapsulation bien inférieures à 50 % w/w_p.

De ce fait, nouveaux développements dans l'encapsulation de molécules hydrophobes via l'auto-assemblabe de copolymères à blocs amphiphiles sont stratégiquement importants pour l'avancée de ce domaine multidisciplinaire. Dans cette direction, les études ont été focalisées sur les objectifs suivants : (i) comprendre de manière claire les processus d'encapsulation et de libération de molécules hydrophobes par des systèmes micellaires obtenus à partir de l'auto-assemblage de copolymères à blocs ; (ii) améliorer significativement la capacité d'encapsulation de nanoparticles micellaires ; (iii) établir une corrélation entre la structure macromoléculaire et la capacité d'encapsulation ; (iv) déterminer l'effet de grandes quantités de molécules hydrophobes encapsulés à l'intérieur des nanocontainers sur leurs paramètres physico-chimiques (taille, forme, polydispersité, stabilité, etc.) ; (v) contrôler le mécanisme et cinétique de libération des molécules hydrophobes par des systèmes micellaires via manipulation intelligente de leur structure.

Les résultats ont montré des différences très intéressantes par rapport à la quantité maximale de molécules hydrophobes encapsulées dans le cœur de la micelle. Ces nanoparticules sont classées en trois groupes principaux, correspondant à leur capacités d'encapsulation (LC) A) faibles ($LC \leq 30$ % w/w_p), B) modérées ($30\ \% < LC < 70\ \%$ w/w_p) et C) élevées ($LC \geq 70$ % w/w_p).

Pour des nanoparticles en catégorie A, une corrélation entre les paramètres physico-chimiques de la structure micellaire ($M_{w,mic}$, N_{agg}, R_H, W, R_c, et V_c) et la capacité maximale d'encapsulation a été établie. En général, la capacité d'encapsulation augmente avec la longueur des blocs qui forment le cœur de la micelle, en conséquence de l'augmentation du volume hydrophobe disponible dans le système.

En utilisant une approche plutôt élaborée et caractérisé par la combinaison d'une fraction de molécule hydrophobe greffées aux chaînes polymériques (B-probe) et une autre fraction libre (F-probe), la capacité d'encapsulation de systèmes micellaire à base de copolymère à blocs a pu être sensiblement améliorée, (nanoparticules en catégorie B).

Des interactions spécifiques du type acide-base dans le cœur de la particule ont été responsables pour l'excellente capacité d'encapsulation systématiquement observée (catégorie C). Cependant, l'incorporation de grandes quantités de matières par des micelles polymériques peut provoquer une augmentation significative de leur taille, ainsi que des transitions de morphologies (de micelles sphériques à cylindres à vésicules). Les résultats suggèrent très clairement que la capacité d'encapsulation des systèmes micellaires stimulables que nous avons développés peut être contrôlée avantageusement via les propriétés structurelles des molécules hydrophobes et des blocs formant le cœur de la nanoparticule.

Experimental Part

This last section describes in detail the experimental procedures for the synthesis, characterization and manipulation of amphiphilic block copolymers herein investigated, as well as the equipments and respective setups used during the present work.

A) Chemicals

α-Methoxy-ω-hydroxy poly(ethylene oxide) (CH_3O-PEO_{113}-OH, Fluka, M_n = 5000 g/mol, M_w/M_n = 1.02), α-bromoisobutyryl bromide (Aldrich, 98%), 1,1,4,7,10,10-hexamethyltriethylenetetramine (HMTETA, Aldrich, 97%), 2,2'-bipyridyl (bpy, Aldrich, 99%), 4-dimethylaminopyridine (DMAP, Aldrich, 98%), copper bromide (CuBr, Aldrich, 99.995%), *N,N'*-Dicyclohexylcarbodiimide (DCC, Fluka, 98%), Ibuprofen (IBPF, Aldrich, 98%), Indomethacin (IND, Fluka, 99%), Indomethacin morpholinylamide (IND-M, Sigma-RBI), *N,N,N',N',N''*-pentamethyldiethylenetriamine (PMDETA, Aldrich, 99%), tin(II) 2-ethylhexanoate ($Sn(Oct)_2$, Aldrich, 95%), *trans*-3,5-Bis(trifluoromethyl)cinnamic acid (F-CIN, Aldrich, 98%), poly(ethylene oxide)-*b*-polycaprolactone block copolymers (PEO-*b*-PCL, Polymer Source Inc.) were used as received. The monomers 2-(diisopropylamino) ethyl methacrylate (DPA, Scientific Polymer Products, 99%), 2-(diethylamino) ethyl methacrylate (DEA, Aldrich, 99%), glycidyl methacrylate (GMA, Aldrich, ≥ 97%) and solketal (SK, Aldrich, 97%) were distilled under reduced pressure before polymerization. e-Caprolactone was distilled under reduced pressure over CaH_2 before polymerization. Glycerol monomethacrylate (G2MA) monomer was kindly donated by Röhm Methacrylates, and was used as received. Triethylamine (Et_3N, $(C_2H_5)_3N$, 99%, Acros), THF (J.T.Baker), and toluene (J.T.Baker) were distilled over BaO, Na/benzophenone and polystyryllithium, respectively.

All other solvents and chemicals were of the highest purity available from Aldrich, were used without any further purification.

B) Synthesis of ATRP Initiators and Active Molecule Derivatives

B-1. Bromo-terminated poly(ethylene oxide) (PEO-Br)

MeO-PEO_{113}-OH (25.0 g, 5.0 mmol) was dissolved in 200 mL of dry toluene in a 500 mL three-neck flask. After azeotropic distillation of ca. 50 mL of toluene at reduced pressure to remove traces of water, dry triethylamine (1.30 mL, 10.0 mol) was added, and the solution

was cooled down to 0 °C. α-Bromoisobutyryl bromide (1.24 mL, 10.0 mmol) was added dropwise via syringe, and the reaction mixture was stirred overnight at room temperature. The stirred solution was treated with charcoal, which was subsequently removed by filtration, and most of the toluene was removed by rotary evaporation prior to precipitation into a 10-fold excess of ether. The crude polymer re-dissolved in 200 mL of CH_2Cl_2, and then extracted with K_2CO_3 saturated aqueous solution (3 x 200 mL). The organic phase was dried over $MgSO_4$, and the final bromo-terminated PEO was obtained after re-precipitation in diethyl ether. Pure white products were obtained after three times precipitation in cold diethyl ether.

B-2. α-(2,2-Dimethyl-1,3-dioxolane-4-methoxy)-ω-bromide poly(ethylene oxide) (SK-PEO-Br)

AROP of EO was performed as previously described by Feng et al.,[211] except that in this work 2,2-dimethyl-1,3-dioxolane-4-methanol (Solketal, SK) initiated the reaction in THF. Dry THF (100 mL) and SK (0.226 mL, 1.82 mmol) were charged into a 250 mL three-neck round-bottomed flask equipped with a magnetic stirrer and an inlet. Subsequently, diphenyl methyl potassium (DPMK) solution in THF (1.731 mL, 1.27 mmol, 0.7 eq. with respect to hydroxyl groups) was slowly introduced, and the orange-red color disappeared as alkoxides were formed. After ca. 4 h, EO (10.0 mL, 200.2 mmol) was added to the system at T < ~ -30°C. The solution temperature was then left to rise to 25 °C, being stirred for 48 under these conditions. The reaction was terminated with the adding 6.0 mL of MeOH. Following, hydroxyl end groups were reacted with α-bromoisobutyryl bromide applying the same procedure as for PEO-Br (*Section B-1*), yielding the title compound.

B-3. α-(2,3-dihydroxypropoxy)-ω-bromide poly(ethylene oxide) (OH_2-PEO-Br)

$(OH)_2$-PEO-Br was prepared by stirring the precursor SK-PEO-Br (4.0 g, 0.95 mmol) in 40 mL of a glacial acetic acid:water 1:4 v/v mixture for 45 min at 80°C. The solution was allowed to cool to room temperature before addition of CH_2Cl_2 (25 mL). The aqueous layer was saturated by slow addition with sodium hydrogen carbonate (10 g), separated from the organic layer and washed with CH_2Cl_2 (3 x 20 mL). The title compound was obtained from after 2x precipitation in cold diethyl ether. Yield = 70%.

B-4. 2,2-Dimethyl-1,3-dioxolane-4-methoxy-(2'-bromo-2'-methylpropionoyl) (SK-Br)[249]

SK (12.0 mL, 96.5 mmol), triethylamine (26.9 mL, 193 mmol) and anhydrous tetrahydrofuran (120 mL) were loaded in a 250 mL round-bottomed flask equipped with a magnetic stirrer and cooled to 0°C with an ice bath. 2-bromo-2-methylpropionyl bromide (13.1 mL, 110 mmol) was added dropwise with a syringe. Next, the mixture was stirred for 45 minutes and allowed to reach room temperature. After this the reaction mixture was stirred into an excess of cold water (200 mL) and extracted with diethyl ether (3 x 125 mL). The organic layer was washed subsequently with a saturated aqueous solution of sodium carbonate (3 x 100 mL), acidified water (pH = 4.0 – 4.5, 3 x 100 mL), and again the saturated solution of sodium carbonate (3 x 100 mL). The organic layer was dried over anhydrous sodium sulfate. Finally the sodium sulfate was removed by filtration and the solvent was removed under reduced pressure using a rotary evaporator to give the title compound as a slightly yellowish oil. Yield = 81%. ^{1}H NMR 400 MHz in $CDCl_3$ (δ, ppm): 4.26 (m, 1H), 4.14 (m, 2H), 4.00 (t, 1H), 3.75 (t, 1H), 3.63 (b, OH), 1.86 (s, 6H), 1.36 and 1.28 (s, 3H each).

B-5. 1-O-(2'-Bromo-2'-methylpropionoyl)-2,3-rac-glycerol ((OH)$_2$-SK-Br)[249]

The same procedure as described for the hydrolysis of SK-PEO-Br (Section B-3, above) was applied in the case of SK-Br, except that in the present case diethyl ether was used as organic solvent during the extraction from aqueous media. The organic layer was dried over anhydrous sodium sulfate. Finally the sodium sulfate was removed by filtration and the solvent was removed under reduced pressure using a rotary evaporator. The crude solid was re-crystallised from toluene to give a white powder. Yield = 80%. ^{1}H NMR 400 MHz in $CDCl_3$ (δ, ppm): 4.95 (d, OH), 4.67 (t, OH), 4.14 (m, 1H), 4.05 (m, 1H), 3.70 (m, 1H), 3.39 (m, 2H), 1.91 (s, 6H).

B-6. Synthesis of Indomethacin Ethyl Ester (IND-Et).

IND (2.0 g, 5.6 mmol) was dissolved in 20 mL of ethanol under nitrogen atmosphere. Subsequently, DMAP (0.07 g, 0.56 mmol) was added to the solution. After 10 min under stirring at 0 ^{o}C, DCC (1.15 g, 5.6 mmol) dissolved in 1.5 mL of ethanol was added dropwise. Subsequently, the solution was stirred for 30 min at 0^{o}C, and then overnight at room temperature. The product was isolated firstly by removing the solvent under reduced pressure. Dichloromethane (30 mL) was added to the residue and the suspension was filtered to remove

solid by-products (urea). The filtrate was extracted with saturated K_2CO_3 (3 x 10 mL) aqueous solution, and the organic phase was dried with anhydrous $MgSO_4$, filtered and evaporated. The product (IND-Et) was finally purified by column chromatography (silica gel) using ethyl acetate and cyclohexane (1:1 v/v) as eluent. The isolated product was obtained as a yellow solid (62 % yield). ^{1}H NMR 400 MHz in $CDCl_3$ (δ, ppm): 7.66 and 7.46 (AB, 2H and 2H), 6.96 (d, 1H), 6.86 (d, 1H), 6.67 (dd, 1H), 4.15 (q, 2H), 3.83 (s, 3H), 3.65 (s, 2H), 2.38 (s, 3H), 1.27 (t, 3H).

C) Polymer Synthesis

C-1. Poly[2-(methacryloyloxy)ethyl phosphorylcholine]-b-poly[2-(diisopropylamino) ethyl methacrylate] (PMPC-b-PDPA)

Within the collaboration framework with Steven P. Armes (University of Scheffield, UK), the PMPC-*b*-PDPA diblocks herein investigated were prepared by his group,[212] using sequential monomer addition (MPC followed by DPA) and ATRP techniques. The polymerization was initiated by an oligo(ethylene glycol)-based water-soluble initiator (OEGBr), and carried out in MeOH at 20 ^{o}C in presence of Cu(I)Br/bpy as catalyst (see also *Section C-3*).

C-2. Poly(ethylene oxide)-b-poly[2-(diisopropylamino) ethyl methacrylate] (PEO-b-PDPA).

In a typical ATRP procedure, DPA monomer (3.0 mL, 12.8 mmol), HMTETA ligand (0.15 mL, 0.54 mmol), and distilled THF as solvent (6.0 mL) were charged into a dry 100 mL Schlenk flask. The tube was sealed with a rubber septum and subjected to four freeze-pump-thaw cycles, then the solution was cannulated under nitrogen into another Schlenk tube, previously evacuated and filled with nitrogen, containing Cu(I)Br (0.04 g, 0.27 mmol), PEO_{113}-Br macroinitiator (1.36 g, 0.27 mmol), and a magnetic stirrer. The solution was then immediately immersed in an oil bath at 60^{o}C to start the polymerization. After 180 min, ^{1}H NMR analysis indicated that 95% of DPA had been polymerized. The reaction was then stopped by cooling down, opening the flask to air and adding 50 mL of aerated THF. The mixture was subsequently passed through a basic alumina column in order to remove the spent ATRP catalyst. The final product was obtained after evaporation of volatiles and precipitation in pentane.

C-3. Poly(ethylene oxide)-b-poly(glycerol monomethacrylate)-b-poly[2-(diisopropyl-amino) ethyl methacrylate] (PEO-b-PG2MA-b-PDPA).

The synthesis of PEO-*b*-PG2MA-*b*-PDPA diblock copolymers was carried out via sequential monomer addition using ATRP protocols.[182] Briefly, G2MA monomer (2.3 g, 14.4 mmol), PEO_{113}-Br macroinitiator (2.4 g, 0.48 mmol) and methanol as solvent (6.0 mL) were charged to a dry 100 mL Schlenk flask. After purging with nitrogen during 30 min to remove dissolved oxygen, the solution was cannulated under nitrogen into another Schlenk tube, previously evacuated and filled with nitrogen, containing Cu(I)Br (0.034 g, 0.24 mmol) and 2,2'-bipyridyl (bpy) ligand (0.075 g, 0.48 mmol), and a magnetic stirrer. The reaction mixture became immediately dark brown and progressively more viscous, indicating the onset of polymerization. The polymerization was allowed to continue for approximately 2 h, at which point the monomer conversion was virtually complete as indicted by ^{1}H NMR. A 30-min N_2-purged mixture of DPA monomer (5.6 mL, 23.9 mmol) and methanol (6.0 mL) was then cannulated into this reaction solution, and ^{1}H NMR used to monitor the reaction until monomer consumption was again complete (typically within 12 h at 20 °C). The reaction solutions were treated with silica gel to remove the ATRP catalyst, and precipitated in to pentane or heptane to remove any traces of residual DPA monomer.

C-4. Poly(glycerol monomethacrylate)-b-poly[2-(diisopropyl-amino) ethyl methacrylate] (PG2MA-b-PDPA).

The same procedure as for PEO_{113}-*b*-$PG2MA_{30}$-*b*-$PDPA_{50}$ (*Section C-2*) was applied in the present case, except that $(OH)_2$-SK-Br (*Section B-5*) was used as ATRP initiator.

C-5. Poly(ethylene oxide)-b-poly(glycidyl methacrylate) (PEO-b-PGMA)

The synthesis of PEO-*b*-PGMA diblock copolymers was performed applying essentially the same ATRP protocol as described in *Section C-1*. In this case, however, the polymerization was carried out in DPE at 30 ^{o}C in presence of Cu(I)Br/PMDETA as catalyst.[214] The reaction was stopped by cooling down, opening the flask to air, and adding 50 mL of aerated $CHCl_3$. The mixture was subsequently passed through a neutral alumina column in order to remove the spent ATRP catalyst. The final product was obtained after evaporation of volatiles and precipitation in pentane.

C-6. Poly(ethylene oxide)-b-Polycaprolactone (PEO-b-PCL)[252]

MeO-PEO-OH (4.51 mg, 0.90 mmol) in distilled toluene (30 mL) was dried azeotropically, and ε-CL (10.0 mL, 90.2 mmol) was added. The polymerization was initiated by the addition of $Sn(Oct)_2$ (7.5 mg, 0.018 mmol) at 120 °C, and the reaction mixture was stirred under nitrogen for 24 h. The PEO-*b*-PCL was isolated by precipitation from toluene into heptane.

C-7. Poly(ethylene oxide)-b-poly(glycerol monomethacrylate) (PEO-b-PG2MA)

The same procedure as for the G2MA monomer in the synthesis of PEO_{113}-*b*-$PG2MA_{30}$-*b*-$PDPA_{50}$ (*Section C-2*), was applied in the present case.

C-8. Poly(ethylene oxide)-b-[poly(glycerol monomethacrylate)-indomethacin] conjugates (PEO-b-(PG2MA-IND)

Conjugation of indomethacin (IND) to pendant hydroxyl groups of PG2MA segments was achieved using Steglich esterification. In a typical procedure, CH_3O-PEO113-*b*-$PG2MA_{40}$ diblock (0.40 g, 0.032 mmol, 2.56 mmol OH groups) and IND (0.46 g, 1.28 mmol) were dissolved in 5.0 mL of dry DMF. Subsequently, DCC (0.26 g, 1.28 mmol) and DMAP (catalytic 10 mol% amount) dissolved in DMF (1.0 mL) were added dropwise. The mixture was left to react at room temperature during 72 h. Afterwards, DMF was almost completely removed under reduced pressure. Then, 10.0 mL of THF were added to re-dissolved polymer-drug conjugate. Remaining solid by-products (urea) were filtered off, and the solvent volume reduced to 4-5 mL. Finally, the copolymer-drug conjugate was obtained after precipitation in a 10-fold excess of cold diethyl ether, conditions at which free IND is soluble, thus allowing the removal of unreacted drug. The IND amount effectively attached to the polymer was determined by ^{1}H NMR and UV-vis spectroscopy.

The efficiency of esterification reactions was calculated using ^{1}H NMR and UV-vis techniques. In the case of NMR analysis, determination was done on basis of the integral ratio between aromatic IND proton at 6.9 ppm and methacrylate signal of PG2MA block in

between 1.6 – 0.5 ppm (normalized to 3H), also taking in account the polymerization degree of PG2MA (DP_{G2MA}).

For UV-vis quantification of B-IND, the standard addition method was used. Firstly, each polymer sample was dissolved in THF to produce an organic solution containing C_{IND} ~ 1.0 mg/mL, on basis of ^{1}H NMR IND content. Subsequently, 40 μL aliquots of such solutions were diluted in 3.0 mL of THF, and the UV-vis absorption spectra were acquired as a function of known added aliquots (0, 20, 40, 60, 80 μL) of 1.0 mg/mL (2.8 mmol/L) IND). Linear fitting of the absorbance intensity at 320 nm (λ_{max}) versus added IND aliquots generated straight lines, from which the "negative volume" of added IND corresponding to zero UV-vis absorption was obtained, and accordingly the concentration of IND present in the original copolymer was calculated.[54]

D) Molecular Characteristics of Initiators and Polymers

D-1. Gel Permeation Chromatography (GPC)

Unless otherwise indicated, number average molar mass (M_n) and molar mass distribution (M_w/M_n) values were determined by GPC either in THF at a flow rate of 1.0 mL/min using a PLgel 5 μm Mixed-C column on a Jasco apparatus equipped with a refractive index detector or in DMF containing 1.0 g/L LiBr at a flow rate of 1.0 mL/min using a series of two PLgel 5 μm Mixed-C columns, equally on Jasco equipment. Calibration was performed using a series of near-monodisperse polystyrene (PS) standards in both cases.

D-2. Nuclear Magnetic Resonance spectroscopy (NMR)

400 MHz ^{1}H and 100 MHz ^{13}C NMR spectra were acquired using an Avance DPX 400 spectrometer. The solvent used for the analyses depended on the polymer solubility properties, and is indicated for each particular case.

E) Physical Chemical Properties of Nanosized Copolymer Assemblies

E-1. Static and Dynamic Light Scattering (SDLS)

SDLS measurements were performed using an ALV laser goniometer, which consists of a 22 mW HeNe linear polarized laser operating at a wavelength of 632.8 nm and an ALV-5000/EPP multiple τ digital correlator with 125 ns initial sampling time. The copolymer solutions were maintained at a constant temperature of 25.0 ± 0.1 °C in all experiments. The accessible scattering angles range from 15° to 150°. The solutions were placed in 10 mm diameter glass cells. The minimum sample volume required for DLS experiments was 1 mL. Data were collected using ALV Correlator Control software and the counting time varied for each sample from 300 to 900 s.

E-2. Transmission Electron Microscopy (TEM)

TEM images were recorded using a CM 120 Philips microscope operating at 120 kV, and equipped with a USC1000-SSCCD 2k x 2k Gatan camera. To prepare the TEM samples, 5 μL of an aqueous solution of block copolymer micelles was dropped onto a carbon-coated copper grid, which was rendered hydrophilic by UV/ozone treatment. Excess micelle solution was gently removed using absorbent paper. Samples were then negatively stained by adding a 5 μL droplet of 2% sodium phosphotungstate solution at pH 7.4, and the excess solution was again removed prior to drying under ambient conditions.

E-3. Fluorescence Spectroscopy

Steady-state fluorescent spectra were measured using a FLX Safas Monaco spectrometer in the right-angle geometry (90° collector optics). For the fluorescence measurements, 2 mL of solution was placed in a 10-mm square quartz cell. All spectra were recorded from air-equilibrated solutions. For the fluorescence emission spectra, λex = 339 nm when pyrene was used as probe, and λex = 415 nm for dipyridamole. Spectra were accumulated with an integration time of 1 second per 0.5 nm.

E-4. UV-vis Spectroscopy

UV-vis spectra were recorded using a Varian Cary 300 UV–vis spectrophotometer. For the measurements, 3.0 mL of solution were placed in a 10-mm square quartz cell. All spectra were recorded after baseline correction for solvent from air-equilibrated solutions in the 300 – 450 nm wavelength range at scan rate of 600 nm/min (0.1 sec integration per 1.0 nm).

E-5. Potentiometric Titration

Systems exhibiting pH-responsiveness were studied by potentiometry. Copolymer solutions at pH = 3.0 were prepared as previously described above. Potentiometric titrations curves were obtained by monitoring the pH increase as a function of added 0.01015 mol/L NaOH (increments of 0.10 mL in a 10 mL aliquot of 0.5 mg/mL diblock copolymer-containing solution). The pH measurements were performed using a Mettler Toledo pH-meter coupled to an InLab 423 combined pH electrode, and titration curves in the pH range of 3 to 10 were recorded.

F) Analytical Methods for Probe Quantification

F-1. UV-vis analysis

The probe content effectively encapsulated inside the micellar nano-carriers was determined by UV-vis spectrometry using analytical curves obtained at probe concentrations ranging from 5.0 to 100.0 μg/mL in THF (or ethanol). In all cases, the UV-vis absorption intensity at λ_{max} depended linearly on the concentration, as illustrated in Figure S1 for Indomethacin morpholinylamide (IND-M).

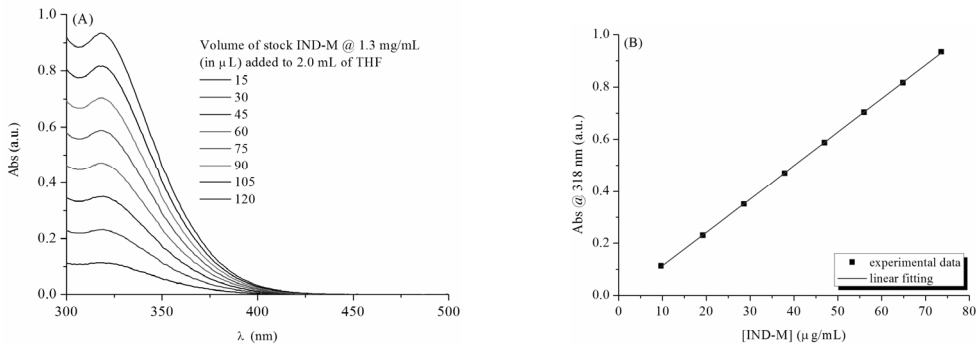

Figure S1. UV-vis absorption spectra acquired as a function of known added aliquots of 1.3 mg/mL IND-M in THF (a), and the respective analytical curve (b).

F-2. Fluorescence analysis

Fluorescence analysis was used for dipyridamole quantification in PMPC-b-PDPA micelles. The loading efficiency was determined using the standard addition analytical method, which is suitable to avoid any possible matrix effects on the quantum yield of DIP fluorescence. Drug-loaded micelles were dissolved in citric acid/sodium citrate buffer at pH = 3.0 to induce dissociation and to ensure a constant fluorescence quantum yield of DIP in aqueous solution. The fluorescence emission intensity at 490 nm (λ_{exc} = 415 nm) was measured as a function of known added aliquots (25, 50, 75, 100, 150, 200 μL) of 3.8 x 10^{-3} mol dm^{-3} DIP. Linear fitting of experimental points generated straight lines, from which the 'negative volume' of added DIP corresponding to zero fluorescence intensity was obtained, and accordingly the amount of DIP present in the original copolymer solution was calculated.

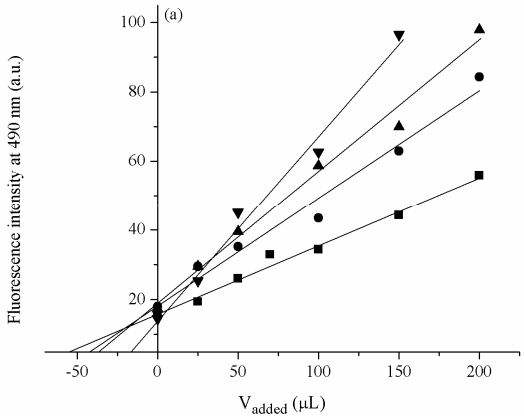

Figure S2. Illustrative plot showing the determination of DIP loadings encapsulated inside $PMPC_{30}$-*b*-$PDPA_{60}$ micelles prepared with varying quantities of added DIP (▼ 5, ▲ 10, ● 15 and ■ 20 % w/w_p (weight/weight of polymer)) employing the standard addition method.

List of Figures

Chapter 1

Chapter II

Chapter III

Chapter IV

List of Schemes

Chapter II

List of Tables

Chapter I

Chapter II

Chapter III

Chapter IV

References

1. Editorial. *Nano Today* **2005,** December, 1.
2. Lovinger, A. J. Nano-, bio-, multi-, inter-,...: Polymer research in an era of prefixes, *Polym. Rev.* **2005,** 45, (3), 195-199.
3. Chow, D. C.; Johannes, M. S.; Lee, W.-K.; Clark, R. L.; Zauscher, S.; Chilkoti, A. Nanofabrication with biomolecules, *Nano Today* **2005,** December, 30-39.
4. Hamley, I. W. Nanostructure fabrication using block copolymers *Nanotechnology* **2003** 14 (10), 39-54.
5. Lazzari, M.; Liu, G.; Lecommandoux, S., *Block Copolymers in Nanoscience*. Wiley-VCH Verlag GmbH & Co.: Darmstadt, 2006.
6. Ikkala, O.; Brinke, G. Hierarchical self-assembly in polymeric complexes: Towards functional materials, *Chem. Comm.* **2004**, 2131-2137.
7. Huang, E.; Rockford, L.; Russell, T. P.; Hawker, C. J. Nanodomain control in copolymer thin films, *Nature* **1998,** 395, (6704), 757-758.
8. Lin, Y.; Boker, A.; He, J.; Sill, K.; Xiang, H.; Abetz, C.; Li, X.; Wang, J.; Emrick, T.; Long, S.; Wang, Q.; Balazs, A.; Russell, T. P. Self-directed self-assembly of nanoparticle/copolymer mixtures, *Nature* **2005,** 434, (7029), 55-59.
9. Hawker, C. J.; Russell, T. P. Block copolymer lithography: Merging "bottom-up" with "top-down" processes, *MRS Bulletin* **2005,** 30, (12), 952-966.
10. Li, M.; Ober, C. L. Block copolymer patterns and templates, *Materials Today* **2006,** 9, 30-39.
11. Gowrishankar, V.; Miller, N.; McGehee, M. D.; Misner, M. J.; Ryu, D. Y.; Russell, T. P.; Drockenmuller, E.; Hawker, C. J. Fabrication of densely packed, well-ordered, high-aspect-ratio silicon nanopillars over large areas using block copolymer lithography, *Thin Solid Films* **2006,** 513, (1-2), 289-294.
12. Matyjaszewski, K.; Gnanou, Y.; Leibler, L., *Macromolecular engineering*. Wiley-VCH: Weinheim, 2007.
13. Taton, D.; Gnanou, Y., Guidelines for Synthesizing Block Copolymers. In *Block Copolymers in Nanoscience*, Lazzari, M.; Liu, G.; Lecommandoux, S., Eds. Wiley-VCH Verlag GmbH & Co.: Darmstadt, 2006; pp 9-35.

14. Hadjichristidis, N.; Pitsikalis, M.; Iatrou, H. Synthesis of block copolymers, *Adv. Polym. Sci.* **2005,** 189, 1-124.
15. Bernaerts, K. V.; Du Prez, F. E. Dual/heterofunctional initiators for the combination of mechanistically distinct polymerization techniques, *Prog. Polym. Sci.* **2006,** 31, (8), 671-722.
16. Lazzari, M.; López-Quintela, A. Block copolymers as a tool for nanomaterial fabrication, *Adv. Mater.* **2003,** 15, (19), 1583-1594.
17. Deming, T. J. Methodologies for preparation of synthetic block copolypeptides: materials with future promise in drug delivery, *Adv. Drug Deliver. Rev.* **2002,** 54, (8), 1145-1155.
18. Klok, H.-A.; Lecommandoux, S. Supramolecular materials via block copolymer self-assembly, *Adv. Mater.* **2001,** 13, (16), 1217-1229.
19. Fontanille, M.; Gnanou, Y., *Chimie et Physico-Chimie des Polymères*. Dunod: Paris, 2002.
20. Matyjaszewski, K.; Davis, T. P., *Handbook of Radical Polymerization*. Wiley-Interscience: New York, 2002.
21. Durmaz, H.; Dag, A.; Altintas, O.; Erdogan, T.; Hizal, G.; Tunca, U. One-pot synthesis of ABC type triblock copolymers via in situ click [3 + 2] and Diels-Alder [4 + 2] reactions, *Macromolecules* **2007,** 40, (2), 191-198.
22. Wu, P.; Fokin, V. V. Catalytic azide-alkyne cycloaddition: Reactivity and applications, *Aldrichim. Acta* **2007,** 40, (1), 7-17.
23. Lutz, J. F. 1,3-dipolar cycloadditions of azides and alkynes: A universal ligation tool in polymer and materials science, *Angew. Chem., Int. Ed.* **2007,** 46, (7), 1018-1025.
24. Binder, W. H.; Sachsenhofer, R. 'Click' chemistry in polymer and materials science, *Macromol. Rapid Comm.* **2007,** 28, (1), 15-54.
25. Yagci, Y.; Tasdelen, M. A. Mechanistic transformations involving living and controlled/living polymerization methods, *Prog. Polym. Sci.* **2006,** 31, (12), 1133-1170.
26. Ladmiral, V.; Mantovani, G.; Clarkson, G. J.; Cauet, S.; Irwin, J. L.; Haddleton, D. M. Synthesis of neoglycopolymers by a combination of "click chemistry" and living radical polymerization, *J. Am. Chem. Soc.* **2006,** 128, (14), 4823-4830.
27. Abetz, V.; Simon, P. F. W. Phase behavior and morphologies of block copolymers, *Adv. Polym. Sci.* **2005,** 189, 125-212.

28. Lecommandoux, S.; Borsali, R.; Schappacher, M.; Deffieux, A.; Narayaman, T.; Rochas, C. Microphase separation of linear and cyclic block copolymers poly(styrene-b-isoprene): SAXS experiments, *Macromolecules* **2004,** 37, (5), 1843-1848.
29. Hanley, K. J.; Lodge, T. P.; Huang, C. I. Phase behavior of a block copolymer in solvents of varying selectivity, *Macromolecules* **2000,** 33, (16), 5918-5931.
30. Förster, S.; Plantenberg, T. From self-organizing polymers to nanohybrid and biomaterials, *Angew. Chem., Int. Ed.* **2002,** 41, (5), 688-714.
31. Bucknall, D. G.; Anderson, H. L. Polymers get organized, *Science* **2003,** 302, 1904-1905.
32. Babin, J.; Rodriguez-Hernandez, J.; Lecommandoux, S.; Klok, H. A.; Achard, M. F. Self-assembled nanostructures from peptide-synthetic hybrid block copolymers: Complex, stimuli-responsive rod-coil architectures, *Faraday Discuss.* **2005,** 128, 179-192.
33. Chen, H. L.; Lu, J. S.; Yu, C. H.; Yeh, C. L.; Jeng, U. S.; Chen, W. C. Tetragonally packed cylinder structure via hierarchical assembly of comb-coil diblock copolymer, *Macromolecules* **2007,** 40, (9), 3271-3276.
34. Grason, G. M. The packing of soft materials: Molecular asymmetry, geometric frustration and optimal lattices in block copolymer melts, *Physics Reports* **2006,** 433, (1), 1-64.
35. Subbotin, A.; Klymko, T.; tenBrinke, G. Lamellar-in-lamellar structure of A-b-(B-b-C)m-b-B-b-A multiblock copolymers, *Macromolecules* **2007,** 40, (8), 2915-2918.
36. Hamley, I. W., *Block Copolymers in Solution: Fundamentals and Applications*. Wiley New York, 2005.
37. Lodge, T. P.; Pudil, B.; Hanley, K. J. The full phase behavior of block copolymers in solvents of varying selectivity, *Macromolecules* **2002,** 35, 4707-4717.
38. Discher, B. M.; Won, Y.-Y.; Ege, D. S.; Lee, J. C.-M.; Bates, F. S.; Discher, D. E.; Hammer, D. A. Polymersomes: Though vesicles made from diblock copolymers, *Science* **1999,** 284, 1143–1146.
39. Discher, B. M.; Hammer, D. A.; Bates, F. S.; Discher, D. E. Polymer vesicles in various media, *Curr. Opin. Colloid Interface Sci.* **2000,** 5, (1-2), 125-131.
40. Allen, C.; Maysinger, D.; Eisenberg, A. Nano-engineering block copolymer aggregates for drug delivery, *Colloid Surf. B-Biointerfaces* **1999,** 16, (1-4), 3-27.
41. Riess, G. Micellization of block copolymers, *Prog. Polym. Sci.* **2003,** 28, (7), 1107-1170.

42. Bates, F. S.; Fredrickson, G. H. Block copolymer thermodynamics: Theory and experiment, *Annu. Rev. Phys. Chem.* **1990,** 41, 525-557.
43. Kataoka, K.; Harada, A.; Nagasaki, Y. Block copolymer micelles for drug delivery: design, characterization and biological significance, *Adv. Drug Deliv. Rev.* **2001,** 47, (1), 113-131.
44. Astafieva, I.; Khougaz, K.; Eisenberg, A. Micellization in block polyelectrolyte solutions. 2. Fluorescence study of the critical micelle concentration as a function of soluble block length and salt concentration, *Macromolecules* **1995,** 28, (21), 7127-7134.
45. Groenewegen, W.; Egelhaaf, S. U.; Lapp, A.; van der Maarel, J. R. C. Neutron scattering estimates of the effect of charge on the micelle structure in aqueous polyelectrolyte diblock copolymer solutions, *Macromolecules* **2000,** 33, (9), 3283-3293.
46. Babin, J. Synthèse et auto-assemblage de copolymères amphiphiles en étoile de type miktoarm. University of Bordeaux I (France), 2006.
47. Liu, L.; Gao, X.; Cong, Y.; Li, B.; Han, Y. Multiple morphologies and their transformation of a polystyrene-bock-poly(4-vinylpyridine) block copolymer, *Macromol. Rapid Comm.* **2006,** 27, (4), 260-265.
48. Ouarti, N.; Viville, P.; Lazzaroni, R.; Minatti, E.; Schappacher, M.; Deffieux, A.; Borsali, R. Control of the morphology of linear and cyclic PS-b-PI block copolymer micelles via PS addition, *Langmuir* **2005,** 21, (4), 1180-1186.
49. Zhang, L. F.; Eisenberg, A. Formation of crew-cut aggregates of various morphologies from amphiphilic block copolymers in solution, *Polym. Adv. Technol.* **1998,** 9, (10-11), 677-699.
50. Zhang, L. F.; Shen, H. W.; Eisenberg, A. Phase separation behavior and crew-cut micelle formation of polystyrene-b-poly(acrylic acid) copolymers in solutions, *Macromolecules* **1997,** 30, (4), 1001-1011.
51. Shen, H. W.; Eisenberg, A. Morphological phase diagram for a ternary system of block copolymer PS310-b-PAA(52)/dioxane/H2O, *J. Phys. Chem. B* **1999,** 103, (44), 9473-9487.
52. Rodríguez-Hernández, J.; Chécot, F.; Gnanou, Y.; Lecommandoux, S. Toward 'smart' nano-objects by self-assembly of block copolymers in solution, *Prog. Polym. Sci.* **2005,** 30, (7), 691-724.

53. Gil, E. S.; Hudson, S. M. Stimuli-responsive polymers and their bioconjugates, *Prog. Polym. Sci.* **2004,** 29, 1173-1222.

54. Giacomelli, C.; LeMen, L.; Borsali, R.; Lai-Kee-Him, J.; Brisson, A.; Armes, S. P.; Lewis, A. L. Phosphorylcholine-based pH-responsive diblock copolymer micelles as drug delivery vehicles: Light scattering, electron microscopy, and fluorescence experiments, *Biomacromolecules* **2006,** 7, (3), 817-828.

55. Du, J.; Tang, Y.; Lewis, A. L.; Armes, S. P. pH-Sensitive vesicles based on a biocompatible zwitterionic diblock copolymer, *J. Am. Chem. Soc.* **2005,** 127, (51), 17982-17983.

56. Borsali, R., In *Handbook of Polyelectrolytes and Their Applications*, Tripathy, S. K.; Kumar, J.; Nalwa, S., Eds. American Scientific Publishers: Los Angeles, 2002; pp 249-265.

57. Borsali, R. Scattering properties of weakly charged polyelectrolytes, *Phys. Chem. Chem. Phys.* **1996,** 100, (6), 836-840.

58. Borsali, R. Scattering properties of multicomponent polymer solutions: Polyelectrolytes, homopolymer mixtures and diblock copolymer, *Macromol. Chem. Phys.* **1996,** 197, (12), 3947-3994.

59. Förster, S.; Abetz, V.; Müller, A. H. E. Polyelectrolyte block copolymer micelles, *Adv. Polym. Sci.* **2004,** 166, 173-210.

60. Lasic, D. D.; Templeton, N. S. Liposomes in gene therapy, *Adv. Drug Deliv. Rev.* **1996,** 20 221-266.

61. Zupancich, J. A.; Bates, F. S.; Hillmyer, M. A. Aqueous dispersions of poly(ethylene oxide)-b-poly(gamma-methyl-epsilon-caprolactone) block copolymers *Macromolecules* **2006,** 39, 4286-4288.

62. Geng, Y.; Discher, D. E. Hydrolytic degradation of poly(ethylene oxide)-block-polycaprolactone worm micelles *J. Am. Chem. Soc.* **2005,** 127, 12780-12781.

63. Bae, K. H.; Lee, Y.; Park, T. G. Oil-encapsulating PEO-PPO-PEO/PEG shell cross-linked nanocapsules for target-specific delivery of paclitaxel, *Biomacromolecules* **2007,** 8, (2), 650-656.

64. Gohy, J. F. Block copolymer micelles, *Adv. Polym. Sci.* **2005,** 190, 65-136.

65. Lodge, T. P.; Bang, J.; Li, Z.; Hillmyer, M. A.; Talmon, Y. Strategies for controlling intra- and intermicellar packing in block copolymer soluitons: Illustrating the flexibility of the self-assembly toolbox, *Faraday Discuss.* **2005,** 128, 1-12.

66. Zhang, L. F.; Eisenberg, A. Multiple Morphologies of Crew-Cut Aggregates of Polystyrene-B-Poly(Acrylic Acid) Block-Copolymers, *Science* **1995,** 268, (5218), 1728-1731.

67. Zhang, L.; Eisenberg, A. Multiple morphologies and characteristics of "crew-cut" micelle-like aggregates of polystyrene-b-poly(acrylic acid) diblock copolymers in aqueous solutions, *J. Am. Chem. Soc.* **1996,** 118, (13), 3168-3181.

68. Lanson, D.; Schappacher, M.; Deffieux, A.; Borsali, R. Synthesis of comblike poly(styrene-b-isoprene) block copolymers and their properties in good and selective solvents, *Macromolecules* **2006,** 39, (20), 7107-7114.

69. Bougard, F.; Jeusette, M.; Mespouille, L.; Dubois, P.; Lazzaroni, R. Synthesis and supramolecular organization of amphiphilic diblock copolymers combining poly(N,N-dimethylamino-2-ethyl methacrylate) and poly(epsilon-caprolactone), *Langmuir* **2007,** 23, (5), 2339-2345.

70. Giacomelli, C.; Borsali, R. Morphology of poly(ethylene oxide)-b-polycaprolatone copolymer micelles controlled via the preparation method, *Macromol. Symp.* **2006,** 245–246, 147–153.

71. Jain, S. J.; Bates, F. S. On the origins of morphological complexity in block copolymer surfactants, *Science* **2003,** 300, 460-464.

72. Discher, D. E.; Eisenberg, A. Polymer vesicles, *Science* **2002,** 297, (5583), 967-973.

73. Zhang, L. F.; Eisenberg, A. Morphogenic effect of added ions on crew-cut aggregates of polystyrene-b-poly(acrylic acid) block copolymers in solutions, *Macromolecules* **1996,** 29, (27), 8805-8815.

74. Zhang, L. F.; Eisenberg, A. Crew-cut aggregates from self-assembly of blends of polystyrene-b-poly(acrylic acid) block copolymers and homopolystyrene in solution, *J. Polym. Sci. Pt. B-Polym. Phys.* **1999,** 37, (13), 1469-1484.

75. Yu, K.; Zhang, L. F.; Eisenberg, A. Novel morphologies of "crew-cut" aggregates of amphiphilic diblock copolymers in dilute solution, *Langmuir* **1996,** 12, (25), 5980-5984.

76. Zhang, L.; Bartels, C.; Yu, Y.; Shen, H.; Eisenberg, A. Mesosized crystal-like structure of hexagonally packed hollow hoops by solution self-assembly of diblock copolymers, *Phys. Rev. Lett.* **1997,** 79, (25), 5034-5037.

77. Eisenberg, A., Personal Communication. In Pessac/France, 2007.

78. Discher, D. E.; Ahmed, F. Polymersomes, *Annu. Rev. Biomed. Eng.* **2006,** 8, 323-341.

79. Halperin, A. Polymeric vs. monomeric amphiphiles: Design parameters, *Polym. Rev.* **2006,** 46, (2), 173-214.
80. de Gennes, P. G., *Solid State Physics*. Academic: New York, 1978.
81. Noolandi, J.; Hong, K. M. Theory of block copolymer micelles in solution, *Macromolecules* **1983,** 16, (9), 1443-1448.
82. Nagarajan, R.; Ganesh, K. Block copolymer self-assembly in selective solvents: theory of solubilization in spherical micelles, *Macromolecules* **1989,** 22, (11), 4312-4325.
83. Leibler, L.; Orland, H.; Wheeler, J. C. Theory of critical micelle concentration of solutions of block copolymers, *J. Chem. Phys.* **1983,** 79, 3550-3557.
84. Hurter, P. N.; Scheutjens, J. M. H. M.; Hatton, T. A. Molecular modeling of micelle formation and solubilization in block copolymer micelles. 1. A self-consistent mean-field lattice theory, *Macromolecules* **1993,** 26, (21), 5592-5601.
85. Daoud, M.; Cotton, J. P. Star shaped polymers, *J. Phys.-Paris* **1982,** 43, 531-538.
86. Zhulina, E. B.; Birshtein, T. M. Scaling theory of solutions of diblock copolymer micelles, *Vysokomol. Soedin.* **1986,** 28, (10), 773-778.
87. Forster, S.; Zisenis, M.; Wenz, E.; Antonietti, M. Micellization of strongly segregated block copolymers, *J. Chem. Phys.* **1996,** 104, (24), 9956-9970.
88. Linse, P. Micellization of poly(ethylene oxide)-poly(propylene oxide) block copolymers in aqueous solution, *Macromolecules* **1993,** 26, (17), 4437-4449.
89. Hoffmann, H. Hundred years of colloid science fascinating phenomena in surfactant solutions, *Phys. Chem. Chem. Phys.* **1994,** 98, (11), 1433-1455.
90. Creutz, S.; van Stam, J.; Antoun, S.; De Schryver, F. C.; Jerome, R. Exchange of polymer molecules between block copolymer micelles studied by emission spectroscopy. A method for the quantification of unimer exchange rates, *Macromolecules* **1997,** 30, (14), 4078-4083.
91. Schillen, K.; Yekta, A.; Ni, S.; Winnik, M. A. Characterization by fluorescence energy transfer of the core of polyisoprene-poly(methyl methacrylate) diblock copolymer micelles. Strong segregation in acetonitrile, *Macromolecules* **1998,** 31, (1), 210-212.
92. van Stam, J.; Creutz, S.; De Schryver, F. C.; Jerome, R. Tuning of the exchange dynamics of unimers between block copolymer micelles with temperature, cosolvents, and cosurfactants, *Macromolecules* **2000,** 33, (17), 6388-6395.
93. Gao, Z. S.; Zhong, X. F.; Eisenberg, A. Chain dynamics in coronas of ionomer aggregates, *Macromolecules* **1994,** 27, (3), 794-802.

94. Nishiyama, N.; Kataoka, K. Current state, achievements, and future prospects of polymeric micelles as nanocarriers for drug and gene delivery, *Pharmacol. Ther.* **2006,** 112, (3), 630-648.

95. Nishiyama, N.; Bae, Y.; Miyata, K.; Fukushima, S.; Kataoka, K. Smart polymeric micelles for gene and drug delivery, *Drug Discov. Today* **2005,** 2, (1), 21-26.

96. La, S. B.; Nagasaki, Y.; Kataoka, K., Poly(ethylene glycol)-based micelles for drug delivery. In *Poly(Ethylene Glycol)*, Am. Chem. Soc.: Washington, 1997; Vol. 680, pp 99-116.

97. Kwon, G. S.; Kataoka, K. Block-copolymer micelles as long-circulating drug vehicles, *Adv. Drug Deliv. Rev.* **1995,** 16, (2-3), 295-309.

98. Kataoka, K.; Kwon, G. S.; Yokoyama, M.; Okano, T.; Sakurai, Y. Block-copolymer micelles as vehicles for drug delivery, *J. Control. Release* **1993,** 24, (1-3), 119-132.

99. Torchilin, V. P. Block copolymer micelles as a solution for drug delivery problems, *Expert Opin. Ther. Pat.* **2005,** 15, (1), 63-75.

100. Torchilin, V. P. Targeted polymeric micelles for delivery of poorly soluble drugs, *Cell. Mol. Life Sci.* **2004,** 61, (19-20), 2549-2559.

101. Torchilin, V. P. Structure and design of polymeric surfactant-based drug delivery systems, *J. Control. Release* **2001,** 73, 137-172.

102. Torchilin, V. P. Micellar nanocarriers: Pharmaceutical perspectives, *Pharm. Res.* **2007,** 24, (1), 1-16.

103. Torchilin, V. P. Multifunctional nanocarriers, *Adv. Drug Deliver. Rev.* **2006,** 58, (14), 1532-1555.

104. Francis, M.; Cristea, M.; Winnik, F. M. Polymeric Micelles for Oral Drug Delivery: Why and How, *Pure Appl. Chem.* **2004,** 76, (7-8), 1321-1335.

105. Tu, R. S.; Tirrell, M. Bottom-up design of biomimetic assemblies, *Adv. Drug Deliver. Rev.* **2004,** 56, (11), 1537-1563.

106. Duncan, R. The dawning era of polymer therapeutics, *Nat. Rev. Drug Discov.* **2003,** 2, (5), 347-360.

107. Kwon, G. S.; Okano, T. Polymeric micelles as new drug carriers, *Adv. Drug Deliv. Rev.* **1996,** 21, (2), 107-116.

108. Vasir, J. K.; Reddy, M. K.; Labhasetwar, V. D. Nanosystems in drug targeting: Opportunities and challenges, *Curr. Nanosci.* **2005,** 1, (1), 47-64.

109. Mainardes, R. M.; Silva, L. P. Drug delivery systems: Past, present, and future, *Curr. Drug Targets* **2004,** 5, (5), 449-455.

110. Ishihara, K.; Ueda, T.; Nakabayashi, N. Preparation of phospholipid polymers and their properties as polymer hydrogel membranes, *Polym. J.* **1990,** 22, (5), 355-360.

111. Lee, J. H.; Lee, H. B.; Andrade, J. D. Blood compatibility of polyethylene oxide surfaces, *Prog. Polym. Sci.* **1995,** 20, (6), 1043-1079.

112. Woodle, M. C. Controlling liposome blood clearance by surface-grafted polymers, *Adv. Drug Deliver. Rev.* **1998,** 32, (1-2), 139-152.

113. Richter, R. P.; Lai Kee Him, J.; Brisson, A. Supported Lipid Membranes, *Materials Today* **2003,** November, 32-37.

114. Kadoma, Y.; Nakabayashi, N.; Masuhara, E.; Yamauchi, J. Synthesis and hemolysis test of polymer containing phosphorylcholine groups, *Kobunshi Ronbunshu* **1978,** 35, (7), 423-427.

115. Miyazawa, K.; Winnik, F. M. Solution properties of hydrophobically-modified phosphorylcholine-based polymers in water and in the presence of surfactants, *J. Phys. Chem. B* **2003,** 107, (38), 10677-10682.

116. Miyazawa, K.; Winnik, F. M. Synthesis of phosphorylcholine-based hydrophobically modified polybetaines, *Macromolecules* **2002,** 35, (7), 2440-2444.

117. Ma, I. Y.; Lobb, E. J.; Billingham, N. C.; Armes, S. P.; Lewis, A. L.; Lloyd, A. W.; Salvage, J. Synthesis of biocompatible polymers. 1. Homopolymerization of 2-methacryloyloxyethyl phosphorylcholine via ATRP in protic solvents: An optimization study, *Macromolecules* **2002,** 35, 9306-9314.

118. Li, Y.; Narain, R.; Ma, Y. H.; Lewis, A. L.; Armes, S. P. Biomimetic thermo-responsive star diblock gelators, *Chem. Comm.* **2004**, 2746-2747.

119. Lobb, E. J.; Ma, I.; Billingham, N. C.; Armes, S. P.; Lewis, A. L. Facile synthesis of well-defined, biocompatible phosphorylcholine-based methacrylate copolymers via atom transfer radical polymerization at 20 degrees C, *J. Am. Chem. Soc.* **2001,** 123, (32), 7913-7914.

120. Lama, J. K. W.; Mab, Y.; Armes, S. P.; Lewis, A. L.; Baldwina, T.; Stolnika, S. Phosphorylcholine–polycation diblock copolymers as synthetic vectors for gene delivery, *J. Control. Release* **2004,** 100, 293–312.

121. Iwata, R.; Suk-In, P.; Hoven, V. P.; Takahara, A.; Akiyoshi, K.; Iwasaki, Y. Control of nanobiointerfaces generated from well-defined biomimetic polymer brushes for protein and cell manipulations, *Biomacromolecules* **2004,** 5, (6), 2308-2314.

122. Ladmiral, V.; Melia, E.; Haddleton, D. M. Synthetic glycopolymers: an overview, *Eur. Polym. J.* **2004,** 40, (3), 431-449.

123. Narain, R.; Armes, S. P. Synthesis and aqueous solution properties of novel sugar methacrylate-based homopolymers and block copolymers, *Biomacromolecules* **2003,** 4, (6), 1746-1758.

124. Dong, C. M.; Chaikof, E. L. Self-assembled nanostructures of a biomimetic glycopolymer-polypeptide triblock copolymer, *Colloid Polym. Sci.* **2005,** 283, (12), 1366-1370.

125. Lu, F. Z.; Meng, J. Q.; Du, F. S.; Li, Z. C.; Zhang, B. Y. Pyrene end-labeled diblock glycopolymers: Synthesis and aggregation, *Macromol. Chem. Phys.* **2005,** 206, (4), 513-520.

126. Lecolley, F.; Waterson, C.; Carmichael, A. J.; Mantovani, G.; Harrisson, S.; Chappell, H.; Limer, A.; Williams, P.; K., O.; Haddleton, D. M. Synthesis of functional polymers by living radical polymerisation, *J. Mater. Chem.* **2003,** 13, 2689 - 2695.

127. Gadelle, F.; Koros, W. J.; Schechter, R. S. Solubilization of aromatic solutes in block copolymers *Macromolecules* **1995,** 28, 4883-4892.

128. Nagarajan, R.; Barry, M.; Ruckenstein, E. Unusual selectivity in solubilization by block copolymer micelles, *Langmuir* **1986,** 2, (2), 210-215.

129. Soo, P. L.; Luo, L. B.; Maysinger, D.; Eisenberg, A. Incorporation and release of hydrophobic probes in biocompatible polycaprolactone-block-poly(ethylene oxide) micelles: Implications for drug delivery, *Langmuir* **2002,** 18, (25), 9996-10004.

130. Li, Z.; Kesselman, E.; Talmon, Y.; Hillmyer, M. A.; Lodge, T. P. Multicompartment micelles from ABC miktoarm stars in water, *Science* **2004,** 306, (5693), 98-101.

131. Li, Z.; Hillmyer, M. A.; Lodge, T. P. Morphologies of multicompartment micelles formed by ABC miktoarm star terpolymers, *Langmuir* **2006,** 22, (22), 9409-9417.

132. Soo, P. L.; Lovric, J.; Davidson, P.; Maysinger, D.; Eisenberg, A. Polycaprolactone-block-poly(ethylene oxide) micelles: A nanodelivery system for 17B-Estradiol, *Mol. Pharm* **2005,** 2, (6), 519-527.

133. Aliabadi, H. M.; Mahmud, A.; Sharifabadi, A. D.; Lavasanifar, A. Micelles of methoxy poly(ethylene oxide)-b-poly([var epsilon]-caprolactone) as vehicles for the solubilization and controlled delivery of cyclosporine A, *J. Control. Release* **2005,** 104, (2), 301-311.

134. Allen, C.; Han, J. N.; Yu, Y. S.; Maysinger, D.; Eisenberg, A. Polycaprolactone-b-poly(ethylene oxide) copolymer micelles as a delivery vehicle for dihydrotestosterone, *J. Control. Release* **2000,** 63, (3), 275-286.

135. Kwon, G.; Naito, M.; Yokoyama, M.; Okano, T.; Sakurai, Y.; Kataoka, K. Block copolymer micelles for drug delivery: loading and release of doxorubicin, *J. Control. Release* **1997,** 48, (2-3), 195-201.

136. Kataoka, K.; Matsumoto, T.; Yokoyama, M.; Okano, T.; Sakurai, Y.; Fukushima, S.; Okamoto, K.; Kwon, G. S. Doxorubicin-loaded poly(ethylene glycol)-poly(beta-benzyl-l-aspartate) copolymer micelles: their pharmaceutical characteristics and biological significance, *J. Control. Release* **2000,** 64, (1-3), 143-153.

137. Hruby, M.; Konak, C.; Ulbrich, K. Polymeric micellar pH-sensitive drug delivery system for doxorubicin, *J. Control. Release* **2005,** 103, (1), 137-148.

138. Shuai, X. T.; Ai, H.; Nasongkla, N.; Kim, S.; Gao, J. M. Micellar carriers based on block copolymers of poly(e-caprolactone) and poly(ethylene glycol) for doxorubicin delivery, *J. Control. Release* **2004,** 98, (3), 415-426.

139. Ahmed, F.; Discher, D. E. Self-porating polymersomes of PEG-PLA and PEG-PCL: hydrolysis-triggered controlled release vesicles, *J. Control. Release* **2004,** 96, (1), 37-53.

140. Nasongkla, N.; Bey, E.; Ren, J.; Ai, H.; Khemtong, C.; Guthi, J. S.; Chin, S. F.; Sherry, A. D.; Boothman, D. A.; Gao, J. Multifunctional polymeric micelles as cancer-targeted, MRI-ultrasensitive drug delivery systems, *Nano Lett.* **2006,** 6, (11), 2427-2430.

141. Dufresne, M. H.; Le Garrec, D.; Sant, V.; Leroux, J. C.; Ranger, M. Preparation and characterization of water-soluble pH-sensitive nanocarriers for drug delivery, *Int. J. Pharm.* **2004,** 277, (1-2), 81-90.

142. Nakanishi, T.; Fukushima, S.; Okamoto, K.; Suzuki, M.; Matsumura, Y.; Yokoyama, M.; Okano, T.; Sakurai, Y.; Kataoka, K. Development of the polymer micelle carrier system for doxorubicin, *J. Control. Release* **2001,** 74, (1-3), 295-302.

143. La, S. B.; Okano, T.; Kataoka, K. Preparation and characterization of the micelle-forming polymeric drug indomethacin-incorporated poly(ethylene oxide)-poly(beta-benzyl L-aspartate) block copolymer micelles, *J. Pharm. Sci.* **1996,** 85, (1), 85-90.

144. Shin, I. L. G.; Kim, S. Y.; Lee, Y. M.; Cho, C. S.; Sung, Y. K. Methoxy poly(ethylene glycol) epsilon-caprolactone amphiphilic block copolymeric micelle containing indomethacin. I. Preparation and characterization, *J. Control. Release* **1998,** 51, (1), 1-11.

145. Kim, S. Y.; Shin, I. L. G.; Lee, Y. M.; Cho, C. S.; Sung, Y. K. Methoxy poly(ethylene glycol) and epsilon-caprolactone amphiphilic block copolymeric micelle containing

indomethacin. II. Micelle formation and drug release behaviours, *J. Control. Release* **1998,** 51, (1), 13-22.

146. Choi, S. K.; Kim, D. Drug-releasing behavior of MPEG/PLA block copolymer micelles and solid particles controlled by component block length, *J. Appl. Polym. Sci.* **2002,** 83, 435-445.

147. Kim, S. Y.; Kim, J. H.; Kim, D.; An, J. H.; Lee, D. S.; Kim, S. C. Drug-releasing kinetics of MPEG/PLLA block copolymer micelles with different PLLA block lengths, *J. Appl. Polym. Sci.* **2001,** 82, (10), 2599-2605.

148. Sant, V. P.; Smith, D.; Leroux, J. C. Novel pH-sensitive supramolecular assemblies for oral delivery of poorly water soluble drugs: Preparation and characterization, *J. Control. Release* **2004,** 97, (2), 301-312.

149. Giacomelli, C.; Schmidt, V.; Borsali, R. Nanocontainers formed by self-assembly of poly(ethylene oxide)-b-poly(glycerol monomethacrylate) – drug conjugates, *Macromolecules* **2007,** 40, 2148-2157.

150. Shuai, X.; Merdan, T.; Schaper, A. K.; Xi, F.; Kissel, T. Core-cross-linked polymeric micelles as paclitaxel carriers, *Bioconjugate Chem.* **2004,** 15, (3), 441-448.

151. Liu, S. Q.; Tong, Y. W.; Yang, Y. Y. Thermally sensitive micelles self-assembled from poly(N-isopropylacrylamide-co-N,N-dimethylacrylamide)-b-poly(D,L-lactide-co-glycolide) for controlled delivery of paclitaxel, *Mol. Biosyst.* **2005,** 1, 158-165.

152. Xie, Z.; Guan, H.; Chen, X.; Lu, C.; Chen, L.; Hu, X.; Shi, Q.; Jing, X. A novel polymer-paclitaxel conjugate based on amphiphilic triblock copolymer, *J. Control. Release* **2007,** 117, (2), 210-216.

153. Lee, S. C.; Huh, K. M.; Lee, J.; Cho, Y. W.; Galinsky, R. E.; Park, K. Hydrotropic polymeric micelles for enhanced paclitaxel solubility: In vitro and in vivo characterization, *Biomacromolecules* **2007,** 8, (1), 202-208.

154. Lee, S. C.; Kim, C.; Kwon, I. C.; Chung, H.; Jeong, S. Y. Polymeric micelles of poly(2-ethyl-2-oxazoline)-block-poly(epsilon-caprolactone) copolymer as a carrier for paclitaxel, *J. Control. Release* **2003,** 89, (3), 437-446.

155. Lee, J. Y.; Cho, E. C.; Cho, K. Incorporation and release behavior of hydrophobic drug in functionalized poly(D,L-lactide)-block-poly(ethylene oxide) micelles, *J Control. Release* **2004,** 94, (2-3), 323-335.

156. Matsumura, Y.; Hamaguchi, T.; Ura, T.; Muro, K.; Yamada, Y.; Schimada, Y.; Shirao, K.; Okusaka, T.; Ueno, H.; Ikeda, M.; Watanabe, N. Phase I clinical trial and

pharmacokinetic evaluation of NK911, a micelle-encapsulated doxorubicin, *Br. J. Cancer* **2004,** 91, 1775-1781.

157. Kato, K.; Hamaguchi, T.; Yasui, H.; Okusaka, T.; Ueno, H.; Ikeda, M.; Shirao, K.; Shimada, Y.; Nakahama, H.; Muro, K.; Matsumura, Y. Phase I study of NK105, a paclitaxel-incorporating micellar nanoparticle, in patients with advanced cancer, *J. Clin. Oncol.* **2006,** 24, (18), 83S-83S.

158. Hamaguchi, T.; Matsumura, Y.; Suzuki, M.; Shimizu, K.; Goda, R.; Nakamura, I.; Nakatomi, I.; Yokoyama, M.; Kataoka, K.; Kakizoe, T. NK105, a paclitaxel-incorporating micellar nanoparticle formulation, can extend in vivo antitumour activity and reduce the neurotoxicity of paclitaxel, *Br. J. Cancer* **2005,** 92, (7), 1240-1246.

159. Higuchi, T. Rate of release of medicaments from ointment bases containing drugs in suspension, *J. Pharm. Sci.* **1961,** 50, 874-875.

160. Hubbell, J. A. Enhancing drug function, *Science* **2007,** 300, 595-596.

161. Jiang, J.; Tong, X.; Morris, D.; Zhao, Y. Toward photocontrolled release using light-dissociable block copolymer micelles, *Macromolecules* **2006,** 39, (13), 4633-4640.

162. Duncan, R. Nanomedicine gets clinical, *Materials Today* **2005,** 8, 16-17.

163. Bontempo, D.; Li, R. C.; Ly, T.; Brubaker, C. E.; Maynard, H. D. One-step synthesis of low polydispersity, biotinylated poly(N-isopropylacrylamide) by ATRP, *Chem. Comm.* **2005**, 4702 - 4704.

164. Tan, J. F.; Ravi, P.; Too, H. P.; Hatton, T. A.; Tam, K. C. Association behavior of biotinylated and non-biotinylated poly(ethylene oxide)-b-poly(2-(diethylamino)ethyl methacrylate), *Biomacromolecules* **2005,** 6, (1), 498-506.

165. Licciardi, M.; Giammona, G.; Du, J. Z.; Armes, S. P.; Tang, Y. Q.; Lewis, A. L. New folate-functionalized biocompatible block copolymer micelles as potential anti-cancer drug delivery systems, *Polymer* **2006,** 47, (9), 2946-2955.

166. Bae, Y.; Jang, W. D.; Nishiyama, N.; Fukushima, S.; Kataoka, K. Multifunctional polymeric micelles with folate-mediated cancer cell targeting and pH-triggered drug releasing properties for active intracellular drug delivery, *Mol. Biosyst.* **2005,** 1, 242-250.

167. Studer, P.; Limal, D.; Breton, P.; Riess, G. Synthesis and characterization of poly(ethylene oxide)-block-poly(methylidene malonate 2.1.2) block copolymers bearing a mannose group at the PEO chain end, *Bioconjugate Chem.* **2005,** 16, (1), 223-229.

168. Bernard, J.; Schappacher, M.; Deffieux, A.; Viville, P.; Lazzaroni, R.; Charles, M. H.; Charreyre, M. T.; Delair, T. Water-soluble dendrigrafts bearing saccharidic moieties: Elaboration and application to enzyme linked oligosorbent assay (ELOSA) diagnostic tests, *Bioconjugate Chem.* **2006,** 17, (1), 6-14.

169. Becker, M. L.; Liu, J.; Wooley, K. L. Functionalized micellar assemblies prepared via block copolymers synthesized by living free radical polymerization upon peptide-loaded resins, *Biomacromolecules* **2005,** 6, (1), 220-228.

170. Schmidt, V.; Giacomelli, C.; Brisson, A.; Borsali, R. Towards an easy access to Annexin-A5 protein binding block copolymer micelles, *Mater. Sci. Eng. C* **2007**, DOI: 10.1016/j.msec.2007.04.025.

171. Schmidt, V.; Giacomelli, C.; Lecolley, F.; Lai-Kee-Him, J.; Brisson, A. R.; Borsali, R. Diblock copolymer micellar nanoparticles decorated with Annexin-A5 proteins, *J. Am. Chem. Soc.* **2006,** 128, (28), 9010-9011.

172. O'Reilly, R.; Hawker, C. J.; Wooley, K. L. Cross-linked block copolymer micelles: functional nanostructures of great potential and versatility, *Chem. Soc. Rev.* **2006,** 35, 1068 - 1083.

173. Liu, S.; Armes, S. P. Recent advances in the synthesis of polymeric surfactants, *Curr. Opin. Colloid In.* **2001,** 6, (3), 249-256.

174. O'Reilly, R. K.; Joralemon, M. J.; Wooley, K. L.; Hawker, C. J. Functionalization of micelles and shell cross-linked nanoparticles using click chemistry, *Chem. Mater.* **2005,** 17, (24), 5976-5988.

175. Qi, K.; Ma, Q.; Remsen, E. E.; Clark, C. G.; Wooley, K. L. Determination of the bioavailability of biotin conjugated onto shell cross-linked (SCK) nanoparticles, *J. Am. Chem. Soc.* **2004,** 126, (21), 6599-6607.

176. Zhang, Q.; Remsen, E. E.; Wooley, K. L. Shell cross-linked nanoparticles containing hydrolytically degradable, crystalline core domains, *J. Am. Chem. Soc.* **2000,** 122, (15), 3642-3651.

177. Thurmond, K. B.; Huang, H. Y.; Clark, C. G.; Kowalewski, T.; Wooley, K. L. Shell cross-linked polymer micelles: stabilized assemblies with great versatility and potential, *Colloid Surf. B-Biointerfaces* **1999,** 16, (1-4), 45-54.

178. Huang, H.; Remsen, E. E.; Kowalewski, T.; Wooley, K. L. Nanocages derived from shell cross-linked micelle templates, *J. Am. Chem. Soc.* **1999,** 121, (15), 3805-3806.

179. Thurmond, K. B.; Kowalewski, T.; Wooley, K. L. Shell cross-linked knedels: A synthetic study of the factors affecting the dimensions and properties of amphiphilic core-shell nanospheres, *J. Am. Chem. Soc.* **1997,** 119, (28), 6656-6665.

180. Thurmond, K. B.; Kowalewski, T.; Wooley, K. L. Water-soluble knedel-like structures: The preparation of shell-cross-linked small particles, *J. Am. Chem. Soc.* **1996,** 118, (30), 7239-7240.

181. O'Reilly, R. K.; Joralemon, M. J.; Hawker, C. J.; Wooley, K. L. Facile syntheses of surface-functionalized micelles and shell cross-linked nanoparticles, *J. Polym. Sci., Part A: Polym. Chem.* **2006,** 44, (17), 5203-5217.

182. Fujii, S.; Cai, Y.; Weaver, J. V. M.; Armes, S. P. Syntheses of shell cross-linked micelles using acidic ABC triblock copolymers and their application as pH-responsive particulate emulsifiers, *J. Am. Chem. Soc.* **2005,** 127, (20), 7304-7305.

183. Rachel K. O'Reilly, M. J. J. C. J. H. K. L. W. Facile syntheses of surface-functionalized micelles and shell cross-linked nanoparticles, *Journal of Polymer Science Part A: Polymer Chemistry* **2006,** 44, (17), 5203-5217.

184. Li, Y.; Lokitz, B. S.; Armes, S. P.; McCormick, C. L. Synthesis of reversible shell cross-linked micelles for controlled release of bioactive agents, *Macromolecules* **2006,** 39, (8), 2726-2728.

185. Liu, S.; Weaver, J. V. M.; Tang, Y.; Billingham, N. C.; Armes, S. P.; Tribe, K. Synthesis of shell cross-linked micelles with pH-responsive cores using ABC triblock copolymers, *Macromolecules* **2002,** 35, (16), 6121-6131.

186. Butun, V.; Wang, X. S.; de PazBanez, M. V.; Robinson, K. L.; Billingham, N. C.; Armes, S. P.; Tuzar, Z. Synthesis of shell cross-linked micelles at high solids in aqueous media, *Macromolecules* **2000,** 33, (1), 1-3.

187. Hales, M.; Barner-Kowollik, C.; Davis, T. P.; Stenzel, M. H. Shell-cross-linked vesicles synthesized from block copolymers of poly(D,L-lactide) and poly (N-isopropyl acrylamide) as thermoresponsive nanocontainers, *Langmuir* **2004,** 20, (25), 10809-10817.

188. Zhu, H.; Liu, Q.; Chen, Y. Reactive block copolymer vesicles with an epoxy wall, *Langmuir* **2007,** 23, (2), 790-794.

189. Opsteen, J. A.; Cornelissen, J.; van Hest, J. C. M. Block copolymer vesicles, *Pure Appl. Chem.* **2004,** 76, (7-8), 1309-1319.

190. Soo, P. L.; Eisenberg, A. Preparation of block copolymer vesicles in solution, *J. Polym. Sci., Part B: Polym. Phys.* **2004,** 42, (6), 923-938.

191. Chen, Z.; Bao, H.; Liu, J. Synthesis of a well-defined epoxy copolymer by atom transfer radical polymerization, *J. Polym. Sci. Part A: Polym. Chem.* **2001,** 39, 3726-3732.

192. Xia, J.; Matyjaszewski, K. Atom transfer radical polymerization, *Chem. Rev.* **2001,** 101, 2921-2990.

193. Patten, T. E.; Matyjaszewski, K. Atom transfer radical polymerization and the synthesis of polymeric materials, *Adv. Mater.* **1998,** 10, (12), 901-915.

194. Wang, J. S.; Matyjaszewski, K. Controlled/"living" radical polymerization. atom transfer radical polymerization in the presence of transition-metal complexes *J. Am. Chem. Soc.* **1995,** 117, 5614.

195. Kato, M.; Kamigaito, M.; Sawamoto, M.; Higashimura, T. Polymerization of methyl methacrylate with the carbon tetrachloride/dichlorotris-(triphenylphosphine)ruthenium(II)/methylaluminum bis(2,6-di-tert-butylphenoxide) initiating system: Possibility of Living Radical Polymerization, *Macromolecules* **1995,** 28, (5), 1721-1723.

196. Matyjaszewski, K.; Dong, H.; Jakubowski, W.; Pietrasik, J.; Kusumo, A. Grafting from surfaces for "everyone": ARGET ATRP in the presence of air, *Langmuir* **2007,** ASAP Article (DOI: http://dx.doi.org/10.1021/la063402e).

197. Ke Min, W. J. K. M. AGET ATRP in the Presence of Air in Miniemulsion and in Bulk, *Macromol. Rapid Commun.* **2006,** 27, (8), 594-598.

198. Kamigaito, M.; Ando, T.; Sawamoto, M. Metal-catalyzed living radical polymerization, *Chem. Rev.* **2001,** 101, (12), 3689-3746.

199. Matyjaszewski, K. Transition metal catalysis in controlled radical polymerization: Atom transfer radical polymerization, *Chem.-Eur. J.* **1999,** 5, (11), 3095-3102.

200. Taton, D.; Gnanou, Y.; Matmour, R.; Angot, S.; Hou, S.; Francis, R.; Lepoittevin, B.; Moinard, D.; Babin, J. Controlled polymerizations as tools for the design of star-like and dendrimer-like polymers, *Polym. Int.* **2006,** 55, (10), 1138-1145.

201. http://www.chem.cmu.edu/groups/maty/ (April 2nd 2007),

202. Penczek, S.; Cypryk, M.; Duda, A.; Kubisa, P.; Slomkowski, S. Living ring-opening polymerizations of heterocyclic monomers, *Prog. Polym. Sci.* **2007,** 32, (2), 247-282.

203. Pang, K.; Kotek, R.; Tonelli, A. Review of conventional and novel polymerization processes for polyesters, *Prog. Polym. Sci.* **2006,** 31, (11), 1009-1037.

204. Albertsson, A. C.; Varma, I. K. Recent developments in ring opening polymerization of lactones for biomedical applications, *Biomacromolecules* **2003,** 4, (6), 1466-1486.

205. Caillol, S. Synthèse et characterization de nouveaux copolymères potentiellment autoassociatifs. Université Bordeaux 1, Pessac, 2002.

206. Stridsberg, K. M.; Ryner, M.; Albertsson, A. C. Controlled ring-opening polymerization: Polymers with designed macromolecular architecture, *Adv. Polym. Sci.* **2002,** 157, 41-65.

207. Mecerreyes, D.; Jérôme, R.; Dubois, P. Novel macromolecular architectures based on aliphatic polyesters: Relevance of the "coordination-insertion" ring-opening polymerization, *Adv. Polym. Sci.* **1999,** 147, 1-59.

208. Carothers, W. H.; Dorough, G. L.; Natta, F. J. v. Studies of polymerization and ring formation. X. The reversible polymerization of six-membered cyclic esters, *J. Am. Chem. Soc.* **1932,** 54, (2), 761-772.

209. Deng, G.; Zhang, L.; Liu, C.; He, L.; Chen, Y. Synthesis of miktoarm star (block) polymers based on a heterofunctional initiator via combination of ROP, ATRP and functional group transformation, *Eur. Polym. J.* **2005,** 41, (6), 1177-1186.

210. Ternat, C.; Kreutzer, G.; Plummer, C. J. G.; Nguyen, T. Q.; Herrmann, A.; Ouali, L.; Sommer, H.; Fieber, W.; Velazco, M. I.; Klok, H. A.; Ma?nson, J. A. E. Amphiphilic multi-arm star-block copolymers for encapsulation of fragrance molecules, *Macromol. Chem. Phys.* **2007,** 208, (2), 131-145.

211. Feng, X.-S.; Taton, D.; Chaikof, E. L.; Gnanou, Y. Toward an easy access to dendrimer-like poly(ethylene oxide)s, *J. Am. Chem. Soc.* **2005,** 127, (31), 10956-10966.

212. Ma, Y. H.; Tang, Y. Q.; Billingham, N. C.; Armes, S. P.; Lewis, A. L.; Lloyd, A. W.; Salvage, J. P. Well-defined biocompatible block copolymers via atom transfer radical polymerization of 2-methacryloyloxyethyl phosphorylcholine in protic media, *Macromolecules* **2003,** 36, (10), 3475-3484.

213. Li, G.; Zhu, X.; Zhu, J.; Cheng, Z.; Zhang, W. Homogeneous reverse atom transfer radical polymerization of glycidyl methacrylate and ring-opening reaction of the pendant oxirane ring *Polymer* **2005,** 46, 12716-12721.

214. Cañamero, P. F.; Fuente, J. F.; Madruga, E. L.; Fernández-García, M. Atom transfer radical polymerization of glycidyl methacrylate: A functional monomer, *Macromol. Chem. Phys.* **2004,** 205, (16), 2221-2228.

215. Krishnan, R.; Srinivasan, K. S. V. Controlled/"living" radical polymerization of glycidyl methacrylate at ambient temperature, *Macromolecules* **2003,** 36, (6), 1769-1771.

216. Krishnan, R.; Srinivasan, K. S. V. Room temperature atom transfer radical polymerization of glycidyl methacrylate mediated by copper(I)/N-alkyl-2-pyridylmethanimine complexes, *Macromolecules* **2004,** 37, (10), 3614-3622.

217. Bories-Azeau, X.; Merian, T.; Weaver, J. V. M.; Armes, S. P.; van den Haak, H. J. W. Synthesis of near-monodisperse acidic homopolymers and block copolymers from hydroxylated methacrylic copolymers using succinic anhydride under mild conditions, *Macromolecules* **2004,** 37, (24), 8903-8910.

218. Sunder, A.; Bauer, T.; Mulhaupt, R.; Frey, H. Synthesis and thermal behavior of esterified aliphatic hyperbranched polyether polyols, *Macromolecules* **2000,** 33, (4), 1330-1337.

219. Sunder, A.; Quincy, M.-F.; Mülhaupt, R.; Frey, H. Hyperbranched polyether polyols with liquid crystalline properties, *Angew. Chem., Int. Ed.* **1999,** 38, (19), 2928-2930.

220. Bertin, P. A.; Watson, K. J.; Nguyen, S. T. Indomethacin-containing nanoparticles derived from amphiphilic polynorbornene: A model ROMP-based drug encapsulation system, *Macromolecules* **2004,** 37, (22), 8364-8372.

221. Quémener, D.; Héroguez, V.; Gnanou, Y. Synthesis of acid-sensitive latices by ring-opening metathesis polymeization, *J. Polym. Sci., Part A: Polym. Chem.* **2005,** 43, 217-229.

222. Pecora, R.; Berne, B. J., *Dynamic Light Scattering With Applications to Chemistry, Biology and Physics*. Dover Publications, INC: Mineola, NY, 2000.

223. Pecora, R. Dynamic light scattering measurement of nanometer particles in liquids, *J. Nanopar. Res.* **2000,** 2, 123–130.

224. Brown, W., *Dynamic Light Scattering. The Method and Some Applications*. Oxford University Press Inc.: New York, 1993.

225. Provencher, S. W. Inverse problems in polymer characterization: Direct analysis of polydispersity with photon correlation spectroscopy, *Makromol. Chem.* **1979,** 180, 201-209.

226. Koppel, D. E. Analysis of macromolecular polydispersity in intensity correlation spectroscopy: The method of cumulants *J. Chem. Phys.* **1972,** 57, (11), 4814-4820.

227. Mountrichas, G.; Mpiri, M.; Pispas, S. Micelles of star block (PSPI)8 and PSPI diblock copolymers (PS = polystyrene, PI = polyisoprene): Structure and kinetics of micellization, *Macromolecules* **2005,** 38, 940-947.

228. Burchard, W. Static and dynamic light scattering from branched polymers and biopolymers *Adv. Polym. Sci.* **1983,** 48, 1-124.

229. Checot, F.; Brulet, A.; Oberdisse, J.; Gnanou, Y.; Mondain-Monval, O.; Lecommandoux, S. Structure of polypeptide-based diblock copolymers in solution: Stimuli-responsive vesicles and micelles, *Langmuir* **2005,** 21, (10), 4308-4315.

230. Yang, M.; Wang, W.; Yuan, F.; Zhang, X.; Li, J.; Liang, F.; He, B.; Minch, B.; Wegner, G. Soft vesicles formed by diblock codendrimers of poly(benzyl ether) and poly(methallyl dichloride), *J. Am. Chem. Soc.* **2005,** 127, (43), 15107-15111.

231. Kalyanasundaran, K.; Thomas, J. K. Environmental effects on vibronic band intensities in pyrene monomer fluorescence and their application in studies of micellar systems, *J. Am. Chem. Soc.* **1977,** 99, 2039-2044.

232. Lee, A. S.; Gast, A. P.; Bütün, V.; Armes, S. P. Characterizing the Structure of pH Dependent Polyelectrolyte Block Copolymer Micelles, *Macromolecules* **1999,** 32, 4302-4310.

233. Yusa, S. I.; Fukuda, K.; Yamamoto, T.; Ishihara, K.; Morishima, Y. Synthesis of well-defined amphiphilic block copolymers having phospholipid polymer sequences as a novel blocompatible polymer micelle reagent, *Biomacromolecules* **2005,** 6, (2), 663-670.

234. Kabanov, A. V.; Nazarova, I. R.; Astafieva, I. V.; Batrakova, E. V.; Alakhov, V. Y.; Yaroslavov, A. A.; Kabanov, V. A. Micelle formation and solubilization of fluorescent-probes in poly(oxyethylene-b-oxypropylene-b-oxyethylene) solutions, *Macromolecules* **1995,** 28, (7), 2303-2314.

235. Allen, C.; Maysinger, D.; Eisenberg, A. Nano-engineering block copolymer aggregates for drug delivery, *Colloids and Surfaces B-Biointerfaces* **1999,** 16, (1-4), 3-27.

236. Kita-Tokarczyk, K.; Grumelard, J.; Haefele, T.; Meier, W. Block copolymer vesicles--using concepts from polymer chemistry to mimic biomembranes, *Polymer* **2005,** 46, (11), 3540-3563.

237. Guerrero-Sanchez, C.; Wouters, D.; Fustin, C. A.; Gohy, J. F.; Lohmeijer, B. G. G.; Schubert, U. S. Structure-property study of diblock copolymer micelles: core and corona radius with varying composition and degree of polymerization, *Macromolecules* **2005,** 38, (24), 10185-10191.

238. Hiemstra, C.; vanderAa, L. J.; Zhong, Z.; Dijkstra, P. J.; Feijen, J. Novel in situ forming, degradable dextran hydrogels by michael addition chemistry: Synthesis, rheology, and degradation, *Macromolecules* **2007,** 40, (4), 1165-1173.

239. Marie-Laure Teyssot, M. F. C. P. C. D. Bis-Heteronucleophilic Michael Addition to Divinyl Sulfone: A New Efficient Access to Macrocycles, *European Journal of Organic Chemistry* **2003,** 2003, (1), 54-62.

240. Reddick, J. J.; Cheng, J.; Roush, W. R. Relative rates of michael reactions of 2'-(phenethyl)thiol with vinyl sulfones, vinyl sulfonate esters, and vinyl sulfonamides relevant to vinyl sulfonyl cysteine protease inhibitors, *Org. Lett.* **2003,** 5, (11), 1967-1970.

241. Zhiju Zheng, C. P. D. W. Y. L. Michael Addition Polymerizations of Trifunctional Amines with Divinyl Sulfone, *Macromolecular Chemistry and Physics* **2005,** 206, (21), 2182-2189.

242. Allen, C.; Yu, Y.; Maysinger, D.; Eisenberg, A. Polycaprolactone-b-poly(ethylene oxide) block copolymer micelles as a novel drug delivery vehicle for neurotrophic agents FK506 and L-685,818, *Bioconjugate Chem.* **1998,** 9, 564-572.

243. Tang, Y.; Liu, S. Y.; Armes, S. P.; Billingham, N. C. Solubilization and Controlled Release of a Hydrophobic Drug Using Novel Micelle-Forming ABC Triblock Copolymers, *Biomacromolecules* **2003,** 4, (6), 1636-1645.

244. Zhao, J. X.; Allen, C.; Eisenberg, A. Partitioning of pyrene between "crew cut" block copolymer micelles and H2O/DMF solvent mixtures, *Macromolecules* **1997,** 30, (23), 7143-7150.

245. Wilhelm, M.; Zhao, C.-L.; Wang, Y.; Xu, R.; Winnik, M. A.; Mura, J.-L.; Riess, G.; Croucher, M. D. Poly(styrene-ethylene oxide) block copolymer micelle formation in water: a fluorescence probe study *Macromolecules* **1991,** 24, 1033-1040.

246. Lutz, J. F.; Laschewsky, A. Multicompartment micelles: Has the long-standing dream become a reality?, *Macromol. Chem. Phys.* **2005,** 206, (8), 813-817.

247. Nokhodchi, A.; Javadzadeh, Y.; Siahi-Shadbad, M. R.; Barzegar-Jalali, M. The effect of type and concentration of vehicles on the dissolution rate of a poorly soluble drug (indomethacin) from liquisolid compacts., *J. Pharm. Pharmaceut. Sci.* **2005,** 8, (1), 18-25.

248. Soyez, H.; Schacht, E.; Vanderkerken, S. The crucial role of spacer groups in macromolecular prodrug design, *Adv. Drug Deliv. Rev.* **1996,** 21, (2), 81-106.

249. Lecolley, F. New polymers from living radical polymerisation for biological applications. PhD thesis, University of Warwick, Warwick, 2004.

250. Albin, P.; Markus, A.; Pelah, Z.; Ben-Zvi, Z. Slow-release indomethacin formulations based on polysaccharides: evaluation in vitro and in vivo in dogs, *J. Control. Release* **1994,** 29, (1-2), 25-39.

251. Wan, H.; Holmen, A.; Nagard, M.; Lindberg, W. Rapid screening of pKa values of pharmaceuticals by pressure-assisted capillary electrophoresis combined with short-end injection, *J. Chromatogr. A* **2002,** 979, (1-2), 369-377.

252. Lee, S. C.; Lee, H. J. pH-Controlled, polymer-mediated assembly of polymer micelle nanoparticles, *Langmuir* **2007,** 23, (2), 488-495.

List of Publications

Articles

Published

1. **Giacomelli, C**.; Schmidt, V.; Borsali, R. Specific interactions improve the payload capacity of block copolymer micelles in aqueous media, *Langmuir* **2007**, 23, 6947-6955. http://dx.doi.org/10.1021/la700337s.

2. Schmidt, V.; **Giacomelli, C**.; Brisson, A.; Borsali, R. Towards an easy access to Annexin-A5 protein binding block copolymer micelles, *Mater. Sci. Eng. C* **2007**, *ASAP article* - http://dx.doi.org/10.1016/j.msec.2007.04.025.

3. **Giacomelli, C**.; Schmidt, V.; Borsali, R. Nano-containers formed by self-assembly of poly(ethylene oxide)-b-poly(glycerol monomethacrylate) – drug conjugates, *Macromolecules* **2007,** 40, 2148-2157.

4. **Giacomelli, C.;** LeMen, L.; Borsali, R.; Lai-Kee-Him, J.; Brisson, A.; Armes, S. P.; Lewis, A. L. Phosphorylcholine-based ph-responsive diblock copolymer micelles as drug delivery vehicles: light scattering, electron microscopy, and fluorescence experiments, *Biomacromolecules* **2006,** 7, (3), 817-828.

5. Schmidt, V.; **Giacomelli, C.;** Lecolley, F.; Lai-Kee-Him, J.; Brisson, A. R.; Borsali, R. Diblock copolymer micellar nanoparticles decorated with annexin-a5 proteins, *J. Am. Chem. Soc.* **2006,** 128, (28), 9010-9011.

6. **Giacomelli, C.;** Borsali, R. Morphology of Poly(ethylene oxide)-b-polycaprolatone copolymer micelles controlled via the preparation method, *Macromol. Symp.* **2006,** 245–246, 147–153.

7. **Giacomelli, C.;** Lafitte, G.; Borsali, R. Polycaprolactone-b-poly(ethylene oxide) biocompatible micelles as drug delivery nanocarriers: Dynamic light scattering and fluorescence experiments, *Macromol. Symp.* **2005,** 229, 107-117.

In preparation

8. Schmidt, V.; **Giacomelli, C**.; Di Cola, E.; Brisson, A. R.; Naraynan, T.; Borsali, R. Polyelectrolyte Behavior of Diblock Copolymer Micelles Having Phosphonic Diacid Groups at the Corona. **2007**, *in prep*.

9. **Giacomelli, C**.; Borsali, R.; Facile approach to highly loaded pH-responsive shell cross-linked micelles. **2007**, *in prep.*

10. Schmidt, V.; **Giacomelli, C**.; Borsali, R.; Brisson, A. R. Nanostructured thin block copolymer films for precise positioning of protein arrays. **2007**, *in prep.*

Nouveaux Développements dans l'Encapsulation de Molécules Hydrophobes via l'Auto-Assemblage de Copolymères à Blocs Amphiphiles

Ce manuscrit décrit le développement de nouvelles stratégies dans la préparation de nanoparticules ayant une excellente capacité d'encapsuler, retenir, transporter et délivrer des molécules hydrophobes (médicaments, fragrances, agents de contraste, pesticides, etc.). Pour cela, sept systèmes de copolymères à blocs amphiphiles bien définis ont été synthétisés (principalement par polymérisation radicalaires par transfert d'atome (ATRP)) et caractérisés par des méthodes classiques. La faculté de ces macromolécules de s'auto-organiser a été utilisée pour obtenir des nanoparticules sphériques (micelles et vésicules avec une taille < 200 nm), dont les propriétés physico-chimiques ont été étudiées en détails par des techniques de diffusion de lumière et d'imagerie. Dans une seconde étape, le processus d'encapsulation de différentes molécules hydrophobes par ces nanoparticules a été mis à profit et exploré en détails. Les résultats ont montré des différences très intéressantes par rapport à la quantité maximale de molécules hydrophobes encapsulées dans le cœur de la micelle. Ces nanoparticules sont classées en trois groupes principaux, correspondant à des capacités d'encapsulation (LC) *A*) faibles (LC ≤ 30 % w/w_p), *B*) modérées (30 % < LC < 70 % w/w_p) et *C*) élevées (LC ≥ 70 % w/w_p). Dans ce dernier cas, des interactions spécifiques du type acide-base dans le cœur de la particule sont responsables pour l'excellente capacité d'encapsulation systématiquement observée. Cependant, l'incorporation de grandes quantités de matières par des micelles polymériques peut provoquer une augmentation significative de la taille, ainsi que des transitions de morphologies (de micelles sphériques à cylindres à vésicules). Les résultats suggèrent très clairement que la capacité d'encapsulation des systèmes micellaires stimulables que nous avons développés peut être contrôlée avantageusement via les propriétés structurelles des molécules hydrophobes et des blocs formant le cœur de la nanoparticule.

Mots-clés: Copolymères à blocs, Polymérisation Radicalaire par Transfert d'Atome, Auto-assemblage, Diffusion de lumière, Techniques d'imagerie, Micelles, Vésicules, Nanoparticules, Encapsulation.

Advances in the Encapsulation of Hydrophobic Molecules via Self-Assembly of Amphiphilic Block Copolymers

This work contemplated the design of original approaches to prepare stimulus-responsive block copolymer nanoparticles having excellent ability to encapsulate, retain, transport and deliver hydrophobic guest molecules (i.e., probes such as drugs, fragrances, contrast agents, pesticides, etc.). To this end, seven well-defined amphiphilic block copolymer systems were synthesized (mainly by atom transfer radical polymerization (ATRP)) and characterized using standard methods. Subsequently, such macromolecules were used as building blocks to obtain self-assembled spherical nanoparticles (micelles and vesicles with size < 200 nm), whose physical chemical parameters were investigated in details by light scattering and imaging techniques. In the last and most important step of this investigation, the loading of hydrophobic probes into the micelles was assessed, as well as the respective release kinetics. The results revealed astonishing differences in terms of loading contents (LC) that could be encapsulated in the particles, which could ultimately be organized in three principal groups: *A*) low (LC ≤ 30 % w/w_p), *B*) moderate (30 % < LC < 70 % w/w_p) and *C*) high (LC ≥ 70 % w/w_p) loading capacity nanoparticles. In the latter case, specific (acid-base) interactions inside the hydrophobic environment of the carrier were responsible for the highly enhanced payload capacity. However, the incorporation of high amounts of hydrophobic guest molecules inside polymeric micelles can provoke not only increases in their hydrodynamic size ($2R_H$), but also substantial changes in the morphology (e.g.: transition from spheres to cylinders to vesicles). The results reported herein suggest that the loading capacity of block copolymer micelles can be tailored through the rational design of core-forming blocks and hydrophobic guest molecules.

Keywords: Block copolymers, Atom transfer radical polymerization, Self-assembly, Light scattering, Imaging techniques, Micelles, Vesicles, Nanoparticles, Encapsulation, Loading content, Release kinetics.